Development of a Biosensing Strategy for Multiplex and Dynamic Quantification of a Secretory Fingerprint from Human Pancreatic Islets

Francisco Rafael Castiello, M. Sc.

Doctor of Philosophy

Department of Biological and Biomedical Engineering

McGill University

Montreal, Canada

Submitted December 2018

A thesis submitted to McGill University in partial fulfillment of the requirements of the degree of Doctor of Philosophy

To my wife…

Abstract

Diabetes mellitus is a chronic disorder occurring when elevated levels of blood glucose, known as hyperglycemia, result from the body's impaired ability to produce or regulate insulin. If left untreated, chronic hyperglycemia can cause cardiovascular disease, neuropathy, nephropathy and eye disease, leading to retinopathy and blindness. In 2017 the number of people with diabetes reached 425 million worldwide. This disease arises from deficiencies in the secretory pathways of the pancreatic islets, a micro-organ constituting 1-2% of the pancreas mass. Recent studies have shown that the cells comprising the islets possess an intricate communication system, in which their secreted hormones exert paracrine interactions on neighbor cells. However, little is understood about the consequences of such communications. Up-to-date most research in the field has focused on understanding the processes related with insulin and glucagon secretion, the main hormones secreted by the two major cell types present in the islets. Thus, monitoring a secretory fingerprint (SF) contemplating more than two hormones, presents a research opportunity to increase our current understanding of diabetes.

Due to their simplicity, ease of use, non-invasive and label-free nature, biosensors provide an excellent basis for the development of analytical tools capable of detecting the SF of islets. Therefore, the main objective of the present thesis was to develop a biosensing strategy for the multiplex detection of a SF composed of the hormones secreted by the three major cell types contained in the pancreatic islets. At first, we explored the use of a capacitance-based biosensor for the detection of insulin. This biosensing technique was selected, since it could offer high sensitivity, potential for multiplexing and capabilities for integration with microelectronic technologies. Since the performance of this biosensor critically depends on the surface chemistry design of the bioreceptor immobilization, a systematic study was performed to evaluate the effect

of common architectures reported in literature. These chemistries included the covalent immobilization of biomolecules on the electrodes, in the gaps between electrodes and a conformal coating covering both. While the development of this capacitive biosensor provided us with very valuable knowledge on the effect of various parameters for the detection of insulin, its implementation for islet continuous SF analysis proved difficult due to its long analysis time. For this reason, we explored surface plasmon resonance imaging (SPRi), an analytical technique with intrinsic real-time analysis and multiplex quantification capabilities, as an alternative to fully reach the thesis objective.

By combining a competitive immunoassay with SPRi and the optimization of the sensor's surface chemistry it was possible to detect, for the first time, insulin, glucagon and somatostatin simultaneously. This biosensing strategy presented a limit of detection (LOD) comparable to previous reports detecting insulin and glucagon secretions individually with a short analysis time. However, detecting the smallest hormone, somatostatin, remained a challenge due to the obtained high LOD compared to insulin and glucagon and a lack of reports providing a desirable reference for its performance. Thus, to address this pitfall and ensure the detection of all targeted hormones in a biologically relevant concentration range, we performed a study comparing three different signal amplification strategies based on gold nanoparticles (GNPs). These strategies included GNPs immobilized on the sensor surface, GNPs conjugated with primary antibodies and GNPs conjugated with a secondary antibody for post competitive assay amplification. Here, multiplexed detection of the three hormones was achieved with an improved LOD of 9 fold for insulin, 10 fold for glucagon and 200 fold for somatostatin when compared to the SPRi biosensor without GNPs signal amplification, successfully addressing the aforementioned challenge. In summary, the results from this thesis work lay the groundwork to begin the investigation of a human islet SF using our newly developed biosensing strategy.

Résumé

Le diabète sucré est une maladie chronique qui arrive quand les taux de sucre dans le sang sont élevés, connu sous le nom d'hyperglycémie, résultant d'une capacité réduite du corps à produire ou à réguler l'insuline. Sans traitement, l'hyperglycémie chronique peut causer des maladies cardiovasculaires, une neuropathie, une néphropathie, et des maladie oculaires, qui peuvent mener à la rétinopathie et la cécité. En 2017, le nombre de personnes affectées par le diabète était de 425 millions à l'échelle mondiale. Cette maladie résulte des carences des voies de sécrétion des îlots du pancréas, ces micro-organes qui représentent 1 - 2 % de la masse du pancréas. Des études récentes montrent que les cellules constituant ces îlots ont un système de communication complexe, dans lequel les hormones qu'elles sécrètent exercent des interactions paracrines sur leurs cellules voisines. Cependant, les conséquences de ces interactions sont encore mal comprises. Jusqu'à présent, beaucoup des recherches dans ce domaine sont concentrées sur la compréhension des procédés de sécrétion d'insuline et de glucagon, qui sont les hormones principales secrétées par les deux principaux types de cellules dans les îlots. Ainsi, le suivi d'une empreinte sécrétoire comprenant plus de deux hormones constitue une opportunité de recherche pour améliorer notre compréhension du diabète.

Par leur simplicité, leur facilité d'utilisation, leur nature non-invasive et l'absence de marquage, les biocapteurs constituent une excellente base pour le développement d'outils analytiques pouvant détecter l'empreinte sécrétoire des îlots. L'objectif principal de cette thèse était donc de développer une stratégie de détection biologique pour la détection multiplexe de l'empreinte sécrétoire composée des hormones secrétées par les trois principaux types cellulaires présents dans les îlots pancréatiques. Dans un premier temps, nous avons exploré l'utilisation d'un biocapteur capacitif pour la détection d'insuline. Cette technique a été choisie pour sa sensibilité

élevée, son potentiel pour le multiplexage et ses capacités d'intégration avec les technologies microélectroniques. La performance de ce biocapteur dépendant essentiellement de la chimie de surface immobilisant le biorécepteur, une étude comparative a permis d'évaluer les effets des architectures communément décrites dans la littérature. Ces chimies consistaient en l'immobilisation covalente des biomolécules sur les électrodes, entre les électrodes et sur le revêtement conforme qui couvre les deux. Tandis que le développement de ce biocapteur capacitif nous a fourni une meilleure compréhension du mécanisme de détection de l'insuline et de certains de ses paramètres, la longueur du temps d'analyse rendait son implémentation pour l'analyse de l'empreintes sécrétoire des îlots difficile. Comme alternative pour réaliser pleinement l'objectif de la thèse, nous avons donc exploré l'imagerie par résonance de plasmons de surface (SPRi), une technique d'analyse présentant des capacités intrinsèques d'analyse en temps réel et de quantification multiplex.

En combinant un immunodosage compétitif avec la SPRi et en optimisant la chimie de surface du biocapteur, il a été possible de détecter simultanément pour la première fois l'insuline, le glucagon et la somatostatine. Cette stratégie de biodétection présentait une limite de détection pour le glucagon et l'insuline comparable aux méthodes reportées antérieurement pour un temps d'analyse court. Néanmoins, la détection de la plus petite hormone, la somatostatine, demeurait un défi en raison des hautes limites de détection obtenues comparées aux autres hormones et en raison de l'absence de rapports offrant une référence convenable pour ses performances.

Afin d'éviter cet écueil et de garantir une détection de toutes les hormones ciblées dans une gamme de concentration pertinente sur le plan biologique, nous avons mené une étude comparative de trois différentes stratégies d'amplification de signal basées sur des nanoparticules d'or (GNPs). Ces stratégies comprenaient des GNPs immobilisés sur la surface du biocapteur, des GNPs conjugués avec un anticorps primaire et des GNPs conjugués avec un anticorps secondaire pour la

post-amplification d’un immunodosage compétitif. La détection multiplexée des trois hormones a alors été obtenue avec une LOD améliorée de 9 fois pour l'insuline, de 10 fois pour le glucagon et de 200 fois pour la somatostatine comparativement à la détection non-amplifiée, permettant de relever le défi susmentionné. En résumé, les résultats de cette thèse établissent les fondations d’une étude sur l’empreinte sécrétoire d’îlots humains à l’aide de notre nouvelle stratégie de détection biologique.

Acknowledgements

First of all, I would like to thank my supervisor, Dr. Maryam Tabrizian for her continuous mentorship, patience and professionalism throughout my graduate studies. She provided me with a great research environment. She was always available to clarify any aspect of my research project promptly and diligently. She always addressed the human aspect involved with the development of my research project, providing advice when frustration emerged. Her support and motivation helped me greatly during difficult times. I will always be very grateful for the opportunity that she gave me to join her lab.

I would like to thank the members of my advisory committee: Prof. Satya Prakash and Prof. Sacha Omanovic for all their valuable insights and guidance during our meetings. I also want to thank all the staff of the McGill microfabrication facilities for their continuous advice and help during the fabrication of interdigitated electrodes and goal-coated substrates. Special thanks to Pina Sorrini, Nancy Abate, Daniel Caron and Sabrina Teoli in Biomedical Engineering Department for always being available and resourceful.

I would like to thank my former and present lab members. Thanks in particular goes to Dr. Khalil Heileman for his collaboration on our microfluidics systems for pancreatic islet research review paper, to James Porter and Paresa Modarres for their collaboration on our capacitive immunosensor paper and to Celine Agnes for her help with the French translation of the thesis abstract. I would also like to thank Dr. Feriel Melaine for her advice and input regarding SPRi and Dr. Jamal Daoud for his advice with impedance experiments. Thanks to all my friends of the Biomat'X lab, Mina, Amir, Lamees, Rosey, Laila, Meltem, Sandrine, Tim, Selya, Kaushar, Saadia, Reza, Nick, Michael, Brandon and Timothy Johns. Thanks for all of the great moments that we had together. You made this PhD journey agreeable and successful. Working with you all was a

great honor.

I would like to acknowledge the funding sources that made this work possible: Natural Sciences and Engineering Research Council of Canada, the NSERC-CREATE Integrated Sensor Systems (ISS) program, Consejo Nacional de Ciencia y Teconología de México (CONACyT) and Secretaría de Educaión Pública México (SEP) and McGill's Biomedical Engineering Department.

I like to express my most sincere gratitude to my wife Dane Guerra for her unconditional love, support and understanding. Her companionship, constant encouragement and joyful personality kept me sane and away from quitting during the hardest times of my PhD.

Finally, my never ending gratefulness to my parents who have given me everything. Thank you for your devotion, patience and incommensurable encouragement that have always convinced me that I can accomplish anything I can dream of. Words would never be enough to express my gratitude to you both. At last, thanks to my sister. You thought me a lot about sharing, negotiation and persuasion. These skills proved to be very useful during my PhD ordeal.

Table of Contents

List of Figures

List of Tables

List of Abbreviations

2D	Two Dimensional
3D	Three Dimensional
5HT	5-Hydroxytryptamine
AC	Alternating Current
ADMET	Absorption, Distribution, Metabolism, Excretion and Toxicity
AFM	Atomic Force Microscopy
APTES	(3-Aminopropyl)triethoxysilane
ATP	Adenosine Triphosphate
BSA	Bovine Serum Albumin
CEI	Capillary Electrophoresis Immunoassay
CPE	Constant Phase Element
DTSSP	(3,3'-dithiobis(sulfosuccinimidyl propionate))
EDC	N-(3-Dimethylaminopropyl)-N′-ethylcarbodiimide hydrochloride
EIS	Electrochemical Impedance Spectroscopy
ELISA	Enzyme-Linked Immunosorbent Assay
ESI-MS	Electrospray Ionization Mass Spectrometry
FDA	Food and Drug Administration
FEM	Finite Element Modeling
FET	Field Effect Transistors
FITC-insulin	Fluorescein Isothiocyanate Labeled Insulin
GNPs	Gold Nanoparticles
GNPs-Ab1	Gold Nanoparticles-Primary Antibody Conjugates

GNPs-Ab2	Gold Nanoparticles-Secondary Antibody Conjugates
HEGD	Hexa(ethylene glycol) Dithiol
IAPP	Islet Amyloid Polypeptide
IDEs	Interdigitated Electrodes
IS	Impedance Spectroscopy
LOC	Lab-on-a-Chip
LOD	Limit of Detection
LYZ	Lysozyme
MHDA	16-Mercaptohexadecanoic Acid
MPS	Microfluidic Perfusion Systems
MW	Molecular Weight
NHS	N-Hydroxysuccinimide
PA	Passive Adsorption
PBS	Phosphate-Buffered Saline
PBS-T	Phosphate-buffered saline-Tween 20
PDMS	Poly(Dimethylsiloxane)
PEG	Poly(Ethylene Glycol)
PMMA	Poly(Methyl Methacrylate)
RI	Refractive Index
Rq	Root Mean Square
RU	Resonant Units
SAMs	Self-Assembled Monolayers
SD	Standard Deviation
SF	Secretory Fingerprint

SPR	Surface Plasmon Resonance
SPRi	Surface Plasmon Resonance imaging
T1D	Type 1 Diabetes
T2D	Type 2 Diabetes
TBS	Tris-buffered saline

Contribution of Authors

This thesis is presented as a collection of manuscripts written by the candidate with the assistance, collaboration and supervision of the co-authors. The candidate envisioned and developed the multiplex biosensing strategy and its associated methods carrying out all required experiments, characterization analysis and data acquisition presented in this thesis. Mr. Khalil Heileman appears as co-author in the literature review publication (**Chapter 5**) for his contribution with ideas, comments and the preparation of the manuscript. Mr. James Porter appears as co-author in the publication regarding capacitance immunosensing (**Chapter 6**) for his involvement in the collection of data related to this manuscript. Ms. Paresa Modarres appears as co-author in the publication in **Chapter 6** for performing the finite element simulation and analysis of the electric field of the sensor included in the manuscript. Finally, Dr. Maryam Tabrizian appear on all publications for her partaking in the preparation of the manuscripts and her guidance and supervisory role throughout the execution of this work.

Thesis Outline

This thesis is divided into ten chapters:

Chapter 1 presents a general introduction for the thesis. The groundwork to grasp the problem of diabetes in the context of pancreatic islet research along with an overview to the concept of an islet's secretory fingerprint are presented in this chapter.

Chapter 2 discusses the rationality and the urge for developing novel analytical techniques for the analysis of human pancreatic islet secretion.

Chapter 3 presents the research hypothesis and the objectives of this thesis.

Chapter 4 presents the background knowledge concerning major topics of this thesis, such as biosensors, SPR, electrochemical impedance spectroscopy and self-assembled monolayers.

Chapter 5 is a review paper that covers the state-of-the-art regarding applications of microfluidics, secretomics and biosensors in emerging areas of human islet research. These areas include islet transplantation, regeneration and drug screening. This review was published in **Lab-on-a-chip** (Castiello, F. R. *et al*. 2016, 16 (3), 409-431).

Chapter 6 presents the investigation of the potential use of an IDEs capacitance-based biosensor for the detection of insulin. The purpose of this study was to collect the knowledge affecting the detection of small molecules, such as insulin (in the context of this thesis) using this label-free sensing technique, and to build the groundwork for the following objectives. This study will be submitted for publication in ***Sensors and Actuators B***.

Chapter 7 introduces the use of a biosensor for simultaneous quantification of insulin, glucagon, and somatostatin based on SPRi, a technique known for its intrinsic high-throughput and multiplexed quantification capabilities. The results of this study were published in ***Analytical chemistry*** (Castiello, F. R. *et al*. 2018, 90 (5), 3132-3139).

Chapter 8 reports on the implementation of different SPR signal amplification strategies using gold nanoparticles to ensure the multiplex detection of secreted hormones within a range of relevant biological concentrations corresponding to the secretion levels from a small population of islets. This investigation was published in ***Analyst*** (DOI: 10.1039/c9an00140a).

Chapter 9 discusses the original contributions of this thesis to the knowledge advancements in the field of islet research and biosensing technology as well as the general discussion of the thesis results.

Chapter 10 presents the future work required to move to the detection of pancreatic islets secretion, possible integration of the SPRi biosensor with microfluidic technologies along with foreseen application of such platform in pancreatic islet research.

Chapter 11 contains the general conclusion of this thesis.

Finally, a list of the references cited in this work and two appendixes are provided at the end of this dissertation. The appendix section contains the published article reprints along with copyright waivers and the candidate curriculum vitae.

Chapter 1. Introduction

Diabetes mellitus is a chronic disorder that occurs when an elevated level of glucose is present in the blood due to the inability of the body to produce or efficiently regulate the hormone insulin. Insulin is a vital hormone produced in the pancreas that helps to transport glucose from the bloodstream into almost all cells in the body where it is required as energy. The lack of insulin or the inability of the cells to properly sense insulin leads to high levels of blood glucose, a condition known as hyperglycemia, which is the distinctive symptom of diabetes. If hyperglycemia becomes chronic, it can cause irreversible damage to various organs leading to the development of disabilities and life-threatening complications, such as cardiovascular disease, neuropathy, nephropathy and eye disease, leading to retinopathy and blindness [1]. In 2017, the number of people with diabetes reached 425 million worldwide and it is expected that this figure will increase 48% by 2045 [1]. Moreover, in 2017 this disease caused a 400 billion dollars disbursement just in the North America and Caribbean region [1].

Diabetes arises from secretory defects in the pancreatic islets or islets of Langerhans, which are clusters of endocrine of cells with average diameter of 150 μm, that constitute between 1 and 2% of the pancreas mass [2]. The islets of Langerhans are highly vascularized micro-organs composed of five hormone-secreting cells (α, β, δ, PP, and ε) that cooperate to maintain glucose homeostasis in response to metabolic changes [2, 3]. In general, there are two main types of diabetes: type 1 (T1D) and type 2 diabetes (T2D). T1D is caused by an autoimmune reaction where the insulin secreting β-cells are destroyed by the immune system, leaving the body with no means of producing this hormone. In T2D, there is insufficient secretion of insulin and/or an inability of the body's cells to adequately sense insulin. T2D accounts for 90% of all cases of diabetes, and

therefore, has been a major subject in diabetes research, particularly for the development of oral hypoglycemic agents [4].

Recent studies indicate that the hormones secreted from the cells composing the islets have an intricate communication system, exerting paracrine interactions on their neighbor cells [3, 5, 6]. Such interactions may play a dominant role in the achievement of glucose homeostasis, and their further understanding may reveal novel therapeutic avenues for T2D [5, 6]. Although many research groups are interested in investigating the mechanisms of insulin and glucagon secretion from the α and β cells respectively [7-10], very few are particularly focused on studying the paracrine interactions of the other islets cells [5], and none on monitoring a secretory fingerprint (SF) that contemplate secretion from more than two islets' cell types. Moreover, the mechanisms of insulin secretion and islet function within most of these works have been elucidated using animal models. However, in recent years it was demonstrated that the islet anatomy and physiology is species-dependent, and hence, it is ill-advised to generalize findings from any individual species [5, 11]. As result, the anatomy, physiology and all basic cellular mechanisms of human islets are being revised [11-16].

Current models for diabetes drug discovery and research include chemically induced *in vivo* models (streptozotocin and alloxan) and genetic model of diabetes (fa/fa and Goto-Kakizaki rats, db/db and ob/ob mice) [17, 18]. There are also *in vitro* models based on insulin-secreting cell lines (β-TC, MIN6 and INS-1 cells) or in the major tissues involved in the pathophysiology of diabetes [17, 19, 20]. However, despite the demonstrated value of these models, there is a lack of predictability when results are extrapolated to humans, most likely due to the vast anatomical and physiological differences among models [5, 11]. Evidence of this inconsistency can be found in a recent work where re-aggregated human pancreatic islets were assessed and compared to native

human islets and rat islets for secondary drug screening [21]. The response of the different islets were significantly different when tested against a variety of hypoglycemic agents [21].

Therefore, this thesis project proposes to study a relevant SF of human pancreatic islets to emphasize the importance of studying the islets as an interconnected whole and not just as a collection of individual functions. By monitoring changes in such SF, it would be possible to develop a more comprehensive *in vitro* model of diabetes and advance our understanding of the paracrine communications within the isles, opening a novel therapeutic avenue for T2D.

Chapter 2. Rationale and Motivation

2.1. Traditional biochemical assays and islets secretion

Currently, most of the pancreatic islet research depends on traditional bioassays for hormone quantification such as patch clamp [13, 14, 22-24], capillary electrophoresis immunoassays (CEI) [25-27], and ELISA [28, 29]. However, the patch clamp technique requires highly skilled operators to trap and manipulate individual cells, is low throughput, it only provides an indirect measurement of secretion, and it lacks specificity for individual secretion products. As with patch clamp, CEI requires skilled operators to work effectively, precise temperature control, overcoming channel clogging, and the integration of lasers with different wavelengths. Finally, although operationally simpler, ELISA is difficult to use for simultaneous quantification of multiple analytes, is time-consuming and expensive. Furthermore, all mentioned techniques face many challenges when attempting their expansion for the simultaneous analysis of multiple targets.

To monitor an islet's SF, candidate multiplex analytical techniques must be fast, specific and possess high spatio-temporal resolution in order to detect changes in the secretion patterns of the islets. Analytical techniques fulfilling such requirements have been rapidly emerging in the last decades thanks to progress of micro- and nanotechnologies for the development of electrochemical-, electrical-, and optical-based biosensors [30]. Among these technologies, label-free electrical sensors based on interdigitate electrodes (IDEs) and optical sensors using surface plasmon resonance (SPR) have shown potential for multiplexed detection of cell secretion products [30-32].

2.2. Label-free electrical biosensors based on IDEs

Essentially, label-free electrical biosensors report a bio-recognition event on the surface of

electrodes by means of a change in either current or voltage [33]. A particular case of such sensors are capacitance biosensors based on IDEs [34, 35]. This type of thin film electrodes can be fabricated with common microfabrication techniques, and their performance can be adjusted by modifying their dimensions. [36, 37]. Additionally, they provide a large sensing surface, present instrumental simplicity compared to other electrochemical techniques, and by integration with a microfluidic handling system they could easily achieve multiplexed detection of analytes [33]. Studies of islet secretion products using electrical biosensors have mostly focused on the detection of insulin from blood serum [38-40]. These technologies could be adapted to detect glucagon and somatostatin from islet samples, expanding the amount of detected secretion products.

2.3. SPR biosensors

By allowing fast detection of binding interactions due to changes in the surface plasmons of a thin gold film, SPR biosensing has become the gold standard to study biomolecular interactions [41]. The advantage of this technique is its inherent dynamic, label-free and real-time analysis [42]. Additionally, when combined with imaging capabilities (SPRi), high-throughput and multiplexed analysis is possible by making arrays of different molecules on the sensing surface [43]. In the last decade, SPR biosensors have mostly been used to investigate fundamental physiological aspects of various islet hormones, namely insulin [44-46], somatostatin [47], pancreatic polypeptide [48, 49] and ghrelin [50]. However, none of these reports exploited the intrinsic multiplex capabilities of SPRi which could allow quantification of more than two of the islets' major secreted hormones.

Chapter 3. Hypothesis and Thesis Objectives

It is hypothesized that a multiplex biosensing strategy can be developed to dynamically quantify a secretory fingerprint of human pancreatic islets encompassing three of their major secreted hormones.

To validate the aforementioned hypothesis, three main objectives were set:

1. Develop a biosensing strategy capable of detecting in real-time time and under continuous flow the islet's low molecular weight hormones.

   This objective was achieved by developing an immunoassay using two biosensing transduction mechanism, electrical and optical. Experimental conditions were investigated to ensure the ability of the sensor to perform dynamic and specific detection of insulin.

2. Expand the biosensing strategy developed in objective one to achieve simultaneous detection of three islets' hormones as its secretion fingerprint with high sensitivity and specificity.

   This aim was achieved by implementing a multiplex SPRi-based immunosensing through the selection of an optimal surface chemistry that allowed for the target detection with high specificity and sensitivity required to operate in a complex matrix such as an islet's secretome.

3. Achieve a limit of detection and dynamic range that allowed the detection of all hormones composing the secretion fingerprint when secreted from few islets in multiplexed mode.

   This goal was achieved by investigating a gold nanoparticle enhancement strategy for the multiplex SPRi-based biosensor developed in objective two to improve the assay performance for the detection of the three selected hormones.

In this dissertation, each objective is delivered as an article, published or under consideration.

Chapter 4. Background Knowledge

4.1. Biosensors

In a nutshell, a biosensor is an analytical device able to measure a physical quantity and convert it into a signal easily read by the observer. A biosensor consists of two major components, a transducer and a bioreceptor. A bioreceptor is a biological material that includes proteins (enzymes and antibodies), nucleic acids (DNA, RND and aptamers), cell receptors, entire microorganisms and viruses [51]. Bioreceptors are typically retained in direct contact with a transduction element and selectively recognize a single and specific analyte. Due to this highly specific nature, biosensors provide an excellent basis for the development of analytical tools, with potential application in medicine, food testing and environmental monitoring [52]. On the other hand, transducers generate an output signal proportional to the specific biorecognition event. Common transducer types include: electrochemical, mechanical and optical [51].

Electrochemical biosensors typically measure small changes in voltage, current, or resistance/impedance in a three-electrode system composed of a working, reference and counter electrode. The bioreceptors are immobilized on the working electrode surface and binding events are measured by means of charge transfer or accumulation. Traditional electrochemical techniques used for biosensing include cyclic voltammetry, chronoamperometry, chronopotentiometry and impedance spectroscopy [53]. Historically, this kind of biosensors were the first to be developed and they are a popular choice for the development of miniaturized diagnostic devices due to their high sensitivity, compatibility with current microfabrication methods and easiness to integrate with modern electronics [53].

Mechanical biosensors measure force, displacement or mass change. Generally, a small

cantilever is used as a transducer to detect minute mass changes due to the binding of target molecules to bioreceptors. In these biosensors, the minimum detectable mass change is proportional to the total mass of the biosensor itself [54]. Thanks to recent advances in nanofabrication technologies, mechanical biosensors have achieved detection limits between 10^{-9} to 10^{-21} grams depending on the operating conditions [54]. Moreover, their ability to be displaced or deformed, presents opportunities to measure forces produced by biological and biochemical systems with a few pN resolution [54].

Optical biosensors measure changes in signals coming from a light source, typically LED or a laser diode. These biosensors are designed to translate changes in the electromagnetic properties of light propagating through a medium that contains biological material present on the surface of the transducer. They include: ellipsometry, spectroscopy (luminescence and Raman), interferometry and surface plasmon resonance [41]. Optical biosensors are the second major evolutionary line of biosensors and they are commonly found in research and development laboratories [52].

Based on its intended application, a biosensor may require optimization of a variety of parameters to achieve optimal performance. For instance, biosensors tailored for point-of-care applications will require high levels of automation, low cost, ease of use, and miniaturization [55]. Meanwhile, biosensors aimed for fundamental laboratory research will require robustness for long term use and high levels of customization to account for a wide variety of biological systems under investigation [56]. However, sensitivity, specificity, limit of detection and detection time are the most important parameters to characterize for any biosensor.

4.2. Electrochemical Impedance Spectroscopy Principles

Electrochemical Impedance Spectroscopy (EIS) is a technique used for more than a century to perform corrosion analysis, characterize batteries and fuel cells as well as to study the adsorption of molecules at an electrode/electrolyte interface among other applications [57]. This technique was first introduced by Oliver Heaviside in the 1880s and later developed in relation to diffusional electrochemical systems by Warburg in 1899 [58].

In essence, EIS is an alternating current (AC) technique that describes the response of an electrochemical system to a small perturbation using a sinusoidal voltage signal as a function of frequency [59]. Here, the magnitude of impedance (|Z|) is defined as the ratio of the applied voltage (V (t)) and the resulting current (I (t)) of the system. Physically, the impedance (Z) term represents all the phenomena within the electrochemical cell that oppose the flow of electrons and ions, such as electrode kinetics, redox reactions, diffusion phenomena and molecular interactions at the electrode surface [59]. These phenomena can be considered analogous to electrical components (resistors, capacitors, inductors) that hinder the flow of electrons in an AC circuit [59].

EIS is subdivided into Faradic EIS and non-Faradic EIS depending on whether a redox reaction is present or not. Faradic EIS involves an electrochemical reaction as a sensing step. This reaction can come either from an external chemical compound (redox probe) added to the system or from the sample itself. In the absence of a redox probe (non-Faradic EIS), the interfacial capacitance at the electrode/electrolyte can be used as a sensitive way of measuring biomolecular events without the transfer of electric charge, making such systems commonly known as capacitive sensors [34]. This makes effectively non-Faradaic EIS a label-free detection technique that eliminates costly and cumbersome sample preparation steps compared to its Faradic counterpart [35].

Impedance is expressed as a complex number, where resistance is the real component and capacitance is the imaginary one. The most popular formats for evaluating electrochemical impedance data are the Nyquist (**Fig. 4.1A**) and Bode plots (**Fig. 4.1B**). In the Nyquist format, the imaginary impedance component (Z") is plotted against the real impedance component (Z') as a function of frequency. In the Bode format, both the impedance magnitude (|Z|) and the phase shift (Θ) are plotted against the logarithm of the excitation frequency [59].

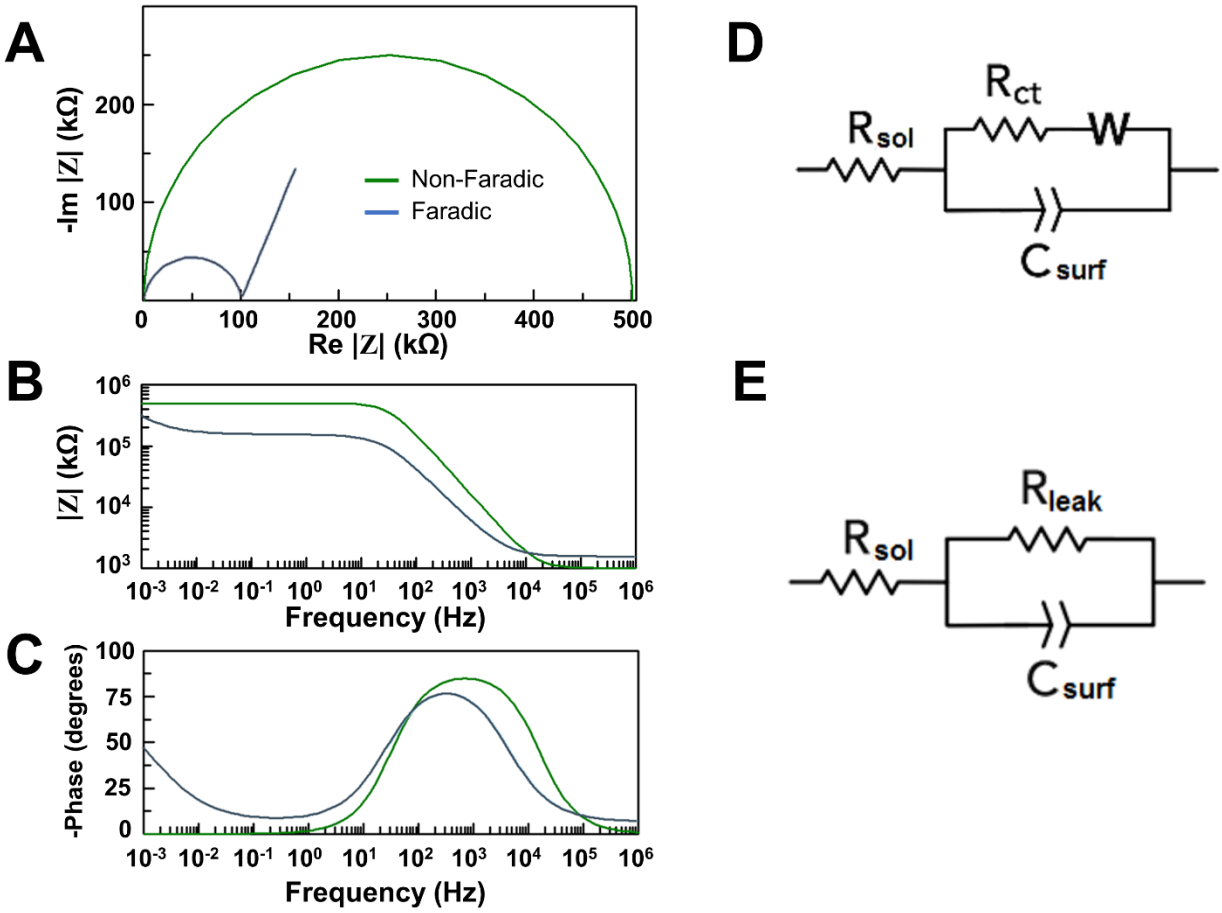

Figure 4.1. Simulated example of non-Faradic and faradic impedance plots. **A**) Nyquist format, Bode format including **B**) magnitude and **C**) phase. **D**) Common circuit models of a faradic system and **E**) common circuit model of a non-faradic system. The analogous electrical components used for these models are the solution resistance (Rsol), the double layer capacitance (Csurf), the Warburg impedance (W), the charge transfer resistance (Rct) and a resistor representing leakage current from a parallel surface capacitor (Rleak). The equivalent circuit models in D and E were used to generate the plots in A, B and C. All the values for the simulation of the presented circuit models were taken from reference [35].

The measured impedance data can be used to extract equivalent values of resistances and capacitances if a circuit model representing physical electrochemical processes is assumed. However, there is not a unique model or even necessarily a one-to-one correspondence between circuit elements and the underlying physical processes [35]. Characteristically, the raw impedance data is fitted to a proposed circuit model and changes in a specific circuit element are reported as the sensor output. Alternatively, the impedance at a particular frequency where the targeted physical phenomena is observed can be used [35]. Common equivalent circuit models found in the literature for faradic and non-faradic electrochemical system are displayed in **Figure 4.1D** and **Figure 4.1E** respectively. Characteristic circuit elements include: the solution resistance (R_{sol}), arising from the conductivity of ions in the solution; the Warburg impedance (W), representing diffusion of the electroactive species to the electrode; the surface capacitance (C_{surf}), representing the capacitance between the metal electrode and ions in solution; the charge transfer resistance (R_{ct}), associated with an oxidation/reduction event or an energy barrier experienced by redox species reaching the electrode. Additionally, in parallel with the surface capacitance a resistive path (R_{leak}) is often modeled for non-Faradaic systems [35].

4.3. Surface Plasmon Resonance Principles

The phenomenon of uneven distribution of light on a metal-dielectric interface was first described by R. W. Wood in the beginning of the twentieth century [60]. This phenomenon is caused by free electrons on the surface of transition metals that propagate along their surface, performing coherent oscillations known as surface plasmon resonance (SPR). These charge-density oscillations are associated with an electromagnetic wave, with maximum intensity at the interface decaying evanescently into the medium [61]. Typically the depth of the evanescent wave is within ≈200 nm

of the metal surface [61]. Most commercial SPR systems nowadays use the so-called Kretschmann configuration which consists of a thin metal film deposited on a glass prism that facilitates total internal reflection of the incident light beam (**Fig. 4.2A**).

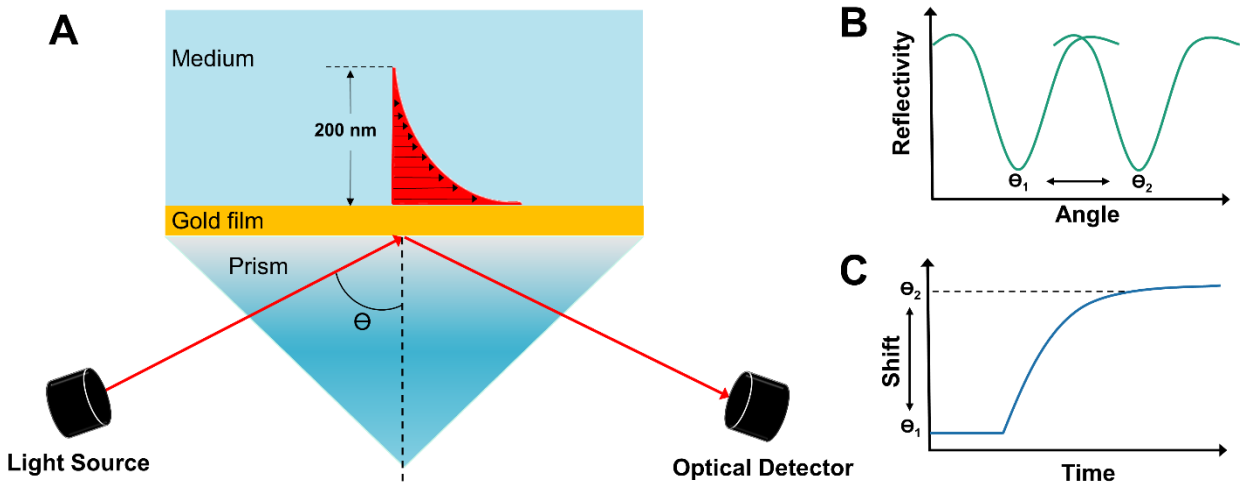

Figure 4.2. A) Typical Kretschmann configuration for an SPR system. When incident light with a defined angle (Θ) excite the surface plasmons of the gold film an evanescent wave is produced within 200 nm of the metal surface. **B)** Representative SPR angle shift due to changes in the refractive index on the vicinity of the metal film. **C)** Typical detection output of an SPR instrument where changes in the angle of the reflected light are tracked over time.

Based on the property measured, an SPR sensogram can be obtained by wavelength, reflectivity or angle shift. In the wavelength shift mode, the SPR is achieved using multiple wavelengths, such as polychromatic light at a constant incident angle. In the reflectivity (% R, *y*-axis **Fig. 4.2B**) and angular shift (Θ at the dip of the curve in **Fig. 4.2B**) modes the SPR is observed by scanning the incident angle at a constant wavelength [62].

On the conditions of a light source with a constant wavelength, the defined SPR angle (Θ) at which resonance occurs is dependent on the refractive index (RI) of the material near the metal surface. Therefore, changes occurring in the RI in the vicinity of the metal surface with the medium cause a change in the plasmon resonance angle which can be monitor by the optical detector (**Fig.**

4.2B). This angle shift can then be tracked over time indicating detection of particular events happening at the film surface (**Fig. 4.2C**). In SPR experiments the angle shift can be directly expressed in degrees or in resonance units (RU) where 1 RU is equivalent to an angle shift of 10^{-4} degrees [63]. Typical metal films used for SPR are silver, gold, copper, aluminum, sodium and indium with an approximate thickness of 50 nm. However, gold films are the most widely used in the field, since SPR can be generated using visible wavelengths of light, it is an inert metal, and various molecules can be easily immobilized on its surface through gold-thiol interactions [61].

An additional advantage of SPR detection systems is that they can provide simultaneous visualization of multiple areas of the metal film when combined with the imaging capabilities of a CCD camera. This multiplexed detection format which was first introduced by Rothenhäuslar and Knoll in 1988 [64], is known as SPR microscopy or SPR imaging (SPRi). Due to the use of a CCD camera for signal detection, sensograms and images of an arrayed metal surface can be recorded in real-time allowing high-throughput analysis of biomolecular or chemical interactions [43]. In this detection technique, differences in the chemical composition or the thickness of the layer close to the metallic film produce changes in the local dielectric constant values, which ultimately generate image contrast. Binding events can be visualized by collecting difference images after a binding event has occurred and subtracting a reference image. This approach allows simultaneous and independent measurements on different areas of the sensor's surface [43].

4.3.1. SPR signal amplification

Despite its advantage for label-free and real-time analysis, SPR detection systems present a major limitation for the detection of highly dilute analytes (<1 pM) or analytes with low molecular weight (<8 kDa) such as cancer biomarkers, hormones and antibiotics [65]. Consequently, to overcome this limitation, sensitivity enhancement methods have been researched to increase the detection

capabilities of SPR systems. Most of these enhancement methods are mainly based in the use of nanomaterials, either as a substrate or as an amplification label, including metallic nanoparticles, magnetic nanoparticles, liposome-based nanoparticles and carbon-based nanomaterials, as well as two-dimensional nanostructures on surface of SPR metallic films [65].

An advantage of metal nanoparticles over other nanostructures is that they exhibit localized surface plasmon resonance (LSPR), which can be observed as a strong UV-Vis absorption band that is not present in absorption spectrum of bulk metals. Gold nanoparticles (GNPs) are among the most popular nanomaterial for SPR signal enhancement [65]. The phenomena of SPR signal enhancement based on GNPs was first applied to biosensors by L. Andrew Lyon *et al*. [66] in 1998, when it was shown that the use of GNPs resulted in over 25 times higher sensitivity than a conventional SPR device when detecting protein-protein interactions. This strategy relies mostly on the coupling of the LSPR of the GNPs with the propagating surface plasmon resonance of the system's metallic film which results in large increase in the plasmon resonance angle [65]. The degree of change in the plasmon resonance angle depends on the GNP size, morphology, interparticle distance and wavelength use during measurements [65, 67]. However, in order to achieve coupling of the plasmon resonance modes, the GNPs must be in close proximity to the SPR metallic surface (< 50 nm) [61]. This is particularly important when using GNPs as tags on analytes or recognition elements, since the distance of the GNP-bioreceptor conjugates after surface binding could be not sufficient for LSPR activation. Additionally to LSPR coupling, GNPs can produce a large SPR signal amplification when they are used as tags. This is due to the artificially increased mass they provided to the analyte, resulting in a high refractive index change on the SPR surface when a binding event occur [68]. However, the LSPR coupling factor is expected to play the dominant role for signal enhancement [67].

An advantage of nanostructures integrated into the SPR metallic films over their use as tags is that the sensitivity enhancement is achieved while preserving the label-free characteristic of SPR systems. Examples include the direct immobilization of GNPs on the SPR sensing film using self-assembled monolayers of alkane dithiols [69], the microfabrication of nanorods [70], and nanohole arrays in the metallic films [71], to name a few. Recently, graphene-modified SPR sensing films have been reported to improve the SPR detection sensitivity [72]. This is mainly due to the charge transfer from graphene to the surface of the metal film leading to a strong excited electric field enhancement at the sensing area [72].

4.4. Self-assembly Monolayers Chemistry

Pristine surfaces of metals and metal oxides are highly reactive. For this reason, they are inclined to the chemisorption of atoms and molecules that lowers the free energy between their surface and the environment [73]. This adsorption predisposition can be exploited to alter the metal and metal oxides interfacial properties depending on their intended application. For instance, adsorbed organic materials can act as an electrically insulating film in conducting materials or they can act as a physical barrier against aggregation of biomolecules. However, random adsorption of foreign materials could lack chemical functionality and reproducibility [74].

A solution to this problem is the used of the fundamental chemical principle of self-assembly molecular organization [75]. Self-assembled monolayers (SAMs) are produced by the adsorption of molecules from solutions or vapors onto the surface of solids in regular arrays on the surface. This process occurs spontaneously, forming highly ordered structures by non-covalent interactions (electrostatic, π-effects, van der Waals forces, and hydrophobic effects) [74]. Therefore, SAMs can provide a simple and reproducible system to tailor the interfacial properties

of metals and metal oxides.

The molecules used for the formation of SAMs naturally possess a chemical functional "head group" with high affinity for the surface. The most extensively studied class of SAMs is produced from the adsorption of thiolated linear compounds (alkanethiols) on noble metals such as gold, silver, copper, palladium and platinum generally possessing a functional chemical group that presents a wide variety of organic functionalities (**Fig. 4.3A**). In these SAMs, sulfur donor atoms strongly coordinate with the metal surface and Van der Waals forces between methylene groups to orient and stabilize the monolayer [76]. Moreover, it has been shown that solutions of mixed alkanethiols allows the formation of highly packed nanometric surfaces SAMs with a wide variety of compositions [74]. Noteworthy when preparing mixed monolayers, the mole fraction in the final SAM adsorbed on the surface will not the same as that in the immersion solution. The choice of solvent, the polar nature of the functional group and the difference in chain lengths of the *n*-alkanethiols mixtures would alter the relative ration of the adsorbed molecular components where the SAM composition is usually enriched with the longer alkanethiol. This effect is more evident when the difference in the number of chain units is greater than three [77, 78].

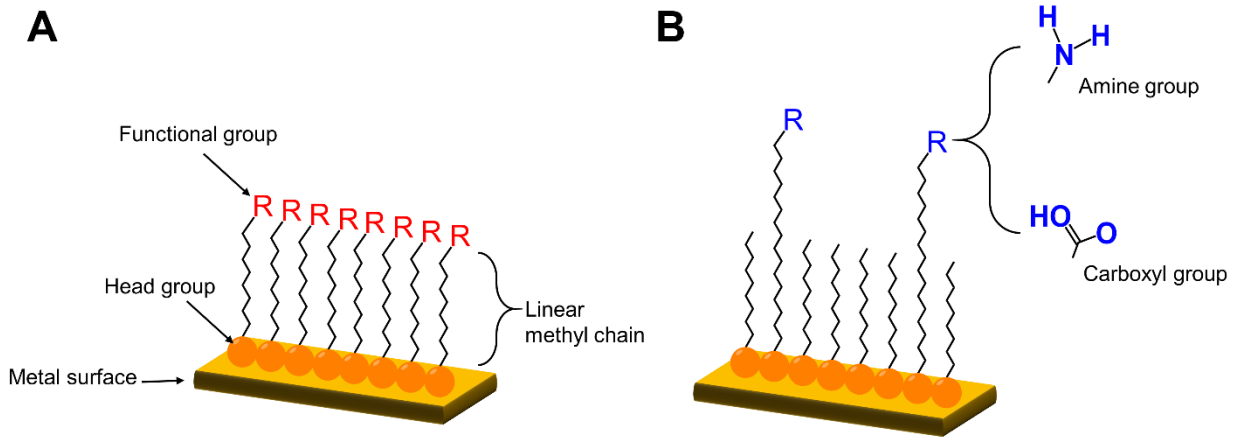

Figure 4.3. Basic structure of **A)** a single alkanethiol self-assembly monolayer and **B)** a mixed self-assembly monolayer with examples of chemical functional groups.

Several studies performed with a wide variety of thiol mixtures and under different conditions, have shown some controversy regarding the possibility to produce separated domains depending on the used solvent, the nature of the thiolated compounds or the temperature used during SAM formation [79]. However, it has been showed that some degree of phase segregation can occur when the mixed SAM components have very different chain lengths and/or a large difference in the degree of polarity regarding their functional groups [80]. Additionally, it is worth mentioning that mixed monolayers typically present a higher level of defects compared to the corresponding single-component SAMs [79].

In general, the use of mixed alkanethiol SAMs offers many advantages for the development of analytical applications [81]. For instance, it has been shown that the co-adsorption of two thiols can prevent denaturation and improve the bioactivity of proteins such as bioreceptors deposited on surfaces, and they can shield the adsorptions of undesired organic matter [76]. These characteristics have a great impact in the development of biosensing techniques where the quality of the bio-interface governs the sensitivity and specificity of the biosensor [82]. These mixed SAMs are generally composed of an alkanethiol with a functional group such as a carboxylic acid or an amine at a low mole fraction, and second "spacer" thiolated compound at a high mole fraction (**Fig. 4.3B**). The first thiol is used for the covalent immobilization of a bioreceptor while the second spacer group reduces the surface concentration of functional groups, and thus minimizes steric hindrance and partial denaturation of the immobilized the bioreceptor [82]. Additionally, the spacer thiol can be used to tune the physicochemical properties of the sensor surface preventing non-specific interaction that can produce interfering signals [82].

Chapter 5. Human Pancreatic Islet Research: State-of-the-Art

The following chapter provides a review paper published in the journal *Lab on a Chip* by the candidate with a comprehensive literature review required for the completion of this thesis project. This review covers the state-of-the-art regarding applications of microfluidics, secretomics and biosensors in emerging areas of human islet research; namely, islet transplantation, regeneration and drug screening. Moreover, the review offers insights on opportunities and challenges for tissue culture on-chip encountered when working with 3D organoids such as the pancreatic islets. In addition, the review identifies gaps in the current technology for multiplexed screening of islet secretion products highlighting promising biosensing tools to achieve this purpose.

Microfluidic Perfusion Systems for Secretion Fingerprint Analysis of Pancreatic islets: Applications, Challenges and Opportunities

F. Rafael. Castiello[a], Khalil Heileman[a], and Maryam Tabrizian[a*]

[a] Biomedical Engineering Department, McGill University, Montreal, QC, H3A 2B4, Canada. E-mail: Maryam.Tabrizian@mcgill.ca; Fax: +1-514-298-7461; Tel: +1-514-398-8129

5.1. Abstract

A secretome signature is a heterogeneous profile of secretions present in a single cell type. From the secretome signature a smaller panel of proteins, namely a secretion fingerprint, can be chosen to feasibly monitor specific cellular activity. Based on a thorough appraisal of the literature, this review explores the possibility of defining and using a secretion fingerprint to gauge the functionality of pancreatic islets of Langerhans. It covers the state of the art regarding microfluidic perfusion systems used in pancreatic islet research. Candidate analytical tools to be integrated within microfluidic perfusion systems for dynamic secretory fingerprint monitoring were identified. These analytical tools include patch clamp, amperometry/voltammetry, impedance spectroscopy, field effect transistors and surface plasmon resonance. Coupled with these tools, microfluidic devices can ultimately find applications in determining islet quality for transplantation, islet regeneration and drug screening of therapeutic agents for the treatment of Diabetes.

5.2. Introduction

Agrawal *et al*. [83] defined the cell secretome as: "the collection of proteins secreted by a cell's tissue, organ or organism at any given time and condition, regardless of secretion mechanism, being constitutive or regulated secretion". A secretome can control and regulate a multitude of biological and physiological processes [84]. In addition, it reflects the functionality of a cell in a given environment [85]. For instance, chronic alteration or aberrant secretion within a cell secretome could be indicative of a pathological condition. Thus, secretome analysis or secretomics is becoming a clinically relevant research field for biomarkers and therapeutic targets discovery [85].

Although the general definition of secretion includes metabolites and ions, in literature, the definition of the secretome only refers to proteins. As such, this review is focused on global secretion of proteins unless otherwise specified. Ions and small molecules will only be mentioned when they are used as an indirect way to measure protein secretion or when a platform that measures them can be adapted for protein secretion detection.

A cell's secretome can be comprised of a considerable amount of proteins (up to 1000) making its continuous monitoring difficult. Moreover, it has been shown that a genetically identical cell population can present functional heterogeneity [86], which can create a potential barrier to accurately screen the response to a stimulus or to pharmacological therapies [87, 88]. To overcome this problem, it is possible to study the secretome of individual cells within a population, and establish a particular secretome signature for each cellular phenotype.

A cell secretome signature is composed of a smaller number of proteins (around 100) compared to the whole cell secretome. However, it will be more convenient to monitor an even smaller set of proteins within the secretome signature, encompassing a particular secretory fingerprint (SF). This SF can be selected on a case-by-case basis and dynamically monitored to

find relationships between secreted proteins and their secretagogues.

While complete secretomic analysis of pancreatic islets has not yet been performed, current knowledge still allows definition of a SF composed of relevant hormones and other biomarkers. To date, the majority of islet studies have focused at most on the simultaneous measurement of two secreted hormones. Herein, we propose that a SF composed of a larger number of secretion products can yield a deeper understanding of islet physiology and its secretory response. The present review is not attempting to cover pancreatic islets secretomics. It rather suggest that the determination of an islet secretome will expand our current knowledge of islet secreted biomarkers. This in time will allow definition and measurement of a more pertinent SF depending on the application (e.g. drug screening, transplantation or islet regeneration).

First, this review presents important concepts of pancreatic islet physiology and species-dependent characteristics. It then covers current methods and challenges for determining a cell secretome. Then it exposes the state of the art regarding microfluidic perfusion systems (MPS) for pancreatic islets. Subsequently, it overviews analytical tools with a proven potential to dynamically monitor islet secretion processes when integrated in MPS. These platforms could be very useful for investigating islets as whole micro-organs and identifying the roles of individual secretion factors. Additionally, they can comprehensively assess the behavior of islets in complex metabolic networks, recapitulate the dynamics of hormone secretion and help discover new therapeutics to treat diabetes mellitus.

5.3. Pancreatic islet physiology and species dependent characteristics

The islets of Langerhans, which constitute 1 to 2% of the pancreas mass, are vascularized micro-organs with an average diameter of 150 μm. The pancreatic islets are composed of five different

endocrine cells (α, β, δ, PP, and ε cells) each secreting characteristic hormones in response to metabolic changes [3]. They are also composed of vascular cells, resident immune cells, neurons and glial cells. Additionally, human islets are surrounded by a complex double basement membrane [89]. Each islet is a functional unit with the physiological role of maintaining glucose homeostasis, mainly through β-cell insulin and α-cell glucagon secretion.

Insulin secretion is a complex and dynamic process, and detailed knowledge of it is critical for understanding diabetes mellitus. Insulin release by β-cells is an electrically excitable process in which changes in membrane potential is coupled to variations in blood glucose concentrations. In the absence of glucose (glucose concentration < 1mM), the membrane resting potential of human β-cells is approximately -70 mV [10]. Once glucose concentration increases, glucose transporters (GLUT) are activated and glucose metabolism occurs inside β-cells through glycolysis, the Krebs cycle and the electron transport chain, generating adenosine triphosphate (ATP) (**Figure 5.1-A**). The generated ATP closes the ATP-sensitive potassium channels (KATP), reducing the resting membrane potential until a threshold of -60 mV is exceeded, initiating membrane depolarization. Once membrane depolarization occurs, the voltage-gated Ca^{2+} channels open (reaching a peak influx at around -30 mV) and Ca^{2+} concentration increases. This in turn, triggers insulin vesicle fusion with the cell membrane by inhibiting the activity of the Ca^{2+} sensitive protein synaptotagmin, and subsequently insulin exocytosis occurs.

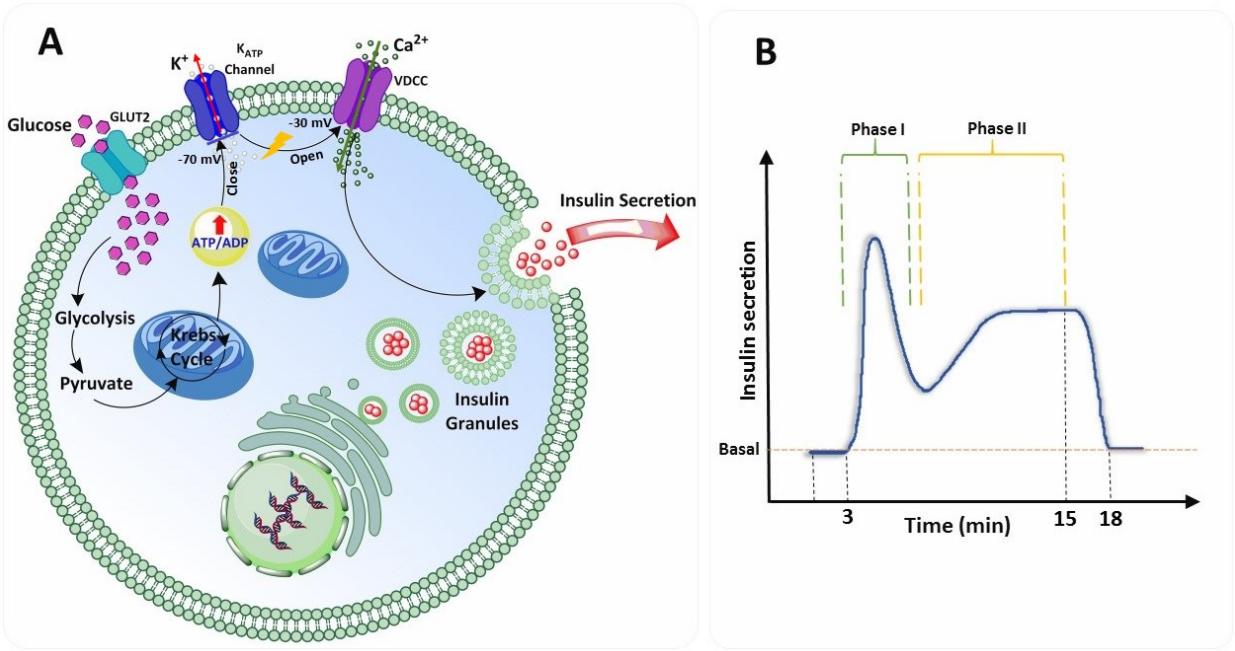

Figure 5.1. A) Glucose-stimulated insulin secretion pathway in pancreatic β-cells and **B)** biphasic insulin release profile.

Induced insulin exocytosis follows a biphasic time course (**Figure 5.1-B**) [90, 91]. The first phase corresponds to a fast transient increase rate of insulin secretion, usually within 5 minutes of glucose stimulation. Afterward, a decrease in insulin secretion takes place, followed by a gradual incremental second phase that lasts as long as the glucose stimulus is applied. As with most secretory cells, the biphasic secretion of insulin is pulsatile by nature. Moreover, insulin secretion has been demonstrated to oscillate in a synchronous manner with cytoplasmic Ca^{2+} concentration [92], indicating that Ca^{2+} oscillations are direct regulators of insulin pulsatility.

Co-secreted peptides and ions during insulin exocytosis, such as C-peptide, Zn^{2+} ions and amylin, can be used to indirectly quantify insulin secretion or measure secretion kinetics. In addition, it has been shown that these co-secreted factors have clinical relevance in diabetes mellitus diagnosis and treatment [93-96]. For the interested reader, in-depth detail of insulin secretion in human islets has been reviewed elsewhere [10].

As in any biological research, the mechanisms of insulin secretion and islet function have

been mostly elucidated using animal models. However, recent studies have demonstrated that islet anatomy and physiology is species-dependent, and therefore one has to be careful when generalizing findings from any individual species [5, 11]. As a consequence, many concepts related to anatomy, physiology and basic cellular mechanisms of human islets are currently being refined [11-16].

As an example, Cabrera *et al*. [11], studied the differences in islets cyto-architecture and functionality amongst four different species (**Figure 5.2-i**). Their findings showed that in the case of mouse, large spatial segregation of cell types exists, suggesting an anatomical subdivision within islets. However, when the authors compared the degree of segregation of cell types between mice and human islets, they found that in mice, 71% of the insulin-containing cells showed exclusively homotypic (same type) associations, whereas, in human, this was only 29%. As a consequence, β-cells are intermingled randomly with α- and δ-cells throughout the entire islet in close association with the islet microcirculation system (**Figure 5.2-ii**). Additionally, Cabrera *et al*. [11] demonstrated that islets from different regions of the human pancreas possess different cell compositions, and that on average, the cell composition of human islets contained proportionally fewer β-cells and more α-cells than that of mouse islets (**Figure 5.2-i**).

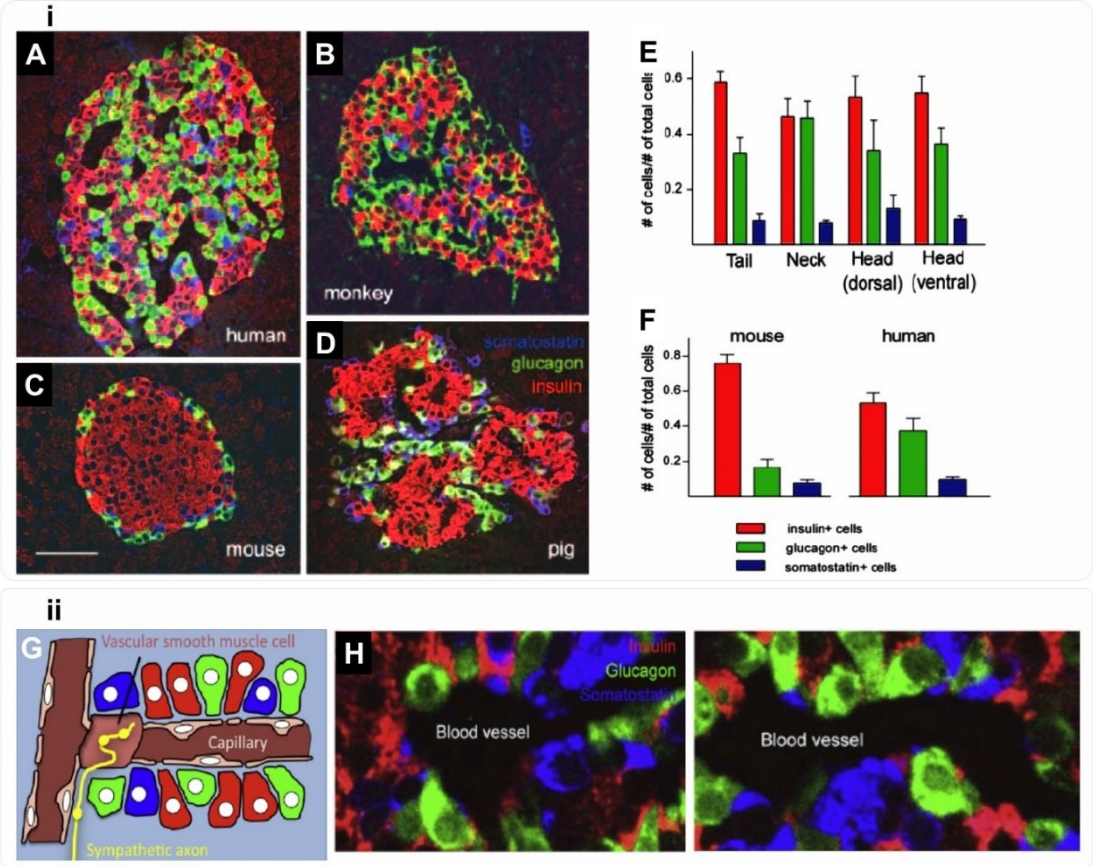

Figure 5.2. Illustration of differences in islet cytoarchitecture among species. **(i)** Confocal images of islets of Langerhans of human (**A),** monkey (**B**), mouse (**C**) and pig (**D**). (**E**) Human islet cell composition depending on the region of the pancreas from which they were obtained. (**F**) Comparison of cell composition between human and mouse islets (Reproduced from Ref. [11] with permission from National Academy of Sciences, U.S.A, Copyright 2006). **(ii)** Human islet cell distribution. (**G**) Schematic representation and (**H**) confocal image of human islet cell distribution around a capillary vessel. For all images, red: insulin-immunoreactive cells; green: glucagon-immunoreactive cells; blue: somatostatin-immunoreactive cells (Reproduced from Ref. [5] with permission from Elsevier).

The anatomy of human islets has significant consequences for cell-to-cell communication within the islets. Recent evidence suggests that the unique cytoarchitecture of human islets give rise to relevant paracrine and autocrine interactions that play a dominant role in their overall endocrine response [3, 5, 6, 16, 97-100]. For instance, it has been shown that somatostatin and ghrelin inhibit glucose-dependent insulin secretion [6, 16, 100], that pancreatic polypeptide (PP) [3] and co-secreted ions and amino acids [97, 98] exert a stimulatory and inhibitory effect respectively on glucagon secretion, and that neurotransmitters released from islet cells may shape

the pulsatile behavior in auto/paracrine feedback loops [99]. These aforementioned paracrine/autocrine interactions along with many others have been recently reviewed in detail [5, 99]. However, more research is needed in order to fully understand these paracrine interactions, particularly in the context of diabetes.

Finally, another critical aspect of islet physiology is functional heterogeneity, since human islets differ in size and composition. However, little is known about how such differences impact islet function [101-103]. Studying the secretome signature of single islets as it is done for other biological systems such as tumors, may allow investigation of this functional heterogeneity. For example, one can determine the secretome signature profile for islets in response to glucose stimulation, which can then be used as a baseline to select "functional" islets before transplantation, or to understand how secreted proteins exert paracrine/autocrine influence in islets.

As demonstrated in this section, our current knowledge of human islet physiology allows definition of a functional SF to monitor hormone secretion. However, once important protein biomarkers are found within the secretome signature profile, it will be possible to conceive systems to monitor the dynamics of a wider and more relevant SF to study particular aspects of islet physiology.

5.4. Current methods to determine a cell secretome

The Bergsten group described the first proteomic reference map of human pancreatic islets [104]. This report represented the first preliminary functional profile of the human islet proteome, in which many of the identified proteins have been implicated in the pathophysiology of diabetes. Since then, the aim of most islet protein profiling studies has been to elucidate the different mechanism involved in diabetes-associated β-cell deterioration [105]. However, because of the

complexity of cell proteomes, in some cases it is more practical to focus on a sub-proteome which only encompasses secreted proteins. Hence, many opportunities exist in the field of pancreatic islet research to focus specifically on the islet secretome and to determine a functional secretome signature. More information regarding islet protein profiling can be found in recent reports [105, 106].

To date, determination of the secretome has focused mostly on cells such as lung [107], colon [108] and glial [109, 110] cancer cells. Determining such cancer cell secretomes has unveiled mechanisms related to angiogenesis, invasion and metastasis, helping to develop new strategies to control cancer [107]. Additionally, there are some reports where the secretome of skeletal muscle cells [111] and human adipocytes during adipogenesis [112] has been determined.

Current methods to determine an unknown cell secretome involve placing cells in culture media for a period of time under controlled conditions, after which the media is analyzed for identification and quantification of secreted proteins. However, proteins secreted by dead cells in the media and serum proteins can mask the proteins of interest, making their isolation a challenge [113]. Hence, it is a common practice to use serum-free media and cytosolic extract as a control for dead cell proteins [113]. Nevertheless, little is known about how this affects cell secretion. Some evidence suggests that serum deprivation can cause apoptosis [114, 115], and can trigger different responses across various cell types [116]. Additionally, secreted proteins can be present at very low concentrations in the culture media, and on top of that, media is usually diluted before analysis, increasing the chances for analytical instruments to miss relevant biomarkers.

Traditional methodologies to decipher a cell secretome can be divided in two broad categories, the ones that analyze RNA/DNA to provide mostly qualitative information on gene-products (including computational methods), and the ones that analyze proteins directly, mostly

based on proteomic methods [84] (**Figure 5.3**). These methods may be restricted depending on whether the secretory protein sequence is known or not. Detailed information about the principle advantages and drawbacks of each has been reviewed elsewhere [84]. Usually a combination of RNA/DNA and protein quantification methods is used to acquire a bigger picture of the secretome by correlating gene expression and protein secretion. However this can be time-consuming.

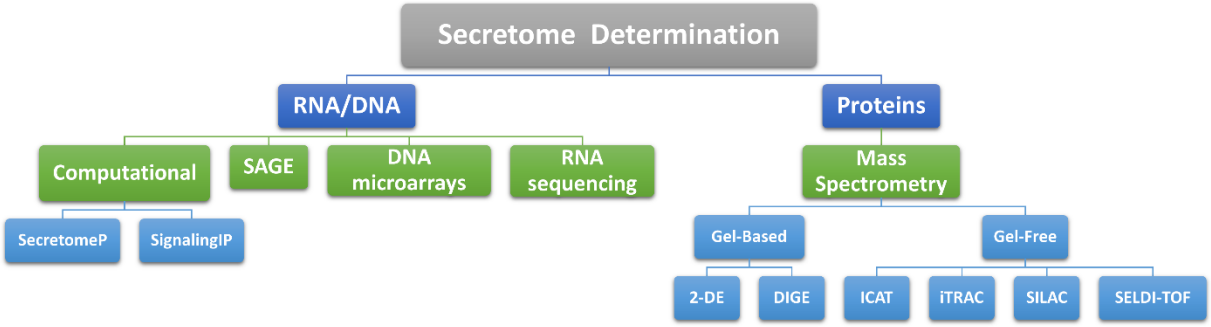

Figure 5.3. Classification of common techniques to decipher an unknown secretome. RNA/DNA methods comprise: serial analysis of gene expression (SAGE), DNA microarrays, RNA sequencing and computational methods such as SecretomeP for non-classical secretion and SignalingIP for classical secretion. Proteomic analysis techniques are mostly based on mass spectrometry, particularly liquid chromatography tandem mass spectrometry (LC-MS/MS). These methods can be subdivided into gel-based techniques, such as two-dimensional gel electrophoresis (2-DE) and differential gel electrophoresis (DIGE), and gel-free techniques, such as isotope-coded affinity tag (ICAT), isobaric tag for relative and absolute quantification (iTRAQ), stable isotope labeling by amino acids in cell culture (SILAC) and surface-enhanced laser desorption ionization-time of flight mass spectrometry (SELDI-TOF MS).

Once a cell secretome signature has been identified, other techniques such as immunoassays (e.g. ELISA, western blot and antibody microarrays) can be used to monitor small changes in the secretome, or as a complementary method with mass spectrometry for secretome identification [84]. Additionally, among these immunoassay techniques, antibody microarrays can be used in a high-throughput and multiplexed manner [117].

5.5. Multiplex screening

Multiplexing is desirable in most biological analyses since it reduces analysis time, sample volumes, and hence the cost of analysis [35]. However, multiplexed protein detection is

complicated due to cross-reactivities. This usually limits the degree of multiplexing, particularly in complex solutions, such as those containing cell secretion products. Nonetheless, a panel of several biomarker measurements can yield far more information than a single biomarker. Thus, efforts to develop multiplexed protein detection technologies represent great opportunities in many research fields.

A traditional technique used for multiplexed analysis of secreted proteins is antibody microarrays. Antibody arrays are a part of miniaturized devices in which antibodies can be immobilized on a planar surface or on microbeads, usually by micro-printing, to capture and quantify specific proteins [117]. The protein binding event is then detected in a label-based or sandwich configuration with a fluorophore, quantum dot or an enzyme [117]. Antibody arrays have been used so far to study proteins secreted by human adipocytes [112], mesenchymal stem cells [118] and cardiomyocyte cells [119].

However, these methods require a large number of cells for the analysis and obtained results will reflect the averaged features of cell populations. This may present disadvantages in many cases, since cell populations are heterogeneous in nature, and hence, population data can mask functional heterogeneity and associated molecular mechanisms [120]. The desirable solution would therefore be to study secretion from a single cell or a very small population of cells in order to identify phenotypes of interest and determine their respective secretome signature.

Microfluidic platforms can enhance spatio-temporal control of the cell microenvironment compared to traditional biological assays, allowing single cell analysis [121]. For instance, the sample volume can be reduced, avoiding dilution of secreted proteins and hence maximizing the information collected. Such platforms make it possible to use traps to immobilize single cells for multiplexed genetic/protein quantification [120, 122]. An example of this is a microfluidic chip for

isotope labeling coupled with electrospray ionization mass spectrometry (ESI-MS) [123], that was used for qualitative and quantitative analysis of drug-induced apoptosis of MCF-7 cells. The chip was designed to perform cell loading, microfluidic cell culture, drug solution injection, microfluidic cell staining, imaging analysis and ESI-MS detection (**Figure 5.4-i**). The authors demonstrated that when combining microfluidics and mass spectrometry, a multiplexed analysis of proteins could be carried out, despite the complexity of the MCF-7 secretome.

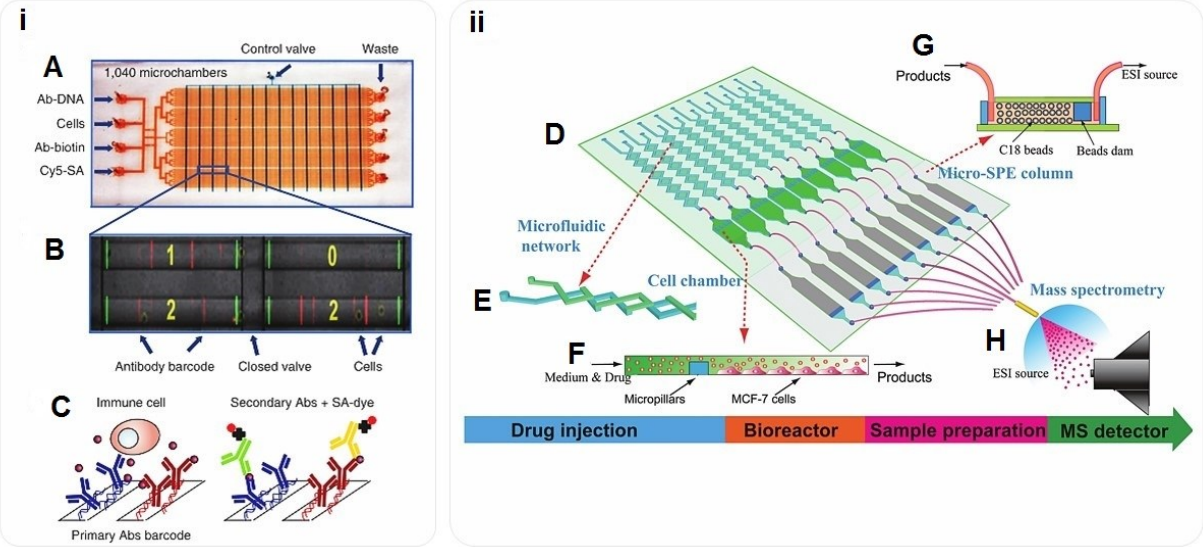

Figure 5.4. Examples of microfluidic devices for cell secretion analysis. **(i)** Barcode chip. **A**) Image of the device's assay channels shown in red and control channels in blue. **B)** Micrograph showing isolated cells and a fluorescent bar code assay. Yellow digits indicate number of cells per micro-chamber. **C)** Schematic representation of the multiplexed primary antibody barcode array used for capture of secreted proteins. SA stands for Streptavidin. (Reproduced from Ref. [124] with permission from Nature Publishing Group). **(ii)** Microfluidic chip for isotope labeling coupled with ESI-MS. **D)** Schematic representation of the ESI-MS chip consisting of a microfluidic network for culture medium delivery and drug injections, cell culture chambers, and on-chip micro-solid-phase extraction (micro-SPE) columns for sample desalting and purifying. **E)** Microfluidic network to generate concentration gradients during cell culture and drug screening. **F)** Side view of MCF-7 cells culture chamber. **G)** Close-up of an integrated micro-SPE column. (H) Micro-SPE column joined by capillaries. (Reproduced from Ref. [123] with permission from American Chemical Society Copyright 2012).

Another example is the evaluation of functional heterogeneity of immune T cells and human macrophages on a single-cell barcode chip [124]. The chip is composed of 1,040 microchambers with a 3 nL volume, each containing a single cell. Protein concentration is determined with sandwich immunoassays from spatially encoded antibodies. This forms a barcode that represents a

complete panel of protein assays (**Figure 5.4-ii**), allowing for highly multiplexed detection of proteins and statistical analysis of single cell protein secretion. Further information on single cell analysis and related microfluidic devices is available in two recent reviews by Galler *et al*. and Liu *et al*. [125, 126].

5.6. Current microfluidic perfusion systems for pancreatic islet research

A particular type of microfluidic device designed to control the media flow over single cells or cell culture chambers are microfluidic perfusion systems (MPS). In the case of pancreatic islets, MPS can simulate the islet *in vivo* environment. For instance, the pressures and flow volume of the islet vascular system can be reproduced [127], making these platforms ideal for islet *in vitro* analysis. In the past decade, many research groups have specialized in MPS development for islet research [127]. These devices generally possess two major components. The first component is a trapping mechanism capable of immobilizing single or multiple islets (**Figure 5.5)** while maintaining constant perfusion. Lack of perfusion on previous islet devices presented serious limitations for secretion studies [128]. For instance, dynamic measurement of islet secretion cannot be obtained since the concentration of secreted products constantly increases within a static chamber. Many experiments require a perfusion system that can rapidly vary the concentration of secretagogues delivered to the islets. Finally, without perfusion, islets cannot obtain fresh nutrients, which limits islet long term survival [128].

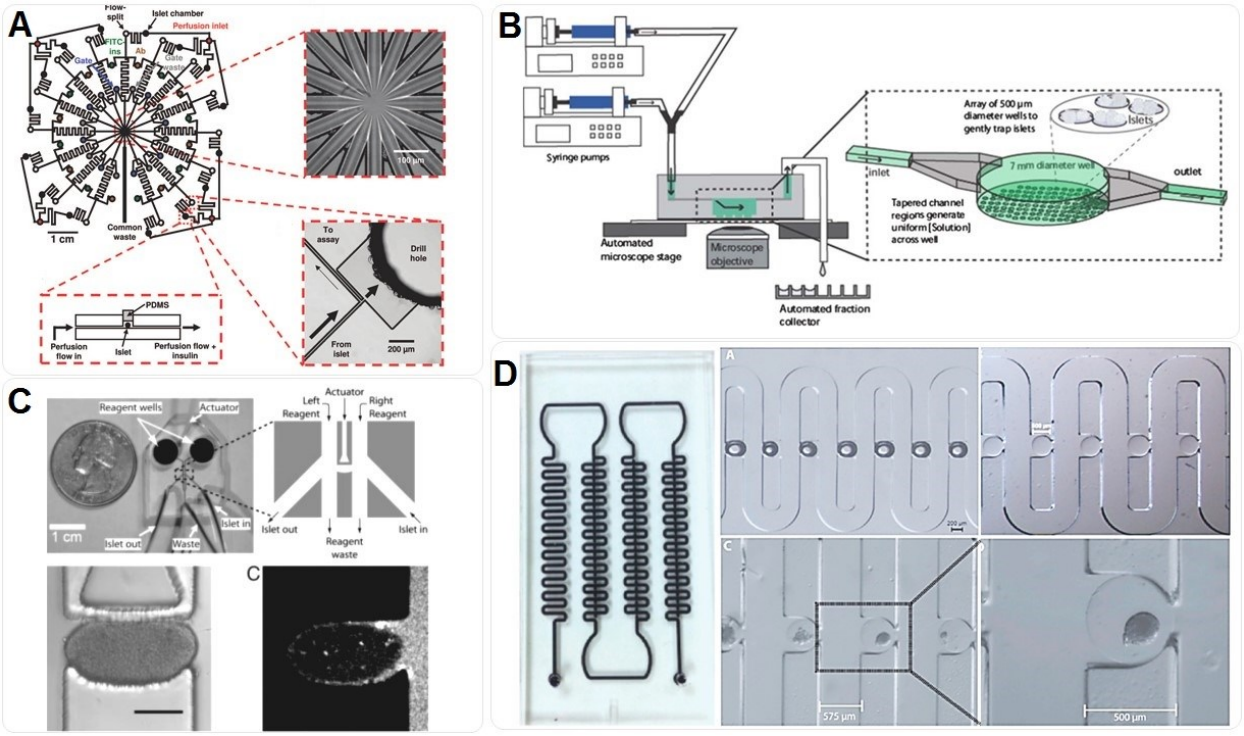

Figure 5.5. Examples of various MPS developed for pancreatic islet research. **A**) Schematics of a microfluidic chip for monitoring insulin secretion from 15 independent islets (Reproduced from Ref. [129] with permission from American Chemical Society Copyright 2009). The device is comprised of a microfluidic channel network, which is indicated by solid black lines. Circles represent the fluidic reservoirs. A side-view representation of an islet perfusion chamber and an on-chip flow-split is also presented. **B**) A microfluidic perfusion device for multiparametric islet function assessment through imaging and ELISA (Reproduced from Ref. [130] with permission from Springer). **C**) A microfluidic device with a single-islet piston-like trap to asses glucose-induced intracellular oscillations of calcium in pancreatic islets (Reproduced from Ref. [131] with permission from National Academy of Sciences, U.S.A, Copyright 2004). **D**) A Microfluidic array for real-time live-cell imaging of microencapsulated pancreatic islets to assess the effect of hypoxia (Reproduced from Ref. [132] with permission from American Chemical Society Copyright 2013).

Additionally, particular features should be considered in perfusion system design to account for the unique 3D cytoarchitecture of islets and their vulnerability to mechanical stress. The first major component of the MPS is the trapping mechanism for islet immobilization. To date, some trapping mechanisms found on MPS are dam wall-like or nozzle-like traps [132, 133] or circular wells located at the bottom of perfusion chambers [130, 134]. Moreover, it is necessary to integrate stable and flexible fluid control for investigating hormone secretion kinetics and biochemical events. This can be achieved either by external or integrated micropumps or by combining capillary forces and electrokinetic mechanisms inside MPS [127]. Although still in development, in the last

decade these features have been successfully introduced to MPS design for applications in islet research (**Table 5.1**).

The second major component of islet MPS is an analytical tool or method to monitor glucose-dependent response of the islets. The principal techniques that have been successfully incorporated in MPS up-to-date are capillary electrophoresis immunoassay (CEI) and intracellular Ca^{+2} oscillation monitoring.

CEI provides a technique for the direct detection of secretion from islets with a detection limit of 3 nM for insulin [25] (**Figure 5.5-A**). During experiments, islets are placed in a chamber and effluent is mixed with anti-insulin antibody and fluorescein isothiocyanate-labeled insulin (FITC-insulin). Insulin from the islets competes with FITC-insulin for binding sites on the antibody. The mixture is passed into an electrophoresis channel where bound and unbound FITC-insulin is separated. Insulin secretion is then quantified fluorescently through establishing the ratio between bound and free insulin. Similarly, this technique has been applied for detecting glucagon, with a detection limit of 1 nM [26]. Noteworthy, investigating glucagon secretion presents an additional challenge, since α-cells comprise a smaller proportion of the islet than β-cells, resulting in a relatively low amount of glucagon secreted per islet and making it difficult to detect variations in glucagon secretion [26]. This demonstrates that the non-insulin islet hormones, which are secreted in small quantities, can be detected when combining analytical tools with the fluid handling capabilities of microfluidics.

Although many microfluidic devices have employed CEI to perform high-throughput immunoassays on-chip [135, 136], their design was not well-suited for continuous monitoring of living cells [137]. This was mostly because the reported methods required off-line preparation of samples which are not amenable for repetitive sampling and continuous reactions [137]. In this

regard, the Kennedy group pioneered the development of a microfluidic CEI to monitor online the fast kinetics of hormone secretion from a single islet with high temporal resolution [25, 129, 137]. One of the advantages of CEI is that it can be fully integrated on-chip. This technique has proven to be fast and accurate and has been able to detect secretion changes within a few seconds [25]. Recently, the use of this technique has been extended to monitor insulin and islet amyloid polypeptide (IAPP) secretion profiles simultaneously [27].

However, the setup can be complex since it involves integrating precise external pumps for fluid flow control, power supplies and electrodes for electro-osmotic flow control. Moreover, since most of the secretion products from islets have similar molecular weights, multiplexing using this technique presents a great challenge. Channel clogging, precise temperature control, and requirement of lasers with different wavelengths remain the main issues of working with such a set-up [27]. Nevertheless, this technique has been useful for long term monitoring of insulin secretion [25, 128], and for understanding heterogeneity in insulin secretion [129, 137, 138].

Calcium-sensitive dyes [139] (e.g. Fluo-3, Indo 1, Quin 2, Calcium Green, Fura Red, etc.) have been used to visualize the calcium oscillations that precede insulin exocytosis and thereby to study secretion mechanisms and to indirectly measure islet secretion. Observing these oscillations is often challenging on many of the macro systems commonly employed in biological studies, because of the difficulty in differentiating physiological events that trigger Ca^{2+} oscillation. In contrast, imaging with microfluidic devices can allow exclusive observation of the Ca^{2+} oscillations associated with exocytosis.

Despite the advantages of this method, it presents some limitations regarding quantification and selectivity. For instance, calcium oscillations from different types of cells in the islet may be difficult to distinguish. Moreover, quantification of secretion products is required off-chip using

traditional immunoassays such as ELISA.

Nevertheless, this technique has furthered our knowledge regarding important aspects of islet secretion such as the limited coordination of Ca^{2+} oscillations in islets when stimulated with glucose [131] (**Figure 5.5-C**). The mentioned study found that β-cells are electrically coupled through gap junctions, being able to synchronize calcium oscillations but only within glucose-stimulated regions[131]. In addition, this technique has shed light on the cellular dynamics of islets when stimulated with different glucose wave forms, analogous the glucose variations that occur *in vivo* [140]. For instance, Dhumpa *et al*. [141] developed a MPS to test the hypothesis that negative feedback from the liver synchronizes islet secretion by controlling the blood glucose level. To introduce negative feedback to the on-chip islets, the glucose stimulation level was updated based on the insulin secretion by employing a model. In response to negative feedback, synchronized secretion was observed within groups of islets using calcium imaging and insulin ELISA.

The Ca^{+2} oscillation technique have also been applied to a microfluidic device able to trap single cells, spatially deliver analytes of interest and assess their effects with subcellular resolution [142]. The device employed pancreatic islet β-cells (MIN6) transfected to express insulin-GFP. The cell response evoked by different analytes was visualized using optical microscopy to monitor Ca^{+2} oscillations and insulin-GFP secretion. In particular, the group found that sub-cellular exposure of glucose-induced a modification in the spatial distribution of insulin granules (cell polarity) within the β-cell toward the site where glucose was delivered. This tool can help to increase the understanding the dynamics of insulin granules exocytosis due to its precise control of the surrounding chemical environment; however it was only demonstrated with single β-cells.

There are examples of microfluidic platforms specifically designed for pre-assessment of islets destined for transplantation to treat type I diabetes. For instance, Mohammed *et al*. [134]

developed a microfluidic islet perfusion device for the assessment of dynamic insulin secretion of multiple pancreatic islets with simultaneous fluorescence imaging of Ca^{2+} oscillations and mitochondrial potential changes. This device was further optimized in order to achieve efficient mixing and uniform distribution of solutions in the perfusion chamber [130] (**Figure 5.5-B**). In another example, Silva *et al*. [133] developed a microfluidic device that traps islets in cup-shaped nozzles, which are connected by channels to allow fluid to bypass the islets. This reduces shear stress on the islet, as demonstrated by healthy islet Ca^{2+} signaling. In addition, the nozzle stimulated intracellular flow through the islets, enhancing β-cell and endothelial cell preservation. This helps address the issue of endothelial cell necrosis in isolated islets, with the goal of stimulating re-vascularization of islets when transplanted.

Another microfluidic device, developed by Nourmohammadzadeh *et al*. [132] (**Figure 5.5-D**), determines the effects of hypoxia on alginate-encapsulated islets for transplantation. The device simultaneously assesses islet functionality and viability by imaging mitochondrial membrane potential, NADPH and intracellular calcium oscillations. They demonstrated that islet functionality decreases with the increasing hypoxic conditions.

Although some of the aforementioned MPS devices can perform multi-parametric characterization of islets [27, 130], most of them monitor a single parameter to study islet hormone secretion and functionality. Many focus solely on a single islet hormone, mainly insulin or glucagon, which may provide an incomplete profile of islet physiological functionality. Hence many research opportunities exist to expand the amount of hormones detected to measure a larger SF. Here is where one of the major challenges for future islet MPS reside. Additionally, the majority of the MPS have used mouse islets as a proof of concept. Consequently, findings on these devices may require translation to human islets. **Table 5.1** summarizes some of the MPS devices for islets

developed to date.

Table 5.1. Summary of selected microfluidic perfusion systems publication used in pancreatic islet research.

Detection method	# Islets	Specie	Type of Trap	Aspect Study	Year	Ref
Capillary electrophoresis immunoassay	1	Mouse	Dam wall-like	Insulin Secretion	2003	[25]
Intracellular calcium oscillation	1	Mouse	Movable wall	Coordination of Ca^{2+}Oscillation in islets	2004	[131]*
Capillary electrophoresis immunoassay	1	Mouse	Dam wall-like	Insulin Secretion	2005	[128]
Intracellular calcium oscillation	1	Mouse	Dam wall-like	Role of Gap junction on regulating Insulin secretion	2006	[143]
Capillary electrophoresis immunoassay	4	Mouse	Dam wall-like	Continues monitor of Insulin Secretion on-chip	2007	[137]
Fluorescence, Competitive Immunoassay and MALDI-MS	1	Mouse	Hand trapping with micromanipulator	Insulin secretion of a single islet	2008	[144]
Fluorescence Imaging	1	Mouse	Dam wall-like	Effects of glucose gradients on insulin secretion	2009	[140]
Capillary electrophoresis immunoassay in parallel	15	Mouse	Dam wall-like	Secretion patterns of insulin and free fatty acid lipotoxicity	2009	[129]*
Intracellular calcium oscillation and ELISA	25/100	Mouse/Human	Chamber with wells	Islet functionality (mitochondrial potential, insulin secretion)	2009	[134]
Fluorescent (Zinc trapped on droplets)	1	Mouse	Dam wall-like	Insulin Secretion	2009	[96]
Intracellular calcium oscillation	1-15	Mouse	Dam wall-like	Variation of insulin secretion from different mice "Islet imprinting"	2009	[145]
Capillary electrophoresis immunoassay in parallel	1	Mouse	Dam wall-like	Long term operation and performance of electrophoresis device	2009	[146]
Intracellular calcium oscillation and ELISA	25-30	Mouse	Chamber with wells	Islet functionality under glucose gradients	2010	[130]*
Intracellular calcium oscillation	1	Mouse	Dam wall-like	Insulin secretion cause by different glucose waveforms	2010	[147]
Intracellular calcium oscillation	100-200	Mouse	Different size of dam wall-like	Separation of islet by size and viability after separation	2010	[148]
Intracellular calcium oscillation and ELISA	8	Mouse	Dam wall-like	Single islet insulin secretion with passively operated device	2011	[149]
Mass spectrometry and ELISA	24	Mouse	Polycarbonate or Nylon membranes	Collection and concentration of islet secretion	2011	[150]
Intracellular calcium oscillation /Two-photon excitation	4-6	Mouse	Dam wall-like	Effect of microfluidic culture on islet-associated endothelial cells	2011	[151]
Intracellular calcium oscillation and ELISA	10-20	Mouse	Chamber with wells	Effect of hypoxia on insulin secretion	2012	[152]
Intracellular calcium oscillation and ELISA	4-55	Mouse	Chamber with wells	Insulin secretion kinetics on islet	2012	[29]

				population and mitochondrial potential		
Intracellular calcium oscillation /Two-photon excitation	1	Mouse	Dam wall-like	Dynamics of lipid partitioning in living pancreatic islets	2012	[153]
Capillary electrophoresis immunoassay	10	Mouse	Dam wall-like	Glucagon secretion	2012	[26]
Intracellular calcium oscillation	100	Mouse	Chamber with wells	Long term bubble prevention on pancreatic islet culture	2012	[154]
Fluorescent Competitive immunoassay	1	Mouse	Nozzle-like	Secretory dynamics of insulin and IAPP	2013	[27]
Intracellular calcium oscillation	100	Rat/Human	Nozzle-like (Encapsulate islets)	Effect of hypoxic conditions on islet viability	2013	[132]*
Intracellular calcium oscillation	5-10	Mouse	Nozzle-like/Dam wall-like	Insulin secretion related to epithelial cell loss and effect of shear stress on islets	2013	[133]
Intracellular calcium oscillation	5-10	Mouse	Dam wall-chamber	Coordination of insulin secretion	2014	[141]
Intracellular calcium oscillation	16**	Single β cell	Micro-orifice driven by pressure	The effect of glucose biases on the spatial distribution of insulin granules	2014	[142]
Capillary electrophoresis immunoassay	1-10	Mouse	Dam wall-like	Oscillation patterns of Insulin secretion	2014	[138]

*Device shown in **Figure 5.5**
**Estimated from images

5.7. Potential analytical tools for islet secretory fingerprint analysis

The analytical techniques mentioned in the previous section prove to be sufficient to follow the fast kinetics of insulin secretion. However, in order to monitor a wide islet SF, integration of novel multiplexed detection tools into MPS is required. The major considerations for detecting secretion from islets are: 1) the temporal resolution of the sensor to assure capturing the fast kinetics of islet hormonal secretion, 2) the dimensions of the sensors to spatially locate islet secretions, 3) the stability of the sensor to allow continuous operation and real-time secretion-monitoring, and 4) the selectivity of the sensor for a single secreted biomolecule, such as insulin, and not co-secreted products such as amylin and C-peptide. Therefore, the sensing tools must be fast, specific and possess high spatio-temporal resolution in order to simultaneously detect changes in the secretion

patterns of the different cells composing the islets. In addition, these tools need to be adapted for easy integration with MPS, since the reduced volume of MPS can concentrate analytes allowing easier detection, particularly for hormones secreted in small quantities (e.g. glucagon, PP and somatostatin). Furthermore, since the islet hormones are usually measured in a carrier solution, calibrating the sensor to the respective pH, salts and other molecules is a prerequisite.

The main reported techniques that could provide multiplexed detection of islet secretion kinetics include electrochemical techniques, patch clamp techniques, field effect transistors (FET) and surface plasmon resonance (SPR) [30]. The following sections will cover the potential of aforementioned technologies to conceive lab-on-a-chip (LOC) devices for assessing a pancreatic islet SF.

5.7.1. Patch Clamp

The patch clamp technique is a tool to study the electrophysiological properties of cells by bringing a pipette containing an electrode in contact with the cell membrane. Suction is applied to the pipette to create an ultrahigh resistance seal with the cell membrane. Rupturing the membrane provides electrical contact between the cell interior and the electrode. This setup enables measurement of whole cell currents and cell membrane capacitance, both of which are correlated with exocytosis of cell secretion products [155].

Patch clamp has been used to study secretion from human β-cells [15, 156-158] and α-cells [23, 24, 97]. During capacitance measurements, exocytosis in β-cells can be invoked using induced voltage clamp depolarisations and secretagogues[155]. This technique can provide quantitative information regarding exocytosis, for example through correlating the rate of capacitance change with the quantity of granules released at a given time [159].

Since the pipette allows infusion (or dialyzing) of substances into the intracellular

environment, observations can be made of the effects of substances on hormone secretion (i.e. cyclic AMP, calcium chelators, GTP analogs and sulfonylureas). Likewise, stimulants can be added in the extracellular bathing solution. Furthermore, fluorescent probes can be injected into the cell cytoplasm through the patch pipette. Therefore, a wealth of data can be obtained by simultaneous membrane capacitance and whole-cell current measurements obtained using the patch pipette while combining fluorescence imaging.

However, some disadvantages of the patch clamp technique are that it is very low throughput, it provides an indirect measurement of secretion, it can be interfered by endocytic processes, it lacks specificity for individual secretion products and it is invasive. Additionally, this technique requires highly skilled operators in order to trap and manipulate cells.

With the current microfabrication technologies microfluidic platforms with small apertures can be fabricated, which act as the pipette tip. These apertures allow automated trapping lateral to [160] or on the bottom of microfluidic channels [161-163]. For instance, Lau *et al*. [160] developed a PDMS microfluidic patch clamp array that incorporates on-chip lateral cell trapping sites and an open-access chamber at the top for easy media changes (**Figure 5.6-i**). A challenge associated with using this technique for on-chip applications is the choice of fabrication materials, since fabrication methods can be expensive and complicated. Additionally, the use of substrates with poor dielectric properties can produce low seal resistance, hence decreasing the signal-to-noise ratio. To overcome this problem, Bruhn *et al*. [161] developed a glass pore chip by taking advantage of the high dielectric properties of glass. The device was able to obtain a similar seal resistance as the conventional micropipettes, to automatically trap cells at the bottom and to perform single membrane channel recording (**Figure 5.6-ii**). Currently, some automated patch-clamp systems with multiplexed recording electronics and microfluidics layers, that enable high-throughput

measurements, are commercially available [164, 165].

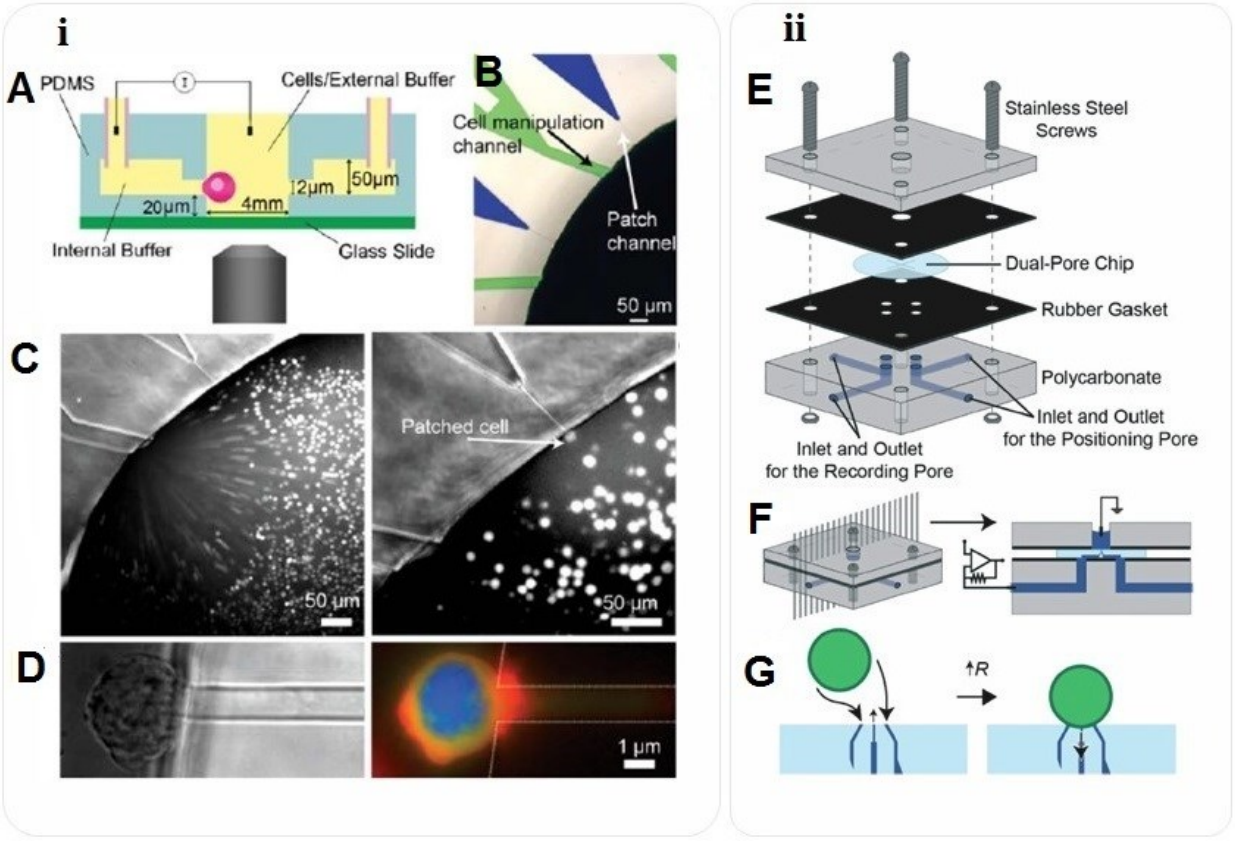

Figure 5.6. (i) A microfluidic patch clamp array chip with lateral cell trapping sites. **A)** Cross-sectional representation showing a cell being trapped in a microfluidic device. (B) Close-up of the device where a channel for patch trapping and cell manipulation can be observed. **C)** Optical microscope image of cells being manipulated in order to bring them close to the patch channel. **D)** Image showing a cell being trapped and patched on the small channel (Reproduced from Ref. [160] with permission from the Royal Society of Chemistry) **(ii)** Dual pore glass chip. **E)** Schematic representation of the assembly of the dual-pore glass chip for cell-attached single-channel patch clamp recording. **F)** Cross-sectional view of an assembled chip. **G)** Representation of a cell trapping mechanism used to establish a high-resistance seal with a cell (Reproduced from Ref. [161] with permission from the Royal Society of Chemistry).

Patch clamp investigations of pancreatic islets have focused primarily on β-cells. But to understand the secretion mechanism of islets as a whole, the technique needs to be extended to other islet cells (δ, ε, etc.). However, the lack of reliable methods to identify islet cells adds an extra challenge for patch clamp measurements of intact islets [97]. One proposed solution is to produce genetically modified mice that express fluorescent proteins in α- and β-cells to distinguish them *in situ* [97]. Still, doing this for the various cell types in the islet is time-consuming and expensive,

and novel identification methods may be required. Nevertheless, studies exist for attaching the patch pipette to single cells within intact islets [166-168].

The patch clamp technique possesses the required temporal resolution (milliseconds) to monitor secretion kinetics and has sufficient sensitivity to detect single vesicle fusion. After proper identification of individual islet cells, microfluidic devices containing multiple patch clamps can measure secretion kinetics simultaneously. To complement patch clamp measurements, electrochemical sensors can be added on-chip to obtain selective quantification of secretion products as has been previously demonstrated in non-LOC setups [14, 169]. Thus, this would provide a high-throughput tool to analyze a single islet SF.

5.7.2. Amperometry/Voltammetry

Amperometric/Voltammetric (A/V) techniques provide a method to detect and quantify cell secretions through electrochemical reactions. In amperometry, a potential is applied while the resulting current from oxidized or reduced species is recorded. Conversely, voltammetry measures current as a function of applied potential.

Insulin is an electroactive molecule and hence it can be detected with unmodified electrodes. This has made insulin the prime focus of islet secretion research by means of A/V sensing. However, electrochemical sensing of insulin with unmodified electrodes has been shown to be characterized by fouling, slow kinetics and low sensitivity [170]. To overcome these limitations coating catalysts have been developed for the electrodes. Several of these catalysts include those containing ruthenium, iridium oxide, metallo-dendrimers, and carbon nanotubes. The sensing performance of some of these catalysts have been previously summarized by Rafiee *et al*. [171] and Amini *et al*. [172]. Additionally, insulin-specific recognition elements can be added to the electrodes. For instance, insulin aptamers [173] and electrodes modified with molecular

imprinted polymers [174] have shown promise for sensing insulin with high specificity. An additional advantage of using aptamers and molecular imprinted polymers as recognition elements is that binding is highly reversible so it is possible to regenerate the sensors with great efficiency[175]. These kinds of selective recognition elements can be developed for other islet hormones which can be advantageous for multiplexed detection.

The majority of A/V sensors have been designed for detecting insulin in blood samples, hence some modification will be required for monitoring insulin secretion from single islets. In addition, some electrodes used a flow injection analysis setup [171, 172], in which the electrode is situated in a constant flow environment. This setup is analogous to the environment in MPS, demonstrating the potential adaptability of these sensors for MPS.

A few A/V sensors have been developed for direct detection of secretions from islets and dispersed β-cells. When monitoring β-cell secretion, alternatives to electrochemically detecting insulin may be preferred to avoid electrode modification steps. For instance, other factors co-secreted with insulin can be readily detected electrochemically. These factors include the electro-active amine, 5-hydroxytryptamine (5HT) [176] and zinc [177] . Zinc is complexed with insulin inside β-cell vesicles and during secretion, the complex dissociates into insulin and free zinc ions. The insulin concentration can be indirectly determined via A/V detection of zinc [178]. Conversely, 5HT needs to be incubated with islets prior to experiments, such that the 5HT becomes localized in insulin vesicles, and is subsequently co-secreted with insulin. In this manner, A/V sensing of 5HT has been used to measure secretion from mouse β-cells [179-182] and mouse islets [183, 184].

There are limited reports where A/V sensors have been integrated in MPS systems for monitoring islet secretion. An example is a microphysiometer chamber containing islets under perfusion, which was coupled with an amperometric insulin sensor composed of a multiwall carbon

nanotube film electrode [185]. This platform serves as a proof of concept for LOC devices, which can take advantage of microfabrication and electrode printing technologies to elaborate probes with high spatio-temporal resolution. Additionally, nanomaterial modified electrodes with sufficient limit of detection (nM) for single cell analysis are becoming robust and have made inroads into the microfluidic domain, presenting opportunities to apply these sensors to islet research. However, research needs to be expanded into multiplexed A/V detection of islet secretion products to allow screening of an islet SF.

5.7.3. Impedance Spectroscopy

Impedance spectroscopy (IS) (also called electrochemical impedance spectroscopy) is a technique that measures changes in the electrical impedance of a sample over a range of applied electrical frequencies. IS biosensing is based on spectrum changes that take place in response to binding events and reactions associated with analytes of interest. This technique is subdivided into Faradic IS and non-Faradic IS depending on whether a redox reaction is present or not. Faradic IS involves an electrochemical reaction as a sensing step. This reaction can come either from an external chemical compound (redox probe) added to the system or from the sample itself. In contrast, the redox probe is absent in non-Faradaic IS. As a label-free technique, IS eliminates costly and cumbersome sample preparation steps [35]. However, as mentioned in the previous section, the electrochemical detection of biological molecules can be non-specific, requiring surface modifications with biomolecules (antibodies, affirmers, aptamers, etc.). Additionally, direct detection of analytes can have insufficient sensitivity, requiring catalytic modification of the sensing interface.

Non-Faradic IS has many advantages over Faradaic IS. Firstly, the absence of a redox probe in non-Faradic IS makes the experimental setup simpler and eliminates the need for catalytic

modification of the sensing interface. Secondly, the redox probe employed in Faradic IS can be highly toxic for cells. Moreover, depletion of the redox probe can occur, so Faradic IS platforms need to be designed to avoid this issue. Hence, non-Faradic IS is considered more appropriate for integration with LOC devices [33], especially for investigation of complex biological systems such as human pancreatic islets.

Faradaic IS has been used to detect insulin using immobilized antibodies [38] or silica nanoparticles/nafion [39]. These technologies can be adapted to detect insulin from islet samples. A shared drawback of most electrochemical biosensors is the non-specific interactions that are usually present in complex samples such as blood serum or cell secretions. However, a recent report detected insulin with a non-Faradaic impedance biosensor using a chemically adsorbed zwitterionic polymer (polymer with net charge of zero, but with negative and positive charges within its structure) with attached monoclonal insulin antibodies [40]. Noteworthy, this functionalization confers high specificity to the mentioned sensor, enabling it to detect insulin in the femtomolar concentration in undiluted blood serum. In a similar fashion, the same group developed a non-Faradic IS detection array for protein marker detection [186]. Thermally cross-linked poly(ethylene glycol) on the chip surface provided a simple and robust interface with high antifouling properties. Here, insulin and C-reactive peptide were simultaneously measured in human serum with little cross-reactivity despite similarities between the two peptides. The limit of detection was as low as 171 fM and 10 pM respectively.

However, despite the remarkable limit of the detection and antifouling properties of the aforementioned biosensors, as with most biosensors, regeneration of the sensing surface for continuous monitoring of secretion products still remains an issue. A recent review by Goode *et al*. [187] summarizes possible strategies to achieve successful biosensor regeneration. Nevertheless

interesting research opportunities exist to extrapolate this technique for multiplexed measurement of islet secretion products. In addition, thin film electrodes modified with robust polymer interfaces can be easily integrated on microfluidic devices with islet perfusion chambers.

5.7.4. Field effect transistors

A field effect transistor (FET) biosensor is built by modifying the gate surface of a transistor with recognition elements capable of binding an analyte, such as antibodies, antibody fragments, aptamers or DNA (**Figure 5.7-i**). When binding events occur, the electric field is modified, resulting in a detectable change in the transistor conductance.

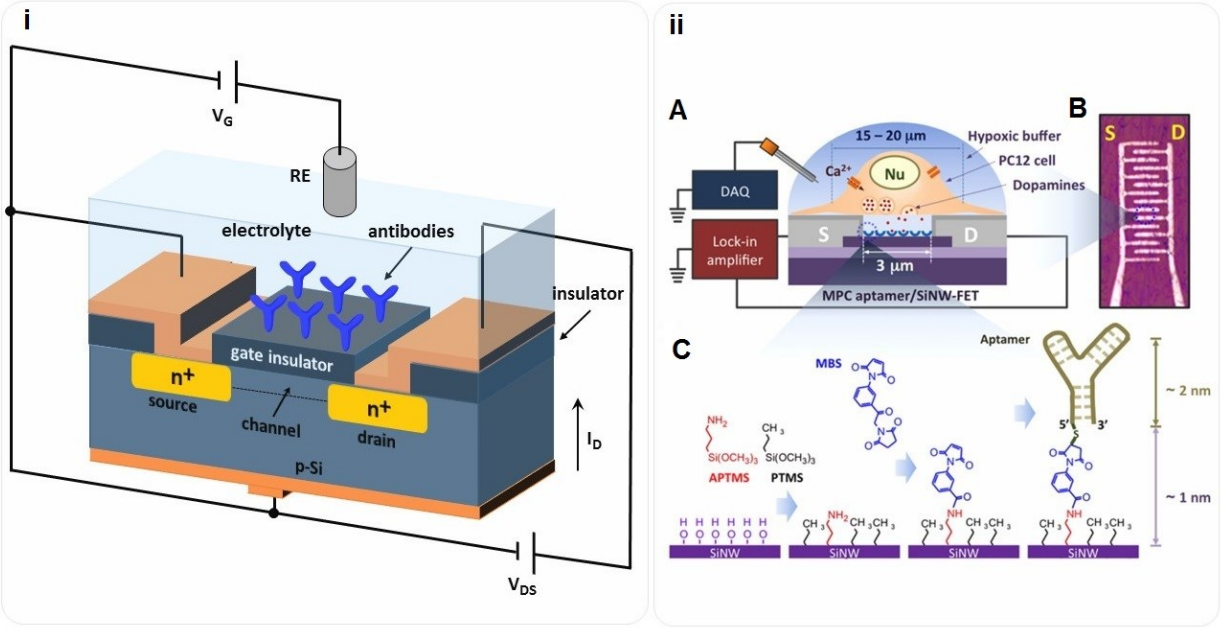

Figure 5.7. (i) A typical structure of a FET sensing device functionalized with antibodies. RE stands for reference electrode, VG for gate voltage, VDS for drain-source voltage and ID for drain current. **(ii)** Multi-parallel connected (MPC) silicon nanowire FET. **A)** Schematic representation of a DNA-aptamer modified MPC SiNW-FET device for detecting dopamine from stimulated PC12 cells. **B)** Microscope image of a SiNW-FET device where "S" stands for source, and "D" for drain. **C)** Schematic representation of the DNA-aptamer immobilization procedure on a SiNWFET. APTMS stands for (3-aminopropyl)trimethoxysilane, PTMS for propyltrimethoxysilane and MBS for 3-maleimidobenzoic acid N-hydroxysuccinimide ester (Reproduced from Ref. [188] with permission from American Chemical Society, Copyright 2013).

The concept of FET biosensors has been developed for more than two decades, but only recently has the interest in them increased due to the development of novel nanomaterials. When

FETs are coupled with highly conductive nanomaterials, such as nanowires (e.g. metal oxide, silicon and carbon-based nanowires) and graphene, a very sensitive tool (pg mL^{-1}) for the detection of biomolecules can be fabricated [188-190].

However, all FET biosensors operate on the principle that the electric field seen by the current carrying element is sensitive to target binding. When immersed in an electrolyte, this requires that binding occur within the order of the Debye length. Beyond this distance the electric field seen by the surface becomes independent of solution composition and binding events [33]. The Debye length is typically restricted to a few nanometers under physiological ionic strength conditions and becomes smaller as the ionic strength increases [191]. Thus, any recognition element must be anchored within this distance, which presents a problem with large macromolecules, such as antibodies (~10 nm). However, it has been demonstrated that recognition elements such as DNA and aptamer (1-2 nm) can efficiently work with FETs [191]. Alternatively, dilution of analytical samples to low ionic strength prior to analysis can be performed.

The aforementioned limitations have not discouraged the application of this highly sensitive type of biosensor to study cell physiology, especially by coupling them with microfluidics. For instance, Li *et al*. [188] developed a highly specific nanowire FET biosensor embedded in a PDMS microfluidic channel (**Figure 5.7-ii**) to detect dopamine secretion from living chromaffin cells (PC12 cell). The biosensor specificity was achieved using DNA-aptamers, which distinguishes dopamine from other analogs such as catechol, phenethylamine, tyrosine, among others. Although this device does not measure proteins, it is a proof of concept that real-time and label-free quantification of secretion products can be achieved with sufficient sensitivity ($<10^{-11}$ M) and selectivity to perform single cell analysis with this technology.

Investigation into the use of FETs to monitor islet secretion products has been limited.

Sakata *et al*. [192] developed a FET sensor to monitor the electrical activity of rat pancreatic β-cells by culturing these cells on the FET gate surface. This FET sensor monitored insulin secretion indirectly by measuring pH changes once the β-cells are stimulated with glucose. Sakata identified a correlation between H^+ ion accumulation and insulin secretion through the activation of β-cell respiration activity.

The major advantage of FETs compare to other type of biosensors is that they can be easily multiplexed, miniaturized and manufactured on a large scale, which makes them a good candidate for mass production. Additionally, their small size enables detection of a large islet SF and potentially allow on-chip screening of several secretagogues. As the FET field continues to evolve with improvements in FET microfabrication and nanomaterials development that increase their sensing capabilities, their potential role in secretome research will undoubtedly expand.

5.7.5. Surface plasmon resonance

By allowing fast detection of binding interactions due to changes in the surface plasmon of a thin gold film, surface plasmon resonance (SPR) sensing has become the gold standard to study biomolecular interactions, particularly affinity-based interactions such as DNA-RNA hybridization or antigen-antibody.

The advantage of this technique is its intrinsic dynamic, label-free and real-time analysis capabilities. Additionally high-throughput and multiplexed analysis are possible by making arrays of different molecules on the sensing surface [193].

However, the sensitivity of this technique is insufficient to detect highly diluted analytes or small molecular weight biomolecules such as cancer biomarkers, hormones and antibiotics. To overcome this challenge, sensitivity-enhancing methods have been proposed such as integration of nanostructures, either as amplification tags or as enhancing substrates [65]. As a result, this

technique has been able to reach limits of detection of picomolar and attomolar order [65], opening the possibility to detect protein secretion from single cells. In addition, the single cell, high-throughput and multiplexed capabilities of this technique can be greatly enhanced by its coupling with microfluidic devices.

There are few reports that attempt to detect cell secretion by the direct application of SPR biosensors [194-197]. Oh *et al*. [197] developed a nanoplasmonic device to study cytokine secretion from immune cells directly derived from human blood (**Figure 5.8-i**). In order to separate the immune cells from the blood, antibody functionalized microbeads targeting specific cell surface biomarkers were employed. Later, these cell/bead conjugates were loaded into the device where they were trapped around a micro-pillar array. The cells were then stimulated and the cytokine secretion was detected on the SPR surface. Another example is a SPR microfluidic device to monitor the dynamic secretion from human monocytic leukemia cells developed by Wu *et al*. [196]. The SPR chip was composed of gold nano-slits with immobilized antibodies on a polycarbonate film (**Figure 5.8-ii**). The nano-slit array was integrated with a cell-trapping microfluidic device, to allow for examination of cell secretion dynamics. The cell-trapping system was designed to allow a micrometer separation of target cells from the sensing surface to minimize non-specific signals from cell bodies. An interesting characteristic of this device is the small number of cells required to detect secretion (<10).

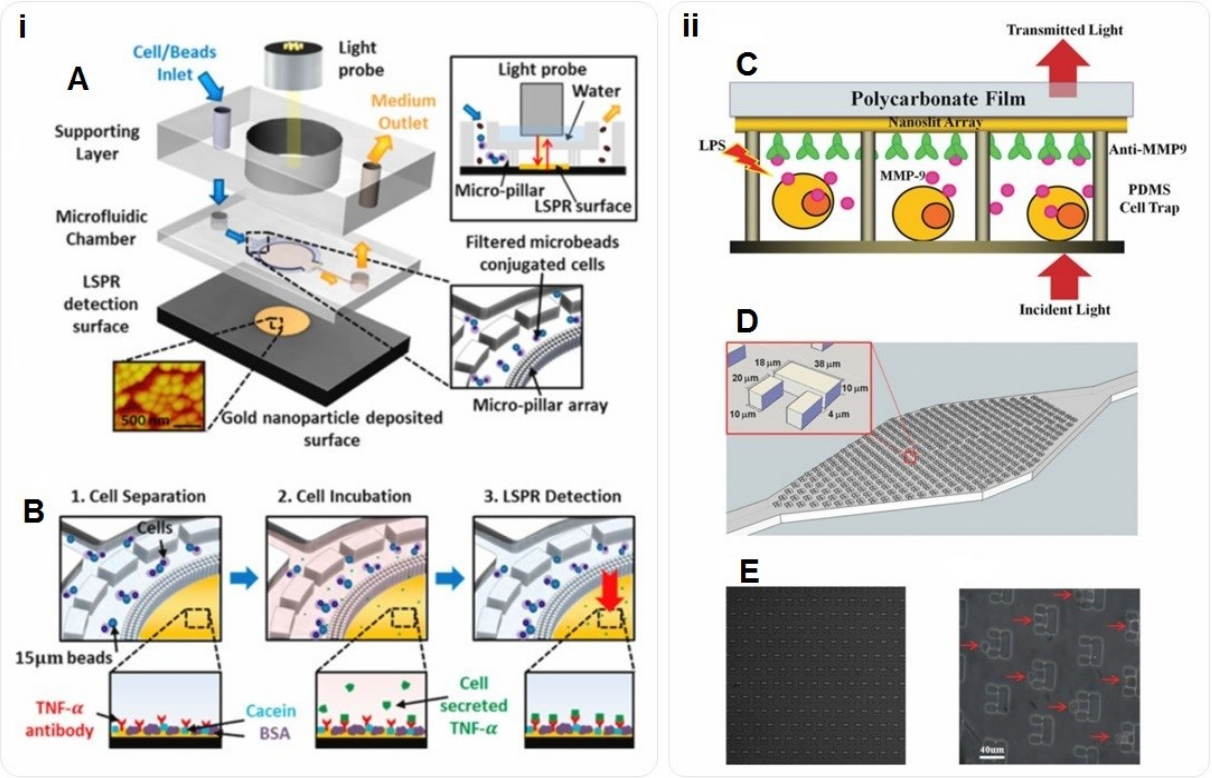

Figure 5.8. (i) A microfluidic device with integrated nanoplasmonic sensing for cellular functional immune analysis of human blood. **A)** Schematic representation of an integrated localized surface plasmon resonance (LSPR) optofluidic device. The bottom layer is composed of deposited gold nanoparticles. The magnified image at the bottom left is an AFM image of the gold nanostructured surface. The middle layer is composed of a microfluidic chamber and channels. The chamber was integrated with micropillar arrays, as shown in the middle right schematic, to trap target cells. The cross-sectional view of the device is shown at the upper right corner. **B)** The middle layer is composed of a microfluidic chamber and channels. (Reproduced from Ref. [197] with permission from American Chemical Society, ACS Author Choice 2014). **(ii)** An optofluidic platform for real-time monitoring of live cell secretion. **C)** Schematic representation of the experimental setup to measure cell secretion. The target cells are immobilized in cell traps incorporated in a microfluidic channel. After stimulation, cell secretions bind to antibodies immobilized on a gold nanoslit SPR sensor located above the cells. **D)** Schematic representation of the entire microfluidic chamber containing an array of cell traps. The dimensions of the cell traps are shown in the inset on the top left corner. **E)** Optical microscope images of the cell trap array showing cells captured in the traps. Each red arrow points to one cell (Reproduced from Ref. [196] with permission from John Wiley and Sons).

Of all analytical techniques mentioned, SPR has been used to detect the widest variety of islet secretion products. SPR biosensors have been used to investigate binding interactions of major secreted islet hormones, namely insulin [44, 198, 199], somatostatin [200], pancreatic polypeptide [201, 202] and ghrelin [203]. Thus, the simultaneous detection of several islet-secreted products in a single device is feasible. However, as with most label-free biosensors, specificity can be a challenge, particularly for applications that involve measurements in a complex matrix such as a

cell secretome. Thus, novel anti-fouling strategies are a central part of ongoing research in the field. For instance, Frasconi *et al*. [204] were able to detect insulin in human serum using SPR sensing with a surface modified with polymeric dendrimers encapsulated gold nanoparticles. This surface preparation reduced non-specific interaction and provided a limit of the detection in the order of pM in complex biological media. Additionally, a less than 5% loss in performance was observed over 40 regeneration cycles. However, the complex competitive immunoassay scheme, requiring several minutes to perform, reduced its real-time capabilities. Nevertheless, this report presented a strategy to reduce non-specific interaction in SPR sensing when measuring small peptides.

Commercial SPRs are generally based on the traditional prism-coupled SPR configuration. The approach is simple and robust, but not amenable to miniaturization and integration [205]. However, SPR technologies have taken advantage of new advances such as optical fibers and waveguide nanostructures for miniaturization, which have opened new avenues for easy fabrication of SPR LOC devices [206]. With the latter setups, islets can potentially be immobilized in proper microenvironments for secretion detection, similar to devices developed for other cell types (see **Figure 5.8**).

5.8. Applications of on-chip monitoring of relevant islet secretory fingerprints

5.8.1. Quality assessment of islet preparations for transplantation

A promising therapeutic avenue for T1D is pancreatic islet transplantation [207-209]. This therapy has provided proof of concept that normoglycemia can be restored in patients with T1D by isolating islets from a cadaveric donor's pancreas and infusing them into the patient's hepatic portal vein (**Figure 5.9**). One of the main limitations of this therapy is the need for more than one donor for each recipient, due to islet apoptosis following isolation [210]. It was estimated that over 50% of

the transplanted islets are lost within hours post infusion [211-215].

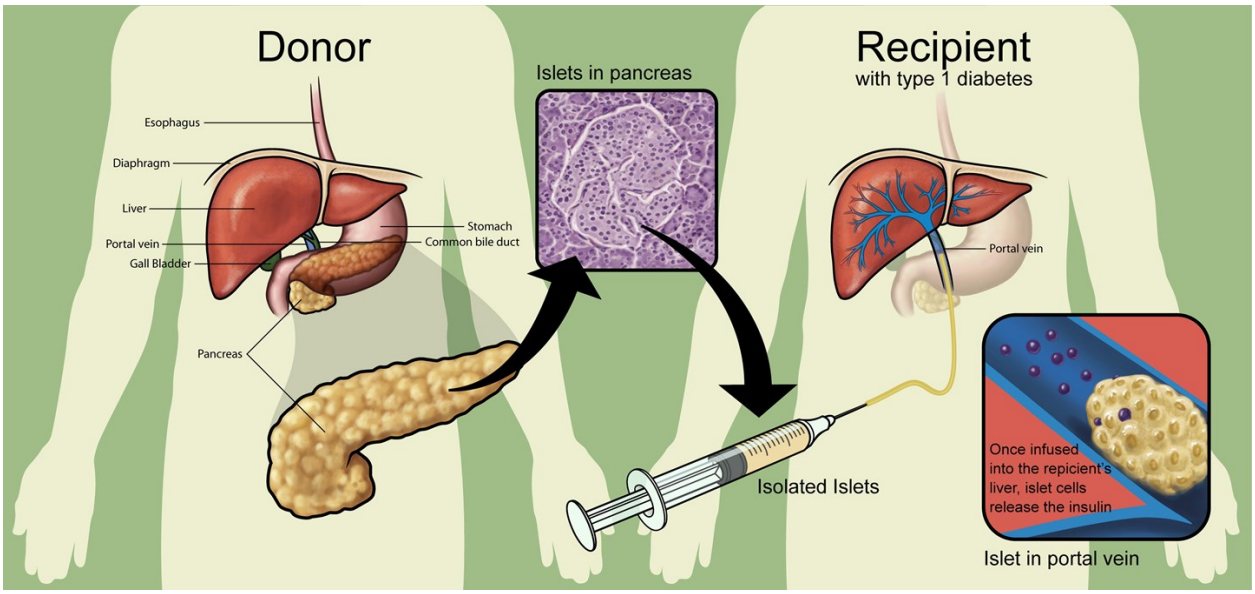

Figure 5.9. Islet transplantation through the Edmonton protocol. First, islets are isolated from a donor by collagenase digestion and then they are assessed for identity and quality. Finally the islets are introduced into the hepatic portal veins of the recipient where they are trapped and are able to respond to glucose concentration changes by secreting insulin and glucagon (Reproduced from Ref. [216] under the terms of the Creative Commons Public Domain Declaration).

This has stimulated interdisciplinary research to increase the long-term survival and functionality of grafted islets [211, 217]. LOC technology offers a tremendous opportunity to assess islet quality for transplantation and islet functionality, all of which are part of emerging fields of research. These opportunities can be further increased by analyzing the islet secretome and by defining an islet secretory fingerprint that encompass biomarkers that rapidly measures its quality. For the interested reader, other aspects and challenges involved in islet transplantation are thoroughly reviewed elsewhere [217-219].

Although there are current regulations from the U.S. Food and Drug Administration (FDA) that state the minimum required characteristics for islet preparations, such as safety, identity, purity, viability and potency [220]; it is currently accepted that these specifications provide reasonable estimates of safety, identity, and purity, but do not deliver meaningful measures of viability or

potency of the preparation [221-224].

The current gold standard testing for islet potency is the nude mice bioassay. This bioassay is based on diabetes reversal after islets engraftment under the mouse's kidney capsule [225-228]. Due to the nature of this assay (immune inhibited mice), it is compatible with human islets. This gives the assay a great advantage when predicting the outcome of human engraftments. However, the nude mice bioassay involves a complex surgical procedure, and only works in a retrospective manner, where results are interpretable and accurate only after diabetes reversal has occurred [226]. Despite the drawbacks, whenever a new potency or viability assay is proposed, the predictability of the method should be tested with the nude mice bioassay.

Some promising islet potency and viability assays developed in the last decade include cell membrane integrity tests, cell death, mitochondrial health assays and oxygen consumption rate [221]. Tests that assess mitochondrial function, particularly those measuring oxygen consumption rates of islets, seem to be the most promising and correlate best with transplantation outcomes in the nude mice bioassay. Nevertheless, pancreatic islets are complex micro-organs, and a multiparametric approach can be more accurate than individual assays.

There are few examples of multiparametric tools for assessing islet quality, and the majority of them are based on MPS [130, 132, 134, 152]. For instance, the Eddington and Oberholzer group developed a microfluidic device where islets are trapped in a well array at the bottom of a micro-chamber. There, mitochondrial membrane potential and Ca^{2+} oscillations were simultaneously measured [130, 134]. This device was improved by adding dynamic oxygen control during glucose stimulation [152]. Later, the group developed a microfluidic islet array with hydrodynamic trapping for islet immobilization and an improved oxygen control in order to assess the response of microencapsulated islets to hypoxic conditions [132]. With this configuration, simultaneous

analysis of Ca^{2+} oscillations, mitochondrial potential and NAD(P)H of human pancreatic islets was achieved. The advantages of such multiparametric MPS for islet quality assessment and functionality are numerous. It enables precise control over the islet microenvironment, it has high spatio-temporal resolution, and it avoids damaging the islets during measurements.

Similar multiparametric MPS could potentially become a new gold standard for islet quality assessment. However, in order to fully establish a new standard, it is still necessary to corroborate the device outcome of islet quality assessment with the nude mice bioassay. Furthermore, these kinds of MPS still rely on elaborate imaging techniques that require trained personnel, complicating their use as point-of-care devices and compromising their commercialisation potential. The development of fully automated LOC devices with integrated sensors that reduce the human factor from the measurements is needed to allow surgeons to immediately assess islet quality prior to transplantation.

By defining a SF for viable and functional islets, it should be possible to develop novel LOC devices to assess in real-time a complex SF of islets in an automated manner. This SF can be comprised of different protein biomarkers for cell death (apoptosis, anoikis, etc), mitochondrial health and secreted hormones. Moreover, assessment of other criteria suggested by the FDA, such as safety and purity, may be also integrated and performed on such LOC devices.

5.8.2. Islet regeneration

Regeneration of functional pancreatic endocrine tissue in the form of islets, β-cells or other hormone-secreting cells, is a potential method to address the issue of donor islet shortages for treating T1D [229, 230]. In addition, understanding regeneration pathways could unlock *in vivo* mechanisms for replenishment of pancreatic endocrine tissue.

The activation of transcription factors during fetal pancreatic development has generated

interest in their potential applications in β cell regeneration [231-235]. Through better understanding of these transcription factors, new strategies to generate islet tissue from existing β-cells or from pancreatic duct and acinar tissue can be developed [235]. Another strategy is trans-differentiation of cells within islets, for example from α to β-cells [234]. Some members of the Reg family have been shown to affect β cell regeneration and/or neogenesis [230, 236]. Another family of proteins, namely the incretins, have also been shown to have implications in regeneration of pancreatic endocrine tissue [234, 237-239]. Many of these factors have shown regenerative potential both *in vivo* and *in vitro*.

MPS can enable screening of a large number of transcription factors involved in islet differentiation and thereby improve existing islet regeneration strategies and uncover new regeneration pathways and agents. Such devices would allow the control of the physical and biochemical environment needed to induce differentiation, support long term culture of islets and their differentiation processes (which last several days), and enable the evaluation of the initial state and result of islet differentiation. The microfluidic devices can also serve as a pre-screening tool for regenerating agents, before testing novel strategies *in vivo*.

In addition, the on-chip microenvironment can be tailored to mimic *in vivo* conditions. For instance, incorporation of 3D extracellular matrices that maintain islet-matrix interaction would provide a more optimum environment for islet regeneration. An example of such a platform is reported by Wan *et al*., where embryoid bodies were differentiated on-chip during long term cultures in 3D collagen matrices [240]. Immunofluorescent staining was then utilized to assess the differentiation of embryoid bodies within 3D extracellular matrix cultures [240]. These types of platforms have been recently upgraded by adding microfluidic well arrays to capture embryoids, exposing them to stimulation gradients and allowing easier imaging and more reproducible results

[241]. Such platforms can be easily translated for islet studies where immobilization, stimulation and imaging of islets can be performed.

Since islets have been shown to be harmed by shear stress in microfluidic environments [151], MPS devices can be designed to reduce fluid-induced shear stress on cells. For instance, such devices have been developed to facilitate cell differentiation in sheltered regions away from main flow channels [241, 242]. In addition, the perfusion environment can be tailored to control media delivery across cells. Fung *et al*. [243] showed that by exposing both halves of a single embryoid body to different flows, expression of differentiation markers varied across the embryoid body. Such a setup would be very useful to examine the long term effects of stimulation gradients across different regions of the islet. Some microfluidic devices have been developed for delivery of stimulation gradients to islets [131] and β-cells [142]. These can be adapted to observe the effect of gradients on islet regeneration.

Evaluating the expression and secretion of islet proteins enables tracking of the differentiation process and determination of the regenerated tissue functionality. For instance, when Hui *et al*. [238] induced pancreatic ductal cells to differentiate into insulin-secreting cells using an incretin, these cells were tested for insulin gene expression, intracellular insulin content and insulin secretion. Zhou *et al*. [244] differentiated a pancreatic duct cell line into endocrine cells, and used staining for insulin, glucagon and pancreatic polypeptide to evaluate this transformation. Another study demonstrated that islets could be differentiated towards highly proliferative duct-like structures, and then back into islet-like structures, through the action of a Reg family protein [230]. Here, immunodetection of insulin, glucagon, somatostatin and pancreatic polypeptide on different days allowed the differentiation process to be tracked. In addition, immunostaining these hormones within the islet-like structures established their islet-like phenotype. Furthermore the functionality

of the islet-like structures was demonstrated based on their comparable glucose-stimulated insulin release to freshly isolated islets. These studies provide proof of concept for using the SF to monitor and assess islet regeneration. Multiplexed detection of key islet proteins comprising a relevant SF can provide a more comprehensive evaluation of the islet regeneration process.

Integrated on-chip biosensing tools for an islet SF, as covered in previous sections, can provide tools to assess the success of an islet regeneration strategy. An established SF for freshly isolated islets can be used as a baseline for assessing the functionality of regenerated pancreatic endocrine tissue. The real-time capability of cell secretion biosensors can provide continuous assessment of the multiple phases of regeneration processes. In addition to SF biosensing, multiple cell parameters can be measured using other techniques, for example by coupling with fluorescence imaging for differentiation markers. Hence, MPS coupled with real-time monitoring of a relevant SF have the potential to provide powerful tools to enhance understanding and control over islet regeneration strategies and furthermore provide quality assessment of regenerated endocrine tissue.

5.8.3. Drug development and screening for Diabetes

Type II diabetes (T2D) is usually characterized by insulin resistance in adipose tissue, skeletal muscles and liver tissue, and by a reduction in insulin production by the pancreas. In order to treat this disease, different therapeutic agents are used to stimulate insulin production (e.g. sulfonylureas and meglitinides), or to reduce insulin resistance in target tissues (e.g. thiazolidinediones and metformins).

The process for developing new anti-diabetic drugs usually starts with *in vivo* and *in vitro* models. These models are used to assess the absorption, distribution, metabolism, excretion and toxicity (ADMET) of the novel therapeutics. Current models for diabetes drug discovery and research include: chemically induced *in vivo* models (streptozotocin and alloxan) and genetic

models of diabetes such as the fa/fa rat, Goto-Kakizaki rats, the db/db mouse, and the ob/ob mouse. The advantages and disadvantages of these models have been extensively reviewed elsewhere [17, 18]. Additionally, *in vitro* models include: islet preparations from humans and other species along with insulin-secreting cell lines (RIN, HIT, β-TC, MIN6 and INS-1 cells), to assess compounds that enhance insulin secretion; hepatocytes, muscle cells (L6 and C2C12) and adipocytes (3T3-L1 cells) for compounds that reduce insulin resistance. The interested reader is redirected to relevant reviews of these *in vitro* models [17, 19, 20].

Despite the demonstrated value of these *in vivo* and *in vitro* models to better understand diabetes, as in islet transplantation, there is a lack of predictability when results are extrapolated to humans. This predictability challenge may have its origin in vital anatomical and physiological differences that are rarely taken into account [5]. Evidence of these differences can be found in a recent work where re-aggregated human pancreatic islets were assessed and compared to native human islets and rat islets for secondary drug screening [21]. The response of the different islets were significantly different when tested against a variety of compounds such as the calcium channel agonist Bay K 8644, glibenclamide, tolbutamide, caffeine, carbachol, glucagon-like peptide-1, among others. As the authors pointed out, islet re-aggregates may represent a more homogenous model for drug screening since native islets present size and compositional heterogeneity. As a result, they can improve assay repeatability and quality and due to their enhanced response to therapeutics and secretagogues, islet re-aggregates may also provide an important alternative source for transplantation. However, caution may be needed when studying ADMET in clinical trials, since ultimately islet re-aggregates will not reflect the response of native islets due to possible alterations of important cell-cell contacts (juxtacrine signaling) or paracrine effects [97, 245]. This may have important consequences for the outcome of human trials.

In a distorted metabolic disease such as T2D, glucose homeostasis is achieved through systemic signaling between different cells and tissues. Thus, an *in vitro* metabolic network comprising human primary cells represents a more accurate model of T2D pathophysiology. However, long term culture is a key consideration when designing such network platforms for drug screening (ADMET), particularly for toxicity studies where 28-90 days culture is usually required [246]. Moreover, interconnected cell networks bring additional challenges because contamination or death of one cell line within the network will compromise the entire network. Despite the challenges, these networks have promise to replace animal models and to provide a more reliable clinical model for drug screening, as shown by the emerging concept of body-on-a-chip [247].

To date, there is no report of a pancreas-on-chip and there are few reports of metabolic networks aiming to assess the pathophysiology of T2D and the effect of therapeutics. One of such reports is a setup that incorporates a 3D culture of pancreatic islets and adipocytes derived from Sprague-Dawley rats [248]. A perfusion system was used to stimulate glucose-dependent insulin secretion from the islets within a 3D scaffold seeded with adipocytes. After long term exposure to high glucose, the adipocytes started behaving like obese adipocytes secreting more leptin and resistin. This in time decreased and delayed the insulin secretion from the islets.

Another report shows a 3D tissue *in vitro* model where hepatocytes, adipocytes and endothelial cells were cultured in modular bioreactors with a common medium flowing between them [249] (**Figure 5.10**). The goal of this work was to probe crosstalk between tissues and determine how each tissue contributes to the entire body metabolic profile. In this system, inflammatory markers (IL-6, TNL-α, and E-selectin) and metabolites (glucose, FFA, triacylglycerides, alanine, lactate, glycerol, and albumin) were monitored over time in response to energetic substrate imbalances such as glucose excess or reduced insulin within the system.

Noteworthy, the system was developed using human cells exclusively. It also demonstrated how an imbalance of energetic substrates changes the overall equilibrium of the model system, just as it occurs in a complex *in vivo* model. If islets are incorporated in such a system, it could provide a useful model for islet response in a metabolic network.

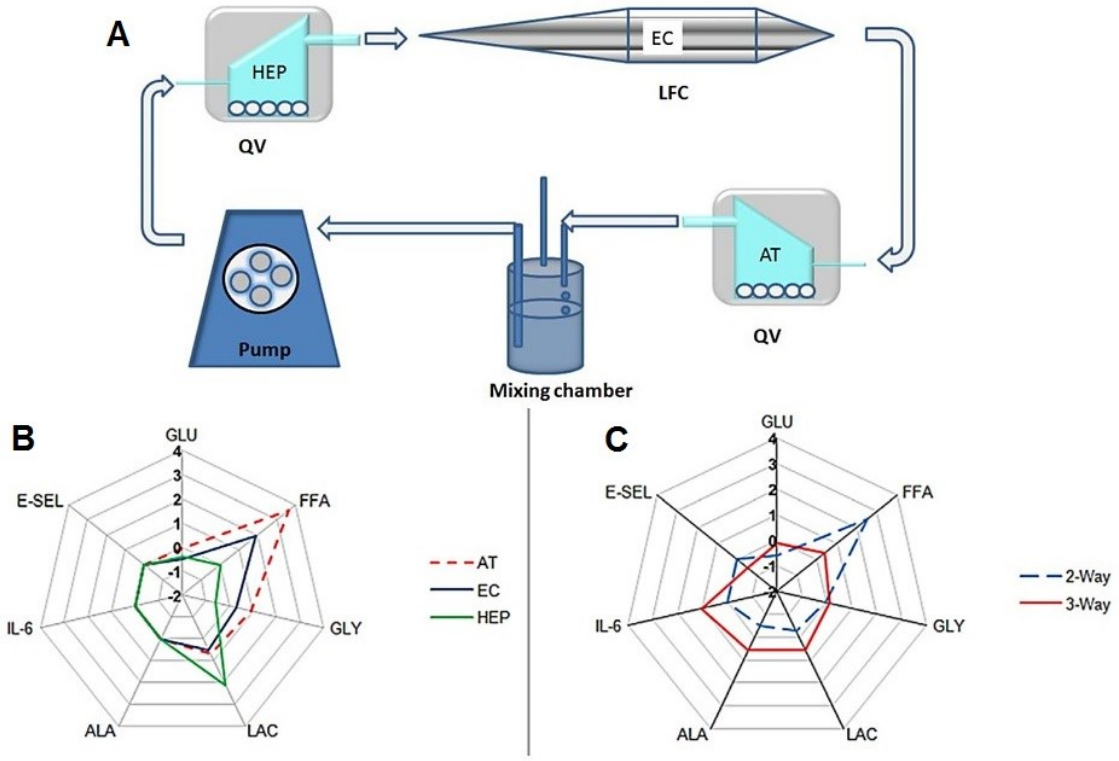

Figure 5.10. A) Schematic representation of a 3D tissue network. In the *quasi-vivo* (QV) chambers, hepatocytes (HEP) and adipocytes (AT) are cultured in a low shear laminar flow regimen. In the laminar flow chamber (LFC), endothelial cells (EC) are cultured under a high shear laminar flow regimen. **B)** Fractional variation in metabolite concentrations for 1-way dynamic cultures of AT, EC and HEP. **C)** Fractional variation in metabolite concentrations for a 2-way (AT+EC) cell culture network and 3-way (AT+EC+HEP) cell culture network. GLU (glucose), GLY (glycerol), LAC (lactate), ALA (L-alanine), E-SEL (E-selectin). (Reproduced from Ref. [249] under the terms of the Creative Commons Public Domain Declaration)

By defining a meaningful SF of healthy pancreatic islets and monitoring it in real-time for ADMET, it may be possible to monitor a future *in vitro* pancreas model that replaces the equivalent animal model. Likewise, the concepts of a secretome signature and a SF can be extended to other cells in a metabolic network such as the aforementioned. Thus, different subpopulations of cells

with the potential to become the target of novel T2D therapeutic agents might be identified. Additionally, a platform with real-time capabilities will be able to simultaneously monitor many aspects of ADMET within these networks, comprising a high-throughput screening system. These platforms should minimize resource consumption and increase the correlation between clinical trials and *in vitro* models, hence reducing costs from drug discovery to commercialization.

Thus, different subpopulations of cells with the potential to become the target of novel T2D therapeutic agents might be identified. Additionally, a platform with real-time capabilities will be able to simultaneously monitor many aspects of ADMET within these networks, comprising a high-throughput screening system. These platforms should minimize resource consumption and increase the correlation between clinical trials and in vitro models, hence reducing costs from drug discovery to commercialization.

5.9. Conclusion and future perspective

In this review, we have provided a general overview of the secretome and the potential determination of it for pancreatic islets. We presented the state of the art of analytical tools and microfluidic platforms for monitoring a relevant islet SF. We have also proposed that defining a particular SF for healthy islets, diseased islets and viable islets can be used as a baseline to dynamically monitor islet functionality and viability. Thus, SF monitoring has applications in islet quality assessment before transplantation, islet regeneration studies and drug screening. In the case of transplantation, monitoring a SF can provide an assessment of islet viability and potency from both human and alternative sources. For islet regeneration, the SF can be used to assess the quality and functionality of pancreatic endocrine tissue after testing the outcome of a regeneration strategy. LOC platforms can provide tools to more easily screen a wide variety of biochemical environments

and reagents as candidates for improved regeneration strategies in a repeatable manner. For drug screening, SF monitoring can be integrated with a pancreas organ-on-chip device to assess ADMET. Moreover, by extending this concept to a cell network, it will be possible to model a complex metabolic disease such as T2D, where novel mechanisms for therapeutics based on the cross talk within the cell network can be discovered. This in time may replace the expensive use of animal models and increase the correlation between *in vitro* models and human trials. Noteworthy, due to the challenges and complexity of maintaining islets in long term culture, to date there is no reports of a pancreas-on-chip for drug screening. In addition to these applications, novel physiological aspects of human pancreatic islets, such as islet paracrine and autocrine effects in native and re-aggregated islets can be studied. This may lead to the discovery of novel therapeutic agents able to regulate these effects.

Biomedical problems often require creative multidisciplinary approaches, especially in the case of pancreatic islets. Interest in secretomics has increased in recent years, because it has the potential to provide new libraries of diagnostic biomarkers and to identify novel therapeutic targets. Increasing collaboration between different fields such as engineering, biology, medicine and analytical chemistry may contribute in developing functional technologies to investigate the secretome of a wide variety of cells and to define and dynamically monitor relevant SFs.

Available platforms for single islet analysis and drug screening do not yet offer multiplexed techniques and are burdened by highly complex operation. The ability to easily monitor several functional parameters from a single human islet would offer a significant technical advantage over current techniques.

MPS are well-established tools and their technology continues to evolve. Once more advanced micro- and nano-analytical technologies are incorporated into MPS, entire metabolic

networks or a body-on-chip can be achieved. Furthermore, these platforms can combine SF monitoring techniques with traditional techniques employed in the "-omic" fields such as mass spectrometry or RNA sequencing to comprise a robust tool for systems biology. The potential of these platforms is enormous, but many challenges still remain to be addressed. Herein lays considerable opportunities for interdisciplinary research teams, particularly in secretion biosensing and in coupling and automatizing "-omics" tool with MPS. This in time may provide relevant applications in systemic or metabolic diseases such as diabetes, lowering the economic burden on health systems and increasing the quality of life of diabetic patients.

Acknowledgments

The authors acknowledge the financial support from the Natural Science and Engineering Research Council of Canada (NSERC), the Fonds de recherche nature et technologies-Team Grant, the NSERC-CREATE in ISS, and FRC scholarship from Consejo Nacional de Ciencia y Teconología de México (CONACyT) and Secretaría de Educación Pública de México (SEP). The authors are also thankful to T. Johns, M. Mekhail, for their insightful comments and editing of this manuscript.

Chapter 6. Evaluation of a capacitive immunosensor based on IDEs for the detection of insulin

The following chapter provides the results corresponding to the investigation of the potential use of an IDEs capacitance-based biosensor for the detection of insulin. This label-free sensing technique was explored since non-faradic electroanalytical methods have been previously reported to offer extraordinary high sensitivity for the detection of small molecules. This chapter presents a thorough study comparing four different insulating/immobilization chemistries commonly used for the construction of capacitive sensors. This study was essential to gain a better understating of the effect of the surface chemistry in the sensor's capacitive behavior, and to obtain a sensitive and highly specific detection system for our targeted hormone. This chapter will be submitted to the journal *Sensors and Actuators B*.

Interfacial Capacitance Immunosensing Using Interdigitated Electrodes: Effect of the Insulation/Immobilization Chemistry

F. Rafael. Castiello[a], James Porter[a], Paresa Modarres[a] and Maryam Tabrizian[a,b]
[a] Biomedical and Biological Engineering Department, McGill University, Montreal, QC, Canada.
[b] Faculty of Dentistry, McGill University, Montreal, QC, Canada.

6.1. Abstract

With the aim of improving the reproducibility of capacitive immunosensors, we performed a comparative study of four different insulating/immobilization chemistries. Each chemistry targeted different areas of an interdigitated electrode including an alkyl thiol monolayer on the electrode surface, an amino silane monolayer on the gaps between electrodes, and conformal coatings via passive adsorption of the probe and a spin-coated layer of poly(methyl methacrylate) (PMMA). We analyzed the dielectric properties of these chemistries by comparing their capacitive behavior through equivalent circuit modeling and correlate the observed behavior with their surface characteristics using atomic force microscopy and finite element modeling. We found that surface binding events occurring in the interdigitated electrode gaps play a major role in the overall change in capacitance. This was confirmed via finite element modeling showing an increased electric field intensity in the electrode gaps by 14%, as compared to directly above the electrodes. Among the investigated surface chemistries, PMMA conformal coating produced a smooth surface (Rq roughness = 0.21 ± 0.02 nm) providing the most reproducible and stable capacitance change (15.6 ± 0.4 %) in response to specific antigen-antibody binding.

6.2. Introduction

The most basic architecture of an immunosensor consists of a receptor, either antibody or antigen,

and a transducer which is capable of detecting binding between the two [250]. A wide range of transduction mechanisms can be used for the development of immunosensors including: optical, electrical, mechanical and magnetic [251]. Among such transduction mechanisms, electrical analytical methods commonly present instrumental simplicity and high sensitivity. This has encouraged the miniaturization of electrical immunosensors in recent years, making them ideal for the growing field of point of care diagnostic devices [33].

A particular case of electrical transductions methods is impedance sensing, which in essence measures changes in the electrical impedance of an electrode/electrolyte interface over a range of applied frequencies. In the absence of a redox probe (non-Faradic), the interfacial capacitance at the electrode/electrolyte interface can be used as a sensitive way of measuring binding events, hence making such sensors commonly known as capacitive immunosensors [34]. The absence of a redox probe in these types of sensors provides design and experimental advantages over its Faradic counterparts where a three-electrode system is required, depletion of the probe can occur and catalytic modification of the sensing interface is needed [33]. The most common kind of capacitive immunosensor is based on coplanar interdigitated electrodes (IDEs) [34]. This type of electrodes provides a large sensing surface, and their performance can be adjusted by modifying their dimensions.

However, while practically simpler, relative unpredictability and limited reproducibility have made capacitive immunosensors unfavored compared to analogous Faradaic approaches [33, 34, 59]. A possible reason for this unpredictable response is difficulties associated with the production of compact and pinhole-free insulating/immobilization layers. Such defects can cause a "short circuit" on the capacitive layer, ultimately decreasing its sensitivity [34]. Some common insulating/immobilization strategies include self-assembled monolayers (SAM) of alkyl thiols [37,

252-254], polymers [40, 186, 255, 256], and silanes [257-259]. The "short circuit" problem could be particularly troublesome when using a SAM of alkyl thiols on gold electrodes since small SAM defects can lead to large changes in capacitance or a complete loss of sensitivity [250, 260, 261]. Furthermore, a variety of architectures have been reported in literature investigating the covalent immobilization of biomolecules on different regions of the sensor such as on the electrodes [37, 252-254, 262], in the gaps between electrodes [257-259, 263] and a conformal coating covering both [255, 256, 264, 265]. However, so far, no systematic studies have been performed to evaluate the effect of these architectures on the sensor performance. This suggests the need for further research in probe immobilization chemistry and architecture to improve reproducibility [59].

In this work, we aim to investigate the insulation/immobilization chemistry and architecture that renders the largest capacitance change detectable for antigen-antibody binding with the most reproducible results. To achieve this, we compared four different insulating/immobilization chemistries commonly found in literature, targeting different areas of a capacitive immunosensor which included: an alkyl thiol SAM on the electrode surface, an amino silane monolayer on the gaps between electrodes, conformal coatings via passive adsorption of the probe and a spin-coated layer of poly(methyl methacrylate) (PMMA). Insulin and its antibody was used as a representative immunosensing system due to the interest of the authors in pursuing detection of such hormone in complex matrices. First, we evaluated the quality of these insulation/immobilization layers through equivalent circuit analysis using the fractional value of the exponential coefficient of a constant phase element (CPE). Next, we correlated the obtained CPE fractional values to the surface characteristics of each chemistry using atomic force microscopy (AFM). Then, the different insulation/immobilization layers were further functionalized with antigen, and the capacitance change in response to antigen-antibody binding was evaluated. After selecting the most

reproducible chemistry, we evaluated the effect of IDEs size on the sensor performance. Finally, two negative controls (PMMA-coated IDEs functionalized with a non-specific antigen, and with no antigen on their surface, respectively) were used to validate the optimized surface chemistry through assessing the specificity of the immunosensor via a secondary antibody assay.

6.3. Materials and Methods

Absolute ethanol and phosphate-buffered saline (PBS) 10X were purchased from Fisher Scientific (Fair Lawn, NJ, USA). Phosphate-buffered saline 1X (PBS) tablets and Tween 20 were purchased from BioShop Canada Inc. (Burlington, Ontario, Canada). N-(3-Dimethylaminopropyl)-N′-ethylcarbodiimide hydrochloride (EDC), N-Hydroxysuccinimide (NHS), (3-Aminopropyl)triethoxysilane 99% (APTES), bovine serum albumin (BSA) and Hydrochloric acid (HCl) were purchased from Sigma-Aldrich (St. Louis, MO, USA). 16-Mercaptohexadecanoic acid (MHDA) was purchased from ProChimia Surfaces Sp. (Zacisze, Sopot, Poland). Tris-buffered saline (TBS) with 1% Casein from BIO-RAD. Anti-insulin antibody (6.2 mg/mL) and human insulin were purchased from PROSPECT (Ness, Ziona, Israel). Anti-glucagon antibodies (200 μg/mL) were purchased from Santa Cruz Biotechnologies, Inc. (Mississauga, ON, Canada). Poly(methyl methacrylate) (PMMA 950 A2) was purchased from MicroChem Corp.

6.3.1. Microfluidic handling system

A microfluidic chamber was designed using a CAD software. Using a clear FLGPCL02 resin (a mixture of methacrylate monomers and oligomers), the device was then constructed by 3D printing (Form2 printer from FormLabs) with a post-cured tensile strength of 65 MPa

6.3.2. Impedance spectra acquisition

Impedance measurements were carried out using a 4294A Agilent precision impedance analyzer with a frequency range of 40 Hz -110 MHz. Interdigitated electrodes were connected through the fixture 16089B and spring loaded pins to the analyzer. Frequency scans were performed over the range of 40 Hz -10 MHz with an oscillating AC potential of 10 mV with 0 V DC bias. All frequency scans were taken at bandwidth 5 (highest precision), and for all measurements, the spectrum was captured 3 times, 3 minutes apart and then averaged.

6.3.3. Microscopy image acquisition

Image acquisition was performed with an inverted microscope (Eclipse TE 2000-U, Nikon Corp, Mississauga, ON, Canada), with fluorescence capabilities. All images were captured using a CCD camera (Retiga-2000R, Q imaging, Surrey, BC, Canada) and Nikon NIS-Elements D software.

6.3.4. Atomic Force Microscopy

AFM surface analysis were performed using a Nanoscope III instrument (Digital Instruments, USA) and Nanoscope v 5.12r5 software. AFM images were acquired in tapping mode in air at room temperature with a silicon probe having a nominal spring constant of 42 N/m and a nominal resonance frequency 330 kHz (model PPP-NCHR, NANOSENSORSTM).

6.3.5. Interdigitated electrode fabrication

Three electrode sets of IDEs 5 × 5, 10 × 10 and 15 × 15 μm (width (w) × spacing (s) in size were fabricated were fabricated in a cleanroom environment. The IDEs fingers length was 1 mm, and a total surface area of 0.5 mm^2 was kept constant by varying the total number of fingers when changing the electrode finger width and spacing. Glass wafers 1 mm thick and 127 mm in diameter

were used as substrates. The wafers were cleaned with acetone under sonication for 5 min, rinsed with isopropyl alcohol (IPA), distilled water and dried with N_2. The substrate was then heated to 100 °C in a YES priming oven under vacuum for 5 min to evaporate any leftover solvents and then cooled with a steam of N_2. Next, LOR5B™ (Microchem, Newton, MA) was spin-coated at 1000 rpm for 45 s onto the glass substrate and baked at 180 °C for 5 min. After allowing the wafer to cool down, Microposit™ S1813™ (Shipley, Marlborough, MA) was spin-coated at 4000 rpm for 30s and baked at 115 °C for 1 min. The substrate was then exposed to UV light with a dose of 136 mJ/cm^2 under a chrome photomask. Finally, the substrate was developed by immersing the substrate in Microposit MF®–319 (Shipley) developer for 70 s without agitation and immediately washed with deionized water and dried with N_2. A 10 nm titanium adhesion layer and a 50 nm gold layer were deposited using a NexDep E-beam evaporator (Angstrom Engineering Inc). The substrate was then immersed in Microposit Remover 1165 (Shipley) at 70 °C under sonication to lift off the metal layer and reveal the patterned electrodes. Finally, the wafer was diced using a diamond saw (Disco DAD3240) into individual sensor chips (20 cm × 19 cm).

6.3.6. Immobilization chemistry

Prior to use, all IDEs were cleaned with acetone under sonication for 5 min then rinsed with IPA, distilled water, and dried with a stream of N_2. Additionally, Kapton stickers were placed on the IDEs connection pads to protect them from surface functionalization which could hinder their conductivity.

6.3.6.1. Poly(methyl methacrylate) (PMMA) coating and functionalization

The PMMA functionalization of the IDEs was adopted from a protocol reported by K. Kamgil *et al*. [266] with minor modifications. First, commercially obtained PMMA was spin-coated undiluted onto IDEs at 5000 rpm for 45 s and baked at 180 °C for 90 s, obtaining a final thickness of 66 nm,

measured by ellipsometry. Then, the IDEs were treated with O_2 plasma at 100 W for 150 s to create hydroxyl groups on its surface and immediately immersed in a 10% (v/v) solution of APTES in MQ water at 70 °C for 5 min. Finally, they were quenched in ethanol and baked at 110 °C for 10 min.

6.3.6.2. Alkyl thiol self-assembly monolayer (SAM) functionalization

IDEs were immersed in an ethanolic solution of 2 mM MHDA overnight (≈18h) at room temperature to allow self-assembly monolayer (SAM) formation. The substrates were then thoroughly rinsed with absolute ethanol, DI water and dried under a stream of N_2.

6.3.6.3. (3-Aminopropyl)triethoxysilane (APTES) functionalization on IDEs gaps

IDEs were treated with O_2 plasma at 100 W for 150 s and immediately immersed in a 10% (v/v) solution of APTES in MQ water (Barnstead, 18.2 MΩ distilled water) at 70 °C for 5 min. The chip was then quenched in ethanol, rinsed with MQ water, dried with N_2 and baked at 110 °C for 10 min. The APTES form a self-assembly layer directly to the glass, which leads to functionalization of the gaps only, leaving the gold surfaces bare.

6.3.6.4. Passive adsorption (PA) functionalization

The PA functionalization of the IDEs was performed following a protocol reported by H. Cui *et al*. [267] with few modifications. First, the IDEs were treated with O_2 plasma at 50 W for 30 s to make the electrode surface hydrophilic. Immediately after, the chip was immersed in a solution containing 1 mg/mL insulin in PBS and incubated at 4 °C overnight. Then, the chip was rinsed with copious amounts of PBS and the surface blocked by immersion in a solution containing 5% (v/v) BSA, 1% (v/v) Casein and 0.05% (v/v) Tween-20 in TBS buffer (BCB buffer) for 30 min.

6.3.7. Covalent immobilization of insulin

After SAM, APTES and PMMA functionalization, the chips were loaded into the microfluidic chamber for the remaining steps of insulin immobilization. **Figure 6.2** shows a schematic summary of all peptide immobilization chemistries performed.

For IDEs functionalized with PMMA and APTES, 5 mg/mL NHS and 2 mg/mL EDC were mixed in MES buffer (pH 6.0). Then, 125 μL of the NHS/EDC mixture was added to 100 μL of an aqueous solution of insulin with a concentration of 1 mg/mL. After reacting for 15 min, 825 μL of PBS 10X was added to the mixture to raise its pH to 7.4 and immediately injected into the system. Finally, the mixture was incubated for 1 h, allowing the covalent bonding between carboxyl groups on insulin and amine groups on APTES to occur.

For IDEs functionalized with alkyl thiol SAM, the NHS/EDC mixture in MES buffer was first injected into the chamber allowing it to react for 15 min. Then, a PBS solution of insulin with a concentration of 1 mg/mL was injected into the chamber and allowed to react for 1 h to form a covalent bond between carboxyl groups on the SAM and the amine groups on the insulin.

After insulin incubation, all surfaces were rinsed by flowing 1 mL of PBS (1X) with 0.05% Tween-20 (PBS-T) through the chamber for 10 min. Next, any remaining reactive sites and non-specific binding sites on the surface were blocked by injecting BCB buffer and incubating for 30 min. A final rinsing step was performed using 1 mL of PBS-T.

6.3.8. Antigen-antibody binding detection

Insulin monoclonal antibody was injected into the system with a final concentration of 10 µg/mL. Once the solution reached the sensing chamber, the flow was stopped and the antibody was incubated for 1 h. Then, the surface was rinsed with 1 mL of PBS-T for 10 min. After rinsing, the

system was allowed to equilibrate for at least 60 s, and then the impedance spectrum was captured. The impedance spectra from the antigen-functionalized and blocked surface were used as a baseline, to determine the capacitance change caused by antibody binding.

To assess the assay specificity and as an additional way to evaluate the sensor functionalization, a secondary fluorescence antibody (Alexa Fluor 647 goat anti-mouse) was injected into the system with a final concentration of 20 μg/mL and incubated for 1 h. Then, the surface was rinsed with 1 mL of PBS-T for 10 min, the system was allowed to equilibrate for at least 60s, and the impedance spectrum was recorded. As with the primary antibody, the impedance spectra from the antigen-functionalized and blocked surface were used as a baseline, to determine the total capacitance change caused by secondary antibody binding.

6.3.9. Statistics

For all impedance spectra analysis, 3 independent experiments were performed, where an equivalent circuit fitting was accomplished with a confidence interval of 95%. Then, the mean value of these circuit elements was calculated and is presented in the manuscript as mean ± standard deviation (SD). Similarly, for AFM analysis the data is express as the mean of at least 3 independent experiments ± SD. Means that are statistically different are indicated with a subscript asterisk (*). Microsoft Excel 2016 was used to perform the One-way ANOVA test followed by Bonferroni's test correction to evaluate the statistical difference of multiple samples, where $P<0.05$ was considered a significant difference.

6.4. Results and Discussion

6.4.1. Microfluidic device fabrication and experimental setup

For stable and consistent measurements the sensor was interfaced with the analytes using a microfluidic chamber constructed via 3D printing. The microfluidic device consists of an inlet and outlet of 1 mm in diameter and an elliptical chamber with a height of 0.93 mm, a small radius (r_a) of 2.06 mm, and large radius (r_b) 4.05 mm, with a total volume of approximately 25 µL. **Figure 6.1** shows the final experimental setup that includes a microfluidic chamber (**Fig. 6.1A**) and the electrical connection between the IDEs and the impedance analyzer (**Fig. 6.1B**). **Figure 6.1C** displays a schematic presentation of the dimension of the microfluidic chamber.

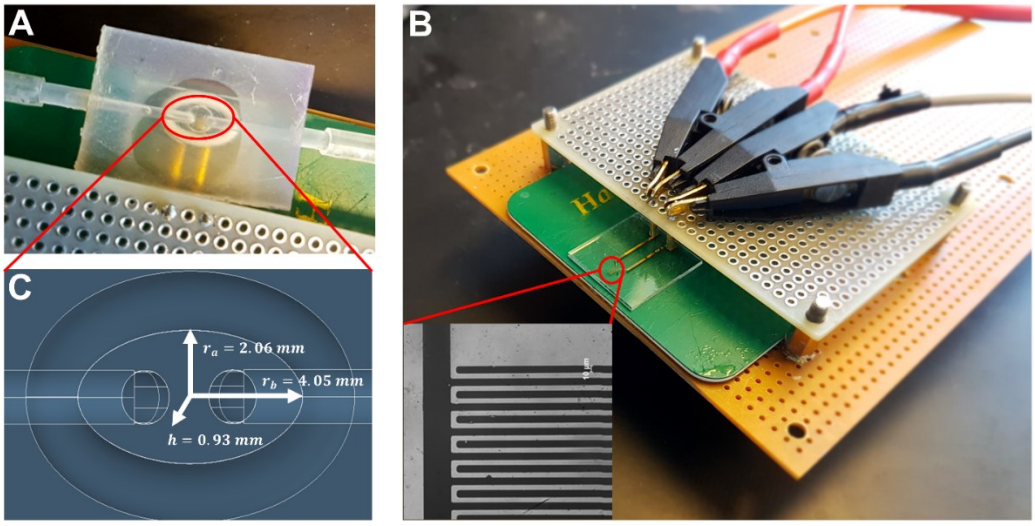

Figure 6.1. Experimental setup for impedance measurements: **A)** the microfluidic chamber, **B)** the electrical connection between the IDEs and to the impedance analyzer and **C)** the schematic representation of the 3D printed chamber showing its dimensions.

6.4.2. Insulation/immobilization chemistries

One of the crucial aspects affecting the reproducibility of capacitive immunosensors is the appropriate design of the sensor surface. The surface morphology of the insulating layer needs to be homogeneous and densely packed to prevent a decrease in the sensor's sensitivity due to surface

irregularities such as pin holes [34, 35, 268, 269]. Therefore, we investigated the effect of four of the most commonly encountered insulating/immobilization strategies in literature for capacitive sensing. In capacitive sensing, the binding of a molecule is expected to produce a change in thickness on the dielectric double layer directly proportional to the molecule size [270]. For this reason, insulin (MW=5807.57 Da) was immobilized onto the IDEs surface, and sensing was performed by detecting attachment of the much larger insulin antibody (MW=150kDa).

Four of the more commonly reported surface chemistries and architectures targeting different areas on the surface of the sensor were chosen: a conformal functionalization with PMMA that covers the entire sensing area (**Fig. 6.2A**), a SAM using 16-mercaptohexadecanoic acid (MHDA) covering only the electrodes (**Fig. 6.2B**), a layer of (3-aminopropyl)triethoxysilane (APTES) covering the space between the electrodes (**Fig. 6.2C**) and the passive adsorption (PA) of the antigen covering both electrodes and spaces (**Fig. 6.2D**).

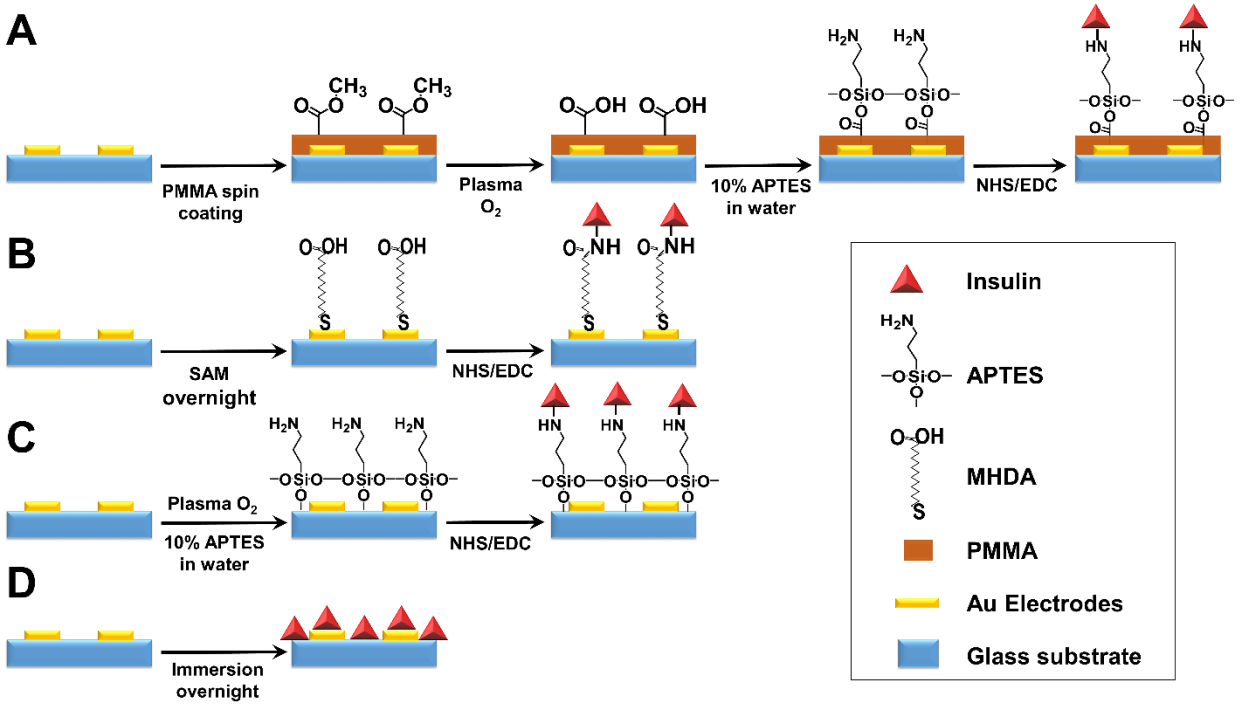

Figure 6.2. Schematic representation of the different insulin immobilization chemistries and architectures used on IDEs. **A)** PMMA, **B)** SAM, **C)** APTES, **D)** PA.

6.4.3. Equivalent circuit model fitting

The equivalent circuit representation is commonly used in literature as a powerful tool that allows the characterization of an electrode-electrolyte system [35, 57]. This representation approximates the experimental impedance data with ideal impedance elements arranged in series and/or in parallel [35, 57]. In this manner, the change of impedance in one element such as a resistance or a capacitance can be evaluated by correlating the overall impedance change to a physical phenomenon such as antigen-antibody binding.

The spectra of the interfacial impedance of an IDEs in the absence of a redox probe (non-Faradaic regime) and in aqueous media is shown in **Figure 6.3A** [271, 272]. The total impedance of this system is typically represented by the equivalent circuit depicted in **Figure 6.3B** [37, 271]. It is observed that there are three clearly defined zones in the spectra (**Fig. 6.3A**), corresponding to the three elements in the equivalent circuit that include the two parallel branches (**Fig. 3B**). Then, the total impedance of the system (Z) as a function of frequency (*f*) is expressed as:

$$\frac{1}{|\mathrm{Z}|} = \frac{1}{\sqrt{R_{Sol}^2 + \frac{1}{(\pi f C_{dl})^2}}} + 2\pi f C_{de} \tag{6.1}$$

For frequency ranges below 10^5 Hz (**Fig. 6.3A**), current does not flow through the dielectric capacitor (C_{de}), leaving it inactive [272]. In this case, the total impedance of the system corresponds only to the double layer capacitance (C_{dl}) and solution resistance (R_{sol}) in series, and the total impedance of the system simplifies to:

$$|Z| = \sqrt{R_{Sol}^2 + \frac{1}{(\pi f C_{dl})^2}} \tag{6.2}$$

Since the solution composition is usually constant during experiments, in essence, the system reports changes on the interfacial capacitance. The interfacial capacitance can be represented by a model of various capacitive layers in series [34]. **Figure 6.3C** shows a schematic representation of such capacitors in series which define the total capacitance of the biosensor. C_{ins} corresponds to an insulating/immobilization layer. C_{rec} includes the contribution of the immobilized antigen layer, any additional blocking proteins, and the specific antibody recognition layer. C_{SL} represents the final Stern Layer. Thus, during biosensing, the antigen-antibody binding is responsible for the overall change in the total capacitance. The total capacitance of the double layer (C_{dl}) is then expressed as:

$$\frac{1}{C_{dl}} = \frac{1}{C_{ins}} + \frac{1}{C_{rec}} + \frac{1}{C_{SL}} \tag{6.3}$$

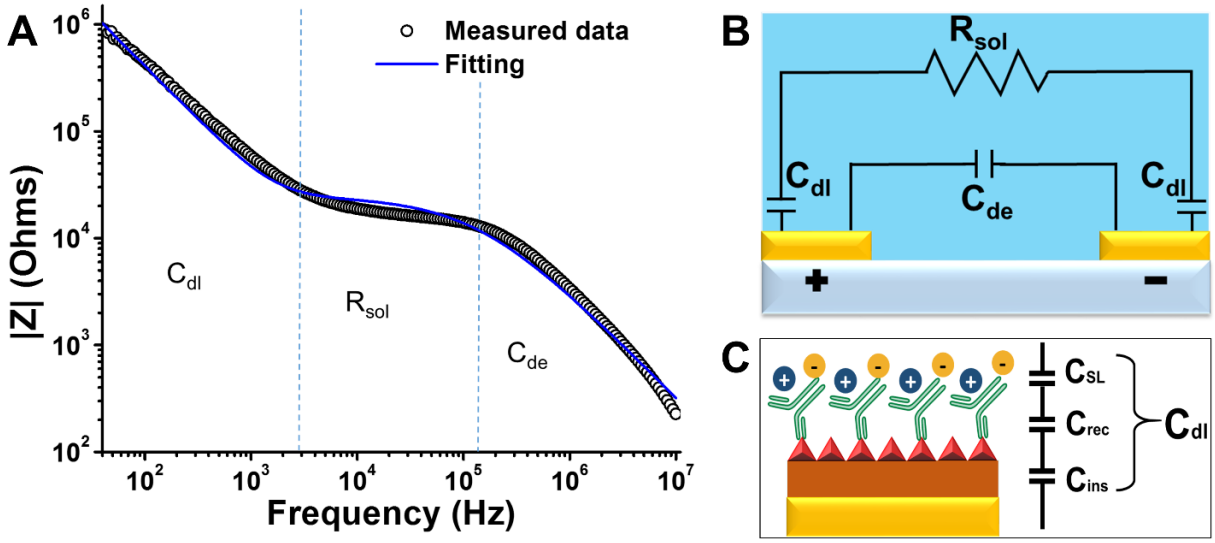

Figure 6.3. A) Interfacial impedance spectra of IDEs in the absence of a redox probe in MQ water. Cdl corresponds to the double layer capacitance, Rsol to the solution resistance and Cde to the dielectric capacitance of the media. **B)** Schematic representation of the equivalent circuit model used for fitting measured data in A. **C)** Schematic representation of a model of capacitors in series that define the double layer capacitance for a typical capacitive biosensor with an electrode–solution interface. Cins corresponds to an insulating/immobilization layer. Crec includes the contribution of the immobilized antigen layer, any additional blocking proteins, and the specific antibody binding layer. CSL represents the final Stern Layer.

Overall, the model shows that the total capacitance in the system is governed by the smallest capacitance of the contributing layers. Additionally, equation 3 assumes an ideal insulation/immobilization and recognition layers where the effect of holes and other chemical heterogeneities are neglected [34]. This emphasizes the fact that the careful design and implementation of insulating layers is a crucial step for the development of capacitive immunosensors [273].

Moreover, it has been empirically demonstrated that the capacitive behavior from the formation of an ionic double layer in solid electrodes does not behave ideally [274]. Instead, it has been observed that the double layer capacitance has a functional form that is frequency dependent [275]. This functional form is commonly known as a constant phase element (CPE), defined as:

$$CPE = \frac{1}{(j\pi f)^n Q} \tag{6.4}$$

Here, j is the imaginary unit and Q is equivalent to the capacitance (C_{dl}) of a perfect capacitor. The coefficient n of the CPE varies between 0 and 1, where $n = 1$ (**Eq. 6.4**) represents the impedance of an ideal capacitor where Q has units of capacitance (F); otherwise ($n<1$), Q has units of $F/s^{(1-n)}$. Therefore, the experimental impedance data can be fitted to the following equation:

$$|Z| = \sqrt{R_{Sol}^2 + \frac{1}{[(\pi f)^n Q]^2}} \tag{6.5}$$

The fractional value of the CPE coefficient n has been shown to account for a variety of the non-ideal conditions present in the capacitive sensing system, such as surface irregularities, chemical heterogeneities, and uneven ion adsorption onto the electrode surface [275-277]. Thus,

the *n* coefficient can represent a powerful parameter to assess the quality of the insulation/immobilization layer during the design of capacitive immunosensors.

To validate the application of the proposed CPE circuit model (**Eq. 6.5**), the impedance spectra of the electrode/electrolyte interface was recorded for a clean IDEs chip (**Fig. 6.4A**) and for IDEs functionalized with the four insulating/immobilization chemistries described in the previous section (**Fig. 6.4B-E)**. For this analysis, IDEs chips with a 10 × 10 µm (width (w) × spacing (s)) were used. After functionalization, the chips were placed in the microfluidic chamber and the impedance spectra were recorded in PBS (1x).

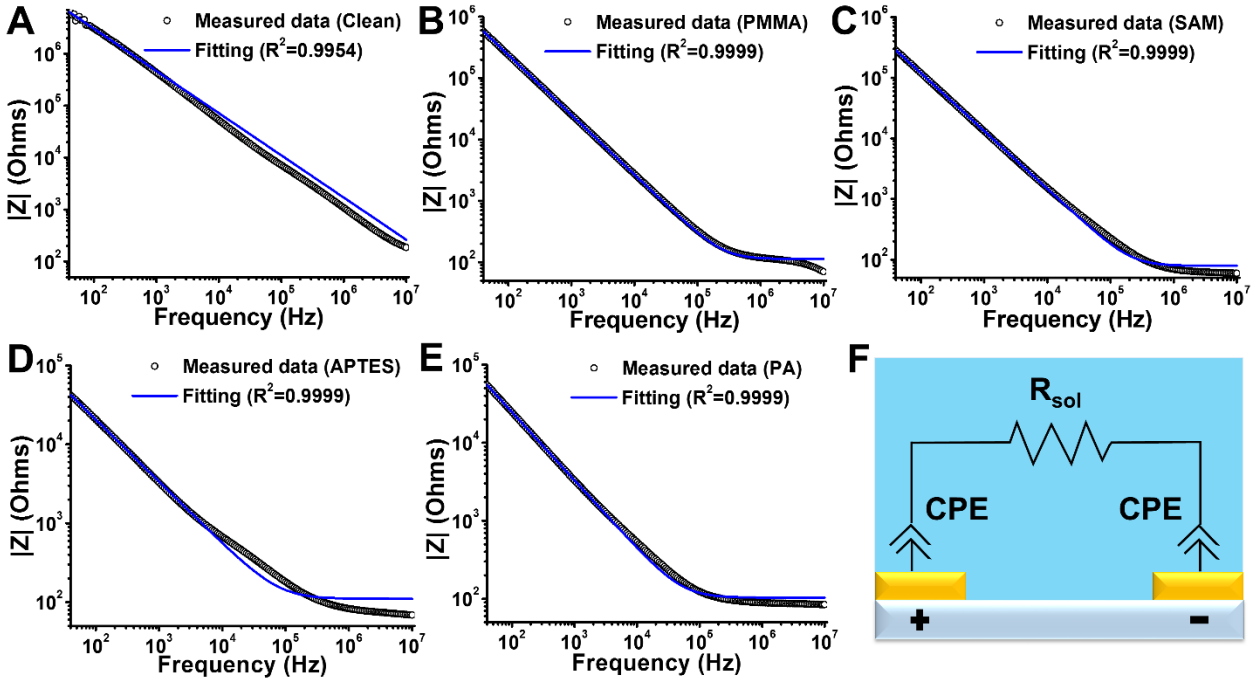

Figure 6.4. Representative impedance spectra and fitted curves in PBS 1x between the frequency range of 40 Hz–10 MHz for 10 × 10 µm IDEs: **A)** clean, **B)** spin-coated PMMA, **C)** a SAM of alkyl thiol, **D)** a self-assembled layer of APTES in the space between the IDEs fingers, and **E)** a passively adsorbed (PA) layer of insulin and BCB buffer blocking. **F)** Schematic representation of the equivalent circuit model used for the fitting.

According to the analysis and measurements from the fitted curves shown in **Figure 6.4** and the extracted circuit parameters provided in **Table 6.1**, one can notice that for the working

frequency range, the C_{de} term coming from the dielectric properties of the PBS 1x solution can be neglected for all insulation/immobilization chemistries. It is also inferred that the behavior of the IDEs is predominantly capacitive for all insulating/immobilization chemistries in the frequency range between 0.1 to 1 MHz. On the other hand, the CPE *n* coefficient of clean electrodes was found to be around 0.9 (**Table 6.1**) showing good agreement with previous reported data for experiments performed under similar conditions [278-280]. The insulation/immobilization chemistries that showed the largest deviation from ideal capacitive behavior were PA and APTES, while the ones showing the best capacitive behavior were SAM and PMMA. Additionally, PA presented the highest standard deviation values for the CPE *n* coefficient from all surfaces while PMMA exhibited the lowest. Noteworthy, APTES showed a large change in capacitance (*Q*) despite only modifying the gaps between electrodes. This is an interesting observation since little experimental research has been conducted regarding the optimal position for the recognition elements immobilization. To understand this phenomenon, further experiments were carried out and the results are reported in the following sections.

Table 6.1. Equivalent circuit parameters obtained by curve-fitting the experimental data with the equivalent circuit in Fig. 1B using Eq. 5. For this analysis 3 independent experiments were performed where a fitting was accomplished with a confidence interval of 95%. All reported values correspond to the mean ± standard deviation (SD) of the circuit element obtained from each independent fitting.

Surface	CPE *n* coefficient	Rsol (Ω)	Q (nF/s$^{(1-n)}$)
Au clean	0.90 ± 0.05	42 ± 0.2	3 ± 1.5
APTES	0.83 ± 0.02	91 ± 13.0	233 ± 36
SAM	0.95 ± 0.01	81 ± 3.0	32 ± 6.0
PMMA	0.97 ± 0.005	111 ± 2.0	15 ± 0.3
PA	0.91 ± 0.46	138 ± 32	238 ± 43

6.4.4. Morphological characterization of the insulating/immobilization layer

AFM was used to characterize the surface morphology of the different insulating/immobilization chemistries. **Figure 6.5** shows a representative 3D image of a 1 μm^2 area of two controls (a clean electrode and clean glass in the gaps between electrodes) (**Fig. 6.5A-B**) and coated IDEs sensing surfaces as described in the previous section (**Fig. 6.5C-F**). The images are presented using the same XY scale and a vertical scale ranging from 0 to 10 nm (deep red to white) to allow proper comparison of the surface morphology among the different insulating/immobilization chemistries. Changes in surface features from the clean Au and glass surfaces confirmed the successful deposition of the different insulation/immobilization layers. For all functionalization strategies, a significant change in surface roughness expressed by root mean square roughness (Rq) in **Table 6.2** was observed. The largest change in surface roughness was found for the PMMA coated surfaces. The large decrease of Rq was consistent with other published works where deposited PMMA films significantly changed surface morphology and smoothed out rough surfaces [281, 282]. The PA antigens-modified surfaces seemed to provide the most heterogeneous surface as the Rq measurements presented the largest standard deviation. This large standard deviation is likely due to the formation of aggregates in some areas of the surface, as clearly observable in **Figure S6.2** provided in supporting information.

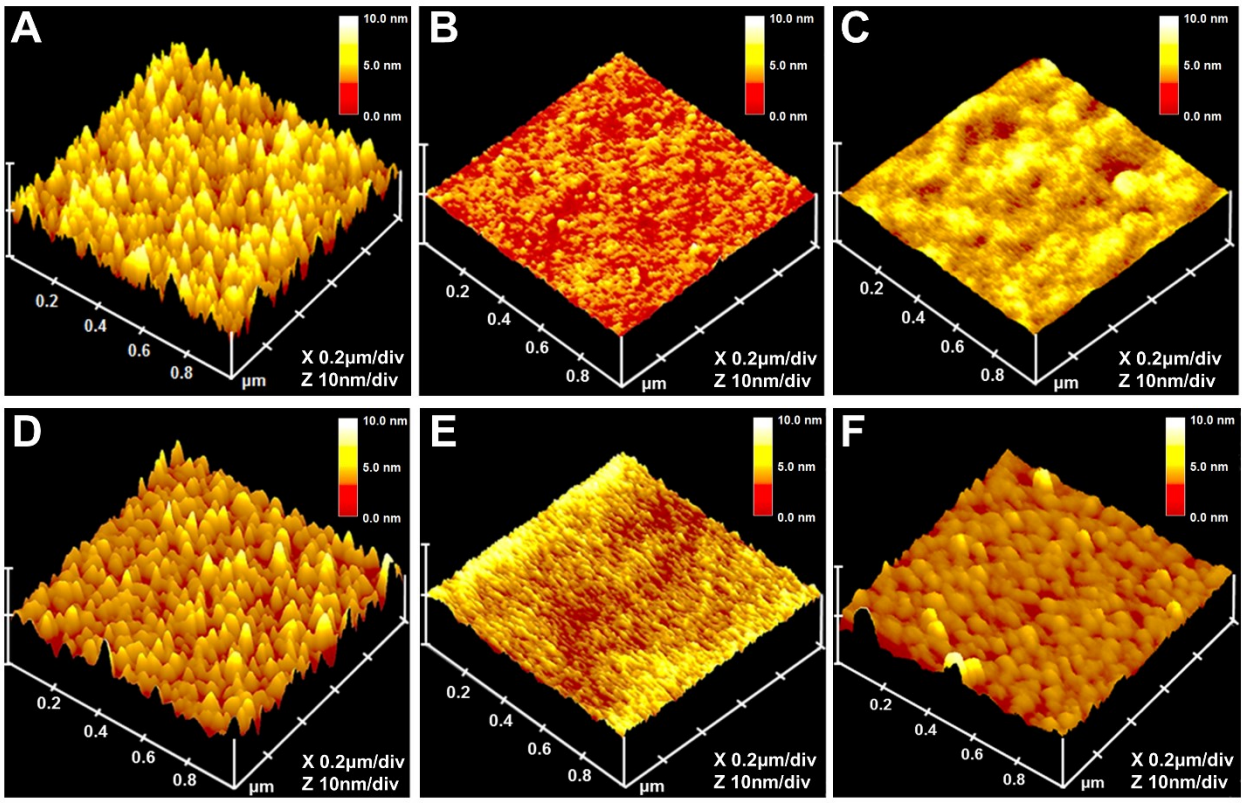

Figure 6.5. Representative 3D images of a 1 µm^2 area of the IDEs sensing surface for: **A)** a clean Au electrode, **B)** clean glass in the gaps between electrodes, **C)** spin-coated PMMA on a gold electrode, **D)** MHDA SAM on a gold electrode, **E)** APTES on the IDEs gaps and **F)** PA of antigens on top of a gold electrode.

The AFM surface analysis matches well with the trend observed for the CPE *n* coefficient analysis. Since the surface roughness is expected to have a significant impact on the capacitive behavior, we observed that the non-ideal capacitive behavior decreases with the decrease in surface roughness. Indeed, the IDEs coated with PMMA provided a small Rq of 0.21 nm and an *n* coefficient as high as 0.97. Conversely, the IDEs prepared with PA antigens presented an Rq of 1.39 and an *n* coefficient of 0.9. Additionally, the large standard deviation in CPE *n* coefficient measurement was consistent with that observed for Rq. Surprisingly, while the Rq for the APTES-coated IDEs was comparable to that of the clean glass, a noticeable decrease in its CPE *n* coefficient was observed. A possible explanation could be that the APTES chemistry targeting only the gaps

between the electrodes, produced a heterogeneous surface morphology seen in **Figure 6.5E**. In this case, the principle of a current leakage passing through an insulating layer does not apply, since in this sensing layout only the space between the IDEs were functionalized. To have a plausible explanation for this effect, the electric field intensity of IDEs was evaluated using finite element modeling (FEM).

Table 6.2: AFM root mean square roughness (Rq) data for three independent samples (n=3) of the different functionalization chemistries on IDEs. The data is presented as mean ± SD of at least 3 independent experiments.

Surface	Image Rq (nm)
Au clean	1.11 ± 0.03
Glass clean	0.23 ± 0.01
APTES	0.19 ± 0.01
SAM	0.90 ± 0.04
PMMA	0.21 ± 0.02
PA	1.39 ± 0.13

6.4.5. FEM of the electric field intensity for IDEs

The electric field inside the chamber for IDEs with a 5µm width, 5µm spacing, and 100nm height was simulated by FEM using COMSOL 5.2 software (Burlington, MA). The simulated 2-D cross section of the device included the glass substrate, gold electrodes, the fluid (PBS), and PDMS as the ceiling (**Fig. 6.6A**, PDMS is not shown). The simulation was performed using the Electric Current Module in frequency domain. The constituent equations included:

$$\nabla . J = Q \tag{6.6}$$

$$J = (\sigma + j\omega\varepsilon_o\varepsilon_r)E + J_e \tag{6.7}$$

$$E = -\nabla V \tag{6.8}$$

where J is the current density, J_e is the externally generated current, E is the electric field intensity, V is the applied voltage, and Q is the charge. Furthermore, ε_0 and ε_r are the electrical permittivity of the free space and the medium, respectively. The symbol ω represents the angular frequency of the applied voltage. Current conservation and electric insulation conditions were applied to all domains and outer geometry boundaries, respectively. The fluid, electrodes, and insulating layer domains were meshed with 15058 triangular elements with a minimum element quality of 0.73.

The electrodes were biased with 0.1 volts at 100 Hz frequency and the electric field intensity values (*E)* was calculated at 80 nm above electrode surfaces (black line) and above the spacing between electrodes (red line) (**Fig. 6.6B**). This distance was chosen as a reasonable distance at which the binding events are expected, taking into account the thickness of all the elements involved and the different immobilization chemistries used on the sensor surface.

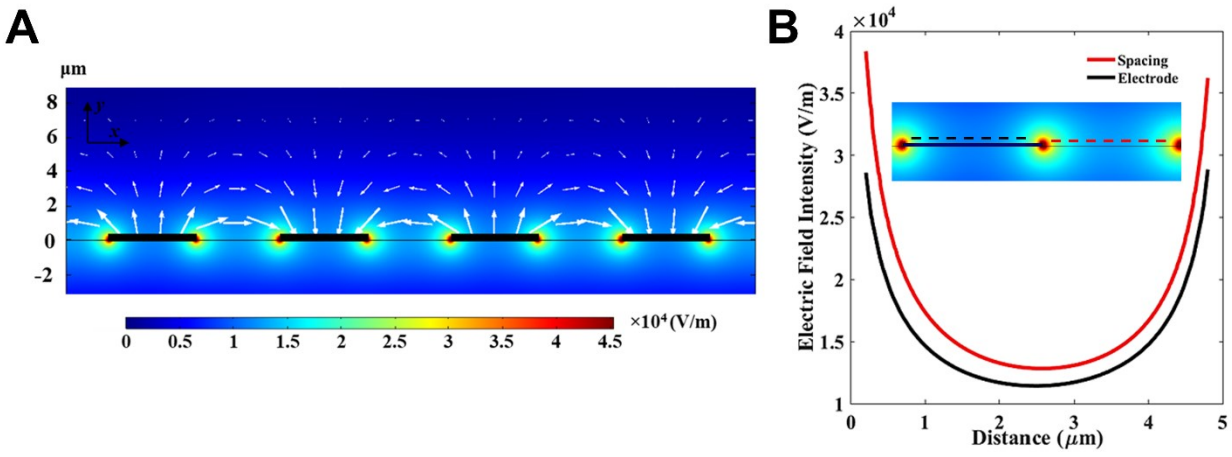

Figure 6.6. A) 2-D cross section simulation of electric field intensity along the longitudinal axis of the chamber (x-direction). **B)** Electric field intensity values 80 nm above electrode and spacing surfaces (dotted lines). The inset shows the enlarged electric field intensity around a single electrode and the gap using the same color scale as **A**.

The average electric field intensity within the spacing (17.35 kV/m) was found to be

14.34% higher than the average electric field intensity above electrode surfaces (15.19 kV/m). This could explain the CPE *n* coefficient decrease and the large capacitance change after APTES functionalization of the IDEs spaces. Furthermore, the enhanced electric field intensity within the space separating two electrodes suggests that the events occurring in such spaces carry a significant weight in the overall change in capacitance. The FEM analysis is consistent with a previous report suggesting that the space between the electrodes significantly contributes to the total electric field intensity and current density distributions around the IDEs [283]. Accordingly, it is important to consider the contribution of functionalized electrode spacing to the overall immunosensor performance in terms of sensitivity and reproducibility. As such, the insulating/immobilization chemistries that do not target the spacing betweens electrodes during functionalization would not profit from this enhanced electric field. Conversly, by not functionalizing the gaps between electrodes or properly blocking it, non-specific adsorption in this area could induce a large change in capacitance, ultimately reducing reproducibility.

6.4.6. Capacitive immunosensing performance of the insulating/immobilization chemistries

After depositing the different insulating/immobilization layers, covalent functionalization of the antigen was carried out. Since the measured impedance largely depends on the target size [34, 35, 260], the small targeted antigen was immobilized on the surface and used as a probe for detection of the antibody in solution. With the exception of PA coating, the antigen was covalently bound to the insulating layer via NHS/EDC chemistry (**Fig. 6.2**). Then, all surfaces were blocked using buffer containing bovine serum albumin and casein to prevent non-specific binding.

Using the impedance spectra from the functionalized and blocked surfaces as the new baseline, the change in capacitance after the antibody binding could be quantified as follows:

$$Capacitance\ change = \frac{C_B - C_0}{C_0} * 100 \quad (6)$$

C_0 corresponds to the capacitance of the blocked surface and C_B corresponds to the capacitance after binding. **Figure 6.7A** illustrates the capacitance change measured for the four surface chemistries.

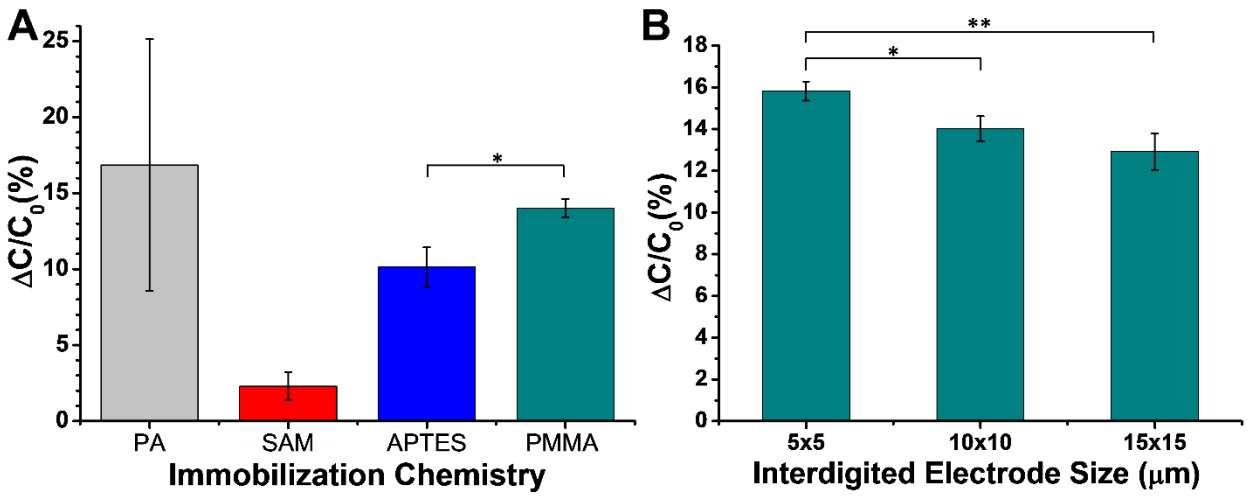

Figure 6.7. Capacitance change for specific antibody binding represented as mean ± SD calculated for three independent samples (n=3) for: **A)** different immobilization/insulation chemistries, where the significant difference between APTES and PMMA chemistries was (*) $P < 0.02$. **B)** different size of IDEs functionalized with PMMA, where the significant difference between 5 × 5 µm and 10 × 10 µm was (*) $P < 0.02$ and 15x15 µm was (**) $P < 0.01$.

Despite the large average change in capacitance, PA was the least reproducible sample, as indicated by a large standard deviation. This is probably caused by defects due to lack of covalent binding and heterogeneity on this surface, both of which also contribute to a much lower CPE *n* coefficient. The SAM chemistry showed the smallest capacitance change despite having a homogeneous surface and an increase in the CPE *n* coefficient. This poor performance might be associated with an interacion of the SAM with the tween 20 used during the blocking and washing steps [251]. This was however necessary to avoid signal drifting during impedance measurement

for all surface chemistries.

A one-way ANOVA test followed by Bonferroni's test correction showed that the change in capacitance for PA-functionalized IDEs was not significantly different from those functionalized with APTES and PMMA. Interestingly, APTES-functionalized IDEs showed a similar change in capacitance for antigen-antibody binding to that of the PMMA conformal coating despite only having the antigen immobilized in the space between electrodes. This can be explained by the increased electric field intensity in this region, shown by CPE *n* coefficient analysis and FEM.
On the other hand, the capacitance change for PMMA-functionalized IDEs proved to be significantly different from APTES ($P = 0.02$). Additionally, the capacitance change for PMMA-coated IDEs was reproducible and stable as this surface chemistry provided a compact and smooth surface (RMS roughness = 0.21 ± 0.02 nm), and a more ideal capacitive behavior (CPE *n* coefficient = 0.97). These findings corroborate other reports on PMMA showing good thermal and mechanical stability, along with dielectric properties suited for metal-insulator applications.[284]
For the aforementioned reasons, PMMA-functionalized IDEs were further investigated regarding the effect of the electrode size on the sensor performance. **Figure 6.7B** shows the capacitance change for antigen-antibody binding for three different sizes of IDEs. In contrast to the large change in capacitance found among the different insulation/immobilization layers, the variation in the IDE sizes does not seem to greatly affect the sensor response. However, the capacitance change from 5 × 5 μm (w × s) IDEs was slightly larger and presented a smaller standard deviation compared to 10 × 10 μm and 15 × 15μm IDEs. This was expected since it has been shown that for IDEs, 80% of the electric field flows within half of the sum of the width and spacing of the electrode digits.[285] This means that smaller electrodes are more specifically tuned to surface events and less sensitive to noise sources coming from the bulk of the solution.[285]

6.4.7. Specificity of the capacitive immunosensor

Finally, to assess the specificity of the PMMA capacitive immunosensors, we performed a specificity assay using a fluorescently labeled secondary antibody. Two negative controls were used consisting of PMMA coated IDEs functionalized with a non-specific antigen, and with no antigen on their surface, respectively. The results clearly indicated the specificity of the capacitive immunosensors using our approach (**Fig. 6.8**). Interestingly, when fluorescence imaging was performed to visually confirm the presence of the primary antibody in all surface, no fluorescence was detected for both controls (**Fig. S6.5** provided in supporting information). This result could suggest that the capacitance immunosensing is more sensitive than fluorescence under our experimental conditions.

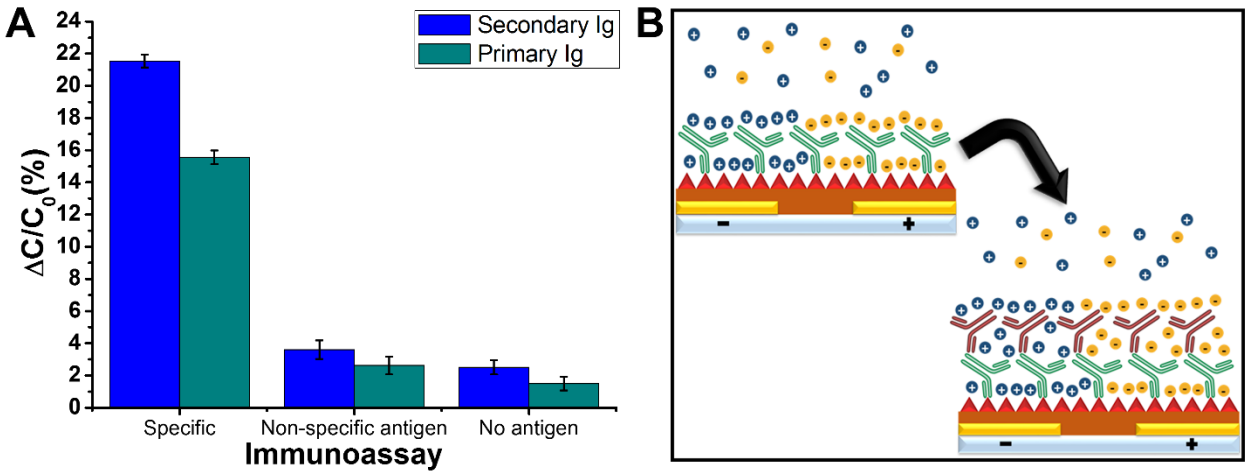

Figure 6.8. A) Capacitance change for a specific assay and two negative controls consisting of a PMMA surface functionalized with a non-specific antigen and no antigen. **B)** Schematic representation of the specificity assay with a secondary antibody performed for this experiment.

6.5. Conclusions

In this work, we assessed the insulation properties of four different chemistries by comparing the CPE *n* coefficient obtained through an equivalent circuit fitting. We found that spin-coated PMMA

on IDEs presented the most ideal capacitive behavior (CPE *n* coefficient = 0.97) among the investigated surface chemistries due to the formation of a packed and smooth surface, as indicated by AFM analysis (Rq = 0.21). Additionally, events occurring in the spacing areas between the IDEs showed to carry a significant weight in the overall change in capacitance. This was confirmed by: 1) the large change in capacitance for the APTES functionalization of the spacing area, 2) FEM simulations showing a 14% increase in the electric field intensity in IDEs spacing area compared to that on top of the electrodes and 3) a similar capacitance change in response to antigen-antibody binding to that of conformal coatings, despite having only half of the surface area functionalized. Comparing the capacitance change in response to antigen-antibody binding among chemistries, spin-coated PMMA IDEs produced the most reproducible and stable capacitance change. Additionally, we found that decreasing the IDEs size makes the system less sensitive to noise sources coming from the bulk of the solution, improving reproducibility. Overall, our finding suggests that polymeric conformal coatings are the most suitable candidates to improve the reproducibility and stability of capacitive immunosensors allowing them to become a reliable option for miniaturized devices and application in the rapidly growing field of point of care diagnostic devices.

Acknowledgments

The authors acknowledge the financial support from the Natural Science and Engineering Research Council of Canada (NSERC), the Fonds de Recherche Nature et Technologies-Team Grant, the NSERC-CREATE in ISS, and FRC scholarship from Consejo Nacional de Ciencia y Teconología de México (CONACyT) and Secretaría de Educación Pública de México (SEP). The authors will also like to thank all the staff from McGill University Nanotools-Microfab for their insights for the fabrication of the IDEs used in this work.

Supplementary information

Microfabrication protocol for IDEs, additional characterization measurement, and typical impedance spectra change for capacitive detection of antigen-antibody binding of the different insulation/immobilization chemistries.

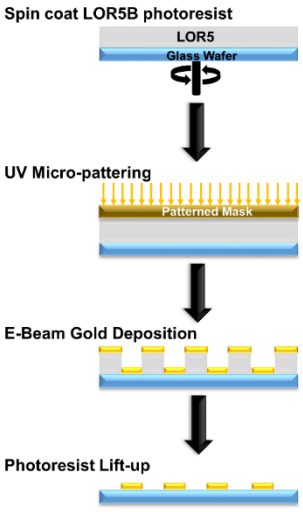

Figure S6.1. Schematic representation of the microfabrication process used to produce interdigitated electrodes (IDEs). First, LOR5B™ (Microchem, Newton, MA) is spin-coated onto the glass substrate and baked. Subsequently, a layer of Microposit™ S1813™ (Shipley, Marlborough, MA) is spin-coated and baked. The substrate is then exposed to UV light under a chrome photomask. After development of the IDE patterns with Microposit MF®–319 (Shipley) developer, 10 nm of titanium and 50 nm of gold are deposited onto the wafer. Finally, the substrate is immersed in Microposit Remover 1165 (Shipley) to lift off the metal layer and reveal the patterned electrodes.

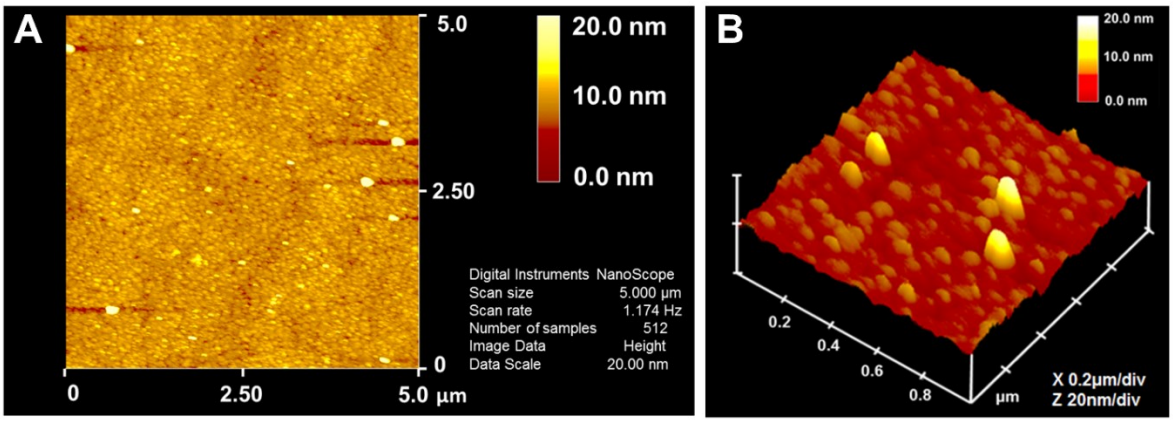

Figure S6.2. 5 µm^2 area on top of IDE electrode with passively adsorbed sensing antigens and blocking proteins in **A)** 2D, and **B)** 3D views.

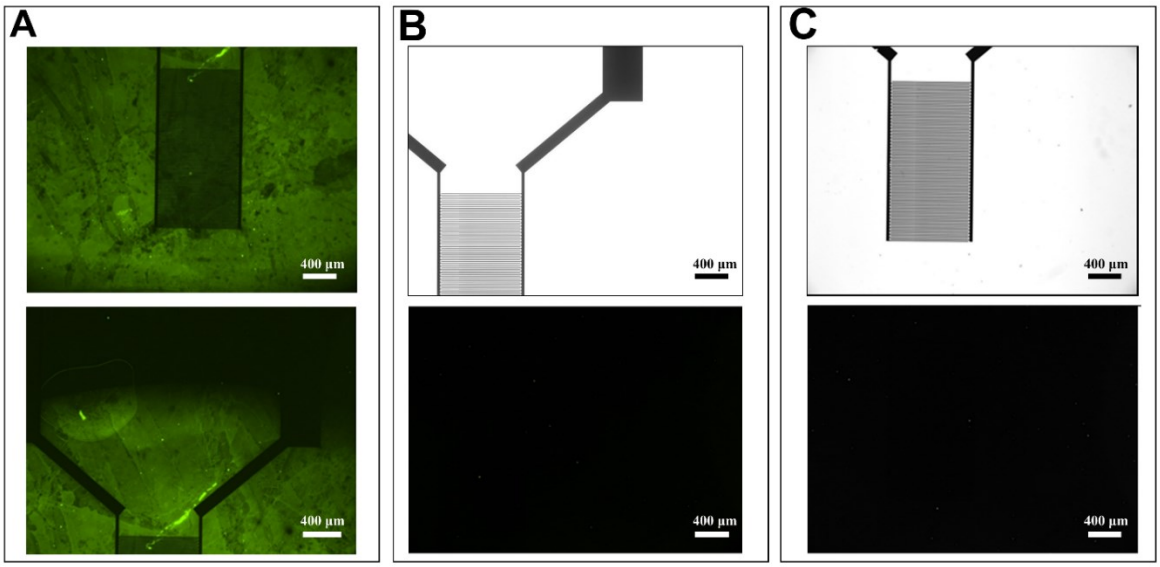

Figure S6.3. Fluorescent images of an immunoassay using fluorescently labled secondary antibodies for: **A)** an specific assay, **B)** non-specific antigen and **C)** no antigen. The images seen on the top and bottom correspond to the same area in light and fluorescent mode, respectively.

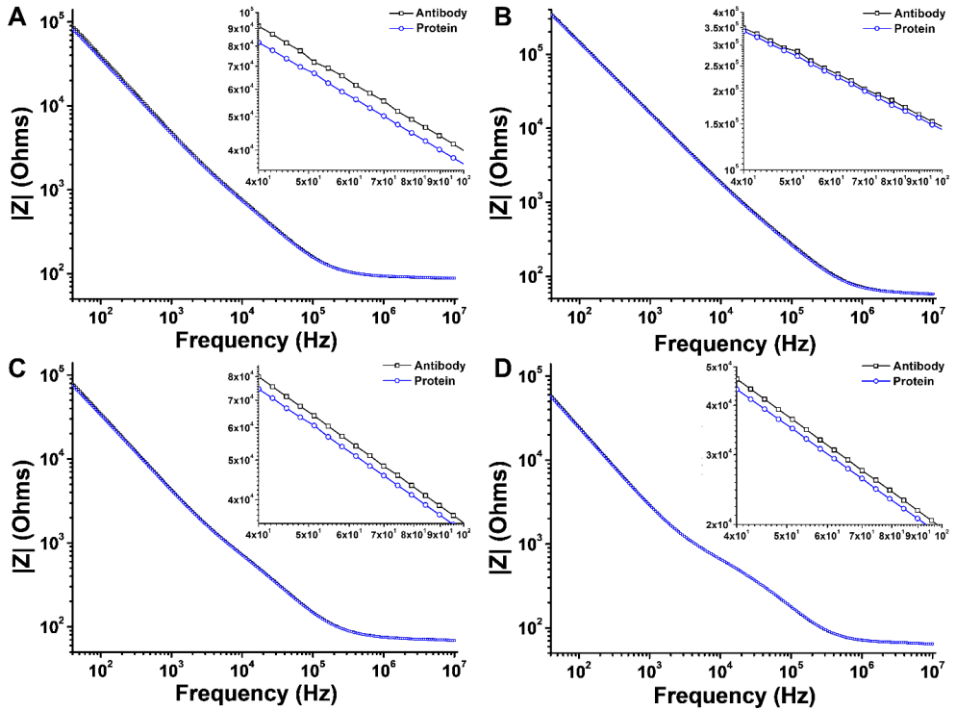

Figure S6.4. Typical impedance spectra before and after antigen-antibody binding for: **A)** PMMA conformal coating, **B)** alkyl thiol SAM on the Au electrode surface, **C)** APTES on the gaps between electrodes, **D)** conformal coatings via

passive adsorption of the antigen. Graph insets show a zoom on the graph to illustrate the line shift.

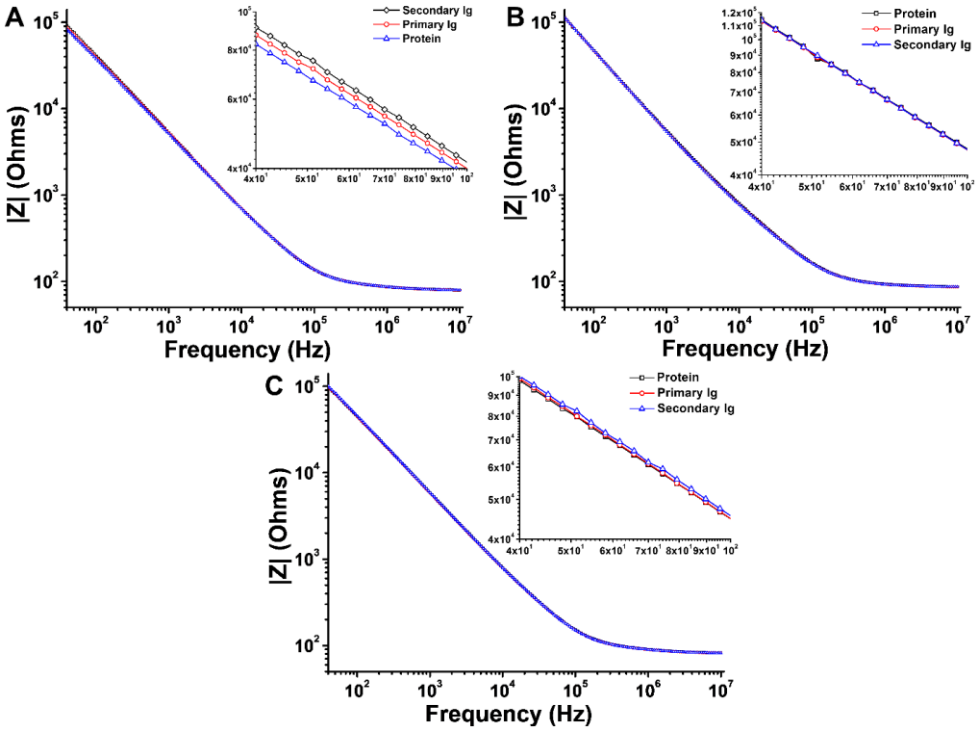

Figure S6.5. Typical impedance spectra before and after antigen-primary antibody binding and binding of a secondary antibody for: **A)** the specific assay, **B)** negative and **C)** positive control.

Chapter 7. Development of a multiplex biosensing strategy based on SPRi

Despite finding a robust insulation/immobilization chemistry for capacitive immunosensing in the previous chapter, it was found that further implementation for multiplex analysis could pose a challenge, due the sensor's long analysis time, which could hinder the dynamic detection of the islet secreted products. For these reasons, in this chapter a biosensor for simultaneous quantification of insulin, glucagon, and somatostatin was introduced. This sensor was based on SPRi, a technique known for its intrinsic high-throughput and multiplex quantification capabilities. Herein, the investigation of the optimal surface chemistry to maximize the assay's sensitivity and specificity was performed. The LOD and dynamic range on biosensor was evaluated for individual hormone detection and later for the multiplex mode achieving simultaneous detection of the three targeted hormones with a short analysis time. This chapter was published as an article in *Analytical Chemistry*.

Multiplex Surface Plasmon Resonance Imaging-Based Biosensor for Human Pancreatic Islets Hormones Quantification

F. Rafael. Castiello[†] and Maryam Tabrizian[*,†,‡]

[†]Biomedical and Biological Engineering Department, [‡]Faculty of Dentistry, McGill University, Montreal, QC, H3A 2B4, Canada.

7.1. Abstract

Diabetes arises from secretory defects in vascularized micro-organs known as the islets of Langerhans. Recent studies indicated that furthering our understanding of the paracrine effect of somatostatin on glucose-induced insulin secretion could represent a novel therapeutic avenue for diabetes. While many research groups are interested in insulin and glucagon secretion, few are particularly focused on studying the paracrine interaction in islets' cells, and none on monitoring a secretory fingerprint that contemplates more than two hormones. Surface plasmon resonance imaging can achieve high-throughput and multiplexed biomolecule quantification, making it an ideal candidate for detection of multiple islet's secretion products if arrays of hormones can be properly implemented on the sensing surface. In this study, we introduced a multiplex surface plasmon resonance imaging-based biosensor for simultaneous quantification of insulin, glucagon, and somatostatin. Performing this multiplex biosensing of hormones was mainly the result of the design of an anti-fouling sensing surface comprised by a mixed self-assembly monolayer of CH_3O-PEG-SH and 16-mercaptohexadecanoic acid, which allowed it to operate in a complex matrix such as an islet secretome. The limit of detection in multiplex mode was 1 nM for insulin, 4 nM for glucagon and 246 nM for somatostatin with a total analysis time of 21 min per point, making our approach the first reporting a label-free and multiplex measurement of such combination of human

hormones. This biosensor holds the promise of providing us with a mean for the further understanding of the paracrine effect of somatostatin on glucose-induced insulin secretion and consequently help develop novel therapeutic agents for diabetes.

7.2. Introduction

Diabetes mellitus affects 12.9% of the adult population in North America and the Caribbean region, from which type 2 diabetes (T2D) accounts for 90-95% of the cases [286]. Diabetes arises from secretory defects in the pancreatic islets of Langerhans, which are endocrine clusters of cells with an average diameter of 150 μm^2. The islets are vascularized micro-organs with five different types of cells (α, β, δ, PP, and ε) that cooperate for hormone secretion in response to metabolic changes [2, 3].

Recent studies indicate that the pancreatic islet's anatomy and physiology are species-dependent and that the unique cytoarchitecture of human islets has significant consequences for cell-to-cell communication within the islets [11]. For instance, secreted hormones from the different islets' cells may exert paracrine interaction on their neighbor cells [3, 5, 6]; particularly somatostatin whose inhibition has been shown to increase glucose-induced insulin secretion [16]. Further understanding of these paracrine effects may represent a therapeutic avenue for T2D [5, 6].

Up-to-date, most of the pancreatic islet research depends on traditional bioassays for hormone quantification such as patch clamp [13, 22-24, 287], capillary electrophoresis immunoassays (CEI) [25-27, 288], and ELISA [28, 29, 288]. Patch clamp has been used to study the secretion from individual islet β-cells [13, 22, 287] and α-cells [23, 24]. This technique provides quantitative information regarding exocytosis, by correlating the rate of capacitance change with the number of granules released at a given time [289]. However, the patch clamp technique requires

highly skilled operators to trap and manipulate individual cells, is low throughput, it only provides an indirect measurement of secretion, and it lacks specificity for individual secretion products. On the other hand, CEI has been used for direct detection of insulin [26] and glucagon [27] from pancreatic islets. During CEI experiments, islets are placed in a chamber, the effluent is mixed with the targeted hormone antibodies and fluorescent-labeled hormones. The secreted hormones from the islets then compete with fluorescent-labeled hormones for binding sites on the antibody. This mixture is then passed into an electrophoresis channel where bound and unbound fluorescent hormones are separated. Hormone secretion is then quantified fluorescently by establishing the ratio between bound and free hormone. As with patch clamp, CEI requires skilled operators to work effectively, precise temperature control, overcoming channel clogging, and the integration of lasers with different wavelengths [27]. Finally, although operational simpler, ELISA is difficult to use for simultaneous quantification, is time-consuming and expensive. Moreover, all mentioned techniques face many challenges when trying to expand them for simultaneous analysis of multiple targets.

While many research groups are interested in insulin and glucagon secretion [7-10], few are particularly focused on studying the paracrine interaction in islets' cells [5], and none on monitoring a secretory fingerprint (SF) for more than two hormones. Hence, to monitor an islets' SF, implementation of multiplexed analytical tools is required.

In this context, surface plasmon resonance imaging (SPRi) could be a useful tool to measure a pancreatic islet's SF. SPRi is now established as the gold standard to study biomolecular interactions such as antigen-antibody [42]. In addition to label-free and real-time analysis, SPRi can achieve high-throughput and multiplexed measurements through arrays of different molecules on the sensing surface [42]. In the last decade, SPR biosensors have mostly been used to investigate

fundamental physiological aspects of the major secreted islet hormones, namely insulin [44-46], somatostatin [47], pancreatic polypeptide [48, 49] and ghrelin [50]. However, there are no reports of a SPRi multiplex biosensor aiming to dynamically quantify more than two of the major secreted hormones. SPRi biosensors present an additional advantage for this particular application that involves measurements in a complex matrix such as the islet secretome. This advantage is provided by designing anti-fouling surfaces using self-assembled monolayers (SAM) that reduce interferences caused by non-specific adsorption of molecules on the sensor surface [74].

Here in, we introduce an SPRi-based biosensor for multiplexed detection of insulin, glucagon, and somatostatin. First, we studied the effect of composition on the anti-fouling properties of a mixed SAM of a thiolated polyethylene glycol (CH3CH3CHO-PEG-SH) and 16-mercaptohexadecanoic acid (MHDA). The antifouling properties of the biosensor were investigated by injecting two proteins: bovine serum albumin (BSA) and lysozyme (LYZ). Next, a competitive immunoassay protocol for insulin, glucagon, and somatostatin was implemented and the biosensor performance for individual hormones was determined. Finally, the biosensor performance was tested in multiplex mode performing simultaneous competitive immunoassays for the three hormones, and the limit of detection (LOD) and dynamic range were determined for each hormone in the mixture.

7.3. Experimental Section

7.3.1. Materials and Apparatus

Absolute ethanol was purchased from Fisher Scientific (Fair Lawn, NJ, USA), Phosphate-buffered saline (PBS) tablets, Tween 20, Glycine were purchased from BioShop Canada Inc. (Burlington, Ontario, Canada). Ethanolamine hydrochloride, N-(3-Dimethylaminopropyl)-N′-

ethylcarbodiimide hydrochloride (EDC), N-Hydroxysuccinimide (NHS), bovine serum albumin (BSA), Hydrochloric acid (HCl), human glucagon, human somatostatin, and Lysozyme (LYZ) were purchased from Sigma-Aldrich (St. Louis, MO, USA). Tris-buffered saline (TBS) with 1% Casein from BIO-RAD. Anti-insulin antibody (6.2 mg/mL) and human insulin were purchased from PROSPECT (Ness, Ziona, Israel). Anti-glucagon and Anti-somatostatin antibodies (200µg/mL each) were purchased from Santa Cruz Biotechnologies, Inc. (Mississauga, ON, Canada). CH_3O-PEG-SH (MW 1200 Da) was purchased from Rapp Polymere GmbH (Tübingen, Germany). 16-mercaptohexadecanoic acid (MHDA) was purchased from ProChimia Surfaces Sp. (Zacisze, Sopot, Poland).

SPRi detection was performed using a scanning-angle SPRi instrument (model SPRi-Lab+, Horiba, France). The SPRi apparatus, equipped with an 800 nm LED source, a CCD camera, and a microfluidic flow cell, was placed in an incubator at 25 °C (Memmert Peltier, Rose Scientific, Canada).

7.3.2. SPRi Measurements

For all experiments, the slope of the plasmon curves was automatically computed by the instrument's software to facilitate the selection of the working angle for kinetic analysis. This slope corresponds to the point of the plasmon curve at which the slope was maximum. Reflectivity shift (ΔR (%)) for all experiments was acquired upon stabilization of the baseline. Measured values were averaged of at least three spots for each sample including controls, and each experiment was repeated at least three times. At each step, the substrate was washed with the running buffer PBS-T (PBS with 0.002% Tween 20), and the difference in the reflected intensity was measured by taking into account the difference between the initial and final buffer signal. An injection loop with a fixed volume of 200 µL was used during experiments. A flow rate of 20 µL/min was used for all

experiments, with the exception of functionalization steps where the flow rate was adjusted depending on the required contact time.

7.3.3. Substrate Preparation

For single hormone-sensing, cleaned microscope glass slides (12 mm x 25 mm x 1 mm, n = 1.518) substrates were coated with 2 nm Cr as an adhesion layer, followed by the deposition of a thin Au layer of 48 nm using Electron-beam physical vapor deposition under high vacuum. Microscope glass slides were then coupled to an SF11 equilateral triangular prism (n_{SF-11} = 1.765) using a refractive index matching liquid. For multiplex sensing, similar gold-coated prisms (n = 1.765) purchased from Horiba Scientific-GenOptics, France, were used as received.

7.3.4. Surface Functionalization

Substrates were cleaned by subsequent immersion in absolute ethanol and deionized (DI) water and dried with a stream of nitrogen. Ethanolic solutions of 0.5 mM CH_3O-PEG-SH and 0.5 mM MHDA were prepared and mixed at different molar ratios from 100% MHDA to 90% CH_3O-PEG-SH: 10% MHDA. Substrates were immersed in the above mentioned ethanolic solutions overnight to allow self-assembly monolayer (SAM) formation. Finally, the substrates were thoroughly rinsed with absolute ethanol and DI water and dried under a stream of nitrogen.

Microscope slides with freshly prepared SAMs were immediately placed on the SPRi system for subsequent functionalization. First, conditioning was performed by 4 serial injections (contact time of 2 min each) of a regeneration solution containing 1M glycine pH 2.5 (1M-Gly). Then, the surface was rinsed with PBS-T until the baseline was stable. Next, NHS/EDC chemistry was used to covalently bind insulin, glucagon or somatostatin as reported by Gobi *et al*. [290]. Briefly, 200 µL of an aqueous solution containing 2 mg/mL NHS, 2 mg/mL EDC and 50 µg/mL of

the desired hormone were flowed over the sensor with a contact time of 1 h. Next, an injection of 200 µL (contact time 10 min) of 1M Ethanolamine hydrochloride pH 8.5 was performed to inactivate unfunctionalized -COOH groups on the sensor surface. Then, two serial injections of regeneration solution (contact time 1 min each) were performed to remove weakly bound hormones. Finally, a blocking solution containing 1% casein and 5% BSA in TBS buffer was injected with (contact time of 30 min) and subsequently, at least 3 injections of the regeneration solution were made to remove weakly bound proteins. **Figure 7.1** shows a graphical representation of a typical sensor functionalization.

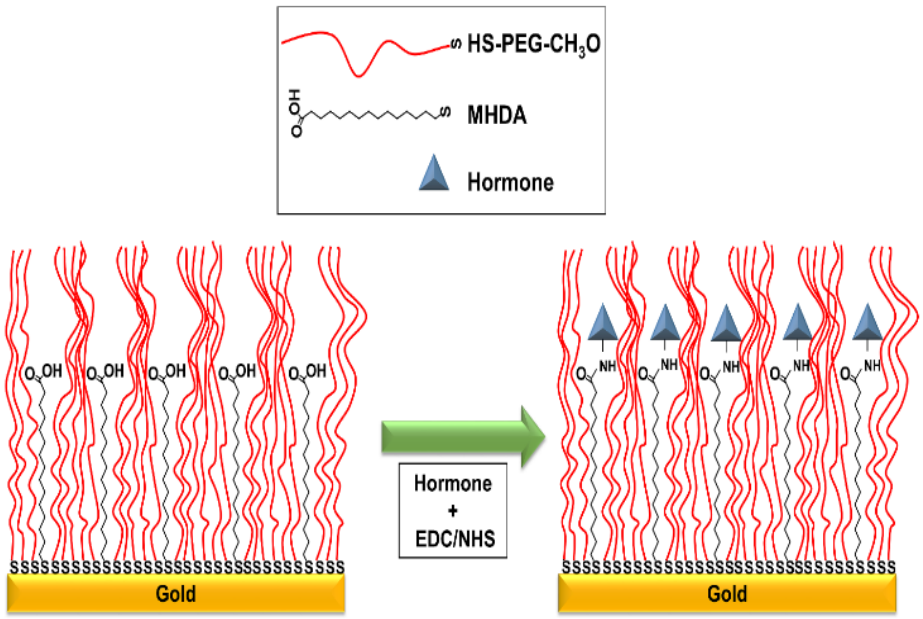

Figure 7.1. Schematic representation of the surface functionalization of thin Au films used in this study. The surface is composed of a mix SAM of 16-Mercaptohexadecanoic (MHDA) as a linker and a thiolated PEG (CH_3O-PEG-SH) as a spacer and anti-fouling agent incubated overnight. Targeted hormones are covalently immobilized to the surface using EDC/NHS chemistry in an aqueous solution.

For the functionalization of gold-coated prisms in multiplex measurement mode, the procedure described for microscope slides was followed with some minor changes. After conditioning, 4 individual solutions containing NHS/EDC (2 mg/mL each) and 50 µg/mL of insulin, glucagon, somatostatin or BSA were spotted (150 nL) in triplicate on the surface of the

prism and incubated in a humidity chamber for 1h. Immediately after, the prism was rinsed with a copious amount of DI water and subsequently immersed in 1M ethanolamine hydrochloride pH 8.5 for 10 min. Next, the prism was immersed in the blocking solution for 30 min, subsequently rinse with DI water and placed in the SPR flow chamber. Then, the regeneration solution was injected at least three times to obtain a stable baseline before beginning with the competitive immunoassays.

7.3.5. Competitive Immunoassay

For multiplex assays, standard solutions containing insulin, glucagon and somatostatin were prepared in PBS-T buffer at a concentration range of 1-4000 ng/mL and mixed with a cocktail of antibodies containing anti-insulin (1 μg/mL), anti-glucagon (2 μg/mL) and anti-somatostatin (2 μg/mL). These mixtures were incubated for 2 min under gently mixing and serially injected over the spotted sensor chip from highest to lowest hormone concentration (contact time of 10 min) starting with a blank solution containing only the antibody cocktail. Each sensing cycle comprised: sample injection 10 min, 5 min buffer washing and 2 injections of regeneration solution (1M-Gly) with a contact time of 25s with 3 min washing with buffer in-between. For individual immunoassays, same conditions were used, with the exception of somatostatin, for which the assay concentration ranged from 50 to 8000 ng/mL.

For all competitive immunoassays, the optimal antibody concentration was defined as the concentration that could generate a small but detectable SPR signal of $\Delta R \approx 1$ which has been previously reported as a reliable ΔR for this type of assays [291].

7.3.6. Statistics

For all competitive immunoassays, relative binding (C/C_0) was calculated by dividing the response of the standard solutions containing hormones (C) by the response of the blank solution containing

only a fixed concentration of antibodies (C_0). To generate calibration curves C/C_0 was plotted against hormone concentration. The calibration curves were fitted using a non-linear 4 parameter logistic (4PL) model. The lower limit of detection (LOD) for all immunoassays was calculated from the calibration curves as the blank signal (C_0) minus three times the standard deviation. The dynamic range for the competitive immunoassay was established between 0.2 C/C_0 and 0.8 C/C_0. All data is expressed as the average of at least 3 independent experiments ± standard deviation (SD).

7.4. Results and Discussion

7.4.1. Effect of SAM Composition on the Sensor Response

SAMs are typically used as a linker layer for immobilization of biological components at the transducer surface of biosensors [74]. A necessary procedure when developing a competitive immunoassay is limiting the amount of competing antigen and antibody in order to maximize the assay's sensitivity. Typically, commercial SPR chips achieve this by fixing the SAM composition and controlling the surface density of the analyte, either by changing the contact time or the concentration of the analyte during functionalization [292]. However, in a mass-sensitive technique such as SPR, the detection of small molecules (such as the target peptides in this study) is challenging, requiring careful design of the surface chemistry to ensure optimal sensitivity [293]. Thus, the linker to spacer ratios must be studied in detail on a case basis.

In this work, a mixed SAM comprised of a linear thiol with a carboxyl end group (MHDA) was used for hormone immobilization, along with a low molecular weight thiolated PEG (CH_3O-PEG-SH) that acts as a spacer and as an anti-fouling agent [294]. These compounds are used in a regular basis for biosensor development; however, this work presents the first report using them in

combination. Additionally, contrary to the majority of the reports in literature [74], our study presents a long chain compound as a spacer and a short chain as anchor. Thus, the results obtained could be counter intuitive when compared to previous reports. In addition, SAM composition plays an important role on the final surface density of immobilized biomolecules; thus, a preliminary study was performed to evaluate its effect on the sensor's response. Since somatostatin was the smallest of the targeted hormones, it was used as the 'reference' hormone for this study.

Figure 7.2 shows the change in reflectivity for a fixed amount of anti-somatostatin antibodies (1µg/mL) over different SAM compositions. With 100% and 50% MHDA a large signal can be observed. Interestingly a change occurred after 50% PEG molar fraction, the signal abruptly diminished and it was barely present for 70% and 90% PEG molar fractions. This could be explained by the fact that mixtures of n-alkanethiols of different chain lengths tend to form SAMs with a composition enriched with the longer alkanethiol [74]. Thus, very little amount of linker is left on the surface to covalently bind somatostatin.

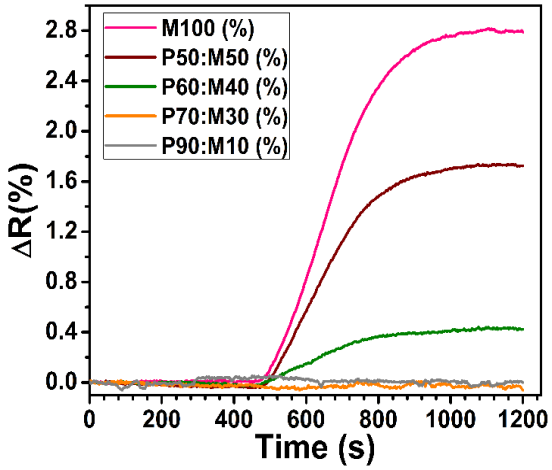

Figure 7.2. SPR reflectivity change response of 1µg/mL of anti-somatostatin antibody for different SAM compositions. P and M stand for CH_3O-PEG-SH and MHDA respectively.

For 70% and 90% PEG molar fractions, it was necessary to increase 20-30 times the anti-somatostatin antibody concentration, to obtain a measurable SPR signal. This presents some

disadvantages for the sensor operation for the following reasons: 1) for a competitive immunoassay, a large amount of antibodies will be poorly inhibited by a small amount of analytes [295]. 2) Each data point in this type of assays requires the injection of a fresh antibody solution; hence, a high amount of antibodies will increase reagent consumption and operational costs.

On the other hand, with 100% and 50% MHDA surface regeneration proved to be challenging when compared to 40% MHDA (**Figure S7.1**). Thus, we set the final composition of SAM as 60% PEG-40% MHDA to incorporate the maximum amount of PEG and still get a detectable signal, even with a relatively low antibody concentration.

7.4.2. Single Step Hormone Immobilization

The hormones used in this work are small peptides possessing an N-terminal group which could be used for immobilization on the sensor surface, through an amide bond formation with the carboxyl group on the MHDA. The surface functionalization was performed in a single step as reported by Gobi *et al*. [290]. Compared to typical two-step NHS/EDC processes where buffer solutions with a variety of pH are required [296, 297], the single step functionalization offers the advantage of reducing the functionalization time and pH adjustments for all hormones since the reaction is performed in aqueous solution. This is particularly advantageous when preparing SPR surfaces using several hormones solutions.

After chip conditioning, individual hormones and the immobilization reagent (a mixture of NHS/EDC) were injected over the sensor chip. Once the solution reached the surface, the SPR angle decreased slightly follow by a steady angle increase to reach nearly a plateau representing surface saturation. At the end of the injection, the surface was washed with running buffer until a stable baseline was obtained. Finally, in order to make the sensor surface homogeneous, a blocking agent containing 5% BSA and 1% casein (w/w) in TBS buffer was injected with a total contact

time of 30 min. At the end of the injection, running buffer was allowed to wash the surface until stabilization of the SPR signal occurred. After this point, at least 2 injections of regeneration solution were used to remove any weakly adsorbed BSA and casein. Once the baseline was stabilized, the difference in SPR angle before and after the blocking step was measured.

Table 7.1 shows the corresponding mean reflectivity change observed after the individual hormone functionalization and its corresponding blocking step (n=3). Interestingly, since the available functionalization sites are fixed, the reflectivity change values for each hormone functionalization proved to be proportional to their differences in molecular weight (MW insulin>glucagon>somatostatin).

Table 7.1. SPR mean reflectivity change after individual hormone functionalization and their corresponding blocking step.

Hormone	ΔR (%) Functionalization	ΔR (%) Blocking
Insulin	8.26 ± 0.57	0.3 ± 0.07
Glucagon	4.57 ± 0.32	0.26 ± 0.06
Somatostatin	3.36 ± 0.66	0.89 ± 0.17

7.4.3. Biosensor performance for individual immunoassays

Direct immunoassays of small molecules by SPR can be challenging since the SPR signal is directly related to the change in mass at the sensor surface. Consequently, the immunoassays in the present work were performed in a competitive manner where inhibition of antibody binding is due to binding occurring with hormones in solution. Thus, the higher the concentration of hormones in solution, the smaller the SPR signal and vice versa (**Figure 7.3).**

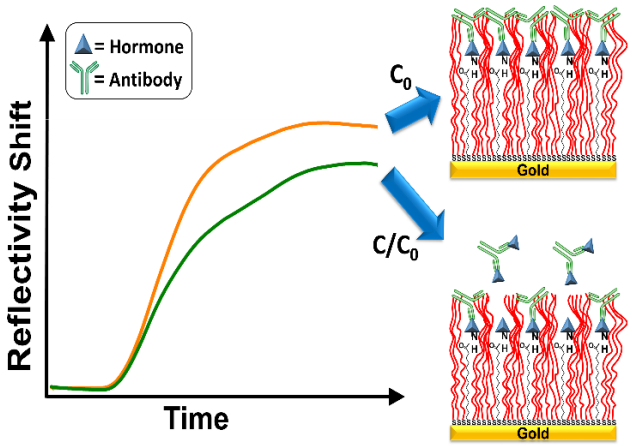

Figure 7.3. Graphical representation of a competitive immunoassay over the sensor surface. After formation of a mixed SAM and functionalization with the targeted hormone covalently linked to the SAM, inhibition of the blank solution with optimal antibody concentration (C_0) follows due to binding occurring with hormones in solution (C/C_0). Thus, the higher the concentration of hormones in solution, the smaller the SPR signal and vice versa.

In general, competitive immunoassays require the use of a small antibody concentration so that slight amounts of the analyte can inhibit antibody binding to the surface [295]. For this reason, the optimal antibody concentration for each hormone was defined as the concentration of the antibody that could generate a small but detectable SPR signal of $\Delta R \approx 1$ [291]. This corresponded to an antibody concentration of 1, 2 and 2 μg/mL for anti-insulin, anti-glucagon and anti-somatostatin respectively.

To study the sensor performance, standard solutions containing either insulin, glucagon or somatostatin were prepared in PBS-T. Then, the optimal amount of antibody was added to the standard solution and gently mixed for a pre-defined period of time before injecting into the SPR system. Somatostatin was particularly sensitive to incubation conditions during this step. After testing different time and mixing conditions, it was found that 2 min incubation under gently manual agitation provided optimal conditions for sensing (data not shown).

Figure 7.4 shows the sensor calibration curves for insulin (**Figure 7.4A**), glucagon (**Figure 7.4B**) and somatostatin (**Figure 7.4C**). For each hormone, mean relative binding values (C/C_0) were plotted as a function of hormone concentration (ng/mL). For each experiment, the entire sensor

surface was functionalized and the mean SPR shift was measured on at least 10 spots from different regions of the chip. Then, an average of these SPR shifts from 3 independent sensors was calculated and the bars in **Figure 7.4** represent the corresponding SD. The LOD and dynamic range for individual immunoassays are shown in **Table 7.2.**

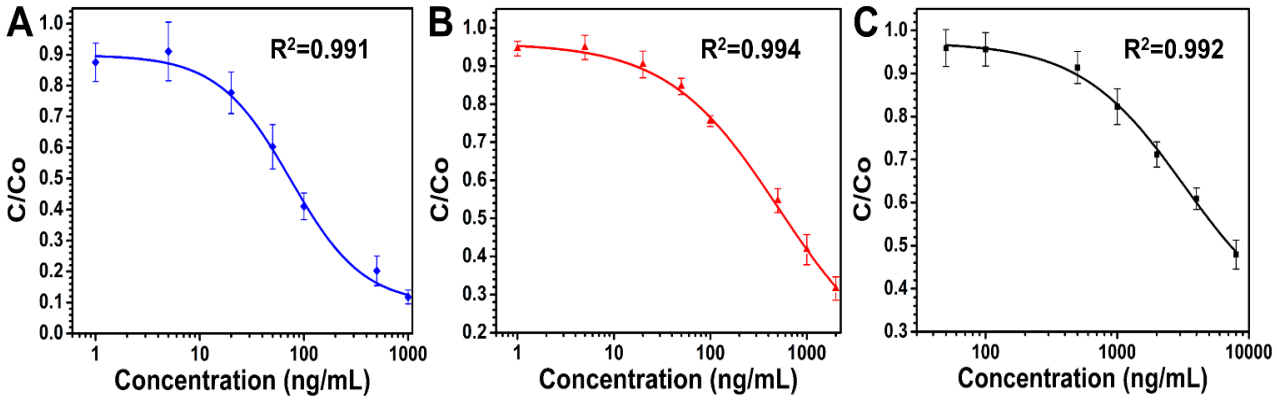

Figure 7.4. Individual hormone calibration curves in PBS-T for **A)** insulin, **B)** glucagon and **C)** somatostatin. For each hormone mean relative binding values (C/C_0) were plotted as a function of hormone concentration (ng/mL). Relative binding was calculated by dividing the response for each concentration (C) by the response from a solution containing only the optimal concentration of individual antibodies (C_0). Solid lines correspond to the fitting of a non-linear 4PL model. Error bars represent the standard deviation from 3 independent experiments (n=3).

Additionally, we tested different sensor regeneration solutions including: 10-50mM NaOH, 10mM NaOH-1-20% (v/v) acetonitrile, 0.1-1M glycine (pH 2-3), 0.1-1M glycine-1% (v/v) DMSO and 2M $MgCl_2$, 0.1-1M glycine-1% (v/v) DMSO and 2M $MgCl_2$ (data not shown). From these solutions, 1M glycine with a pH=2.5 provided the more efficient conditions for surface regeneration.

Table 7.2. SPR sensing performance for single hormones. All values were calculated from the non-linear 4PL fit equation derived from individual calibration curves. The reported LOD was calculated as the response of the blank (C_0) minus 3 times the standard deviation. *Highest concentration tested.

Hormone	ΔR (%) (C0)	LOD [ng/mL]	LOD [nM]	Dynamic Range [ng/ml]
Insulin	1.47±0.06	12	2	15-338
Glucagon	1.25±0.02	4	1	72-2000*
Somatostatin	1.11±0.03	409	250	1237-8000*

Finally, the sensor's resistance to non-specific absorption of proteins was determined by separately injecting BSA and LYZ with a final concentration of 1 mg/mL. The injection of these solutions was performed at the end of each calibration curve experiment under the same experimental condition as the standard solutions used during hormone sensing. The shift in reflectivity was measured after 10 minutes of contact time and 5 minutes PBS-T wash. For all cases, during BSA injection the SPR angle increased abruptly and later returned to a slightly smaller baseline value, likely due to the high bulk refractive index change during the injection. This can be interpreted as a negligible accumulation of BSA on the sensor surface. In the case of LYZ injection, the sensor registered a positive increase in the baseline value immediately after the buffer washing step. The adsorbed amount of LYZ was less than 100 pg/mm^2 for all hormone-functionalized surfaces. This value is consistent with the definition of an antifouling surface [294]. Moreover, a single injection of regeneration solution for 25 s returned the baseline to its original value, indicating a weak interaction of LYZ on the sensor's surface. **Table S7.1** in supporting information shows the mean (n=3) SPR response to BSA and LYZ immediately after buffer washing.

7.4.4. Biosensor performance for multiplex immunoassays

Multiplex hormone detection was achieved by simultaneously performing 3 immunoassays. Once the different hormones were immobilized on the surface and the chip blocked, the spot cross-reactivity was investigated. **Figure 7.5** shows the sensor response to individual injection of the optimal antibody concentration of anti-insulin (**Figure 7.5A**), anti-glucagon (**Figure 7.5B**) and anti-somatostatin (**Figure 7.5C**). The typical sensor response to a blank solution (mix of all antibodies) is shown in **Figure 7.5D**. Each injection caused an increase in SPR signal on the relevant spot, indicating specific binding and low cross-contamination between the spots. A certain level signal variation was observed between individual injections of antibodies (**Figure 7.5A-C**)

and the injection of the antibody mix (**Figure 7.5D**). This signal variability may arise due to subsequent injection and regeneration of the sensor's surface since the multiplex sensor presented a similar performance to that of the individual sensors, as shown later in this section. This did not represent a major drawback during the sensor operation, as we recorded consistent and reproducible measurement during all of our experiments.

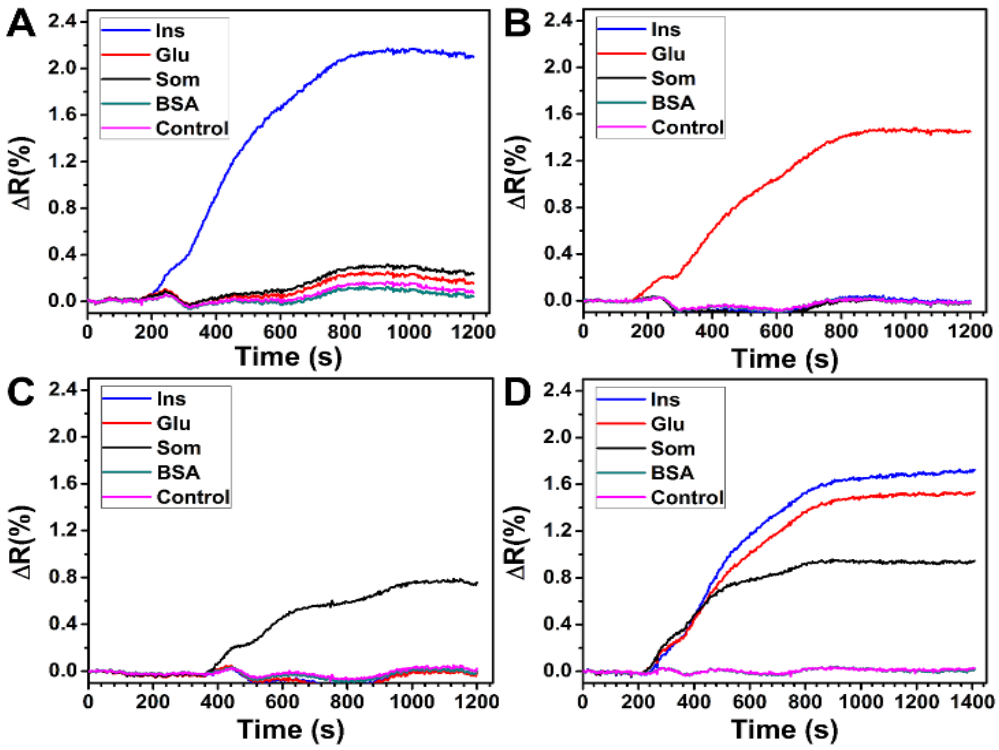

Figure 7.5. Spot specificity on a multiplex sensing surface for **A)** anti-insulin, **B)** anti-glucagon and **C)** anti-somatostatin. **D)** Typical blank solution response (C_0) for multiplex immunoassays. Immobilized BSA (green line) and the bare SAM surface, identified in the graphs as "Control" (pink line), were used as negative controls.

For this experiment, two negative controls were used: the bare SAM surface and spots functionalized with BSA, as identified by "Control" (pink color) and BSA (green color) in **Figure 7.5**. As it can be seen in **Figure 7.5D**, there was a negligible response on the BSA and "Control" spots when exposed to the blank solution, indicating the high anti-fouling properties of the sensor. To further determine the anti-fouling properties of the sensor in multiplex mode, separate injections of BSA and LYZ with a final concentration of 1 mg/mL were performed. As with individual sensing

experiments, BSA injection resulted in a small decrease of the baseline while LYZ lead to a slight increase in the baseline value measured after buffer washing. Similarly to individual assays the adsorbed amount of LYZ was well within the definition of an antifouling surface [294] (less than 100 pg/mm^2). The mean SPR response of the multiplex sensor for BSA and LYZ immediately after buffer washing is reported in supporting information (**Table S7.2**).

For the multiplex assays, freshly prepared standard solutions (PBS-T) containing a mixture of insulin, glucagon, and somatostatin were prepared. The optimal amount of antibodies was then added and gently mixed for 2 min before injecting into the SPR system. **Figure 7.6** shows the calibration curves for multiplex sensing of insulin (blue), glucagon (red) and somatostatin (black). For each hormone, mean relative binding values (C/C_0) were plotted as a function of hormone concentration (ng/mL). During experiments, the mean SPR shift was measured in at least 3 spots for each hormone and the controls. Then, an average of these SPR shifts from 3 independent sensors was calculated, and the bars in **Figure 7.6** represent the corresponding SD. The LOD and dynamic range for multiplex immunoassays is shown in **Table 7.3.** Typical SPR curves for the multiplex detection mode can be found in supporting information (**Figure 7.S3-6**).

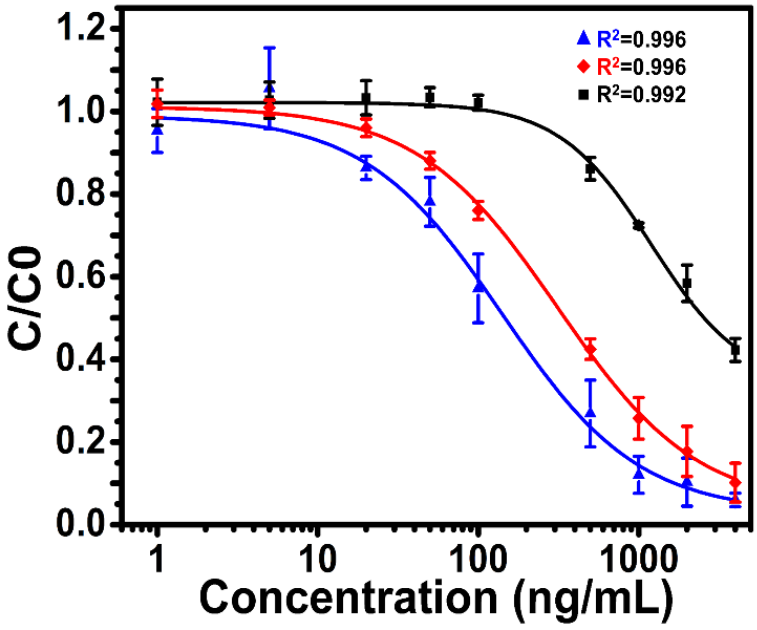

Figure 7.6. Multiplex hormone calibration curves in PBS-T for insulin (blue), glucagon (red) and somatostatin (black). For each hormone, mean relative binding values (C/C_0) were plotted as a function of hormone concentration (ng/mL). Relative binding was calculated by dividing the response of a range of standard solutions containing a mix hormones (C) by the response of the blank solution containing only a fixed concentration of antibodies (C_0). Solid lines correspond to the fitting of a non-linear 4PL model. Error bars represent the standard deviation from 3 independent experiments (n=3).

The LOD of the sensor in multiplex mode was very similar to that of individual sensors. However, it can be noticed that the dynamic range for each hormone is different from each other. This could be as a result of variations in the hormones' surface density caused by the surface functionalization of the gold-coated prism outside of the SPR system.

Table 7.3: SPR sensing performance for multiplexed immunoassays. All values were calculated from the non-linear 4PL fit equation derived from individual calibration curves. The reported LOD was calculated as the response of the blank (C_0) minus 3 times the standard deviation.

Hormone	Max ΔR (%) (C0)	LOD [ng/mL]	LOD [nM]	Dynamic Range [ng/ml]
Insulin	1.69 ± 0.02	8	1	34-633
Glucagon	1.52 ± 0.01	14	4	85-1592
Somatostatin	0.93 ± 0.03	403	246	719-4000*

*Highest concentration tested

Interestingly, the LOD of the SPR immunoassays in the multiplex mode were one order of magnitude higher than their corresponding ELISA assays (pg/mL). However, the high sensitivity

of the ELISA method is not necessarily required for the detection of hormones directly secreted by a population of islets. For instance, previous reports demonstrated individual detection of insulin [25] and glucagon [26] secreted (LOD) from 10 islets was 10 and 5 nM respectively at 15mM glucose.

Since the number of somatostatin secreting cells within the islets is usually smaller than that of insulin or glucagon-secreting cells [11], further protocol optimization could be required. Nevertheless, if the future detection of islet secretion products requires signal amplification, this could be readily addressed using gold nanoparticles, either within the sensing surface itself or as signal enhancing agent to increase the LOD of the present SPR immunoassays [298].

7.5. Conclusion

In this work, we introduced a strategy for label-free and multiplex detection of pancreatic islet hormones with a LOD of 1 nM for insulin, 4 nM for glucagon and 246 nM for somatostatin with a total analysis time per point of 21 min using a SPRi-based biosensor. The sensor showed comparable performance to previous reports where direct secretion of insulin and glucagon from a population of islets have been studied. The sensor exhibited excellent anti-fouling properties and specificity due to the design of a mixed SAM of a thiolated polyethylene glycol and 16-mercaptohexadecanoic acid showing a negligible response to a concentration of 1 mg/mL of BSA and a very little response to LYZ. This show promise for the future operation of the sensor in a complex matrix such as a pancreatic islet secretome. The present SPRi-based biosensor could be easily integrated with previously developed microfluidic perfusion devices, which trap and reproduce the natural *in vivo* conditions of the islets, allowing real-time secretion analysis of pancreatic islet secretion. Such biosensing platform holds the potential to monitor a small islet's

secretory fingerprint, allowing further understanding of the paracrine effect of somatostatin on glucose induces insulin secretion as well as comprising a drug screening platform for the discovery of novel therapeutic agents for the treatment of diabetes.

Acknowledgment

The authors acknowledge the financial support from the Natural Science and Engineering Research Council of Canada (NSERC), the Fonds de recherche nature et technologies-Team Grant, the NSERC-CREATE in ISS, and FRC scholarship from Consejo Nacional de Ciencia y Teconología de México (CONACyT) and Secretaría de Educaión Pública de México (SEP). The authors are also thankful to F. Melaine for her insightful discussions during the development of this work.

Associated Content

Supporting Information

Quantitative data of non-specific adsorption of BSA and LYZ on individual and multiplex mode, and typical SPR curves for multiplex mode sensing.

Table S7.1. Individual hormone sensing non-specifics quantification from BSA and LYZ each at 1 mg/mL final concentration.

Hormone	ΔR (%) BSA [1mg/mL]	ΔR (%) LYZ [1mg/mL]	Amount of LYZ absorbed (pg/mm^2)
Insulin	-0.01 ± 0.01	0.19 ± 0.01	110 ± 6
Glucagon	-0.17 ± 0.03	0.14 ± 0.02	81 ± 12
Somatostatin	-0.02 ± 0.01	0.17 ± 0.02	98 ± 12

Table S7.2. Multiplex hormone sensing non-specifics quantification from BSA and LYZ each at 1 mg/mL final concentration. Quantification was performed for negative control spots functionalized with BSA and the bare SAM surface (control).

Spot	ΔR (%) BSA [1mg/mL]	ΔR (%) LYZ [1mg/mL]	Amount of LYZ absorbed (pg/mm^2)
Insulin	-0.06 ± 0.03	0.16 ± 0.02	93 ± 12
Glucagon	-0.07 ± 0.05	0.08 ± 0.03	47 ± 17
Somatostatin	-0.07 ± 0.02	0.17 ± 0.05	99 ± 29
Control	-0.03 ± 0.02	0.15 ± 0.02	87 ± 12
BSA	-0.03 ± 0.02	0.02 ± 0.01	12 ± 6

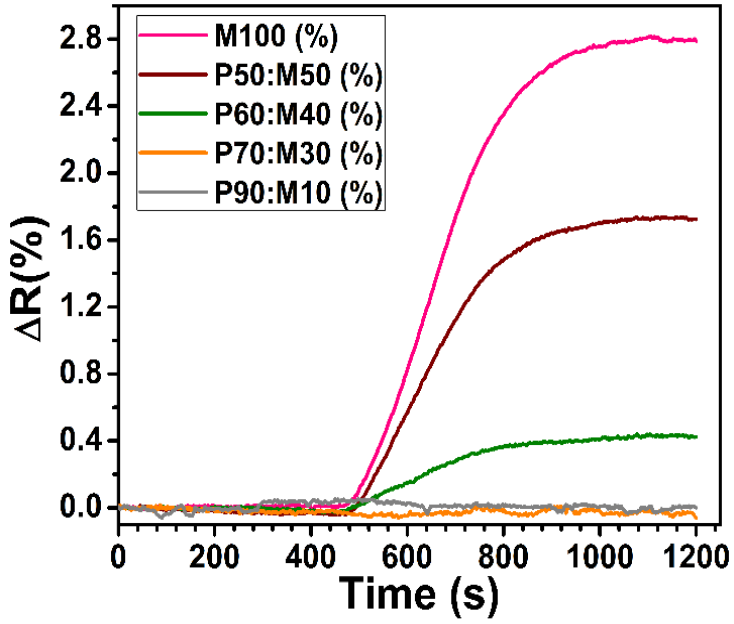

Figure S7.1. SPR reflectivity change response of 1 μg/mL of anti-somatostatin antibody for different SAM compositions. P and M stand for CH_3O-PEG-SH and MHDA respectively.

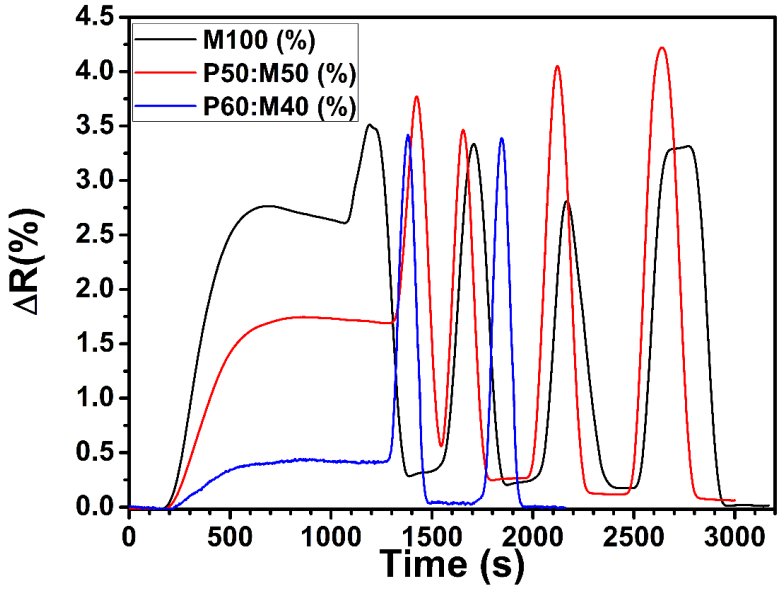

Figure S7.2. Typical regeneration experiment for different composition of SAMs. P and M stand for CH_3O-PEG-SH and MHDA respectively.

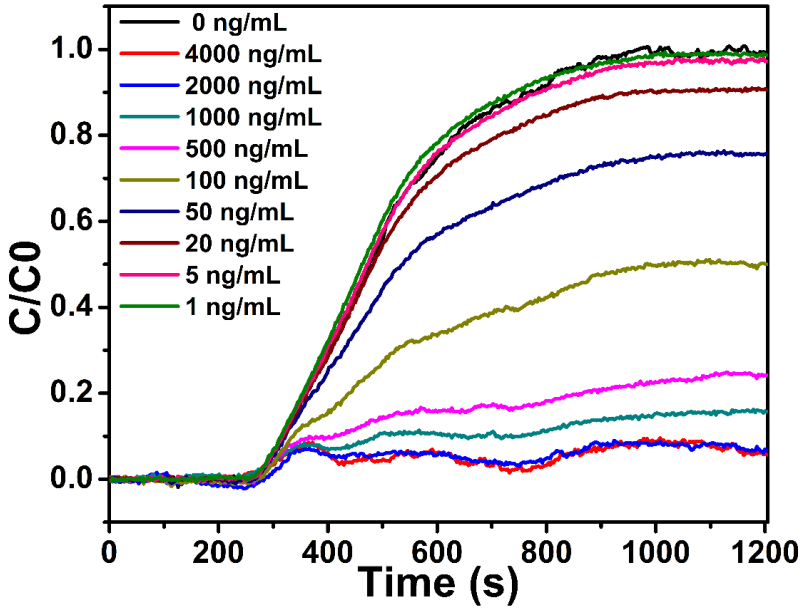

Figure S7.3. Typical insulin SPR curves during multiplex sensing. Relative binding (C/C_0) was calculated by dividing the response for each concentration (C) by the response from a solution containing only the optimal concentration of individual antibodies (C_0).

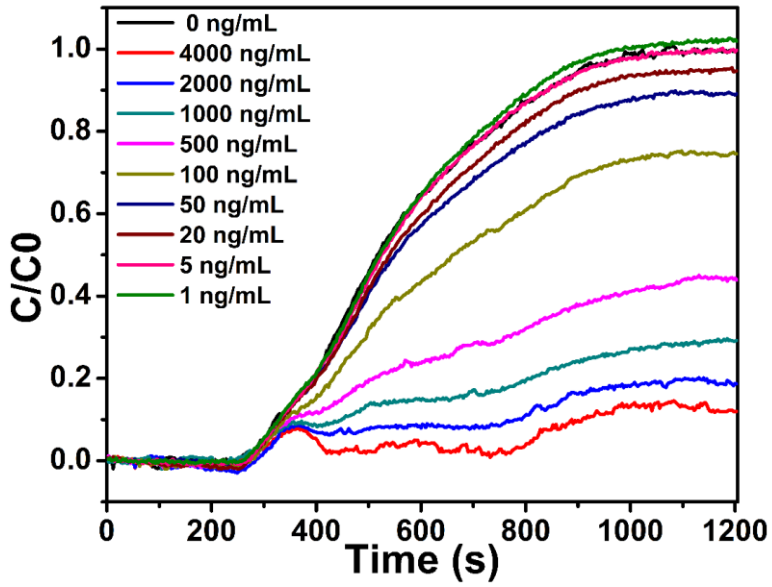

Figure S7.4. Typical glucagon SPR curves during multiplex sensing. Relative binding (C/C_0) was calculated by dividing the response for each concentration (C) by the response from a solution containing only the optimal concentration of individual antibodies (C_0).

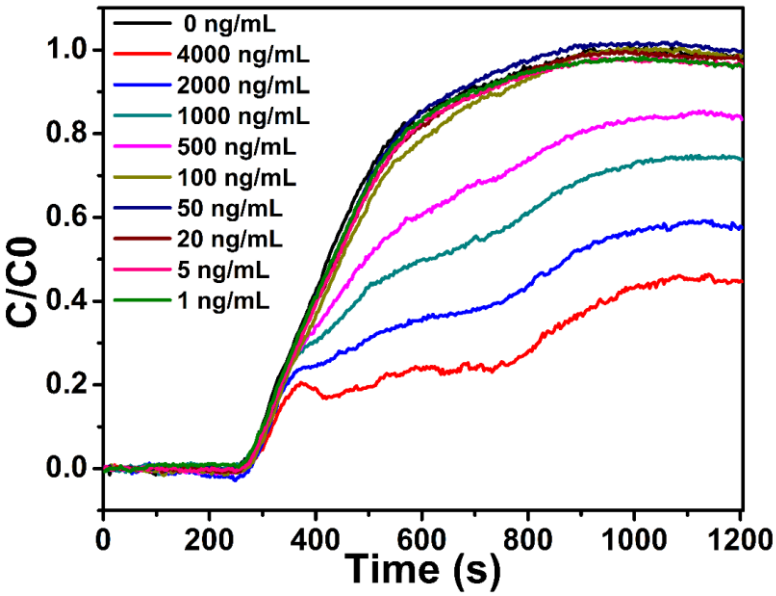

Figure S7.5. Typical somatostatin SPR curves during multiplex sensing. Relative binding (C/C_0) was calculated by dividing the response for each concentration (C) by the response from a solution containing only the optimal concentration of individual antibodies (C_0).

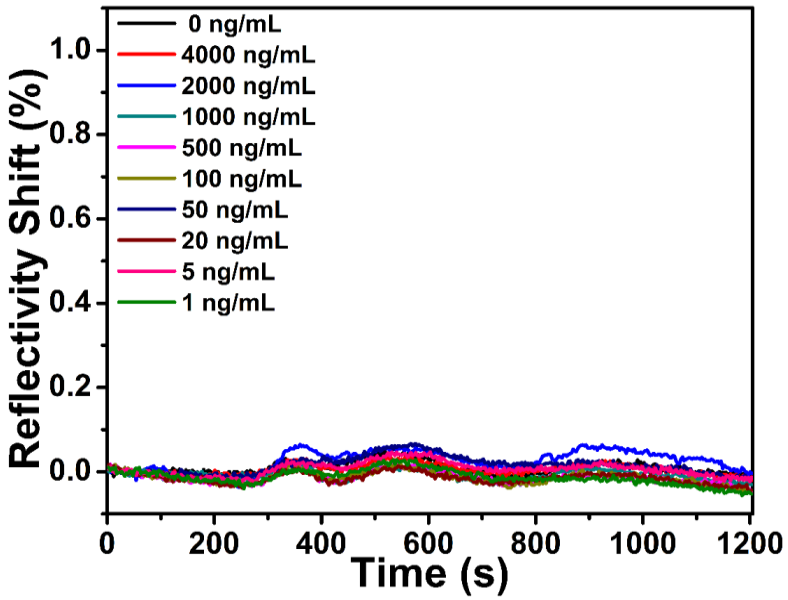

Figure S7.6. Typical BSA spot SPR curves during multiplex sensing.

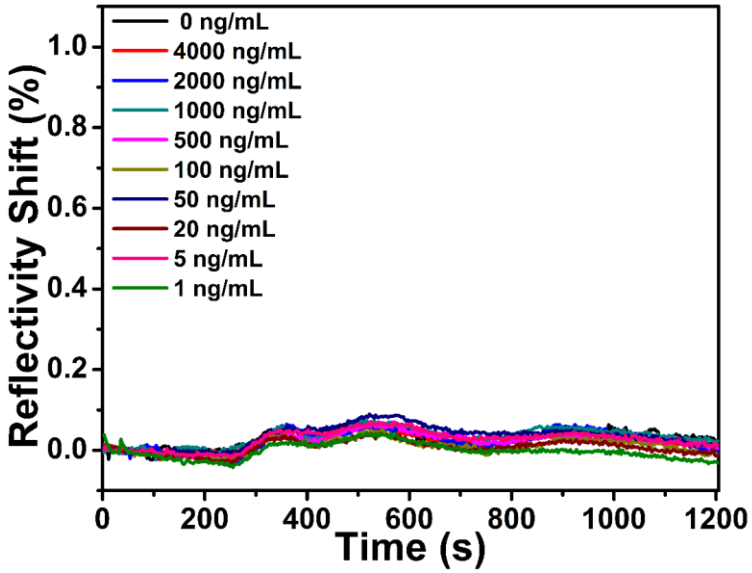

Figure S7.7. Typical control (Bare SAM surface) SPR curves for multiplex sensing.

Chapter 8. Signal amplification strategies for multiplex SPRi-based biosensors

This chapter presents a detailed study that compares three different amplification strategies commonly used for SPRi biosensors. This investigation is essential to enable the possibility of detecting all three targeted hormones in a biologically relevant concentration range with a higher degree of confidence before moving to precious and scares human islets studies. Particularly, to ensure that somatostatin secreted from a small population of islets can be effectively and accurately detected. The dynamic range and sensitivity of the SPRi biosensor presented in Chapter 7 were improved using gold nanoparticles (GNPs). For this study, three GNPs amplification strategies were compared: GNPs immobilized on the sensor surface, GNPs conjugated with primary antibodies and GNPs conjugated with a secondary antibody. The content of this chapter was published in the journal *Analyst*.

Multiplex SPRi-based immunoassay using gold nanoparticle amplification strategies for quantification of human pancreatic islet hormones

F. Rafael. Castiello[a] and Maryam Tabrizian[a,b].

[a] Biomedical Engineering Department, McGill University, Montreal, QC, Canada.
[b] Faculty of Dentistry, McGill University, Montreal, QC, Canada.

KEYWORDS diabetes mellitus, biosensing, pancreatic islets, hormones, gold nanoparticles, amplification.

8.1. Abstract

In this work, we demonstrate the potential use of SPRi for secretion-monitoring of pancreatic islets. The islets are a small micro-organ that regulates glucose homeostasis in the body where somatostatin is used as a potent paracrine inhibitor of insulin and glucagon secretion. However, this inhibitory effect is lost in diabetic individuals and little is known about its contribution to the pathology of diabetes. Thus, the simultaneous detection of these three hormones (insulin, glucagon and somatostatin), collectively considered as an islets' secretory fingerprint (SF), was previously explored by the authors using SPRi. Earlier biosensing reports have shown that the concentration of these hormones vary from nanomolar to picomolar secreted from a tenth of islets. Therefore, to be able to detect these three hormones in multiplexed manner, the dynamic range and sensitivity of our SPRi biosensor were improved using gold nanoparticles (GNPs) for SPRi signal amplification. Three GNPs amplification strategies were compared: 1) GNPs immobilized on the sensor surface, 2) GNPs conjugate with primary antibodies (GNPs-Ab_1) and 3) GNPs conjugated with a secondary antibody (GNPs-Ab_2). Among these strategies an immunoassay using GNPs-Ab_2 conjugates was able to achieve multiplex detection of the three hormones without cross-reactivity and with a LOD improvement of 9 fold for insulin, 10 fold for glucagon and 200 fold for somatostatin when

compared to the SPRi biosensor without GNPs. The present work denotes the first report of the simultaneous detection of such hormones with a sensitivity level comparable to ELISA assays, particularly for somatostatin.

8.2. Introduction

Pancreatic islets are small micro-organ that regulates glucose homeostasis in the body [288]. Deficiencies in the islet's secretory pathways give rise to diabetes mellitus. However, little is understood about the paracrine communication occurring during glucose regulation [288]. For instances, it has been shown that somatostatin, secreted by the third most abundant cell type in the islets, is a potent paracrine inhibitor of both insulin and glucagon secretion [14, 97]. In a healthy adult, somatostatin secretion is normally stimulated by glucose and tolbutamide, however these triggering effects are lost in type 1 and type 2 diabetes. This has been proposed to contribute to the impaired regulation of glucagon secretion in diabetes [299, 300]. Thus, monitoring an islets' secretory fingerprint (SF) including the three most abundant secreting cells in the islet, could help to better understand such paracrine communications.

Pancreatic islet research up-to-date involves mostly the use of traditional bioassays for hormone quantification such as ELISA [21, 28, 301], patch clamp [13, 22-24, 142, 287], and capillary electrophoresis (CE) [25-27]. However, these techniques have a low throughput, are time-consuming, labor extensive and can detect only one hormone at a time. Moreover, they face several challenges when attempting their implementation for multiplex analysis.

Most of these shortcomings could be addressed using optical, electrical, mechanical or magnetic biosensors [302]. Among these biosensing technologies, sensors based on the optical excitation of surface plasmons has increased in popularity in the last decade due to its simple, easy

to use, non-invasive and label-free nature [303]. Surface plasmon resonance (SPR) biosensors present an additional advantage for the multiplex screening of biomolecular interactions when combine with imaging capabilities (SPRi) [43]. For instance, H. J. Lee *et al*. [304] demonstrated the simultaneous detection of 3 low molecular weight protein biomarkers using SPRi, by creating a high-density antibody microarray achieving multiplex detection of the three protein markers down to 1 nM concentrations. This makes SPRi a very desirable technique for secretion-monitoring of pancreatic islets.

In a recent work reported by the authors, a multiplex SPRi-based biosensor was introduced as a viable tool for simultaneous quantification of insulin, glucagon, and somatostatin by performing three simultaneous competitive assays with monoclonal antibodies [305]. In this work an innovative surface chemistry was introduced and optimized for the detection of the three targeted peptides in a competitive immunoassay format with high antifouling properties, obtaining a limit of detection (LOD) of 1 nM for insulin, 4 nM for glucagon, and 246 nM for somatostatin in multiplexed mode with a total analysis time of 21 min per point. These LODs are satisfactory for the detection of insulin [25] or glucagon [26] alone, secreted from a small population of islets, there are no available reports regarding the required LOD for somatostatin within the same population. Moreover, it is known that the number of somatostatin secreting cells within pancreatic islets is usually lower than that of insulin or glucagon-secreting cells [11].

Considering the important role of somatostatin in regulating insulin and glucagon secretion [14, 97], the aim of this work was to improve performance of the previously developed SPRi biosensor to ensure that somatostatin secreted from a tenth of islets can effectively, accurately and simultaneously be detected with other towed hormones.

Since its introduction by L. Lyon *et al*. [66], gold nanoparticles (GNPs) have been the most

commonly used method for improving the performance of SPR immunosensors. Two configurations are typically considered for the use of GNPs in SPR signal amplification: 1) the sensor surface modification with GNPs and 2) the labeling of a recognition element with GNPs. These strategies rely either on the coupling of local plasmon resonance of the GNP with the surface plasmon resonance of the system or in the increased mass attached to the recognition element for signal enhancement [67, 306]. Both GNPs amplification strategies have been frequently reported in the literature for individual detection of hormones such as insulin [307], progesterone[308], testosterone [309] and other small analytes [65, 67, 310], however, studies regarding the application of these strategies for multiplex hormones detection are scarce. Moreover, few reports exist regarding the use of GNPs amplification in a multiplex setting and they are focus on the detection of DNA sequences [311] or cancer biomarkers by means of localized SPR using microscopy [312]. Although these reports demonstrated detection of target analytes in femtomolar levels in multiplex mode, there is a lack of formal studies regarding the optimal GNP amplification strategy for SPRi systems.

Thus, to establish the optimal signal amplification scheme for the multiplexed sensing of the islets' SF with SPRi, three GNPs amplification strategies were investigated including 1) GNPs immobilized on the sensor surface, 2) GNPs conjugate with primary antibodies (GNPs-Ab_1) and 3) GNPs conjugated with a secondary antibody (GNPs-Ab_2). For this study, somatostatin was used as the 'reference' hormone, as it is the smallest among the three islets' SF, to first test the performance of the aforementioned SPR signal amplification strategies in an indirect competitive assay. Then, the biosensor performance was assessed in multiplex mode to determine the LOD and dynamic range for the three targeted hormones.

8.3. Experimental section

8.3.1. Materials and methods

Absolute ethanol was purchased from Fisher Scientific (Fair Lawn, NJ, USA), phosphate-buffered saline (PBS) tablets, tween 20 and glycine were purchased from BioShop Canada Inc. (Burlington, Ontario, Canada). Ethanolamine hydrochloride, N-(3-Dimethylaminopropyl)-N′-ethylcarbodiimide hydrochloride (EDC), N-Hydroxysuccinimide (NHS), hexa(ethylene glycol) dithiol (HEGD), bovine serum albumin (BSA), hydrochloric acid (HCl), glycerol, sodium hydroxide (NaOH), 20 nm gold nanoparticles (GNPs) in citrate buffer, human glucagon and human somatostatin were purchased from Sigma-Aldrich (St. Louis, MO, USA). (3,3'-dithiobis(sulfosuccinimidyl propionate)) (DTSSP) was purchased from Thermo Fisher Scientific. Tris-buffered saline (TBS) with 1% casein, goat anti-mouse IgG1and goat anti-rat IgG2a secondary polyclonal antibodies were purchased from BIO-RAD. Anti-insulin antibody (6.2 mg/mL) and human insulin were purchased from PROSPECT (Ness, Ziona, Israel). Anti-somatostatin monoclonal antibodies (200µg/mL each) were purchased from Santa Cruz Biotechnologies, Inc. (Mississauga, ON, Canada). Anti-glucagon monoclonal antibodies were purchased from Abcam (Cambridge, MA, USA). CH_3O-PEG-SH (MW 1200 Da) was purchased from Rapp Polymers GmbH (Tübingen, Germany). 16-mercaptohexadecanoic acid (MHDA) from ProChimia Surfaces Sp. (Zacisze, Sopot, Poland). Borate buffer 0.5 M pH 8.5 was purchased from Alfa-Aesar (USA).

8.3.2. Substrate preparation

Cleaned microscope glass slides (12 mm x 25 mm x 1 mm, n = 1.518) substrates were coated with 2 nm Cr as an adhesion layer, followed by the deposition of a thin Au layer of 48 nm using E-beam vapor deposition under high vacuum. The slides were then coupled to an SF11 equilateral triangular

prism (nSF-11 = 1.765) using a refractive index matching liquid. Gold-coated prisms (n =1.765) were purchased from Horiba Scientific, France and used as received.

8.3.3. SPRi measurements

SPRi detection was performed using a scanning-angle SPRi instrument (model SPRi Lab+, Horiba, France). The SPRi apparatus is equipped with an 800 nm LED source, a CCD camera, and a microfluidic flow cell. All experiments were performed at 25 °C by keeping the instrument inside an incubator (Memmert Peltier, Rose Scientific, Canada).

To select the working angle for kinetic analysis, the slope of the plasmon curves was computed automatically by the instrument's software. The selected angle corresponds to the point of the plasmon curve at which the slope was maximum. Reflectivity shift (ΔR (%)) was measured upon stabilization of the baseline. After each analyte injection, the substrate was rinsed with running buffer PBS-T (PBS with 0.002% tween 20), and the ΔR was calculated by the difference between the buffer signal before and after the analyte injection. The signal was recorded at least on three spots for each analyte and controls to determine the average ΔR values. All experiments were performed using an injection loop with a fixed volume of 200 µL and a constant flow rate of 20 µL/min, with the exception of functionalization steps where the flow rate was adjusted depending on the required contact time.

All SPR plots are presented as a function of reflectivity shift (ΔR (%)) vs time. A Savitzky-Golay smoothing polynomial function of second order was applied to all plots using OriginLab 2018 (b.9.5.5.409).

8.3.4. Surface immobilization of hormones

Following a protocol previously developed by authors[305], an ethanolic solution of 0.5 mM

CH_3O-PEG-SH and 0.5 mM MHDA were prepared and mixed at a molar ratio of 40% MHDA and 60% PEG (60-PEG/40-MHDA). Gold-coated prisms and slides were immersed in the ethanolic solution overnight to allow self-assembly monolayer (SAM) formation. Finally, they were thoroughly rinsed with absolute ethanol, DI water and dried under a stream of N_2.

For individual somatostatin sensing experiments, SAM-functionalized slides were placed on the SPRi system for subsequent functionalization. An initial conditioning step was performed by four serial injections of a 1M glycine pH 2.5 (1M-Gly) solution (contact time of 2 min each). Then, PBS-T was allowed to run until a stable baseline was obtained. Next, covalent immobilization of insulin, glucagon or somatostatin via NHS/EDC chemistry was performed following Gobi *et al*. protocol [290]. Briefly, an aqueous solution containing 2 mg/mL NHS, 2 mg/mL EDC and 50 μg/mL of the desired hormone was injected into the system with a contact time of 1 h. Next, an injection of 1M ethanolamine hydrochloride pH 8.5 (contact time 10 min) was performed to inactivate any unfunctionalized -COOH groups. Then, two serial injections of 1M-Gly solution (contact time 1 min each) were performed to remove weakly bound hormones. Finally, a blocking solution containing 5% BSA and 1% casein in TBS buffer was injected (contact time of 30 min) and subsequently, at least 3 injections of the 1M-Gly solution were made to remove weakly bound proteins. **Figure 1A** shows a schematic representation of a typical surface hormone functionalization.

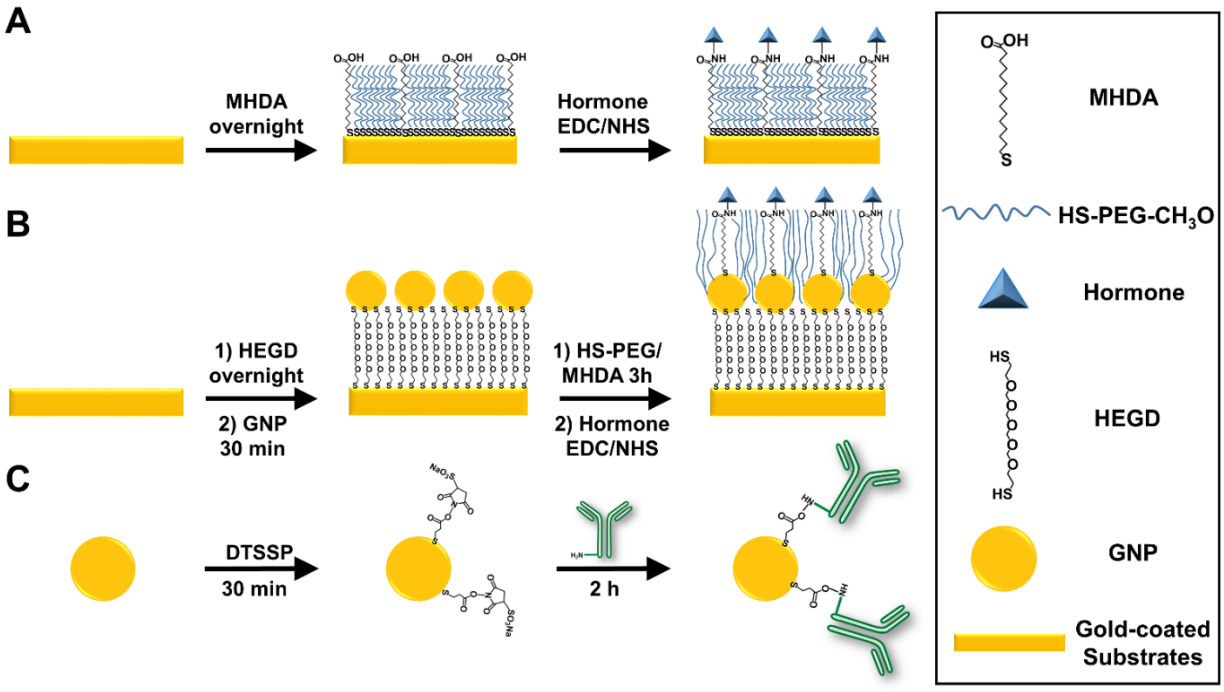

Figure 8.1. Schematic representation of the typical surface functionalization of: **A)** Gold-coated substrates functionalized with a self-assembled monolayer (SAM) of 16-mercaptohexadecanoic acid (MHDA)/CH_3O-PEG-SH (PEG) and subsequently with the targeted hormone, **B)** gold-coated substrate surface functionalized with a SAM of hexa(ethylene glycol) dithiol (HEGD), GNPs and subsequently with the targeted hormone and **C)** covalent antibody functionalization of for the formation of GNPs-conjugates using (3,3'-dithiobis(sulfosuccinimidyl propionate)) (DTSSP).

For multiplex measurements, gold-coated prisms were functionalized using the procedure described for glass slides outside of the SPR system. After conditioning, four individual solutions containing NHS/EDC and each targeted hormone (insulin, glucagon, somatostatin) or a control (BSA) were spotted (150 nL) in triplicate on the prisms and incubated in a humidity chamber for 1h. After incubation, the prisms were rinsed with DI water and exposed to 1M ethanolamine hydrochloride pH 8.5 for 10 min. Next, the prisms were exposed to the blocking solution for 30 min and subsequently, rinsed with PBS-T. Finally, the prisms were placed in the SPR system and a 1M-Gly solution was injected at least three times to obtain a stable baseline before starting with the experiments.

8.3.5. Immobilization of GNPs on the gold-coated sensor's surface

The immobilization of GNPs on the gold-coated sensor's surface was achieved according to a protocol developed by Taufik *et al*. [313] with minor modifications. After cleaning, gold-coated slides were immersed in an ethanolic solution of 2mM HEGD overnight to allow SAM formation. After rinsing with ethanol and DI water, the slides were exposed to an aqueous solution containing 20 nm GNPs (OD_{520} = 1.0) and incubated for one hour. Next, the slides were rinsed with DI water and placed in a 60-PEG/40-MHDA ethanolic solution for 3 hours. Finally, hormone functionalization was performed according to the procedure described in the previous section. **Figure 1B** shows a schematic representation of the surface functionalization with GNPs and hormones.

8.3.6. Antibody-GNP functionalization

The functionalization protocol for 20 nm GNPs (OD_{520} = 1) with primary or secondary antibodies was adapted from a previous report by J. D. Driskell *et al*.[314] using DTSSP as a bifunctional crosslinker. Briefly, 134 µL of 50 mM borate buffer pH 8.5 was added to a 1 mL suspension of 20 nm GNP to adjust the pH. Next, 26 µL of 20 µM DTSSP was added to the GNPs and incubated for 30 min to form a thiolate monolayer through cleavage of the DTSSP disulfide bond. The suspension was then centrifuged at 17,500g for 30 min, the supernatant containing excess DTSSP was removed and the GNPs were resuspended in 1 mL of 2 mM borate buffer. Immediately after, 20 µg of the desired antibody was added to the DTSSP-GNPs suspension and incubated for 90 minutes. The suspension was then centrifuged at 17,500g for 30 min, the supernatant was removed, and the GNPs were resuspended in 1 mL of 2 mM borate buffer containing 1% (m/v) BSA and incubated for 30 min to allow the BSA to block any unreacted DTSSP and nonspecific binding sites. The

centrifugation/resuspension cycle was repeated two additional times using 2 mM borate buffer for resuspension to remove excess antibody and BSA. The final volume of the solution after the centrifugation/resuspension cycles was fixed to approximately 200 μL ($OD_{525} \approx 4$) and the solution was stored at 4 °C. The functionalized GNPs were diluted to the desired concentration in PBS-T prior to use in immunoassays. **Figure 1C** shows a schematic representation of antibody-GNP functionalization. Successful GNPs functionalization for all antibodies was confirmed by the shift in absorbance maxima of the GNPs from 520 to 525 nm (**Fig. S8.2** in supporting information).

8.3.7. Competitive immunoassays

The four configurations used for indirect competitive immunoassays consisted in a surface with (**Fig. 2A**) and without GNPs (**Fig. 2B**), primary antibodies GNPs (GNP-$Ab_{1)}$ conjugates (**Fig. 2C**) and secondary antibodies GNPs (GNP-Ab_2) conjugates (**Fig. 2D**). Since somatostatin was the smallest of the targeted hormones, it was used as the "reference" hormone in all individual hormone assays. The optimal primary anti-somatostatin antibody, GNPs-Ab_1 and GNPs-Ab2 concentration were defined as the concentration that could generate a small but detectable SPR signal of $\Delta R \approx 1$, previously reported as a reliable ΔR for this type of assays [291].

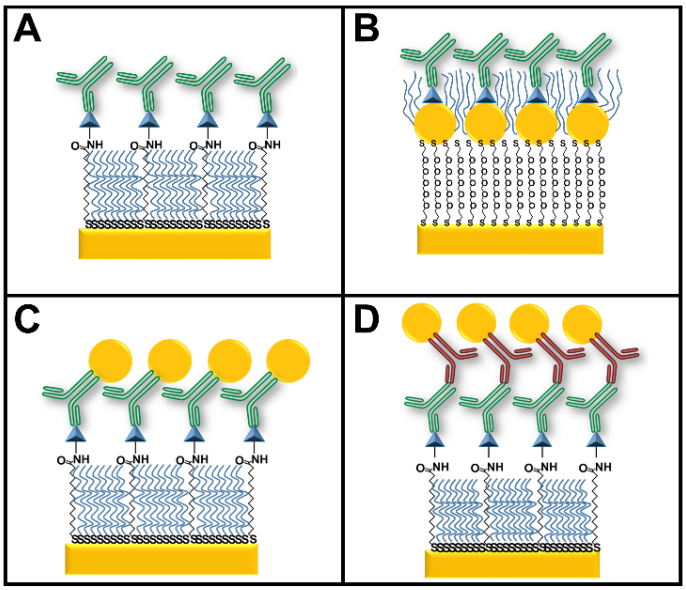

Figure 8.2. Schematic representation of the four configurations of competitive immunoassay used for this work: **A)** an assay involving only primary antibodies and the hormone immobilized on a gold surface used as control, **B)** an assay where GNPs are present on the surface and the hormone is immobilized on top of the GNPs, **C)** an assay where GNPs are conjugated with monoclonal primary antibodies (GNPs-Ab_1) and **D)** an assay involving GNPs conjugated with a polyclonal secondary antibody (GNPs-Ab_2) after a primary competitive assay.

Standard somatostatin solutions were prepared by serial dilution in PBS-T buffer with concentrations ranging between 0.01-4000 ng/mL. These solutions were then mixed with 2 µg/mL of anti-somatostatin antibody for assays involving only primary antibodies, 0.6 µg/mL of antibody for the assay involving GNP-Ab_2 conjugates or a 1:50 dilution (from $OD_{525} \approx 4$) of GNP-Ab_1 conjugates. All mixtures were incubated for 2 min with gentle mixing by inverting upside down and then injected into the system from highest to lowest hormone concentration (contact time of 10 min) starting with a blank solution containing only anti-somatostatin antibodies or GNP-Ab_1 conjugates. For assays involving GNP-Ab_2 conjugates, immediately after anti-somatostatin antibody injection, GNPs-Ab_2 conjugates were injected (1:50 dilution from $OD_{525} \approx 4$). The optimal primary anti-somatostatin antibody, GNPs-Ab_1, and GNPs-Ab_2 concentration were defined as the concentration that could generate a small but detectable SPR signal of $\Delta R \approx 1$, previously reported as a reliable ΔR for this type of assays [291].

During calibration curve experiments, different sensor regeneration solutions were tested including 10−50 mM NaOH, 50 mM NaOH 5−50% (v/v)−glycerol, 0.1−1 M glycine (pH 1.5), 0.1−1 M glycine (pH 1.5) with 1% (v/v) DMSO, and 2 M $MgCl_2$. From these solutions, 50 mM NaOH with 25% glycerol provided the most efficient conditions for regeneration and it was used throughout all the experiments.

For multiplex assays, standard solutions having a mix of insulin, glucagon, and somatostatin were prepared in PBS-T buffer at a concentration range of 0.01-4000 ng/mL and mixed with a cocktail of primary antibodies containing anti-insulin (0.2 µg/mL), anti-glucagon (0.05 µg/mL) and anti-somatostatin (0.6 µg/mL). Similar to individual somatostatin assays, the mixtures were incubated for 2 min with gentle mixing and serially injected over the spotted sensor chip from highest to lowest hormone concentration (contact time of 10 min) starting with a blank solution containing only the antibody cocktail. Subsequently, a GNPs-Ab_2 mixture containing GNPs conjugated to anti-mouse IgG1 (1:100 dilution from $OD_{525} \approx 4$) and anti-rat Ig2a (1:50 dilution from $OD_{525} \approx 4$) was injected into the system. Each sensing cycle comprised: hormone primary antibody mixing and incubation for 2 min, cocktail injection for 10 min, 3 min buffer washing, 10 min injection of a GNPs-Ab_2 mixture and 2 injections of regeneration solution with a contact time of 30s with 3 min washing with buffer in-between.

8.3.8. Statistics

Relative binding (C/C_0) was calculated for all competitive immunoassays, by dividing the response of the standard solutions containing hormones (C) by the response of the blank solution containing only a fixed concentration of antibodies (C_0). To generate calibration curves C/C_0 was plotted against hormone concentration. The calibration curves were fitted using a non-linear 4 parameter logistic (4PL) model. The LOD for all immunoassays was calculated from the calibration curves

as the blank signal (C_0) minus three times the standard deviation. The dynamic range for the competitive immunoassay was established between 0.2 C/C_0 and 0.8 C/C_0. All data are expressed as the average of at least 3 independent experiments ± standard deviation (SD).

8.4. Results and discussion

8.4.1. GNP amplification strategies for competitive immunoassays

First, the formation of a chemically-linked layer of GNPs was performed using a SAM of a dithiol alkane (HEGD). HEGD allowed anchoring of the GNPs to the gold-coated sensor's surface through the thiol group on each end of the molecule [313]. AFM analysis indicated the successful immobilization of the GNPs by a significant change in surface morphology from a clean gold surface to a GNPs-modified surface as clearly observed in **Figure S8.1** provided in supporting information. This was further confirmed by a change in surface RMS roughness from 0.68 nm to 2.41 nm and later to 5.36 nm from a clean surface to a SAM-functionalized surface, and to a GNPs-functionalized surface. The signal amplification rationale here is that the activation of the GNPs localized SPR due to the proximity of the immobilized GNPs to the sensor's surface can lead to different resonance properties of the overall SPR system with additional resonance shifts, resulting in an enhanced sensitivity of the biosensor [306].

For all GNPs-antibody conjugates, functionalization was confirmed by a shift observed in the maximum absorption peak from 520 to 525 nm (**Fig. S8.3** in supporting information). In the case of GNPs-Ab_1 conjugates, the rationale behind this strategy is that the increased mass of the antibody due to the linked GNPs will result in a higher refractive index change on the SPR surface, thereby producing a larger SPR shift [67]. Additionally, due to the close proximity of the GNPs to the SPR surface (<15 nm) signal enhancement is also linked to electromagnetic field coupling

between surface SPR and the GNPs localized SPR [67]. Regarding the use of GNPs-Ab_2 conjugates, the signal amplification is only expected from the increased mass of the antibody due to the linked GNPs, as the GNPs are quite far from the surface [67].

Figure 3 shows the sensor calibration curves for somatostatin detection where the mean relative binding values (C/C_0) were plotted as a function of hormone concentration for all sensing strategies. For these experiments, detection without GNPs was used as a control assay (**Fig. 3A**). Additionally, the entire sensor surface was functionalized with somatostatin, and the SPR shift for all sensing events was obtained as the mean of at least 10 spots from different regions of the chip. Then, an average of ΔR of three independently prepared chips was calculated representing their corresponding standard deviation (SD). The LOD and dynamic range for each sensing strategy are shown in **Table 1**.

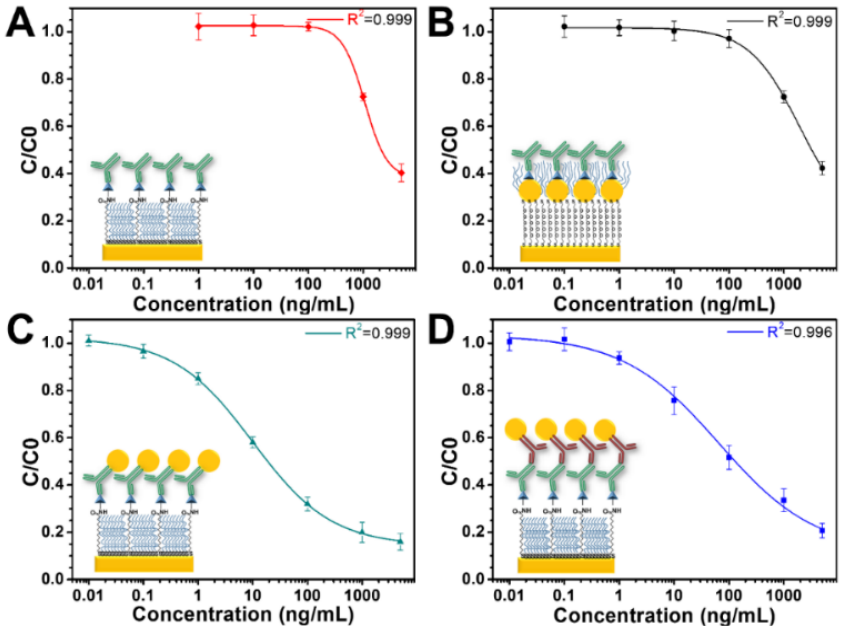

Figure 8.3. Somatostatin sensing calibration curves in PBS-T for **A)** an assay involving only primary antibodies and the hormone immobilized on a gold surface, **B)** an assay where GNPs are present on the surface and the hormone is immobilized on top of the GNPs, **C)** an assay where GNPs are conjugated with monoclonal primary antibodies (GNPs-Ab_1) and **D)** an assay involving GNPs conjugated with a polyclonal secondary antibody (GNPs-Ab_2). Solid lines correspond to the fitting of a nonlinear 4PL model. Error bars represent the standard deviation from 3 independent experiments (n = 3).

Noteworthy, the concentration of the control assay (**Fig. 3A**) and the strategy using a GNPs-modified surface (**Fig. 3B**) was set to 2µg/mL to facilitate comparison and to easily observe SPR signal enhancement. Interestingly, these two sensing strategies presented similar LODs. However, the GNPs-modified surface showed a higher SPR signal (**Figure S8.3** in supporting information) compared to the signal obtained for the surface without GNPs as clearly observable in the ΔR (%) (C_0) values in **Table 1**. Indeed, this seems consistent with recent reports where the LOD of the calibration curve of an indirect competitive immunoassay using GNP-modified sensors did not change even when the SPR signal was enhanced [310, 315]. A possible explanation is that the performance of an indirect competitive immunoassay highly depends on the affinity constant of the immunoreaction [310]. Therefore, only strategies affecting the affinity of the antigen-antibody system such as the GNPs-Ab conjugation could improve the LOD of the SPR sensor [310].

Table 8.1. SPR Sensing Performance for somatostatin using different immunosensing strategies.

Strategy	ΔR (%) (C_0)	LOD [ng/mL]	LOD [nM]	Dynamic Range [ng/mL]
Primary Ig	1.10 ± 0.03	450	275	754-4000[a]
GNPs Surf	1.72 ± 0.05	404	247	626-4000[a]
GNPs-Ab_1	1.26 ± 0.02	0.24	0.15	1.54-780
GNPs-Ab_2	0.93 ± 0.04	1.75	1.07	7.5-4000[a]

[a] Highest concentration tested

Finally, from all immunosensing strategies, the competitive immunoassay using GNPs-Ab_1 conjugates presented the best performance decreasing the LOD three orders of magnitude compared to the control assay from 450 ng/mL to 240 pg/mL. Hence, this immunoassay amplification strategy was selected for further development of the multiplex hormone-sensing assay.

8.4.2. GNP-amplified multiplex immunoassays

Fig. 4A-C shows the assessment of cross-reactivity for primary antibodies. Individual injection of each antibody caused an increase in SPR signal only on its relevant spot, demonstrating specificity and low cross-contamination between spots. Moreover, there was a negligible response on the control spots, indicating good antifouling properties.

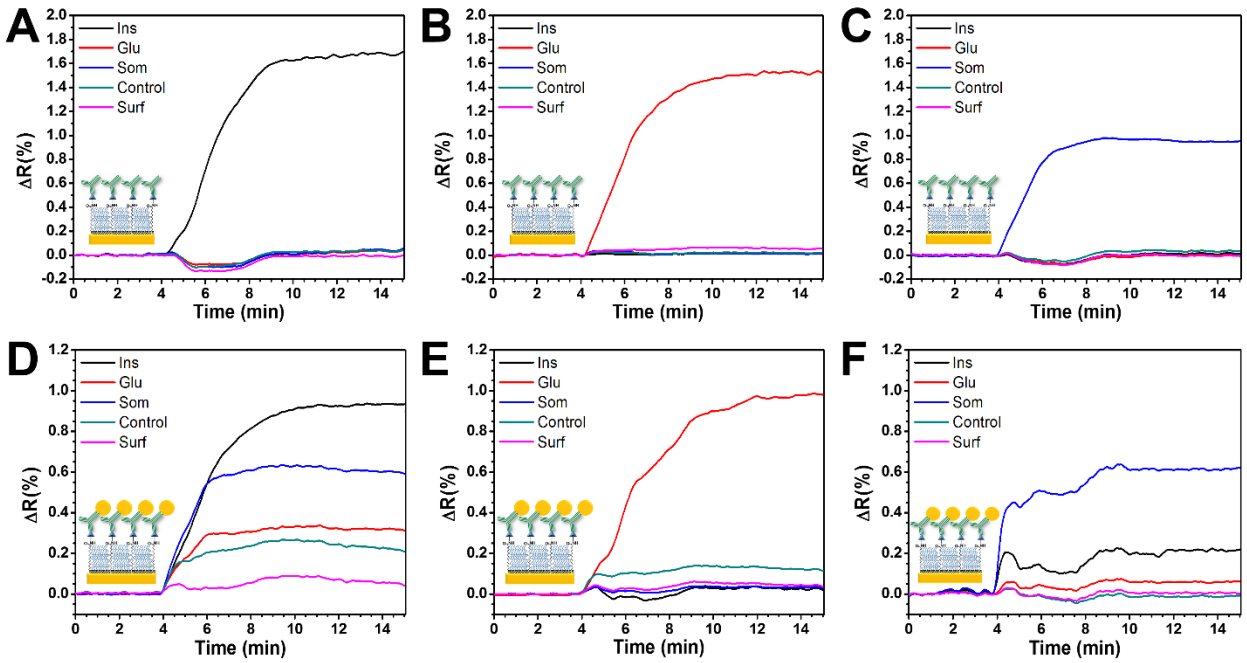

Figure 8.4. Specificity of the sensor for a multiplex immunoassay using only primary antibodies. The first row shows the specificity of the sensor without signal amplification for **A)** anti-insulin, **B)** anti-glucagon, and **C)** anti-somatostatin. Second row shows the specificity of the sensor on the same surface with signal amplification for **D)** GNPs-anti-insulin, **E)** GNPs-anti-glucagon and **F)** GNPs-anti-somatostatin. Immobilized BSA and the bare SAM surface identified in the graphs as "Control" (green line) and "Surf" (pink line) respectively were used as negative controls.

However, when a similar experiment was performed using GNPs-Ab_1 conjugates, high cross-reactivity was observed. This effect was particularly large for GNPs-anti-insulin conjugates which generated a non-specific signal increase in all the functionalized spots including the two negatives controls (**Fig. 4D**). When GNPs-anti-glucagon conjugates were injected, cross-reactivity with insulin and somatostatin spots was not observed, however some degree of non-specific interactions were detected for the negative control spots (**Fig. 4F**). For GNPs-anti-somatostatin

conjugates, cross-reactivity was also observed mostly with insulin spots (**Fig. 4G**). Additional antibodies from different species and companies were used for GNPs-Ab_1 conjugates for anti-insulin and anti-somatostatin. However cross-reactivity was always present (data not shown). This has been reported in literature as a recurring problem for multiplex immunoassays [316, 317], particularly for GNP conjugates since it has been shown that such conjugations can modify the activity of the antibodies. In theory, a combination of GNPs-Ab_1 conjugates with little or null cross-reactivity for our system could be achieved, however testing a library of antibodies would be time consuming and cost-ineffective. Due to this dilemma, the second best amplification strategy (GNP-Ab_2) was selected for further development of our multiplex immunosensor. For this strategy, some degree of cross-reactivity could occur since the secondary antibodies are similarly conjugated to GNPs. In general, antibody conjugation is known to affect the antibody's affinity [310], however this did not seem to hinder the possibility for multiplex sensing as later demonstrate in this section.

The nonspecific binding effect of the GNPs-Ab_2 conjugates on the analyte spots was determined prior to the multiplex assay through the injection of a mix of GNPs-goat anti-mouse IgG1and GNPs-goat anti-rat IgG2a over the sensor surface. As seen in **Figure 5A**, a minimum SPR angle shift was detected during the injection with the signal returning to similar baseline levels after a few minutes of PBS-T washing, indicating a negligible nonspecific binding effect of the GNPs-Ab_2 conjugates to the different surface spots.

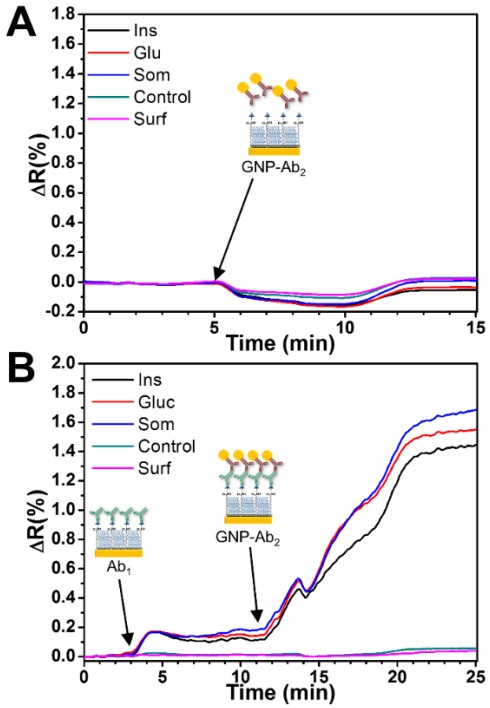

Figure 8.5. Real-time SPR angle shift sensorgrams of: **A)** Nonspecific binding effect of GNPs-Ab_2 conjugates and **B)** specific binding effect of GNPs-Ab_2 conjugates after primary antibody injection (blank injection C_0). Immobilized BSA and the bare SAM surface identified as "Control" and "Surf" were used as negative controls.

Figure 8.5B shows a typical sensor response to a blank solution (mix of all antibodies) and the subsequent amplification effect of the GNPs-Ab_2 conjugates. The injection caused a small increase in SPR signal on the relevant hormone spots while an almost no response for the control spots, indicating specific binding. For these experiments, the initial concentration of primary antibodies (C_0) was fixed to 0.2 µg/mL for anti-insulin, 0.05 µg/mL for anti-glucagon and 0.6 µg/mL for anti-somatostatin. This Ab_1 concentration produced a small signal of ≈0.15 ΔR for all hormone spots. The subsequent injection of GNPs-Ab_2 conjugates generated an SPR signal enhancement of ≈10 times, which was consistent with previous literature reports where 20 nm GNPs-Ab_2 conjugates have been used for signal amplification [308, 318].

It is noteworthy the fact that the C_0 signal obtained for somatostatin during individual GNPs-Ab_2 was smaller (ΔR = 0.93, Table 8.1) compared to that obtained during the multiplex assay

(ΔR = 1.51, Table 2). This difference is likely due to some cross-reactivity between the different species of secondary antibodies in the GNPs-Ab_2. However, due to the absence of non-specific interactions with the hormone spots and the controls, it was possible to use these conjugates for multiplex detection since the sensor response (ΔR) was always consistent and reproducible for all targeted hormones.

To further assess the sensor's resistance to non-specific adsorption of proteins, at the end of each calibration curve two solutions containing either BSA or LYZ, both with a final concentration of 1 mg/mL was injected to the system following the same protocol as for the hormone immunoassay. After an abruptly increased in the SPR signal during the injections due to the high bulk refractive index of the solution, the shift in reflectivity was measured after 10 minutes of contact time and 5 minutes of PBS-T wash. Since LYZ presented the largest ΔR among the two tested proteins, it was used as reference to quantitatively evaluate the antifouling properties of the sensor. The mean (n=3) ΔR response to BSA and LYZ from the hormone-functionalized spots and controls is showed in **Table S8.1** in supporting information. It was found that the adsorbed amount of LYZ was ≈100 pg/mm^2 for all spots assuming that 1RU = 1μRIU = 1pg/mm^2 of surface mass shift for a fixed wavelength of 800 nm [62]. This was very consistent with the definition of an antifouling surface [294]. Moreover, a short (30 s) injection of regeneration solution returned the baseline to its original value, indicating a weak interaction of LYZ and BSA on the sensor's surface.

Figure 8.6 shows the average calibration curves for the multiplex sensing of serially diluted mixtures of insulin, glucagon, and somatostatin in PBS-T obtained from three independent measurements. The calculated LOD and dynamic range obtained (**Table 2**) for the three hormones in multiplexed mode were somehow comparable to that of ELISA kits (0.001-40 ng/mL depending of the hormone targeted) assessing individual hormone quantification. However, our sensing

approach has the advantage of multiplexing, a larger working range and a relatively low analysis time of 32 min per point.

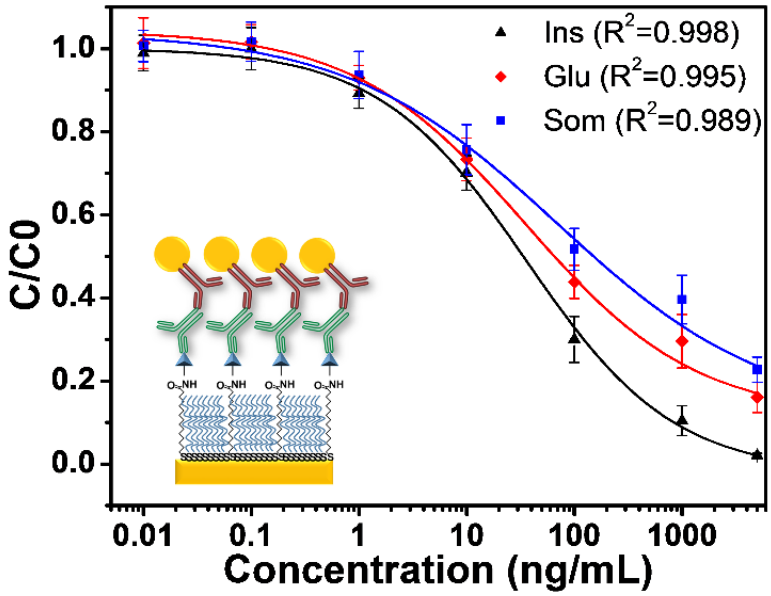

Figure 8.6. Calibration curves for a multiplex immunoassay using GNPs-Ab_2 conjugates as amplification strategy in PBS-T. Solid lines correspond to the fitting of a nonlinear 4PL model for different concentration of insulin (blue), glucagon (red), and somatostatin (black). For each hormone, mean relative binding values (C/C_0) were plotted as a function of hormone concentration (ng/mL). The mean SPR shift was measured in sets of triplicate spots for each hormone and the controls. Then, the average SPR shift was calculated using 3 independent multiplex sensors corresponding to the reported SD.

Moreover, the use of GNPs for SPR signal amplification led to a remarkable LOD improvement for all tested hormones. An increase of 9 fold for insulin, 10 fold for glucagon and 200 fold for somatostatin detection was obtained as compared to the multiplex sensing approach without using GNPs-conjugates amplification [305]. Noteworthy is the fact that somatostatin showed a dramatic improvement in LOD. This could be explained by the fact that somatostatin is the smallest of the targeted hormones in this study (MW=1637.88 Da). Thus, under the same immobilization conditions, the maximum amount of immobilization is expected to be lower than that of the higher MW hormones[78]. This could lead to less steric hindrance for binding of the large GNPs-Ab_2 conjugates. This is corroborated by the fact that despite showing a similar response for primary antibody injection, somatostatin produced a slightly larger SPR shift for GNPs-Ab_2

conjugates (**Fig. 5**).

The LOD achieved in this study is in accordance with previous studies where detection of insulin [25] and glucagon [26] secreted from 10 islets was achieved at 15 mM glucose. Therefore, the somatostatin secreted from this small population of islets could be effectively and accurately detected by our proposed approach, opening the possibility of gaining better understanding of its paracrine communications associated with abnormal islets' function in diabetes.

Table 8.2. SPR sensing performance for a multiplex immune assay for insulin, glucagon and somatostatin. The presented ΔR (%) (C_0) is the sensor's response to the GNPs-Ab_2 conjugates.

Hormone	ΔR (%) (C_0)	LOD [ng/mL]	LOD [nM]	Dynamic Range [ng/mL]
Insulin	1.32 ± 0.03	0.90	0.15	3.9-270
Glucagon	1.40 ± 0.03	1.35	0.39	5.0-1,977
Somatostatin	1.51 ± 0.04	2.00	1.22	6.6-4,000[a]

[a] Highest concentration tested

8.5. Conclusions

To address the challenges in detection of low molecular weight hormones secreted in very low concentration by human islets such as somatostatin, we investigated three GNPs amplification strategies using an SPRi-based biosensing approach. Although the amplification method involving the conjugation of primary antibodies with GNPs showed the best performance for sensing of individual hormones, it presented large cross-reactivity during multiplex experiments. This cross-reactivity was successfully circumvented using secondary antibodies conjugated to GNPs as amplification. We successfully achieved multiplex detection of three pancreatic islet related

hormones with an LOD of 0.15 nM, 0.39 nM and 2.0 nM for insulin, glucagon and somatostatin respectively with a total analysis time of 32 min per point. This performance is comparable with previously reported detection sensitivity of insulin and glucagon secreted from 10 islets as well with the individual hormones sensing using conventional ELISA kits.

The possibility of working with a small pancreatic islet population combined with the advantage of multiplexing, a wide working concentration window and a low analysis time, would make our sensor very suitable for its application in secretion-monitoring of the pancreatic islets, particularly for understanding the paracrine effect of somatostatin on glucose-induced insulin and glucagon secretion. Furthermore, integrating a microfluidic perfusion platform with the proposed sensing approach could allow performing multiparametric analysis of an islets' SF in the context of discovery of novel drugs for diabetes treatment.

ACKNOWLEDGMENT

The authors acknowledge the financial support from the Natural Science and Engineering Research Council of Canada (NSERC) and the NSERC-CREATE in ISS grants, and FRC scholarship from Consejo Nacional de Ciencia y Teconología de México (CONACyT) and Secretaría de Educación Pública de México (SEP). The authors are also thankful to Dr. F. Melaine for her help during the initial exploration of GNPs as amplification strategy.

ASSOCIATED CONTENT

Supporting Information. Gold nanoparticle functionalization characterization: including surfaces and GNPs-Ab conjugates.

Atomic Force Microscopy

Atomic force microscopy (AFM) measurements were performed using a Nanoscope III instrument (Digital Instruments, USA) and Nanoscope v 5.12r5 software. AFM images were acquired in tapping mode in air at room temperature with a silicon probe having a nominal spring constant of 42 N/m and a nominal resonance frequency 330 kHz (model PPP-NCHR, NANOSENSORSTM).

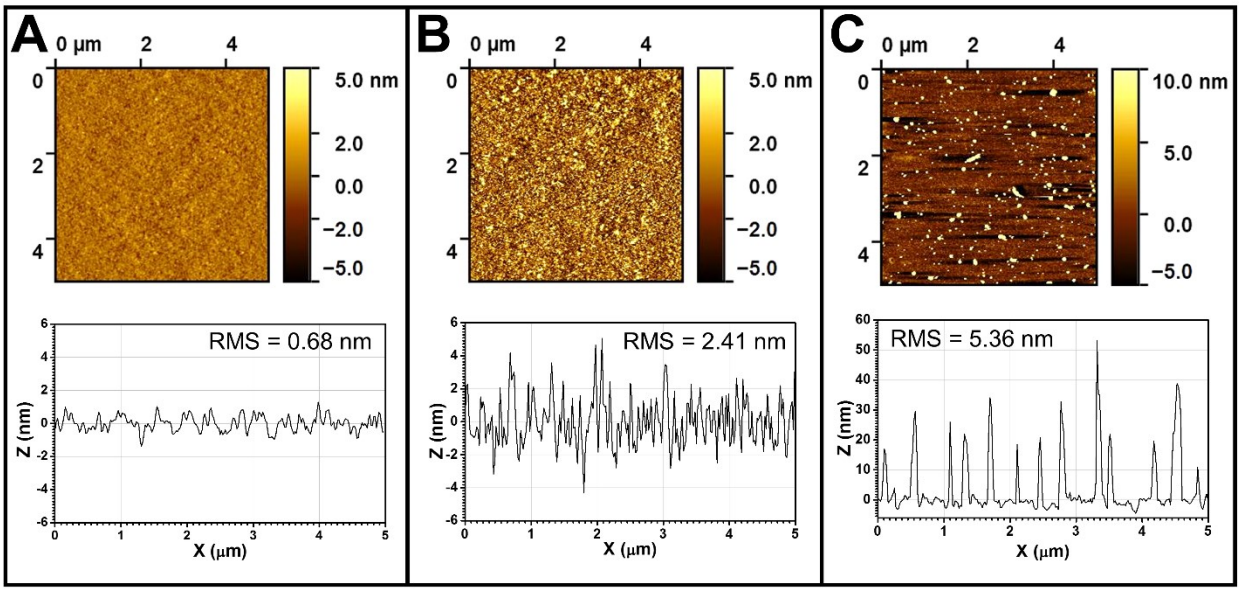

Figure S8.1. 2D AFM images and surface topography of: **A)** a clean gold surface, **B)** a gold surface functionalized with a self-assembled monolayer (SAM) of hexa(ethylene glycol) dithiol and **C)** a gold-SAM functionalized surface with gold nanoparticles.

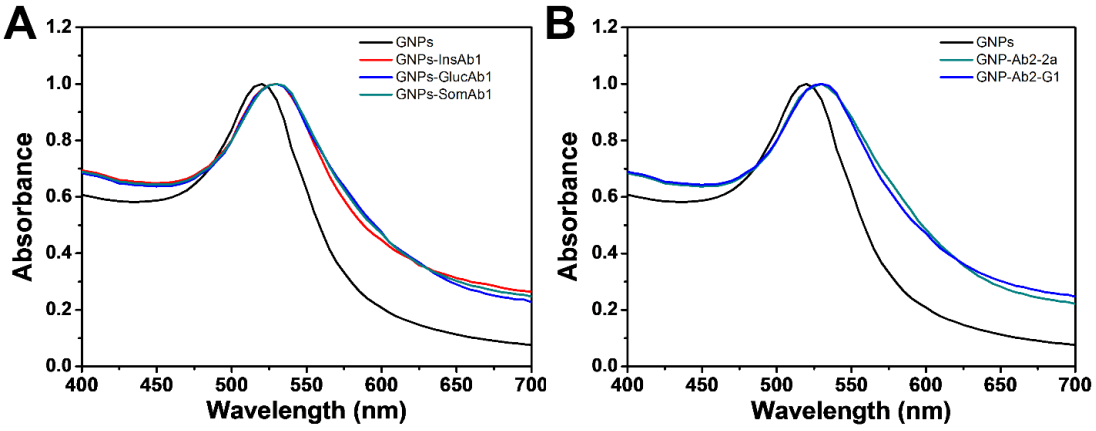

Figure S8.2. UV-vis absorption spectra of functionalized gold nanoparticles with: **A)** primary antibodies and **B)** secondary antibodies.

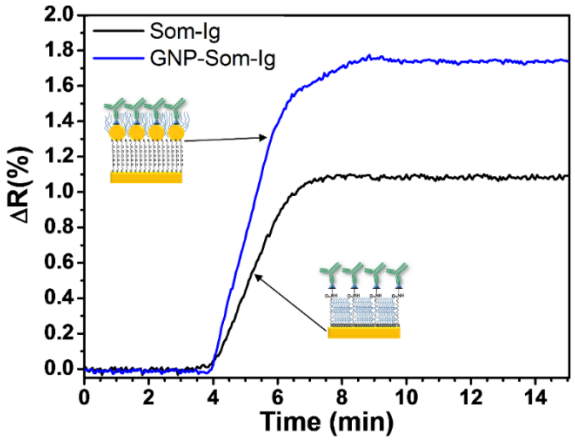

Figure S8.3. Real-time SPR angle shift sensorgrams comparison in response to the injection of 2μg/mL of anti-somatostatin antibody for a surface functionalized with gold nanoparticles and a surface without gold nanoparticles.

Table S8.1. Quantification of non-specific absorption of 1 mg/mL of BSA or LYZ on the sensor's surface during multiplexed analysis. Quantification was performed for two negative control: the bare SAM surface and spots functionalized with BSA (control). This calculation assume that 1RU = 1μRIU = 1pg/mm^2 of surface mass shift at a fixed wavelength of 800 nm. Only LYZ is reported in pg/mm^2 since it produced the largest sensor response.

Spot	ΔR (%) BSA [1mg/mL]	ΔR (%) LYZ [1mg/mL]	Amount of LYZ absorbed (pg/mm^2)
Insulin	0.04 ± 0.02	0.15 ± 0.02	90 ± 12
Glucagon	0.04 ± 0.01	0.11 ± 0.03	66 ±18
Somatostatin	0.04 ± 0.02	0.16 ± 0.03	96 ± 18
Surface	0.06 ± 0.01	0.16 ± 0.04	96 ± 24
Control	0.03 ± 0.02	0.07 ± 0.04	42 ± 24

Chapter 9. Original Contributions and General Discussion

The main motivation for this doctoral project was to develop a multiplexed biosensing strategy capable of detecting a secretion fingerprint comprised of small hormones secreted by the three major cell types contained in the pancreatic islets. Recent studies have clearly demonstrated that the anatomy of human pancreatic islets has significant consequences for cell-to-cell communication within the islets, giving rise to relevant paracrine hormone interactions unique to our species. Moreover, traditional biochemical assays lack the temporal resolution to follow the secretion process dynamically, they are time-consuming, labor extensive and can detect only one hormone at a time. Therefore, the design of novel analytical tools is required in order to detect changes in the secretion patterns of the islets. This was successfully achieved by the development of a multiplexed biosensing strategy able to simultaneously detect insulin, glucagon and somatostatin in the nano- and picomolar range with a short analysis time.

This study led to three major original contributions to the field of biosensors and pancreatic islet research. First was the use of an IDE capacitance-based biosensor for the detection of insulin. This label-free sensing technique was selected due to the fact that non-faradic electroanalytical methods have been reported to offer high sensitivity, ease for automation, and potential multiplex capabilities by means of their integration with microelectronic technologies [40, 186]. However, relative unpredictability has made these immunosensors unfavored compared to other electrochemical approaches. This is mainly due to the fact that the IDE biosensors' performance critically depends on the quality and architecture of the bioreceptor immobilization chemistry [250, 260, 261], which is very often neglected. Through a systematic study, we investigated the effect of the most common architectures reported in the literature, namely the covalent immobilization of biomolecules on the electrodes [37, 252-254, 262], in the gaps between electrodes [257-259, 263]

and a conformal coating covering both [255, 256, 264, 265]. Our results showed that polymeric conformal coatings such as spin-coated PMMA generate the most reproducible and stable capacitance change in response to specific antigen-antibody binding. Additionally, it was found that binding events occurring in the interdigitated electrode gaps play a major role in the overall change in capacitance, a feature that is commonly disregarded when developing biosensing strategies based in IDEs. The development of this sensor allowed us to understand many of the critical variables involved in the detection of small hormones such as insulin (e.g. immunoassay format, immobilization chemistry, etc.). However, we found that this type of sensor requires long analysis time making them unsuited for continuous measurements, which is a prerequisite for their intended used of secretion-monitoring, the main objective of this thesis. This motivated us to explore SPRi as an alternative biosensing method.

The results generated with the used of an SPRi biosensing method, were gathered in two original contributions. We introduced a label-free and multiplex strategy for the simultaneous detection of insulin, glucagon and somatostatin. It is noteworthy that the detection of small molecules, such as these peptide hormones (<10 kDa) presents a challenge in a mass-sensitive technique such as SPR. Thus, it was necessary to combine an innovative design of the surface chemistry with proper optimization of an indirect competitive immunoassay, to detect the three hormones with an LOD comparable to previous reports detecting insulin and glucagon individually secreted from a group of 10 islets. The developed biosensing strategy used a mixed SAM comprised of a linear thiol with a carboxyl end group (MHDA) for hormone immobilization, along with a low molecular weight thiolated PEG (CH_3O-PEG-SH) that acts as a spacer and as an antifouling agent [294, 319]. While each component of this surface chemistry has previously been used for biosensor development, our work was the first report using them in combination.

Additionally, contrary to the majority of the reports in the literature [74, 320], this study presented a long chain compound as a spacer and a short chain as an anchor. This produced a biosensor with excellent antifouling properties and specificity capable of its future operation in a complex matrix such as a pancreatic islet secretome.

The study of different GNPs amplification strategies for the development of a sensitive method for multiplexed hormone detection was the second major contribution to the field of multiplexed SPRi biosensing, which is presented as the third manuscript collected in this thesis. Although GNPs amplification strategies are commonly encountered in the literature, most of these works report only its use for individual detection of analytes [65, 67, 310], or detection in a localized SPR multiplexed format using microscopy [312]. To establish the optimal signal amplification scheme for the multiplexed sensing of the islets' hormones with SPRi, three GNP amplification strategies were investigated including 1) GNPs immobilized on the sensor surface, 2) GNPs conjugated with primary antibodies (GNPs-Ab_1) and 3) GNPs conjugated with a secondary antibody (GNPs-Ab_2). We found that the amplification method involving GNP conjugation with primary antibodies produced the best results in terms of performance for sensing of individual hormones. However, when implemented for multiplex experiments, this amplification scheme presented large cross-reactivity. This pitfall was successfully circumvented by the use of an immunoassay with GNP secondary antibodies conjugates, leading to a significant LOD improvement during the simultaneous detection of the three hormones. By the incorporation of this amplification scheme, the biosensor's LOD decreased 9, 10 and 200 folds for insulin, glucagon and somatostatin, respectively, when compared to the SPRi biosensor without GNP conjugates. This improvement was particularly important for the detection of somatostatin where the LOD decreased from 403 ng/mL to 2 ng/mL, falling within levels comparable to somatostatin ELISA

kits (0.001-10 ng/mL). Since there are reports in literature regarding the required LOD only for the detection of insulin [25] and glucagon [26], the obtained LOD for somatostatin enables its detection with a higher degree of confidence for the future detection of islets secretions.

Finally, we can make a comparison of the SPRi multiplex method developed in this thesis to other multiplex technologies such as Luminex xMAP, Biolayer Interferometry (BLI) and Microscale Thermophoresis (MST). A brief explanation of the operating principles of these techniques is presented next.

Luminex xMAP assays use antibody-conjugated bead sets of approximately 5 microns to detect analytes in a multiplexed sandwich immunoassay format. Each bead in the set is produced with a unique content of two dyes that serve for identification along with an immobilized specific bioreceptor (usually a monoclonal antibody). Later, a third dye conjugated via biotin-streptavidin to an antibody is used to detect binding of the analyte in a sandwich format [321]. Data is acquired on a dedicated flow cytometry-based platform. Although high throughput, this technique require high reagent consumption to functionalize the different sets of beads, no kinetic information can be obtained and long associated assay times could be required.

BLI is a technique that uses white light interferometry to quantify biomolecules adsorbed to the tips of several optical fibers. White light travelling through these optical fibers is reflected at the fiber-biomolecular layer and the reflected beams generate a signal that only depends on the amount of adsorbed molecules eliminating any the effect of the surrounding matrix [322]. Typically, the measurements are performed by dipping the optical fibers into well plates. The major drawback of BLI is its relative lower sensitivity compared to other detection methods such as ELISA and SPR, making the detection of low molecular weight analytes very difficult. In addition, accurate and reproducible measurement of binding rate constants of antibodies is limited due to

challenges such as sensor regeneration, and mass transport limitations due to its static well configuration [323].

MST is performed using thin capillaries in free solution, using a microscopic temperature gradient induced by an infrared laser. This produces the movement of molecules within the capillaries and the detection is achieved using various fluorescent labels on either the recognition element or the analyte. The thermophoretic movement of molecules within the temperature gradient depends on size, charge, hydration shell or conformation that typically changes upon binding interactions, thus allowing the quantification of complex biomolecular interactions [324]. The dynamic range of this technique is usually with the pM to mM range, which is comparable to ELISA measurements. Additionally, the technique requires a small amount of sample and is relatively easy to use. However, this technique cannot provide kinetic information and the requirement of fluorescent labels have been known to cause non-specific binding, thus reducing experimental confidence particularly for a large number of targeted analytes.

Table 9.1 presents a summary of the current multiplex technologies along with their strength and weakness compared to SPRi. Overall, it can be observed that SPRi is a multiplex, label-free and real-time technology that allows the evaluation of the kinetic parameters of the system under study. Additionally, SPRi analysis required low reagent consumption compare to other technologies using sandwich immunoassay such as ELISA or Luminex xMAP. Moreover, this technique possess a short analysis time and reusability. To date, SPRi is the only commercially available technology with a high degree of automation, real-time measurement and imaging of up to several hundred interactions in parallel.

Table 9.1. Summary of current multiplex sensing technologies including their strengths and weakness compared to SPRi.

Technique	Strength	Weakness
SPRi	• Real-time • Kinetic information • Low reagent consumption • Reusability	• Microarray spotter required • Challenge for detection of low MW analytes • Surface immobilization required could alter bioreceptor activity
ELISA	• High sensitivity	• Low-throughput • High reagent consumption • Difficult to multiplex
Luminex xMAP	• High-throughput • High level of multiplexing	• High reagent consumption • Time-consuming • No kinetic information • Lack of real-time measurement
BLI	• Simple measurement set-up • Allows measurement in complex matrices	• Low sensitivity • Mass transport limitations • Low multiplexing
MST	• Small sample volume • No analyte immobilization required • Allow study of conformational changes	• Fluorescent labels required • No kinetic information • Specificity could be challenging with high number of analytes

Chapter 10. Future Work

In this thesis, we established the basic requirements for quantification of a SF from human pancreatic islets using multiplex SPRi-based biosensor. However, work still remains to further push this promising biosensing approach towards its translation as a technology platform. For this reason, foreseen challenges and future directions are discussed in the following section of this chapter.

10.1. Alternative signal amplification strategies

Although we have successfully introduced in Chapter 8 an SPR signal amplification strategy for the multiplexed detection of hormones, this strategy requires the use of GNP-tagged secondary antibodies. Despite the short analysis time of this approach compared to traditional bioassays, the indirect use of a labeled biorecognition element introduced additional steps to the assay, increasing the analysis time from 21 to 32 min. This can potentially be avoided by investigating alternative amplification techniques based on the integration of nanostructures onto the SPR sensing surface, such as nanoholes [71, 325] and nanorods [70]. Additionally, recent studies have shown that graphene-modified SPR substrates lead to a strong excited electric field enhancement producing ultra-high sensitivity in this type of biosensors [72, 326, 327]. These modifications can potentially allow the sensor to operate in a direct detection format, simplifying the assay and generating faster measurements.

10.2. Dynamic range and limit of the detection of the sensor in a complex matrix

In Chapter 8, we showed that the performance of the biosensor using an assay with gold nanoparticles is comparable to ELISA kits detecting somatostatin, also providing a comparable

LOD for insulin and glucagon with previous reports in literature detecting secretion from a group of 10 islets. However, the biosensor performance could be altered due to interaction with the complex matrix presented by the secretome of pancreatic islets, since it is known that many co-secreted peptides such as proinsulin, amylin and C-peptides are towed during glucose-induced section [93-96]. These small by-products of secretion are very similar in structure to the targeted hormones, which could possible give rise to antibody cross-reactivity. Additionally, despite the proven antifouling capabilities of the biosensor against proteins, other small molecules could introduce noise during analyte detection.

For this reason, the biosensor performance should be determined with collected secretions from islets, and if necessary be adjusted by further adapting its surface chemistry or by adjusting the concentration of reagents involved in the immunoassay. Additionally, the number of secreting islets must be studied to ensure that the three targeted hormones are collected within the dynamic range of the multiplex biosensor. In parallel with these measurements, ELISA kits which are the gold standard in the field, must be used to validate the concentration obtained using the developed SPRi biosensor.

10.3. Microfluidic integration

As reported in Chapter 5, in the last decade many microfluidic perfusion systems (MPS) have been developed to simulate *in vivo* environment of the islets, becoming a common *in vitro* model to study the islets' physiology and functionality. These systems provide several advantages for islets' SF analysis, such as 1) prolonging the islets survival for long term examination [127], 2) allowing highly accurate spatio-temporal secretion studies by avoiding accumulation of secretion products present within a static chamber [128] and 3) by rapidly varying the concentration of secretagogues

delivered to the islets, producing an accurate kinetic reading of the secreted products [128]. For future work, we envision to integrate the developed multiplex biosensor with a MPS, not only for the aforementioned reasons, but also to improve the overall fluid handling capabilities. With a more stable and flexible fluid control, the sensor's working volume could be reduced avoiding dilution of the secretions and thereby reaching a higher detection sensitivity. Moreover, the various steps of the competitive immunoassay could be performed in-situ, increasing its efficiency to further improve the overall biosensor's performance [328]. Such system can comprise a self-contained platform for continuous monitoring of a SF from the islets.

10.4. Platform to study the induction of diabetes to healthy human islets

With the integration of a MPS, a multiplexed biosensing tool and further automation, it would be possible to create a platform for the continuous monitoring of islets' SF. This would allow to differentiate a SF from healthy viable islets and diseased ones. Additionally, such a platform can be used to induce diabetes in healthy islets as an "*in vitro* diabetes model", allowing to better understand diverse physiological mechanisms of human pancreatic islets such as the loss of paracrine communications in diseased islets [299, 300]. Moreover, SF monitoring could have applications in islet quality assessment before transplantation, islet regeneration studies and drug screening. For islet transplantation purposes, monitoring a SF could provide an improved assessment of the viability and potency of the islet, as current practices evaluate only secretion of a single hormone to determine the islet's functionality [221-224]. For islet regeneration purposes, an SF could be used to rapidly assessed the functionality of regenerated islets or β-cells [229, 230]. Finally, this device could be used as a screening platform for testing novel therapeutic agents on diabetic islets by assessing the potency of these agents to revert diseased back into a healthy state.

Chapter 11. General Conclusion

The present thesis work introduced a novel multiplex biosensing strategy based on SPRi as a viable technique for detection of a SF from human pancreatic islets composed of insulin, glucagon and somatostatin. The use of a carefully designed SAM for simultaneous hormone immobilization along with an antifouling agent, allowed the development of a biosensor with excellent protein antifouling properties and specificity, capable of potential operation in a complex matrix such as a pancreatic islet secretome. To address the detection challenges of low molecular weight hormones secreted in very low concentration by human islets, a GNP amplification strategy in a competitive immunoassay format was implemented. This strategy led to a comparable sensor performance to proven biosensing technologies measuring secretion from a group of 10 islets. As such, this thesis laid the foundation required to begin with detection of secreted products from human pancreatic islets. The expectation is that with only minor adjustments, the developed biosensing strategy accomplishes the detection of insulin, glucagon and somatostatin from few human islets, further validating the achievements of this work. Moreover, it is expected that our sensing strategy integrated with a MPS to produce a platform that could address various obstacles in the understanding of the mechanism of islets dysfunction, thereby uncovering more novel alternatives for the treatment of diabetes.

References

1. *IDF Diabetes Atlas*. 2017; 8th edn.:[Available from: http://www.diabetesatlas.org.
2. Hall, J.E., *Guyton and Hall textbook of medical physiology.* Saunders, Philadelphia, 2011.
3. Yovos, J.G., *The role of α-, δ-and F cells in insulin secretion and action.* Diabetes research and clinical practice, 2011. **93**: p. S25-S26.
4. Kokil, G.R., et al., *Type 2 diabetes mellitus: limitations of conventional therapies and intervention with nucleic acid-based therapeutics.* Chem Rev, 2015. **115**(11): p. 4719-43.
5. Caicedo, A., *Paracrine and autocrine interactions in the human islet: More than meets the eye.* Seminars in Cell & Developmental Biology, 2013. **24**(1): p. 11-21.
6. Wierup, N., F. Sundler, and R.S. Heller, *The islet ghrelin cell.* Journal of Molecular Endocrinology, 2014. **52**(1): p. R35-R49.
7. Yang, L., et al., *Imaging beta-cell mass and function in situ and in vivo.* Journal of Molecular Medicine, 2013. **91**(8): p. 929-938.
8. Süss, C. and M. Solimena, *Proteomic Profiling of β-cells Using a Classical Approach–Two-dimensional Gel Electrophoresis.* Experimental and clinical endocrinology & diabetes, 2008. **116**(S 01): p. S13-S20.
9. Li, Y.V., *Zinc and insulin in pancreatic beta-cells.* Endocrine, 2014. **45**(2): p. 178-189.
10. Rorsman, P. and M. Braun, *Regulation of Insulin Secretion in Human Pancreatic Islets.* Annual Review of Physiology, Vol 75, 2013. **75**: p. 155-179.
11. Cabrera, O., et al., *The unique cytoarchitecture of human pancreatic islets has implications for islet cell function.* Proceedings of the National Academy of Sciences of the United States of America, 2006. **103**(7): p. 2334-2339.
12. Bosco, D., et al., *Unique arrangement of α- and β-cells in human islets of Langerhans.* Diabetes, 2010. **59**(5): p. 1202-1210.
13. Hanna, S.T., et al., *Kiss-and-run exocytosis and fusion pores of secretory vesicles in human β-cells.* Pflugers Archiv European Journal of Physiology, 2009. **457**(6): p. 1343-1350.
14. Braun, M., et al., *Somatostatin release, electrical activity, membrane currents and exocytosis in human pancreatic delta cells.* Diabetologia, 2009. **52**(8): p. 1566-1578.
15. Braun, M., et al., *Voltage-Gated Ion Channels in Human Pancreatic β-Cells: Electrophysiological Characterization and Role in Insulin Secretion.* Diabetes, 2008. **57**(6): p. 1618-1628.
16. Braun, M., *The Somatostatin Receptor in Human Pancreatic beta-Cells*, in *Pancreatic Beta Cell*, G. Litwack, Editor. 2014, Elsevier Academic Press Inc: San Diego. p. 165-193.
17. Reed, M.J. and K.A. Scribner, *In‐vivo and in‐vitro models of type 2 diabetes in pharmaceutical drug discovery.* Diabetes, Obesity and Metabolism, 1999. **1**(2): p. 75-86.
18. Sakata, N., et al., *Animal models of diabetes mellitus for islet transplantation.* Exp Diabetes Res, 2012. **2012**: p. 256707.
19. Dave, V., et al., *Experimental Models on Diabetes: A Comprehensive Review.* International Journal of Advances in Pharmaceutical Sciences, 2013. **4**(1): p. 01-08.
20. Poitout, V., L.K. Olson, and R.P. Robertson, *Insulin-secreting cell lines: classification, characteristics and potential applications.* Diabetes Metab, 1996. **22**(1): p. 7-14.
21. Ramachandran, K., et al., *Assessment of re-aggregated human pancreatic islets for secondary drug screening.* British Journal of Pharmacology, 2014. **171**(12): p. 3010-3022.
22. Luciani, D.S. and J.D. Johnson, *Acute effects of insulin on beta-cells from transplantable*

human islets. Molecular and cellular endocrinology, 2005. **241**(1): p. 88-98.
23. Braun, M., et al., *γ-aminobutyric acid (GABA) is an autocrine excitatory transmitter in human pancreatic β-cells.* Diabetes, 2010. **59**(7): p. 1694-1701.
24. Ramracheya, R., et al., *Membrane Potential-Dependent Inactivation of Voltage-Gated Ion Channels in α-Cells Inhibits Glucagon Secretion From Human Islets.* Diabetes, 2010. **59**(9): p. 2198-2208.
25. Roper, M.G., et al., *Microfluidic chip for continuous monitoring of hormone secretion from live cells using an electrophoresis-based immunoassay.* Analytical chemistry, 2003. **75**(18): p. 4711-4717.
26. Shackman, J.G., et al., *Dynamic monitoring of glucagon secretion from living cells on a microfluidic chip.* Analytical and Bioanalytical Chemistry, 2012. **402**(9): p. 2797-2803.
27. Lomasney, A.R., L. Yi, and M.G. Roper, *Simultaneous Monitoring of Insulin and Islet Amyloid Polypeptide Secretion from Islets of Langerhans on a Microfluidic Device.* Analytical Chemistry, 2013. **85**(16): p. 7919-7925.
28. Xing, Y., et al., *A pumpless microfluidic device driven by surface tension for pancreatic islet analysis.* Biomedical Microdevices, 2016. **18**(5): p. 9.
29. Lee, D., et al., *Dual microfluidic perifusion networks for concurrent islet perifusion and optical imaging.* Biomedical Microdevices, 2012. **14**(1): p. 7-16.
30. Huang, Y.X., D. Cai, and P. Chen, *Micro- and Nanotechnologies for Study of Cell Secretion.* Analytical Chemistry, 2011. **83**(12): p. 4393-4406.
31. Oh, B.R., et al., *Integrated Nanoplasmonic Sensing for Cellular Functional Immunoanalysis Using Human Blood.* ACS Nano, 2014.
32. Tsouti, V., et al., *Capacitive microsystems for biological sensing.* Biosens Bioelectron, 2011. **27**(1): p. 1-11.
33. Luo, X. and J.J. Davis, *Electrical biosensors and the label free detection of protein disease biomarkers.* Chem Soc Rev, 2013. **42**(13): p. 5944-62.
34. Berggren, C., B. Bjarnason, and G. Johansson, *Capacitive biosensors.* Electroanalysis, 2001. **13**(3): p. 173-180.
35. Daniels, J.S. and N. Pourmand, *Label-free impedance biosensors: Opportunities and challenges.* Electroanalysis, 2007. **19**(12): p. 1239-1257.
36. Igreja, R. and C. Dias, *Analytical evaluation of the interdigital electrodes capacitance for a multi-layered structure.* Sensors and Actuators A: Physical, 2004. **112**(2): p. 291-301.
37. Zou, Z., et al., *Functionalized nano interdigitated electrodes arrays on polymer with integrated microfluidics for direct bio-affinity sensing using impedimetric measurement.* Sensors and Actuators, A: Physical, 2007. **136**(2): p. 518-526.
38. Xu, M., X. Luo, and J.J. Davis, *The label free picomolar detection of insulin in blood serum.* Biosensors and Bioelectronics, 2013. **39**(1): p. 21-25.
39. Wright, J.E.I., et al., *Electrochemical impedance spectroscopy and quartz crystal nanobalance (EQCN) studies of insulin adsorption on Pt.* Journal of Electroanalytical Chemistry, 2004. **564**(1-2): p. 185-197.
40. Luo, X., et al., *Ultrasensitive label free electrical detection of insulin in neat blood serum.* Analytical chemistry, 2013. **85**(8): p. 4129-4134.
41. Homola, J., S.S. Yee, and G. Gauglitz, *Surface plasmon resonance sensors: review.* Sensors and Actuators B: Chemical, 1999. **54**(1): p. 3-15.
42. Singh, P., *SPR Biosensors: Historical Perspectives and Current Challenges.* Sensors and Actuators B: Chemical, 2016. **229**: p. 110-130.

43. Spoto, G. and M. Minunni, *Surface Plasmon Resonance Imaging: What Next?* The Journal of Physical Chemistry Letters, 2012. **3**(18): p. 2682-2691.
44. Nault, L., et al., *Human insulin adsorption kinetics, conformational changes and amyloidal aggregate formation on hydrophobic surfaces.* Acta Biomaterialia, 2013. **9**(2): p. 5070-5079.
45. Ha Minh, H., et al., *A Microfluidic Chip Based on Localized Surface Plasmon Resonance for Real-Time Monitoring of Antigen–Antibody Reactions.* Japanese Journal of Applied Physics, 2008. **47**(2S): p. 1337.
46. Grasso, G., et al., *Enzyme solid-state support assays: a surface plasmon resonance and mass spectrometry coupled study of immobilized insulin degrading enzyme.* Eur Biophys J, 2009. **38**(4): p. 407-14.
47. Gao, J., et al., *Affinity analysis of somatostatin and somatostatin receptor by surface plasmon resonance.* Analytical Methods, 2013. **5**(13): p. 3201-3206.
48. Lerch, M., et al., *Strongly Altered Receptor Binding Properties in PP and NPY Chimeras Are Accompanied by Changes in Structure and Membrane Binding.* Biochemistry, 2005. **44**(25): p. 9255-9264.
49. Zou, C., et al., *Studies of the Structure of the N-Terminal Domain from the Y4 Receptor—a G Protein-Coupled Receptor—and its Interaction with Hormones from the NPY Family.* ChemBioChem, 2008. **9**(14): p. 2276-2284.
50. Takagi, K., et al., *Anti-ghrelin immunoglobulins modulate ghrelin stability and its orexigenic effect in obese mice and humans.* Nature Communications, 2013. **4**.
51. Bahadır, E.B. and M.K. Sezgintürk, *Applications of commercial biosensors in clinical, food, environmental, and biothreat/biowarfare analyses.* Analytical Biochemistry, 2015. **478**: p. 107-120.
52. Turner, A.P.F., *Biosensors: sense and sensibility.* Chemical Society Reviews, 2013. **42**(8): p. 3184-3196.
53. Grieshaber, D., et al., *Electrochemical Biosensors - Sensor Principles and Architectures.* Sensors (Basel, Switzerland), 2008. **8**(3): p. 1400-1458.
54. Arlett, J.L., E.B. Myers, and M.L. Roukes, *Comparative advantages of mechanical biosensors.* Nature Nanotechnology, 2011. **6**: p. 203.
55. Foudeh, A.M., et al., *Microfluidic designs and techniques using lab-on-a-chip devices for pathogen detection for point-of-care diagnostics.* Lab on a Chip, 2012. **12**(18): p. 3249-3266.
56. St John, A. and C.P. Price, *Existing and Emerging Technologies for Point-of-Care Testing.* The Clinical biochemist. Reviews, 2014. **35**(3): p. 155-167.
57. Randviir, E.P. and C.E. Banks, *Electrochemical impedance spectroscopy: an overview of bioanalytical applications.* Analytical Methods, 2013. **5**(5): p. 1098-1115.
58. Lvovich, V.F., *Impedance spectroscopy: applications to electrochemical and dielectric phenomena*. 2012: John Wiley & Sons.
59. Prodromidis, M.I., *Impedimetric immunosensors—A review.* Electrochimica Acta, 2010. **55**(14): p. 4227-4233.
60. Wood, R.W., *On a Remarkable Case of Uneven Distribution of Light in a Diffraction Grating Spectrum.* Proceedings of the Physical Society of London, 1902. **18**(1): p. 269.
61. Hill, R.T., *Plasmonic biosensors.* Wiley Interdisciplinary Reviews-Nanomedicine and Nanobiotechnology, 2015. **7**(2): p. 152-168.
62. Schasfoort, R.B., *Handbook of surface plasmon resonance*. 2nd Edition ed. 2017, United

Kingdom Royal Society of Chemistry.
63. Nguyen, H.H., et al., *Surface Plasmon Resonance: A Versatile Technique for Biosensor Applications.* Sensors, 2015. **15**(5): p. 10481-10510.
64. Rothenhäusler, B. and W. Knoll, *Surface–plasmon microscopy.* Nature, 1988. **332**: p. 615.
65. Zeng, S.W., et al., *Nanomaterials enhanced surface plasmon resonance for biological and chemical sensing applications.* Chemical Society Reviews, 2014. **43**(10): p. 3426-3452.
66. Lyon, L.A., M.D. Musick, and M.J. Natan, *Colloidal Au-Enhanced Surface Plasmon Resonance Immunosensing.* Analytical Chemistry, 1998. **70**(24): p. 5177-5183.
67. Szunerits, S., J. Spadavecchia, and R. Boukherroub, *Surface plasmon resonance: signal amplification using colloidal gold nanoparticles for enhanced sensitivity.* Reviews in Analytical Chemistry, 2014. **33**(3): p. 153-164.
68. He, L., et al., *Colloidal Au-Enhanced Surface Plasmon Resonance for Ultrasensitive Detection of DNA Hybridization.* Journal of the American Chemical Society, 2000. **122**(38): p. 9071-9077.
69. Azzam, E.M.S., et al., *Fabrication of a surface plasmon resonance biosensor based on gold nanoparticles chemisorbed onto a 1,10-decanedithiol self-assembled monolayer.* Thin Solid Films, 2009. **518**(1): p. 387-391.
70. Kabashin, A.V., et al., *Plasmonic nanorod metamaterials for biosensing.* Nature Materials, 2009. **8**: p. 867.
71. Brolo, A.G., et al., *Surface Plasmon Sensor Based on the Enhanced Light Transmission through Arrays of Nanoholes in Gold Films.* Langmuir, 2004. **20**(12): p. 4813-4815.
72. Wu, L., et al., *Highly sensitive graphene biosensors based on surface plasmon resonance.* Optics Express, 2010. **18**(14): p. 14395-14400.
73. van Santen, R.A., *Reactivity of transition-metal surfaces.* Catalysis Letters, 1992. **16**(1): p. 59-69.
74. Love, J.C., et al., *Self-assembled monolayers of thiolates on metals as a form of nanotechnology.* Chemical Reviews, 2005. **105**(4): p. 1103-1169.
75. Mendes, A.C., et al., *Self-assembly in nature: using the principles of nature to create complex nanobiomaterials.* Wiley Interdisciplinary Reviews: Nanomedicine and Nanobiotechnology, 2013. **5**(6): p. 582-612.
76. Wink, T., et al., *Self-assembled monolayers for biosensors.* Analyst, 1997. **122**(4): p. 43R-50R.
77. Shevade, A.V., et al., *Phase Behavior of Mixed Self-Assembled Monolayers of Alkanethiols on Au(111): A Configurational-Bias Monte Carlo Simulation Study.* Langmuir, 2001. **17**(24): p. 7566-7572.
78. Lahiri, J., et al., *A strategy for the generation of surfaces presenting ligands for studies of binding based on an active ester as a common reactive intermediate: a surface plasmon resonance study.* Analytical chemistry, 1999. **71**(4): p. 777-790.
79. Vericat, C., M.E. Vela, and R.C. Salvarezza, *Self-assembled monolayers of alkanethiols on Au(111): surface structures, defects and dynamics.* Physical Chemistry Chemical Physics, 2005. **7**(18): p. 3258-3268.
80. Chen, S., et al., *Controlled Chemical and Structural Properties of Mixed Self-Assembled Monolayers of Alkanethiols on Au(111).* Langmuir, 2000. **16**(24): p. 9287-9293.
81. Islam, N., et al., *Effects of Composition of Oligo(ethylene glycol)-Based Mixed Monolayers on Peptide Grafting and Human Immunoglobulin Detection.* The Journal of Physical Chemistry C, 2014. **118**(10): p. 5361-5373.

82. Briand, E., et al., *Building of an immunosensor: How can the composition and structure of the thiol attachment layer affect the immunosensor efficiency?* Biosensors & Bioelectronics, 2006. **22**(3): p. 440-448.
83. Agrawal, G.K., et al., *Plant secretome: Unlocking secrets of the secreted proteins.* Proteomics, 2010. **10**(4): p. 799-827.
84. Mukherjee, P. and S. Mani, *Methodologies to decipher the cell secretome.* Biochimica Et Biophysica Acta-Proteins and Proteomics, 2013. **1834**(11): p. 2226-2232.
85. Hathout, Y., *Approaches to the study of the cell secretome.* Expert Review of Proteomics, 2007. **4**(2): p. 239-248.
86. Niepel, M., S.L. Spencer, and P.K. Sorger, *Non-genetic cell-to-cell variability and the consequences for pharmacology.* Current opinion in chemical biology, 2009. **13**(5): p. 556-561.
87. Cohen, A.A., et al., *Dynamic proteomics of individual cancer cells in response to a drug.* science, 2008. **322**(5907): p. 1511-1516.
88. Gascoigne, K.E. and S.S. Taylor, *Cancer cells display profound intra-and interline variation following prolonged exposure to antimitotic drugs.* Cancer cell, 2008. **14**(2): p. 111-122.
89. Otonkoski, T., et al., *Unique basement membrane structure of human pancreatic islets: implications for β-cell growth and differentiation.* Diabetes, obesity and metabolism, 2008. **10**(s4): p. 119-127.
90. Polonsky, K., B. Given, and E. Van Cauter, *Twenty-four-hour profiles and pulsatile patterns of insulin secretion in normal and obese subjects.* Journal of Clinical Investigation, 1988. **81**(2): p. 442.
91. Lefebvre, P., et al., *Pulsatility of insulin and glucagon release: physiological significance and pharmacological implications.* Diabetologia, 1987. **30**(7): p. 443-452.
92. Gilon, P., R.M. Shepherd, and J.-C. Henquin, *Oscillations of secretion driven by oscillations of cytoplasmic Ca2+ as evidences in single pancreatic islets.* Journal of Biological Chemistry, 1993. **268**(30): p. 22265-22268.
93. Jones, A.G. and A.T. Hattersley, *The clinical utility of C-peptide measurement in the care of patients with diabetes.* Diabetic Medicine, 2013. **30**(7): p. 803-817.
94. Westermark, P., A. Andersson, and G.T. Westermark, *Islet amyloid polypeptide, islet amyloid, and diabetes mellitus.* Physiological Reviews, 2011. **91**(3): p. 795-826.
95. Brandenburg, D., *History and diagnostic significance of C-peptide.* Exp Diabetes Res, 2008. **2008**: p. 576862.
96. Easley, C.J., et al., *Quantitative measurement of zinc secretion from pancreatic islets with high temporal resolution using droplet-based microfluidics.* Analytical Chemistry, 2009. **81**(21): p. 9086-9095.
97. Le Marchand, S.J. and D.W. Piston, *Glucose Suppression of Glucagon Secretion METABOLIC AND CALCIUM RESPONSES FROM α-CELLS IN INTACT MOUSE PANCREATIC ISLETS.* Journal of Biological Chemistry, 2010. **285**(19): p. 14389-14398.
98. Wang, X., et al., *Micellar electrokinetic chromatography method for measuring amino acid secretions from islets of Langerhans.* Electrophoresis, 2015. **36**(9-10): p. 1172-1178.
99. Gylfe, E. and A. Tengholm, *Neurotransmitter control of islet hormone pulsatility.* Diabetes, Obesity and Metabolism, 2014. **16**: p. 102-110.
100. Dezaki, K., et al., *Ghrelin attenuates cAMP-PKA signaling to evoke insulinostatic cascade in islet β-cells.* Diabetes, 2011. **60**(9): p. 2315-2324.

101. Aizawa, T., et al., *Size-related and size-unrelated functional heterogeneity among pancreatic islets.* Life sciences, 2001. **69**(22): p. 2627-2639.
102. Farhat, B., et al., *Small human islets comprised of more beta-cells with higher insulin content than large islets.* Islets, 2013. **5**(2): p. 87-94.
103. Huang, H.H., et al., *Low insulin content of large islet population is present in situ and in isolated islets.* Islets, 2011. **3**(1): p. 6-13.
104. Ahmed, M., J. Forsberg, and P. Bergsten, *Protein profiling of human pancreatic islets by two-dimensional gel electrophoresis and mass spectrometry.* J Proteome Res, 2005. **4**(3): p. 931-40.
105. Bergsten, P., *Islet protein profiling.* Diabetes Obesity & Metabolism, 2009. **11**: p. 97-117.
106. Ahmed, M., *Proteomics and islet research*, in *The Islets of Langerhans*. 2010, Springer. p. 363-390.
107. Yousefi, Z., et al., *Secretomic analysis of large cell lung cancer cell lines using two-dimensional gel electrophoresis coupled to mass spectrometry.* Folia Histochemica Et Cytobiologica, 2012. **50**(3): p. 368-374.
108. Imperlini, E., et al., *The Secretome Signature of Colon Cancer Cell Lines.* Journal of Cellular Biochemistry, 2013. **114**(11): p. 2577-2587.
109. Formolo, C.A., et al., *Secretome Signature of Invasive Glioblastoma Multiforme.* Journal of Proteome Research, 2011. **10**(7): p. 3149-3159.
110. Jha, M.K., et al., *The secretome signature of reactive glial cells and its pathological implications.* Biochimica Et Biophysica Acta-Proteins and Proteomics, 2013. **1834**(11): p. 2418-2428.
111. Yoon, J.H., et al., *Secretomics for skeletal muscle cells: a discovery of novel regulators?* Advances in biological regulation, 2012. **52**(2): p. 340-50.
112. Zhong, J., et al., *Temporal Profiling of the Secretome during Adipogenesis in Humans.* Journal of Proteome Research, 2010. **9**(10): p. 5228-5238.
113. Chevallet, M., et al., *Toward a better analysis of secreted proteins: the example of the myeloid cells secretome.* Proteomics, 2007. **7**(11): p. 1757-1770.
114. Kulkarni, G. and C. McCulloch, *Serum deprivation induces apoptotic cell death in a subset of Balb/c 3T3 fibroblasts.* Journal of cell science, 1994. **107**(5): p. 1169-1179.
115. Charles, I., et al., *Serum deprivation induces apoptotic cell death of transformed rat retinal ganglion cells via mitochondrial signaling pathways.* Invest Ophthalmol Vis Sci, 2005. **46**(4): p. 1330-8.
116. Pirkmajer, S. and A.V. Chibalin, *Serum starvation: caveat emptor.* American Journal of Physiology-Cell Physiology, 2011. **301**(2): p. C272-C279.
117. Gallotta, A., E. Orzes, and G. Fassina, *Biomarkers quantification with antibody arrays in cancer early detection.* Clinics in laboratory medicine, 2012. **32**(1): p. 33-45.
118. Liu, C.-H. and S.-M. Hwang, *Cytokine interactions in mesenchymal stem cells from cord blood.* Cytokine, 2005. **32**(6): p. 270-279.
119. LaFramboise, W.A., et al., *Cardiac fibroblasts influence cardiomyocyte phenotype in vitro.* American Journal of Physiology-Cell Physiology, 2007. **292**(5): p. C1799-C1808.
120. Lu, Y., et al., *High-Throughput Secretomic Analysis of Single Cells to Assess Functional Cellular Heterogeneity.* Analytical Chemistry, 2013. **85**(4): p. 2548-2556.
121. Sackmann, E.K., A.L. Fulton, and D.J. Beebe, *The present and future role of microfluidics in biomedical research.* Nature, 2014. **507**(7491): p. 181-189.
122. Fan, R., et al., *Integrated barcode chips for rapid, multiplexed analysis of proteins in*

microliter quantities of blood. Nature biotechnology, 2008. **26**(12): p. 1373-1378.
123. Chen, Q., et al., *Qualitative and quantitative analysis of tumor cell metabolism via stable isotope labeling assisted microfluidic chip electrospray ionization mass spectrometry.* Analytical chemistry, 2012. **84**(3): p. 1695-1701.
124. Ma, C., et al., *A clinical microchip for evaluation of single immune cells reveals high functional heterogeneity in phenotypically similar T cells.* Nature medicine, 2011. **17**(6): p. 738-743.
125. Galler, K., et al., *Making a big thing of a small cell - recent advances in single cell analysis.* Analyst, 2014. **139**(6): p. 1237-1273.
126. Liu, Y. and A.K. Singh, *Microfluidic Platforms for Single-Cell Protein Analysis.* Jala, 2013. **18**(6): p. 446-454.
127. Wang, Y., et al., *Application of microfluidic technology to pancreatic islet research: first decade of endeavor.* Bioanalysis, 2010. **2**(10): p. 1729-1744.
128. Shackman, J.G., et al., *Perfusion and chemical monitoring of living cells on a microfluidic chip.* Lab on a Chip, 2005. **5**(1): p. 56-63.
129. Dishinger, J.F., K.R. Reid, and R.T. Kennedy, *Quantitative monitoring of insulin secretion from single islets of Langerhans in parallel on a microfluidic chip.* Analytical chemistry, 2009. **81**(8): p. 3119-3127.
130. Adewola, A.F., et al., *Microfluidic perifusion and imaging device for multi-parametric islet function assessment.* Biomed Microdevices, 2010. **12**(3): p. 409-17.
131. Rocheleau, J.V., et al., *Microfluidic glucose stimulation reveals limited coordination of intracellular Ca2+ activity oscillations in pancreatic islets.* Proceedings of the National Academy of Sciences of the United States of America, 2004. **101**(35): p. 12899-12903.
132. Nourmohammadzadeh, M., et al., *Microfluidic Array with Integrated Oxygenation Control for Real-Time Live-Cell Imaging: Effect of Hypoxia on Physiology of Microencapsulated Pancreatic Islets.* Analytical Chemistry, 2013. **85**(23): p. 11240-11249.
133. Silva, P.N., et al., *A microfluidic device designed to induce media flow throughout pancreatic islets while limiting shear-induced damage.* Lab Chip, 2013. **13**(22): p. 4374-84.
134. Mohammed, J.S., et al., *Microfluidic device for multimodal characterization of pancreatic islets.* Lab Chip, 2009. **9**(1): p. 97-106.
135. Cheng, S.B., et al., *Development of a multichannel microfluidic analysis system employing affinity capillary electrophoresis for immunoassay.* Analytical chemistry, 2001. **73**(7): p. 1472-1479.
136. Bromberg, A. and R.A. Mathies, *Multichannel homogeneous immunoassay for detection of 2, 4, 6 - trinitrotoluene (TNT) using a microfabricated capillary array electrophoresis chip.* Electrophoresis, 2004. **25**(12): p. 1895-1900.
137. Dishinger, J.F. and R.T. Kennedy, *Serial immunoassays in parallel on a microfluidic chip for monitoring hormone secretion from living cells.* Analytical chemistry, 2007. **79**(3): p. 947-954.
138. Yi, L., et al., *Integrated perfusion and separation systems for entrainment of insulin secretion from islets of Langerhans.* Lab on a Chip, 2015. **15**(3): p. 823-832.
139. Takahashi, A., et al., *Measurement of intracellular calcium.* Physiol Rev, 1999. **79**(4): p. 1089-125.
140. Zhang, X. and M.G. Roper, *Microfluidic perfusion system for automated delivery of temporal gradients to islets of Langerhans.* Analytical chemistry, 2009. **81**(3): p. 1162-

1168.
141. Dhumpa, R., et al., *Negative Feedback Synchronizes Islets of Langerhans.* Biophysical Journal, 2014. **106**(10): p. 2275-2282.
142. Terao, K., et al., *Subcellular glucose exposure biases the spatial distribution of insulin granules in single pancreatic beta cells.* Scientific Reports, 2014. **4**: p. 6.
143. Rocheleau, J.V., et al., *Critical role of gap junction coupled KATP channel activity for regulated insulin secretion.* PLoS Biol, 2006. **4**(2): p. e26.
144. Chen, D., et al., *The chemistrode: a droplet-based microfluidic device for stimulation and recording with high temporal, spatial, and chemical resolution.* Proceedings of the National Academy of Sciences, 2008. **105**(44): p. 16843-16848.
145. Nunemaker, C.S., et al., *Glucose metabolism, islet architecture, and genetic homogeneity in imprinting of [Ca2+] i and insulin rhythms in mouse islets.* PloS one, 2009. **4**(12): p. e8428.
146. Reid, K.R. and R.T. Kennedy, *Continuous operation of microfabricated electrophoresis devices for 24 hours and application to chemical monitoring of living cells.* Analytical chemistry, 2009. **81**(16): p. 6837-6842.
147. Zhang, X., et al., *Microfluidic system for generation of sinusoidal glucose waveforms for entrainment of islets of Langerhans.* Analytical chemistry, 2010. **82**(15): p. 6704-6711.
148. Nam, K.H., et al., *Size-based separation and collection of mouse pancreatic islets for functional analysis.* Biomedical Microdevices, 2010. **12**(5): p. 865-874.
149. Godwin, L.A., et al., *Passively Operated Microfluidic Device for Stimulation and Secretion Sampling of Single Pancreatic Islets.* Analytical Chemistry, 2011. **83**(18): p. 7166-7172.
150. Morris, C., et al., *A robust microfluidic in vitro cell perifusion system.* Conf Proc IEEE Eng Med Biol Soc, 2011. **2011**: p. 8412-5.
151. Sankar, K.S., et al., *Culturing pancreatic islets in microfluidic flow enhances morphology of the associated endothelial cells.* PloS one, 2011. **6**(9): p. e24904.
152. Lo, J.F., et al., *Islet Preconditioning via Multimodal Microfluidic Modulation of Intermittent Hypoxia.* Analytical Chemistry, 2012. **84**(4): p. 1987-1993.
153. Lam, A.K., et al., *Quantitative imaging of electron transfer flavoprotein autofluorescence reveals the dynamics of lipid partitioning in living pancreatic islets.* Integrative Biology, 2012. **4**(8): p. 838-846.
154. Wang, Y., et al., *Systematic prevention of bubble formation and accumulation for long-term culture of pancreatic islet cells in microfluidic device.* Biomedical microdevices, 2012. **14**(2): p. 419-426.
155. Misler, S., et al., *Electrophysiology of stimulus-secretion coupling in human β-cells.* Diabetes, 1992. **41**(10): p. 1221-1228.
156. Braun, M., et al., *Exocytotic Properties of Human Pancreatic β-cells.* Annals of the New York Academy of Sciences, 2009. **1152**(1): p. 187-193.
157. Hanna, S., et al., *Kiss-and-run exocytosis and fusion pores of secretory vesicles in human β-cells.* Pflügers Archiv - European Journal of Physiology, 2009. **457**(6): p. 1343-1350.
158. Luciani, D.S. and J.D. Johnson, *Acute effects of insulin on beta-cells from transplantable human islets.* Molecular and Cellular Endocrinology, 2005. **241**(1–2): p. 88-98.
159. Proks, P., et al., *Ca(2+)- and GTP-dependent exocytosis in mouse pancreatic beta-cells involves both common and distinct steps.* The Journal of Physiology, 1996. **496**(Pt 1): p. 255-264.
160. Lau, A.Y., et al., *Open-access microfluidic patch-clamp array with raised lateral cell*

trapping sites. Lab on a Chip, 2006. **6**(12): p. 1510-1515.
161. Bruhn, B.R., et al., *Dual-pore glass chips for cell-attached single-channel recordings.* Lab on a Chip, 2014. **14**(14): p. 2410-2417.
162. Pantoja, R., et al., *Silicon chip-based patch-clamp electrodes integrated with PDMS microfluidics.* Biosensors and Bioelectronics, 2004. **20**(3): p. 509-517.
163. Li, X., et al., *Microfluidic System for Planar Patch Clamp Electrode Arrays.* Nano Letters, 2006. **6**(4): p. 815-819.
164. Dunlop, J., et al., *High-throughput electrophysiology: an emerging paradigm for ion-channel screening and physiology.* Nature reviews Drug discovery, 2008. **7**(4): p. 358-368.
165. Farre, C., et al., *Ion channel screening – automated patch clamp on the rise.* Drug Discovery Today: Technologies, 2008. **5**(1): p. e23-e28.
166. Göpel, S., et al., *Patch‐clamp characterisation of somatostatin‐secreting δ‐cells in intact mouse pancreatic islets.* The Journal of physiology, 2000. **528**(3): p. 497-507.
167. Göpel, S., et al., *Regulation of glucagon release in mouse α‐cells by KATP channels and inactivation of TTX‐sensitive Na+ channels.* The Journal of physiology, 2000. **528**(3): p. 509-520.
168. Göpel, S., et al., *Voltage-gated and resting membrane currents recorded from B-cells in intact mouse pancreatic islets.* Journal of Physiology, 1999. **521**(3): p. 717-728.
169. Paras, C.D., et al., *Localized exocytosis detected by spatially resolved amperometry in single pancreatic β-cells.* Cell biochemistry and biophysics, 2000. **33**(3): p. 227-240.
170. Salimi, A., et al., *Picomolar Detection of Insulin at Renewable Nickel Powder-Doped Carbon Composite Electrode.* Analytical Chemistry, 2007. **79**(19): p. 7431-7438.
171. Rafiee, B. and A.R. Fakhari, *Electrocatalytic oxidation and determination of insulin at nickel oxide nanoparticles-multiwalled carbon nanotube modified screen printed electrode.* Biosensors and Bioelectronics, 2013. **46**(0): p. 130-135.
172. Amini, N., M.B. Gholivand, and M. Shamsipur, *Electrocatalytic determination of traces of insulin using a novel silica nanoparticles-Nafion modified glassy carbon electrode.* Journal of Electroanalytical Chemistry, 2014. **714–715**(0): p. 70-75.
173. Gerasimov, J.Y., et al., *Development of an electrochemical insulin sensor based on the insulin-linked polymorphicregion.* Biosensors and Bioelectronics, 2013. **42**(0): p. 62-68.
174. Prasad, B.B., et al., *Imprinting molecular recognition sites on multiwalled carbon nanotubes surface for electrochemical detection of insulin in real samples.* Electrochimica Acta, 2010. **55**(28): p. 9146-9156.
175. Lee, J.-O., et al., *Aptamers as molecular recognition elements for electrical nanobiosensors.* Analytical and bioanalytical chemistry, 2008. **390**(4): p. 1023-1032.
176. Barbosa, R.M., et al., *Control of pulsatile 5‐HT/insulin secretion from single mouse pancreatic islets by intracellular calcium dynamics.* The Journal of physiology, 1998. **510**(1): p. 135-143.
177. Maghasi, A.T., et al., *Detection of secretion from pancreatic islets using chemically modified electrodes.* Analytical Biochemistry, 2004. **326**(2): p. 183-189.
178. Barbosa, R.M., et al., *Electrochemical studies of zinc in zinc-insulin solution.* Analyst, 1996. **121**(12): p. 1789-1793.
179. Barg, S., et al., *The stimulatory action of tolbutamide on Ca2+-dependent exocytosis in pancreatic β cells is mediated by a 65-kDa mdr-like P-glycoprotein.* Proceedings of the National Academy of Sciences, 1999. **96**(10): p. 5539-5544.

180. Smith, P.A., P. Proks, and F.M. Ashcroft, *Quantal analysis of 5-hydroxytryptamine release from mouse pancreatic β-cells.* The Journal of Physiology, 1999. **521**(3): p. 651-664.
181. Takahashi, N., et al., *Post-priming actions of ATP on Ca2+-dependent exocytosis in pancreatic beta cells.* Proceedings of the National Academy of Sciences, 1999. **96**(2): p. 760-765.
182. Zhou, Z. and S. Misler, *Amperometric Detection of Quantal Secretion from Patch-clamped Rat Pancreatic -Cells.* Journal of Biological Chemistry, 1996. **271**(1): p. 270-277.
183. Barbosa, R.M., et al., *Real Time Electrochemical Detection of 5-HT/Insulin Secretion from Single Pancreatic Islets: Effect of Glucose and K+Depolarization.* Biochemical and Biophysical Research Communications, 1996. **228**(1): p. 100-104.
184. Barbosa, R.M., et al., *Control of pulsatile 5-HT/insulin secretion from single mouse pancreatic islets by intracellular calcium dynamics.* The Journal of Physiology, 1998. **510**(1): p. 135-143.
185. Snider, R.M., et al., *A multiwalled carbon nanotube/dihydropyran composite film electrode for insulin detection in a microphysiometer chamber.* Anal Chim Acta, 2008. **609**(1): p. 44-52.
186. Luo, X.L., et al., *Redox and Label-Free Array Detection of Protein Markers in Human Serum.* Analytical Chemistry, 2014. **86**(11): p. 5553-5558.
187. Goode, J.A., J.V.H. Rushworth, and P.A. Millner, *Biosensor Regeneration: A Review of Common Techniques and Outcomes.* Langmuir, 2015. **31**(23): p. 6267-6276.
188. Li, B.R., et al., *An ultrasensitive nanowire-transistor biosensor for detecting dopamine release from living pc12 cells under hypoxic stimulation.* Journal of the American Chemical Society, 2013. **135**(43): p. 16034-16037.
189. Schöning, M.J. and A. Poghossian, *Recent advances in biologically sensitive field-effect transistors (BioFETs).* Analyst, 2002. **127**(9): p. 1137-1151.
190. Lee, J., S.A. Soper, and K.K. Murray, *Microfluidics with MALDI analysis for proteomics—A review.* Analytica chimica acta, 2009. **649**(2): p. 180-190.
191. Matsumoto, A. and Y. Miyahara, *Current and emerging challenges of field effect transistor based bio-sensing.* Nanoscale, 2013. **5**(22): p. 10702-10718.
192. Sakata, T. and H. Sugimoto, *Continuous Monitoring of Electrical Activity of Pancreatic beta-Cells Using Semiconductor-Based Biosensing Devices.* Japanese Journal of Applied Physics, 2011. **50**(2): p. 3.
193. D'Agata, R. and G. Spoto, *Surface plasmon resonance imaging for nucleic acid detection.* Analytical and bioanalytical chemistry, 2013. **405**(2-3): p. 573-584.
194. Stybayeva, G., et al., *Detecting interferon-gamma release from human CD4 T-cells using surface plasmon resonance.* Colloids and Surfaces B: Biointerfaces, 2010. **80**(2): p. 251-255.
195. Milgram, S., et al., *On chip real time monitoring of B-cells hybridoma secretion of immunoglobulin.* Biosensors and Bioelectronics, 2011. **26**(5): p. 2728-32.
196. Wu, S.H., et al., *Optofluidic Platform for Real-Time Monitoring of Live Cell Secretory Activities Using Fano Resonance in Gold Nanoslits.* Small, 2013. **9**(20): p. 3532-3540.
197. Oh, B.-R., et al., *Integrated Nanoplasmonic Sensing for Cellular Functional Immunoanalysis Using Human Blood.* ACS Nano, 2014. **8**(3): p. 2667-2676.
198. Hiep, H.M., et al., *A microfluidic chip based on localized surface plasmon resonance for real-time monitoring of antigen-antibody reactions.* Japanese Journal of Applied Physics, 2008. **47**(2): p. 1337-1341.

199. Grasso, G., et al., *Enzyme solid-state support assays: a surface plasmon resonance and mass spectrometry coupled study of immobilized insulin degrading enzyme.* European Biophysics Journal with Biophysics Letters, 2009. **38**(4): p. 407-414.
200. Gao, J.H., et al., *Quantification of somatostatin with a surface plasmon resonance-based biosensor.* Gaodeng Xuexiao Huaxue Xuebao/Chemical Journal of Chinese Universities, 2010. **31**(7): p. 1327-1331.
201. Lerch, M., et al., *Strongly altered receptor binding properties in PP and NPY chimeras are accompanied by changes in structure and membrane binding.* Biochemistry, 2005. **44**(25): p. 9255-9264.
202. Zou, C., et al., *Studies of the structure of the N-terminal domain from the Y4 receptor - A G protein-coupled receptor - And its interaction with hormones from the NPY family.* ChemBioChem, 2008. **9**(14): p. 2276-2284.
203. Takagi, K., et al., *Anti-ghrelin immunoglobulins modulate ghrelin stability and its orexigenic effect in obese mice and humans.* Nature communications, 2013. **4**: p. 2685-2685.
204. Frasconi, M., et al., *Multifunctional Au Nanoparticle Dendrimer-Based Surface Plasmon Resonance Biosensor and Its Application for Improved Insulin Detection.* Analytical Chemistry, 2010. **82**(17): p. 7335-7342.
205. Hoa, X.D., A.G. Kirk, and M. Tabrizian, *Towards integrated and sensitive surface plasmon resonance biosensors: A review of recent progress.* Biosensors & Bioelectronics, 2007. **23**(2): p. 151-160.
206. Hoa, X.D., A.G. Kirk, and M. Tabrizian, *Towards integrated and sensitive surface plasmon resonance biosensors: a review of recent progress.* Biosens Bioelectron, 2007. **23**(2): p. 151-60.
207. Robertson, R.P., *Successful islet transplantation for patients with diabetes--fact or fantasy?* The New England journal of medicine, 2000. **343**(4): p. 289.
208. Meloche, R.M., *Transplantation for the treatment of type 1 diabetes.* World Journal of Gastroenterology, 2007. **13**(47): p. 6347.
209. Shapiro, A.J., et al., *Islet transplantation in seven patients with type 1 diabetes mellitus using a glucocorticoid-free immunosuppressive regimen.* New England Journal of Medicine, 2000. **343**(4): p. 230-238.
210. Paraskevas, S., et al., *Cell loss in isolated human islets occurs by apoptosis.* Pancreas, 2000. **20**(3): p. 270-276.
211. Harlan, D.M., et al., *Current advances and travails in islet transplantation.* Diabetes, 2009. **58**(10): p. 2175-2184.
212. Korsgren, O. and B. Nilsson, *Improving islet transplantation: a road map for a widespread application for the cure of persons with type I diabetes.* Current opinion in organ transplantation, 2009. **14**(6): p. 683-687.
213. Korsgren, O., et al., *Optimising islet engraftment is critical for successful clinical islet transplantation.* Diabetologia, 2008. **51**(2): p. 227-232.
214. Bennet, W., et al., *Incompatibility between human blood and isolated islets of Langerhans: a finding with implications for clinical intraportal islet transplantation?* Diabetes, 1999. **48**(10): p. 1907-1914.
215. Bennet, W., et al., *Isolated human islets trigger an instant blood mediated inflammatory reaction: implications for intraportal islet transplantation as a treatment for patients with type 1 diabetes.* Upsala journal of medical sciences, 2000. **105**(2): p. 125-133.

216. Naftanel, M.A. and D.M. Harlan, *Pancreatic islet transplantation.* PLoS medicine, 2004. **1**(3): p. e58.
217. Merani, S., et al., *Optimal implantation site for pancreatic islet transplantation.* British Journal of Surgery, 2008. **95**(12): p. 1449-1461.
218. Pepper, A.R., et al., *Current status of clinical islet transplantation.* World journal of transplantation, 2013. **3**(4): p. 48-53.
219. Ichii, H. and C. Ricordi, *Current status of islet cell transplantation.* Journal of hepato-biliary-pancreatic surgery, 2009. **16**(2): p. 101-112.
220. Administration, U.S.F.a.D. *Guidance for Industry: Considerations for Allogeneic Pancreatic Islet Cell Products*. 2009 October 28, 2014]; Available from: http://www.fda.gov/BiologicsBloodVaccines/GuidanceComplianceRegulatoryInformation/Guidances/CellularandGeneTherapy/ucm182440.htm.
221. Papas, K.K., T.M. Suszynski, and C.K. Colton, *Islet assessment for transplantation.* Current Opinion in Organ Transplantation, 2009. **14**(6): p. 674-682.
222. Yamamoto, T., et al., *Quality control for clinical islet transplantation: organ procurement and preservation, the islet processing facility, isolation, and potency tests.* Journal of hepato-biliary-pancreatic surgery, 2009. **16**(2): p. 131-136.
223. Colton, C.K., et al., *Characterization of islet preparations*. 2007: Elsevier: Amsterdam.
224. Loganathan, G., et al., *Factors Affecting Transplant Outcomes in Diabetic Nude Mice Receiving Human, Porcine, and Nonhuman Primate Islets: Analysis of 335 Transplantations.* Transplantation, 2013. **95**(12): p. 1439-1447.
225. Ricordi, C., J.R.T. Lakey, and B.J. Hering, *Challenges toward standardization of islet isolation technology.* Transplantation Proceedings, 2001. **33**(1-2): p. 1709.
226. Bertuzzi, F. and C. Ricordi, *Prediction of clinical outcome in islet allotransplantation.* Diabetes Care, 2007. **30**(2): p. 410-417.
227. London, N.J., et al., *The diabetic ℓuman reconstituted"severe combined immunodeficient (SCID-hu) mouse: a model for isogeneic, allogeneic, and xenogeneic human islet transplantation.* Transplant Proc, 1991. **23**(1 Pt 1): p. 749.
228. Ricordi, C., D.W. Scharp, and P.E. LACY, *REVERSAL OF DIABETES IN NUDE MICE AFTER TRANSPLANTATION OF FRESH AND 7-DAY-CULTURED (24 [degrees] C) HUMAN PANCREATIC ISLETS.* Transplantation, 1988. **45**(5): p. 994-996.
229. Pagliuca, F.W., et al., *Generation of Functional Human Pancreatic β Cells In Vitro.* Cell, 2014. **159**(2): p. 428-439.
230. Jamal, A., et al., *Morphogenetic plasticity of adult human pancreatic islets of Langerhans.* Cell Death & Differentiation, 2005. **12**(7): p. 702-712.
231. Ben-Othman, N., et al., *From pancreatic islet formation to beta-cell regeneration.* Diabetes Research and Clinical Practice, 2013. **101**(1): p. 1-9.
232. Puri, S. and M. Hebrok, *Cellular Plasticity within the Pancreas— Lessons Learned from Development.* Developmental Cell, 2010. **18**(3): p. 342-356.
233. Kaneto, H., et al., *Role of PDX-1 and MafA as a potential therapeutic target for diabetes.* Diabetes Research and Clinical Practice, 2007. **77**(3, Supplement): p. S127-S137.
234. Mellado-Gil, J.M., N. Cobo-Vuilleumier, and B.R. Gauthier, *Islet -Cell Mass Preservation and Regeneration in Diabetes Mellitus: Four Factors with Potential Therapeutic Interest.* Journal of Transplantation, 2012. **2012**: p. 9.
235. Murtaugh, L.C., *Pancreas and beta-cell development: from the actual to the possible.* Development, 2007. **134**(3): p. 427-438.

236. Liu, J.-L., et al., *Possible Roles of Reg Family Proteins in Pancreatic Islet Cell Growth.* Endocrine, Metabolic & Immune Disorders - Drug Targets(Formerly Current Dru, 2008. **8**(1): p. 1-10.
237. Migliorini, A., E. Bader, and H. Lickert, *Islet cell plasticity and regeneration.* Molecular Metabolism, 2014. **3**(3): p. 268-274.
238. Hui, H., C. Wright, and R. Perfetti, *Glucagon-like peptide 1 induces differentiation of islet duodenal homeobox-1–positive pancreatic ductal cells into insulin-secreting cells.* Diabetes, 2001. **50**(4): p. 785-796.
239. Zhou, J., et al., *Exendin-4 differentiation of a human pancreatic duct cell line into endocrine cells: Involvement of PDX-1 and HNF3β transcription factors.* Journal of Cellular Physiology, 2002. **192**(3): p. 304-314.
240. Wan, C.R., S. Chung, and R.D. Kamm, *Differentiation of Embryonic Stem Cells into Cardiomyocytes in a Compliant Microfluidic System.* Annals of Biomedical Engineering, 2011. **39**(6): p. 1840-1847.
241. Cimetta, E. and G. Vunjak-Novakovic, *Microscale technologies for regulating human stem cell differentiation.* Experimental Biology and Medicine, 2014. **239**(9): p. 1255-1263.
242. Cambier, T., et al., *Design of a 2D no-flow chamber to monitor hematopoietic stem cells.* Lab on a Chip, 2015. **15**(1): p. 77-85.
243. Fung, W.T., et al., *Microfluidic platform for controlling the differentiation of embryoid bodies.* Lab on a Chip, 2009. **9**(17): p. 2591-2595.
244. Zhou, J., et al., *Exendin‐4 differentiation of a human pancreatic duct cell line into endocrine cells: Involvement of PDX‐1 and HNF3β transcription factors.* Journal of cellular physiology, 2002. **192**(3): p. 304-314.
245. Chowdhury, A., et al., *Functional differences between aggregated and dispersed insulin-producing cells.* Diabetologia, 2013. **56**(7): p. 1557-1568.
246. Oecd, *OECD Guidelines for the Testing of Chemicals*. 1994: Organization for Economic.
247. Bhatia, S.N. and D.E. Ingber, *Microfluidic organs-on-chips.* Nature biotechnology, 2014. **32**: p. 760-772.
248. Xu, M.G., et al., *Modeling insulin secretion dysfunction in a three-dimensional culture system by cell-assembly technique*. 2009 Ieee International Conference on Virtual Environments, Human-Computer Interfaces and Measurement Systems. 2009, New York: Ieee. 118-122.
249. Iori, E., et al., *Glucose and fatty acid metabolism in a 3 tissue in-vitro model challenged with normo-and hyperglycaemia.* PloS one, 2012. **7**(4): p. e34704.
250. Mirsky, V.M., M. Riepl, and O.S. Wolfbeis, *Capacitive monitoring of protein immobilization and antigen-antibody reactions on monomolecular alkylthiol films on gold electrodes.* Biosensors and Bioelectronics, 1997. **12**(9-10): p. 977-989.
251. Goode, J.A., J. Rushworth, and P.A. Millner, *Biosensor Regeneration: A Review of Common Techniques and Outcomes.* Langmuir, 2015. **31**: p. 6267-6276.
252. Ghafar-Zadeh, E., et al., *Handheld impedance biosensor system using engineered proteinaceous receptors.* Biomedical microdevices, 2010. **12**(6): p. 967-975.
253. Qureshi, A., et al., *Label-free capacitive biosensor for sensitive detection of multiple biomarkers using gold interdigitated capacitor arrays.* Biosensors and Bioelectronics, 2010. **25**(10): p. 2318-2323.
254. Park, J.-W., et al., *Rapid and sensitive detection of Nampt (PBEF/visfatin) in human serum using an ssDNA aptamer-based capacitive biosensor.* Biosensors and Bioelectronics, 2012.

38(1): p. 233-238.
255. BelBruno, J.J., G. Zhang, and U.J. Gibson, *Capacitive sensing of amino acids in molecularly imprinted nylon films.* Sensors and Actuators B: Chemical, 2011. **155**(2): p. 915-918.
256. Sontimuang, C., R. Suedee, and F. Dickert, *Interdigitated capacitive biosensor based on molecularly imprinted polymer for rapid detection of Hev b1 latex allergen.* Anal Biochem, 2011. **410**(2): p. 224-33.
257. Jacquot, B.C., et al., *Non-Faradaic electrochemical detection of protein interactions by integrated neuromorphic CMOS sensors.* Biosensors and Bioelectronics, 2008. **23**(10): p. 1503-1511.
258. Lee, M., et al., *A novel biosensor based on hafnium oxide: Application for early stage detection of human interleukin-10.* Sensors and Actuators B: Chemical, 2012. **175**: p. 201-207.
259. Gebbert, A., et al., *Real-time monitoring of immunochemical interactions with a tantalum capacitance flow-through cell.* Analytical Chemistry, 1992. **64**(9): p. 997-1003.
260. Riepl, M., et al., *Optimization of capacitive affinity sensors: drift suppression and signal amplification.* Analytica Chimica Acta, 1999. **392**(1): p. 77-84.
261. Zaccari, I., et al., *Improving the Dielectric Properties of Ethylene-Glycol Alkanethiol Self-Assembled Monolayers.* Langmuir, 2014. **30**(5): p. 1321-1326.
262. Arya, S.K., et al., *Capacitive aptasensor based on interdigitated electrode for breast cancer detection in undiluted human serum.* Biosensors and Bioelectronics, 2018. **102**: p. 106-112.
263. Markov, A., et al., *In Situ Analysis of the Growth and Dielectric Properties of Organic Self-Assembled Monolayers: A Way To Tailor Organic Layers for Electronic Applications.* ACS Applied Materials & Interfaces, 2016. **8**(25): p. 16451-16456.
264. Sanguino, P., et al., *Interdigitated Capacitive Immunosensors With PVDF Immobilization Layers.* IEEE Sensors Journal, 2014. **14**(4): p. 1260-1265.
265. Li, S., et al., *AC electrokinetics-enhanced capacitive immunosensor for point-of-care serodiagnosis of infectious diseases.* Biosensors and Bioelectronics, 2014. **51**: p. 437-443.
266. Kim, K., S.W. Park, and S.S. Yang, *The optimization of PDMS-PMMA bonding process using silane primer.* BioChip Journal, 2010. **4**(2): p. 148-154.
267. Cui, H., et al., *An AC electrokinetic impedance immunosensor for rapid detection of tuberculosis.* Analyst, 2013. **138**(23): p. 7188-7196.
268. Wu, Z.-S., et al., *A sensitive immunoassay based on electropolymerized films by capacitance measurements for direct detection of immunospecies.* Analytical Biochemistry, 2005. **337**(2): p. 308-315.
269. Bahadir, E.B. and M.K. Sezginturk, *A review on impedimetric biosensors.* Artificial Cells Nanomedicine and Biotechnology, 2016. **44**(1): p. 248-262.
270. Labib, M., et al., *Competitive capacitive biosensing technique (CCBT): A novel technique for monitoring low molecular mass analytes using glucose assay as a model study.* Analytical and Bioanalytical Chemistry, 2010. **397**(3): p. 1217-1224.
271. Yang, L., et al., *Interdigitated microelectrode (IME) impedance sensor for the detection of viable< i> Salmonella typhimurium</i>.* Biosensors and Bioelectronics, 2004. **19**(10): p. 1139-1147.
272. Ibrahim, M., et al., *Physical and Electrical Modeling of Interdigitated Electrode Arrays for Bioimpedance Spectroscopy*, in *New Developments and Applications in Sensing Technology*. 2011, Springer. p. 169-189.

273. Tsouti, V., et al., *Capacitive microsystems for biological sensing.* Biosensors and Bioelectronics, 2011. **27**(1): p. 1-11.
274. Shoar Abouzari, M.R., et al., *On the physical interpretation of constant phase elements.* Solid State Ionics, 2009. **180**(14): p. 922-927.
275. Pajkossy, T., *Impedance spectroscopy at interfaces of metals and aqueous solutions — Surface roughness, CPE and related issues.* Solid State Ionics, 2005. **176**(25): p. 1997-2003.
276. Pajkossy, T. and L. Nyikos, *Scaling-law analysis to describe the impedance behavior of fractal electrodes.* Physical Review B, 1990. **42**(1): p. 709-719.
277. McRae, G.A., et al., *A comparison of fractal dimensions determined from atomic force microscopy and impedance spectroscopy of anodic oxides on Zr–2.5Nb.* Applied Surface Science, 2002. **191**(1): p. 94-105.
278. Jeon, D.-Y., et al., *Impedance characterization of nanogap interdigitated electrode arrays fabricated by tilted angle evaporation for electrochemical biosensor applications.* Journal of Vacuum Science & Technology B, 2014. **32**(2): p. 021803.
279. Van Gerwen, P., et al., *Nanoscaled interdigitated electrode arrays for biochemical sensors.* Sensors and Actuators B: Chemical, 1998. **49**(1): p. 73-80.
280. Boubour, E. and R.B. Lennox, *Insulating properties of self-assembled monolayers monitored by impedance spectroscopy.* Langmuir, 2000. **16**(9): p. 4222-4228.
281. Subbarao, N.V., et al., *Effect of thickness of bilayer dielectric on 1, 7‐dibromo‐N, N′‐dioctadecyl‐3, 4, 9, 10‐perylenetetracarboxylic diimide based organic field‐effect transistors.* physica status solidi (a), 2014. **211**(10): p. 2403-2411.
282. Nathawat, R., et al., *XPS and AFM surface study of PMMA irradiated by electron beam.* Surface and Coatings Technology, 2009. **203**(17): p. 2600-2604.
283. Singh, K.V., et al., *3D nanogap interdigitated electrode array biosensors.* Analytical and Bioanalytical Chemistry, 2010. **397**(4): p. 1493-1502.
284. Shekar, B.C., S. Sathish, and R. Sengoden, *Spin Coated Nano Scale PMMA Films for Organic Thin Film Transistors.* Physics Procedia, 2013. **49**: p. 145-157.
285. Narakathu, B.B., M.Z. Atashbar, and B.E. Bejcek, *Improved detection limits of toxic biochemical species based on impedance measurements in electrochemical biosensors.* Biosensors and Bioelectronics, 2010. **26**(2): p. 923-928.
286. *IDF Diabetes Atlas*. 2015; 7th edn.:[Available from: http://www.diabetesatlas.org.
287. Braun, M., et al., *Exocytotic Properties of Human Pancreatic β‐cells.* Annals of the New York Academy of Sciences, 2009. **1152**(1): p. 187-193.
288. Castiello, F.R., K. Heileman, and M. Tabrizian, *Microfluidic perfusion systems for secretion fingerprint analysis of pancreatic islets: applications, challenges and opportunities.* Lab on a Chip, 2016. **16**(3): p. 409-431.
289. Proks, P., et al., *Ca (2+)‐and GTP‐dependent exocytosis in mouse pancreatic beta‐cells involves both common and distinct steps.* The Journal of physiology, 1996. **496**(1): p. 255-264.
290. Gobi, K.V., H. Iwasaka, and N. Miura, *Self-assembled PEG monolayer based SPR immunosensor for label-free detection of insulin.* Biosensors & Bioelectronics, 2007. **22**(7): p. 1382-1389.
291. Estevez, M.C., et al., *Indirect competitive immunoassay for the detection of fungicide Thiabendazole in whole orange samples by Surface Plasmon Resonance.* Analyst, 2012.

137(23): p. 5659-5665.
292. Biacore, A., *Biacore sensor surface handbook.* GE Healthcare Bio-Sciences AB: Uppsala, Sweden, 2003.
293. Mitchell, J., *Small Molecule Immunosensing Using Surface Plasmon Resonance.* Sensors, 2010. **10**(8): p. 7323-7346.
294. Vaisocherova, H., E. Brynda, and J. Homola, *Functionalizable low-fouling coatings for label-free biosensing in complex biological media: advances and applications.* Analytical and Bioanalytical Chemistry, 2015. **407**(14): p. 3927-3953.
295. Mitchell, J.S., et al., *Estrogen conjugation and antibody binding interactions in surface plasmon resonance biosensing.* Steroids, 2006. **71**(7): p. 618-631.
296. Cui, X., et al., *Real-time immunoassay of ferritin using surface plasmon resonance biosensor.* Talanta, 2003. **60**(1): p. 53-61.
297. Haasnoot, W., et al., *Biosensor immunoassay for flumequine in broiler serum and muscle.* Analytica Chimica Acta, 2007. **586**(1): p. 312-318.
298. Bedford, E.E., et al., *Surface Plasmon Resonance Biosensors Incorporating Gold Nanoparticles.* Macromolecular Bioscience, 2012. **12**(6): p. 724-739.
299. Grill, V., et al., *A Stimulating Effect of Glucose on Somatostatin Release Is Impaired in Noninsulin-Dependent Diabetes Mellitus*.* The Journal of Clinical Endocrinology & Metabolism, 1984. **59**(2): p. 293-297.
300. Segers, O., et al., *Basal and Tolbutamide-induced Plasma Somatostatin in Healthy Subjects and in Patients with Diabetes and Impaired Glucose Tolerance.* Diabetic Medicine, 1989. **6**(3): p. 232-238.
301. Nguyen, D.T., et al., *Endocrine system on chip for a diabetes treatment model.* Biofabrication, 2017. **9**(1): p. 015021.
302. Lafleur, J.P., et al., *Recent advances in lab-on-a-chip for biosensing applications.* Biosensors & Bioelectronics, 2016. **76**: p. 213-233.
303. Hinman, S.S., K.S. McKeating, and Q. Cheng, *Surface Plasmon Resonance: Material and Interface Design for Universal Accessibility.* Analytical Chemistry, 2018. **90**(1): p. 19-39.
304. Lee, H.J., D. Nedelkov, and R.M. Corn, *Surface Plasmon Resonance Imaging Measurements of Antibody Arrays for the Multiplexed Detection of Low Molecular Weight Protein Biomarkers.* Analytical Chemistry, 2006. **78**(18): p. 6504-6510.
305. Castiello, F.R. and M. Tabrizian, *Multiplex Surface Plasmon Resonance Imaging-Based Biosensor for Human Pancreatic Islets Hormones Quantification.* Analytical Chemistry, 2018. **90**(5): p. 3132-3139.
306. Jung, J., et al., *Enhanced surface plasmon resonance by Au nanoparticles immobilized on a dielectric SiO2 layer on a gold surface.* Analytica Chimica Acta, 2009. **651**(1): p. 91-97.
307. Frasconi, M., et al., *Multifunctional Au Nanoparticle Dendrimer-Based Surface Plasmon Resonance Biosensor and Its Application for Improved Insulin Detection.* Analytical Chemistry, 2010. **82**(17): p. 7335-7342.
308. Mitchell, J.S., et al., *Sensitivity enhancement of surface plasmon resonance biosensing of small molecules.* Analytical Biochemistry, 2005. **343**(1): p. 125-135.
309. Mitchell, J.S. and T.E. Lowe, *Ultrasensitive detection of testosterone using conjugate linker technology in a nanoparticle-enhanced surface plasmon resonance biosensor.* Biosensors and Bioelectronics, 2009. **24**(7): p. 2177-2183.
310. Kabiraz, D.C., et al., *Mechanism of surface plasmon resonance sensing by indirect competitive inhibition immunoassay using Au nanoparticle labeled antibody.* Talanta, 2017.

172: p. 1-7.
311. Sendroiu, I.E., et al., *Ultrasensitive DNA Microarray Biosensing via in Situ RNA Transcription-Based Amplification and Nanoparticle-Enhanced SPR Imaging.* Journal of the American Chemical Society, 2011. **133**(12): p. 4271-4273.
312. Lee, J.U., A.H. Nguyen, and Sang J. Sim, *A nanoplasmonic biosensor for label-free multiplex detection of cancer biomarkers.* Biosensors and Bioelectronics, 2015. **74**: p. 341-346.
313. Taufik, S., et al., *An antifouling electrode based on electrode–organic layer–nanoparticle constructs: Electrodeposited organic layers versus self-assembled monolayers.* Journal of Electroanalytical Chemistry, 2016. **779**: p. 229-235.
314. Driskell, J.D., et al., *One-step assay for detecting influenza virus using dynamic light scattering and gold nanoparticles.* Analyst, 2011. **136**(15): p. 3083-3090.
315. Kawaguchi, T., et al., *Surface plasmon resonance immunosensor using Au nanoparticle for detection of TNT.* Sensors and Actuators B: Chemical, 2008. **133**(2): p. 467-472.
316. Juncker, D., et al., *Cross-reactivity in antibody microarrays and multiplexed sandwich assays: shedding light on the dark side of multiplexing.* Current Opinion in Chemical Biology, 2014. **18**: p. 29-37.
317. Dias, J.T., et al., *Minimizing antibody cross-reactivity in multiplex detection of biomarkers in paper-based point-of-care assays.* Nanoscale, 2016. **8**(15): p. 8195-8201.
318. Martinez-Perdiguero, J., et al., *Surface plasmon resonance immunoassay for the detection of the TNF alpha biomarker in human serum.* Talanta, 2014. **119**: p. 492-497.
319. Lowe, S., N.M. O'Brien-Simpson, and L.A. Connal, *Antibiofouling polymer interfaces: poly(ethylene glycol) and other promising candidates.* Polymer Chemistry, 2015. **6**(2): p. 198-212.
320. Arya, S.K., et al., *Recent advances in self-assembled monolayers based biomolecular electronic devices.* Biosensors and Bioelectronics, 2009. **24**(9): p. 2810-2817.
321. Lin, A., A. Salvador, and J.M. Carter, *Multiplexed Microsphere Suspension Array-Based Immunoassays*, in *ELISA: Methods and Protocols*, R. Hnasko, Editor. 2015, Springer New York: New York, NY. p. 107-118.
322. Shah, N.B. and T.M. Duncan, *Bio-layer interferometry for measuring kinetics of protein-protein interactions and allosteric ligand effects.* Journal of visualized experiments : JoVE, 2014(84): p. e51383-e51383.
323. Kamat, V. and A. Rafique, *Designing binding kinetic assay on the bio-layer interferometry (BLI) biosensor to characterize antibody-antigen interactions.* Analytical Biochemistry, 2017. **536**: p. 16-31.
324. Asmari, M., et al., *Thermophoresis for characterizing biomolecular interaction.* Methods, 2018. **146**: p. 107-119.
325. Lesuffleur, A., et al., *Periodic nanohole arrays with shape-enhanced plasmon resonance as real-time biosensors.* Applied Physics Letters, 2007. **90**(24): p. 243110.
326. Szunerits, S., et al., *Recent advances in the development of graphene-based surface plasmon resonance (SPR) interfaces.* Analytical and Bioanalytical Chemistry, 2013. **405**(5): p. 1435-1443.
327. Zeng, S., et al., *Graphene–gold metasurface architectures for ultrasensitive plasmonic biosensing.* Advanced Materials, 2015. **27**(40): p. 6163-6169.
328. Yu, W., et al., *Microfluidic Chip-Based Immunoassay for Reliable Detection of Cloxacillin in Poultry.* Food Analytical Methods, 2016. **9**(11): p. 3163-3169.

Appendix A: Article Reprints and Copyright Waivers

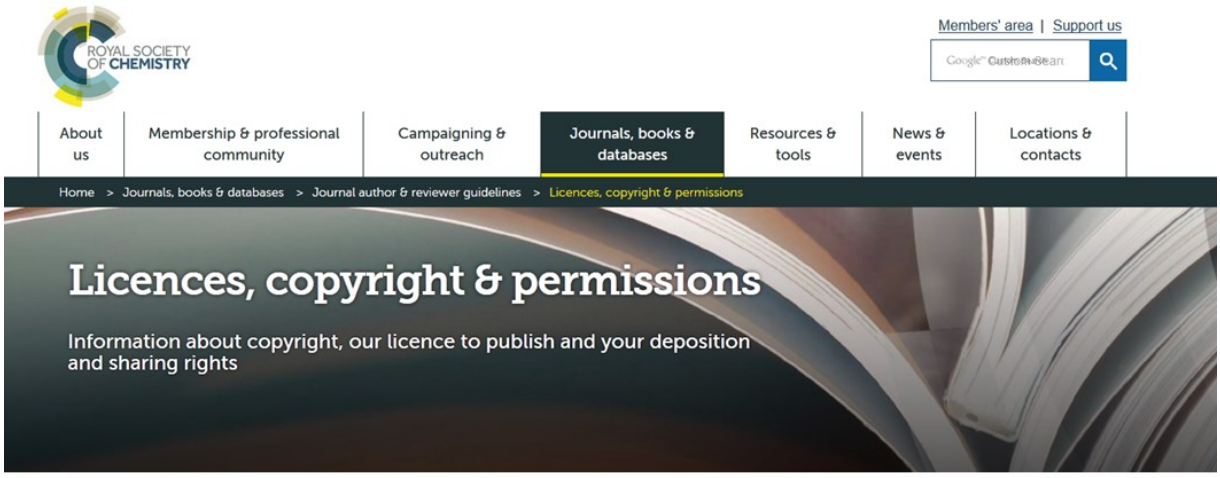

Deposition and sharing rights

The following details apply only to authors accepting the standard licence to publish. Authors who have accepted one of the open access licences to publish, or are thinking of doing so, should refer to the details for open access deposition rights.

When the author accepts the licence to publish for a journal article, he/she retains certain rights concerning the deposition of the whole article. This table summarises how you may distribute the accepted manuscript and version of record of your article.

Sharing rights	Accepted manuscript	Version of record
Share with individuals on request, for personal use	✓	✓
Use for teaching or training materials	✓	✓
Use in submissions of grant applications, or academic requirements such as theses or dissertations	✓	✓
Share with a closed group of research collaborators, for example via an intranet or privately via a scholarly communication network	✓	✓
Share publicly via a scholarly communication network that has signed up to STM sharing principles	⧗	×
Share publicly via a personal website, institutional repository or other not-for-profit repository	⧗	×
Share publicly via a scholarly communication network that has not signed up to STM sharing principles	×	×

⧗ Accepted manuscripts may be distributed via repositories after an embargo period of 12 months

Lab on a Chip

CRITICAL REVIEW

View Article Online
View Journal | View Issue

Cite this: Lab Chip, 2016, 16, 409

Microfluidic perfusion systems for secretion fingerprint analysis of pancreatic islets: applications, challenges and opportunities

F. Rafael Castiello, Khalil Heileman† and Maryam Tabrizian*

A secretome signature is a heterogeneous profile of secretions present in a single cell type. From the secretome signature a smaller panel of proteins, namely a secretion fingerprint, can be chosen to feasibly monitor specific cellular activity. Based on a thorough appraisal of the literature, this review explores the possibility of defining and using a secretion fingerprint to gauge the functionality of pancreatic islets of Langerhans. It covers the state of the art regarding microfluidic perfusion systems used in pancreatic islet research. Candidate analytical tools to be integrated within microfluidic perfusion systems for dynamic secretory fingerprint monitoring were identified. These analytical tools include patch clamp, amperometry/voltametry, impedance spectroscopy, field effect transistors and surface plasmon resonance. Coupled with these tools, microfluidic devices can ultimately find applications in determining islet quality for transplantation, islet regeneration and drug screening of therapeutic agents for the treatment of diabetes.

Received 1st September 2015,
Accepted 15th December 2015

DOI: 10.1039/c5lc01046b

www.rsc.org/loc

1. Introduction

Agrawal *et al.*[1] defined the cell secretome as: "the collection of proteins secreted by a cell's tissue, organ or organism at any given time and condition, regardless of secretion mechanism, being constitutive or regulated secretion". A secretome can control and regulate a multitude of biological and physiological processes.[2] In addition, it reflects the functionality of a cell in a given environment.[3] For instance, chronic alteration or aberrant secretion within a cell secretome could be indicative of a pathological condition. Thus, secretome analysis or secretomics is becoming a clinically relevant research field for biomarkers and therapeutic targets discovery.[5]

Although the general definition of secretion includes metabolites and ions, in literature, the definition of the secretome only refers to proteins. As such, this review is focused on global secretion of proteins unless otherwise specified.

Biomedical Engineering Department, McGill University, Montreal, QC, H3A 2B4, Canada. E-mail: Maryam.Tabrizian@mcgill.ca; Fax: +1 514 398 7461; Tel: +1 514 398 8129

† This author significantly contributed to the present paper.

F. Rafael Castiello

F. Rafael Castiello is a PhD student in the Department of Biomedical Engineering at McGill University. He received his bachelor's degree in Chemical Engineering from Guadalajara University, Mexico and obtained his master's degree in Material Science and Engineering from National Autonomous University of Mexico, CNyN Ensenada, Mexico. During his master's studies, he worked on the fabrication of nanomaterials for the development of biosensors. His current research is focused on developing microfluidic-based biosensors for the dynamic detection of pancreatic islets and cell secretion.

Khalil Heileman

Khalil Heileman is a PhD student in the Department of Biomedical Engineering at McGill University. He received his bachelor's degree in Mechanical Engineering from the University of Toronto, Canada. His primary research interests are integrating microfluidic devices with dielectric spectroscopy for applications in pancreatic islets of Langerhans research.

Ions and small molecules will only be mentioned when they are used as an indirect way to measure protein secretion or when a platform that measures them can be adapted for protein secretion detection.

A cell's secretome can be comprised of a considerable amount of proteins (up to 1000) making its continuous monitoring difficult. Moreover, it has been shown that a genetically identical cell population can present functional heterogeneity,[4] which can create a potential barrier to accurately screen the response to a stimulus or to pharmacological therapies.[5,6] To overcome this problem, it is possible to study the secretome of individual cells within a population, and establish a particular secretome signature for each cellular phenotype.

A cell secretome signature is composed of a smaller number of proteins (around 100) compared to the whole cell secretome. However, it will be more convenient to monitor an even smaller set of proteins within the secretome signature, encompassing a particular secretory fingerprint (SF). This SF can be selected on a case-by-case basis and dynamically monitored to find relationships between secreted proteins and their secretagogues.

While complete secretomic analysis of pancreatic islets has not yet been performed, current knowledge still allows definition of a SF composed of relevant hormones and other biomarkers. To date, the majority of islet studies have focused at most on the simultaneous measurement of two secreted hormones. Herein, we propose that a SF composed of a larger number of secretion products can yield a deeper understanding of islet physiology and its secretory response. The present review is not attempting to cover pancreatic islets secretomics. It rather suggest that the determination of an islet secretome will expand our current knowledge of islet secreted biomarkers. This in time will allow definition and measurement of a more pertinent SF depending on the application (*e.g.* drug screening, transplantation or islet regeneration).

Maryam Tabrizian

Maryam Tabrizian is full professor at the Department of Biomedical Engineering at McGill University. She is FRSQ-Chercheur National awardee and became the Guggenheim Fellow in Biomedical Sciences in 2010. M. Tabrizian's core competency is in the field of bio-interface, biorecognition systems and microfluidics and their integration with biosensing devices for cell behaviour investigation in stimulated microenvironments. For more than 10 years, her laboratories have been working on the development of microfluidic platforms compatible with impedance spectroscopy and surface plasmon resonance spectroscopy for the detection and high throughput analysis of biomarkers, proteins, peptides, DNA, drugs and other biologically active substances.

First, this review presents important concepts of pancreatic islet physiology and species-dependent characteristics. It then covers current methods and challenges for determining a cell secretome. Then it exposes the state of the art regarding microfluidic perfusion systems (MPS) for pancreatic islets. Subsequently, it overviews analytical tools with a proven potential to dynamically monitor islet secretion processes when integrated in MPS. These platforms could be very useful for investigating islets as whole micro-organs and identifying the roles of individual secretion factors. Additionally, they can comprehensively assess the behavior of islets in complex metabolic networks, recapitulate the dynamics of hormone secretion and help discover new therapeutics to treat diabetes mellitus.

1.1. Pancreatic islet physiology and species dependent characteristics

The islets of Langerhans, which constitute 1 to 2% of the pancreas mass, are vascularized micro-organs with an average diameter of 150 μm. The pancreatic islets are composed of five different endocrine cells (α, β, δ, PP, and ε cells) each secreting characteristic hormones in response to metabolic changes.[7] They are also composed of vascular cells, resident immune cells, neurons and glial cells. Additionally, human islets are surrounded by a complex double basement membrane.[8] Each islet is a functional unit with the physiological role of maintaining glucose homeostasis, mainly through β-cell insulin and α-cell glucagon secretion.

Insulin secretion is a complex and dynamic process, and detailed knowledge of it is critical for understanding diabetes mellitus. Insulin release by β-cells is an electrically excitable process in which changes in membrane potential is coupled to variations in blood glucose concentrations. In the absence of glucose (glucose concentration <1 mM), the membrane resting potential of human β-cells is approximately −70 mV.[9] Once glucose concentration increases, glucose transporters (GLUT) are activated and glucose metabolism occurs inside β-cells through glycolysis, the Krebs cycle and the electron transport chain, generating adenosine triphosphate (ATP) (Fig. 1A). The generated ATP closes the ATP-sensitive potassium channels (KATP), reducing the resting membrane potential until a threshold of −60 mV is exceeded, initiating membrane depolarization. Once membrane depolarization occurs, the voltage gated Ca^{2+} channels open (reaching a peak influx at around −30 mV) and Ca^{2+} concentration increases. This in turn, triggers insulin vesicle fusion with the cell membrane by inhibiting the activity of the Ca^{2+} sensitive protein synaptotagmin, and subsequently insulin exocytosis occurs.

Induced insulin exocytosis follows a biphasic time course (Fig. 1-B).[10,11] The first phase corresponds to a fast transient increase rate of insulin secretion, usually within 5 minutes of glucose stimulation. Afterwards, a decrease in insulin secretion takes place, followed by a gradual incremental second phase that lasts as long as the glucose stimulus is applied. As

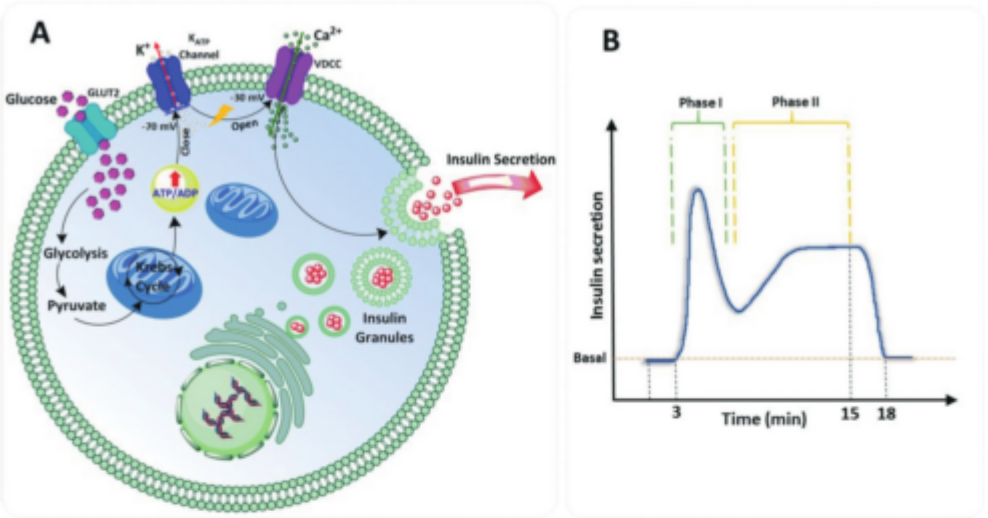

Fig. 1 A) Glucose stimulated insulin secretion pathway in pancreatic β-cells and B) biphasic insulin release profile.

with most secretory cells, the biphasic secretion of insulin is pulsatile by nature. Moreover, insulin secretion has been demonstrated to oscillate in a synchronous manner with cytoplasmic Ca^{2+} concentration,[12] indicating that Ca^{2+} oscillations are direct regulators of insulin pulsatility.

Co-secreted peptides and ions during insulin exocytosis, such as C-peptide, Zn^{2+} ions and amylin, can be used to indirectly quantify insulin secretion or measure secretion kinetics. In addition, it has been shown that these co-secreted factors have clinical relevance in diabetes mellitus diagnosis and treatment.[13–16] For the interested reader, in depth detail of insulin secretion in human islets has been reviewed elsewhere.[9]

As in any biological research, the mechanisms of insulin secretion and islet function have been mostly elucidated using animal models. However, recent studies have demonstrated that islet anatomy and physiology is species-dependent, and therefore one has to be careful when generalizing findings from any individual species.[17,18] As a consequence, many concepts related to anatomy, physiology and basic cellular mechanisms of human islets are currently being refined.[17,19–23]

As an example, Cabrera *et al.*,[17] studied the differences in islets cyto-architecture and functionality amongst four different species (Fig. 2-i). Their findings showed that in the case of mouse, large spatial segregation of cell types exists, suggesting an anatomical subdivision within islets. However, when the authors compared the degree of segregation of cell types between mice and human islets, they found that in mice, 71% of the insulin-containing cells showed exclusively homotypic (same type) associations, whereas, in human, this was only 29%. As a consequence, β-cells are intermingled randomly with α- and δ-cells throughout the entire islet in close association with the islet microcirculation system (Fig. 2-ii). Additionally, Cabrera *et al.*[17] demonstrated that islets from different regions of the human pancreas possess different cell compositions, and that on average, the cell composition of human islets contained proportionally fewer β-cells and more α-cells than that of mouse islets (Fig. 2-i).

The anatomy of human islets has significant consequences for cell-to-cell communication within the islets. Recent evidence suggests that the unique cytoarchitecture of human islets give rise to relevant paracrine and autocrine interactions that play a dominant role in their overall endocrine response.[7,18,23–28] For instance, it has been shown that somatostatin and ghrelin inhibit glucose dependent insulin secretion,[23,24,28] that pancreatic polypeptide (PP)[7] and co-secreted ions and amino acids[25,26] exert a stimulatory and inhibitory effect respectively on glucagon secretion, and that neurotransmitters released from islet cells may shape the pulsatile behavior in auto/paracrine feedback loops.[27] These aforementioned paracrine/autocrine interactions along with many others have been recently reviewed in detail.[18,27] However, more research is needed in order to fully understand these paracrine interactions, particularly in the context of diabetes.

Finally, another critical aspect of islet physiology is functional heterogeneity, since human islets differ in size and composition. However, little is known about how such differences impact islet function.[29–31] Studying the secretome signature of single islets as it is done for other biological systems such as tumors, may allow investigation of this

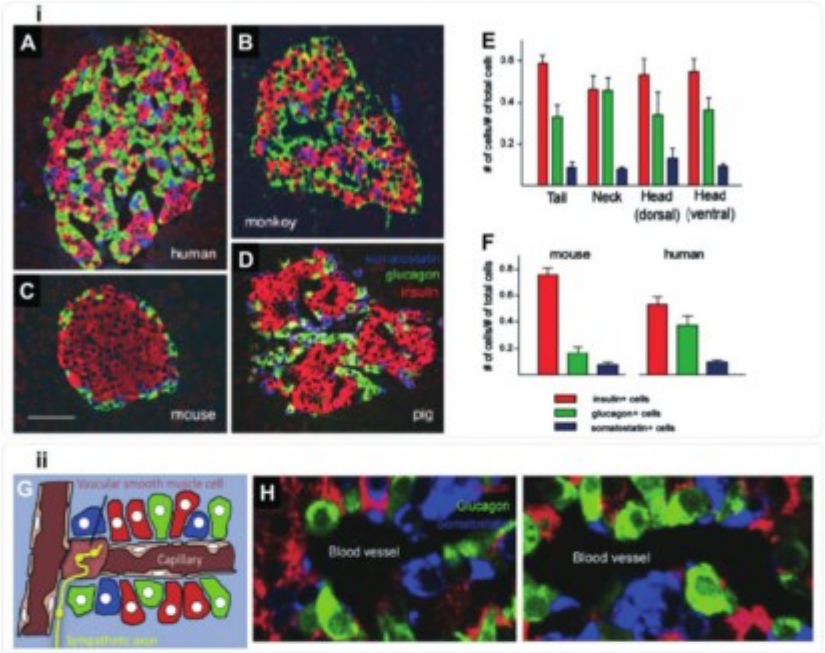

Fig. 2 Illustration of differences in islet cytoarchitecture among species. (i) Confocal images of islets of Langerhans of human (A), monkey (B), mouse (C) and pig (D). (E) Human islet cell composition depending on the region of the pancreas from which they were obtained. (F) Comparison of cell composition between human and mouse islets (Reproduced from ref. 17 with permission from National Academy of Sciences, U.S.A, Copyright 2006). (ii) Human islet cell distribution. (G) Schematic representation and (H) confocal image of human islet cell distribution around a capillary vessel. For all images, red: insulin-immunoreactive cells; green: glucagon-immunoreactive cells; blue: somatostatin-immunoreactive cells (Reproduced from ref. 18 with permission from Elsevier).

functional heterogeneity. For example, one can determine the secretome signature profile for islets in response to glucose stimulation, which can then be used as a baseline to select "functional" islets before transplantation, or to understand how secreted proteins exert paracrine/autocrine influence in islets.

As demonstrated in this section, our current knowledge of human islet physiology allows definition of a functional SF to monitor hormone secretion. However, once important protein biomarkers are found within the secretome signature profile, it will be possible to conceive systems to monitor the dynamics of a wider and more relevant SF to study particular aspects of islet physiology.

1.2. Current methods to determine a cell secretome

The Bergsten group described the first proteomic reference map of human pancreatic islets.[32] This report represented the first preliminary functional profile of the human islet proteome, in which many of the identified proteins have been implicated in the pathophysiology of diabetes. Since then, the aim of most islet protein profiling studies has been to elucidate the different mechanism involved in diabetes associated β-cell deterioration.[33] However, because of the complexity of cell proteomes, in some cases it is more practical to focus on a sub-proteome which only encompasses secreted proteins. Hence, many opportunities exist in the field of pancreatic islet research to focus specifically on the islet secretome and to determine a functional secretome signature. More information regarding islet protein profiling can be found in recent reports.[33,34]

To date, determination of the secretome has focused mostly on cells such as lung,[35] colon[36] and glial[37,38] cancer cells. Determining such cancer cell secretomes has unveiled mechanisms related to angiogenesis, invasion and metastasis, helping to develop new strategies to control cancer.[35] Additionally, there are some reports where the secretome of skeletal muscle cells[39] and human adipocytes during adipogenesis[40] has been determined.

Current methods to determine an unknown cell secretome involve placing cells in culture media for a period of time under controlled conditions, after which the media is analyzed for identification and quantification of secreted proteins.

However, proteins secreted by dead cells in the media and serum proteins can mask the proteins of interest, making their isolation a challenge.[41] Hence, it is a common practice to use serum free media and cytosolic extract as a control for dead cell proteins.[41] Nevertheless, little is known about how this affects cell secretion. Some evidence suggests that serum deprivation can cause apoptosis,[42,43] and can trigger different responses across various cell types.[44] Additionally, secreted proteins can be present at very low concentrations in the culture media, and on top of that, media is usually diluted before analysis, increasing the chances for analytical instruments to miss relevant biomarkers.

Traditional methodologies to decipher a cell secretome can be divided in two broad categories, the ones that analyze RNA/DNA to provide mostly qualitative information on gene-products (including computational methods), and the ones that analyze proteins directly, mostly based on proteomic methods[2] (Fig. 3). These methods may be restricted depending on whether the secretory protein sequence is known or not. Detailed information about the principle advantages and drawbacks of each has been reviewed elsewhere.[2] Usually a combination of RNA/DNA and protein quantification methods is used to acquire a bigger picture of the secretome by correlating gene expression and protein secretion. However this can be time consuming.

Once a cell secretome signature has been identified, other techniques such as immunoassays (*e.g.* ELISA, western blot and antibody microarrays) can be used to monitor small changes in the secretome, or as a complementary method with mass spectrometry for secretome identification.[2] Additionally, among these immunoassay techniques, antibody microarrays can be used in a high-throughput and multiplexed manner.[45]

1.3 Multiplex screening

Multiplexing is desirable in most biological analyses since it reduces analysis time, sample volumes, and hence the cost of analysis.[46] However, multiplexed protein detection is complicated due to cross-reactivities. This usually limits the degree of multiplexing, particularly in complex solutions, such as those containing cell secretion products. Nonetheless, a panel of several biomarker measurements can yield far more information than a single biomarker. Thus, efforts to develop multiplexed protein detection technologies represent great opportunities in many research fields.

A traditional technique used for multiplexed analysis of secreted proteins is antibody microarrays. Antibody arrays are a part of miniaturized devices in which antibodies can be immobilized on a planar surface or on microbeads, usually by microprinting, to capture and quantify specific proteins.[45] The protein binding event is then detected in a label-based or sandwich configuration with a fluorophore, quantum dot or an enzyme.[45] Antibody arrays have been used so far to study proteins secreted by human adipocytes,[40] mesenchymal stem cells[47] and cardiomyocyte cells.[48]

However, these methods require a large number of cells for the analysis and obtained results will reflect the averaged features of cell populations. This may present disadvantages in many cases, since cell populations are heterogeneous in nature, and hence, population data can mask functional heterogeneity and associated molecular mechanisms.[49] The desirable solution would therefore be to study secretion from a single cell or a very small population of cells in order to identify phenotypes of interest and determine their respective secretome signature.

Microfluidic platforms can enhance *spatio-temporal* control of the cell microenvironment compared to traditional biological assays, allowing single cell analysis.[50] For instance, the sample volume can be reduced, avoiding dilution of secreted proteins and hence maximizing the information collected. Such platforms make it possible to use traps to immobilize single cells for multiplexed genetic/protein quantification.[49,51] An example of this is a microfluidic chip for isotope labeling coupled with electrospray ionization

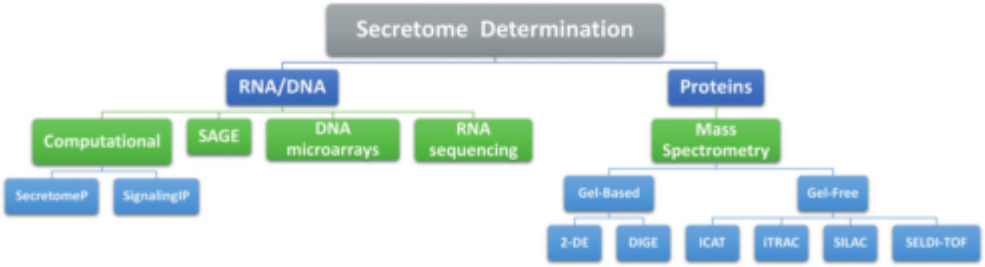

Fig. 3 Classification of common techniques to decipher an unknown secretome. RNA/DNA methods comprise: serial analysis of gene expression (SAGE), DNA microarrays, RNA sequencing and computational methods such as SecretomeP for non-classical secretion and SignalingIP for classical secretion. Proteomic analysis techniques are mostly based on mass spectrometry, particularly liquid chromatography tandem mass spectrometry (LC-MS/MS). These methods can be subdivided into gel based techniques, such as two-dimensional gel electrophoresis (2-DE) and differential gel electrophoresis (DIGE), and gel free techniques, such as isotope-coded affinity tag (ICAT), isobaric tag for relative and absolute quantification (iTRAQ), stable isotope labeling by amino acids in cell culture (SILAC) and surface enhanced laser desorption ionization-time of flight mass spectrometry (SELDI-TOF MS).

mass spectrometry (ESI-MS),[52] that was used for qualitative and quantitative analysis of drug-induced apoptosis of MCF-7 cells. The chip was designed to perform cell loading, microfluidic cell culture, drug solution injection, microfluidic cell staining, imaging analysis and ESI-MS detection (Fig. 4-i). The authors demonstrated that when combining microfluidics and mass spectrometry, a multiplexed analysis of proteins could be carried out, despite the complexity of the MCF-7 secretome.

Another example is the evaluation of functional heterogeneity of immune T cells and human macrophages on a single-cell barcode chip.[53] The chip is composed of 1040 3 nl volume microchambers, each containing a single cell. Protein concentration is determined with sandwich immunoassays from spatially encoded antibodies. This forms a barcode that represents a complete panel of protein assays (Fig. 4-ii), allowing for highly multiplexed detection of proteins and statistical analysis of single cell protein secretion. Further information on single cell analysis and related microfluidic devices is available in two recent reviews by Galler *et al.* and Liu *et al.*[54,55]

2. Current microfluidic perfusion systems for pancreatic islet research

A particular type of microfluidic device designed to control the media flow over single cells or cell culture chambers are microfluidic perfusion systems (MPS). In the case of pancreatic islets, MPS can simulate the islet *in vivo* environment. For instance, the pressures and flow volume of the islet vascular system can be reproduced,[56] making these platforms ideal for islet *in vitro* analysis.

In the past decade, many research groups have specialized in MPS development for islet research.[56] These devices generally possess two major components. The first component is a trapping mechanism capable of immobilizing single or multiple islets (Fig. 5) while maintaining constant perfusion. Lack of perfusion on previous islet devices presented serious limitations for secretion studies.[57] For instance, dynamic measurement of islet secretion cannot be obtained since the concentration of secreted products constantly increases within a static chamber. Many experiments require a perfusion system that can rapidly vary the concentration of secretagogues delivered to the islets. Finally, without perfusion, islets cannot obtain fresh nutrients, which limits islet long term survival.[57]

Additionally, particular features should be considered in perfusion system design to account for the unique 3D cytoarchitecture of islets and their vulnerability to mechanical stress. The first major component of the MPS is the trapping mechanism for islet immobilisation. To date, some trapping mechanisms found on MPS are dam wall-like or nozzle-like traps[58,59] or circular wells located at the bottom of perfusion chambers.[60,61] Moreover, it is necessary to integrate stable and flexible fluid control for investigating hormone secretion kinetics and biochemical events. This can be achieved either by external or integrated micropumps or by combining

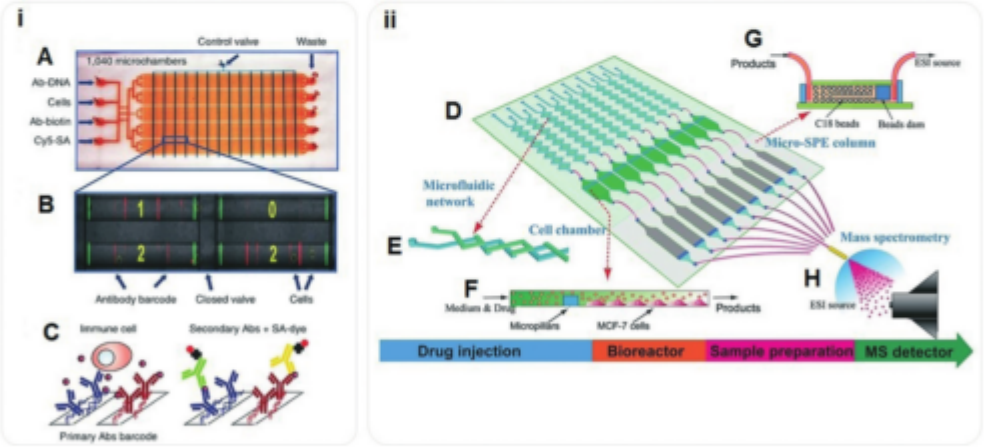

Fig. 4 Examples of microfluidic devices for cell secretion analysis. (i) Barcode chip. (A) Image of the device's assay channels shown in red and control channels in blue. (B) Micrograph showing isolated cells and a fluorescent bar code assay. Yellow digits indicate number of cells per microchamber. (C) Schematic representation of the multiplexed primary antibody barcode array used for capture of secreted proteins. SA stands for Streptavidin. (Reproduced from ref. 53 with permission from Nature Publishing Group). (ii) Microfluidic chip for isotope labelling coupled with ESI-MS. (D) Schematic representation of the ESI-MS chip consisting of a microfluidic network for culture medium delivery and drug injections, cell culture chambers, and on-chip micro-solid-phase extraction (micro-SPE) columns for sample desalting and purifying. (E) Microfluidic network to generate concentration gradients during cell culture and drug screening. (F) Side view of MCF-7 cells culture chamber. (G) Close-up of an integrated micro-SPE column. (H) Micro-SPE column joined by capillaries. (Reproduced from ref. 52 with permission from American Chemical Society Copyright 2012).

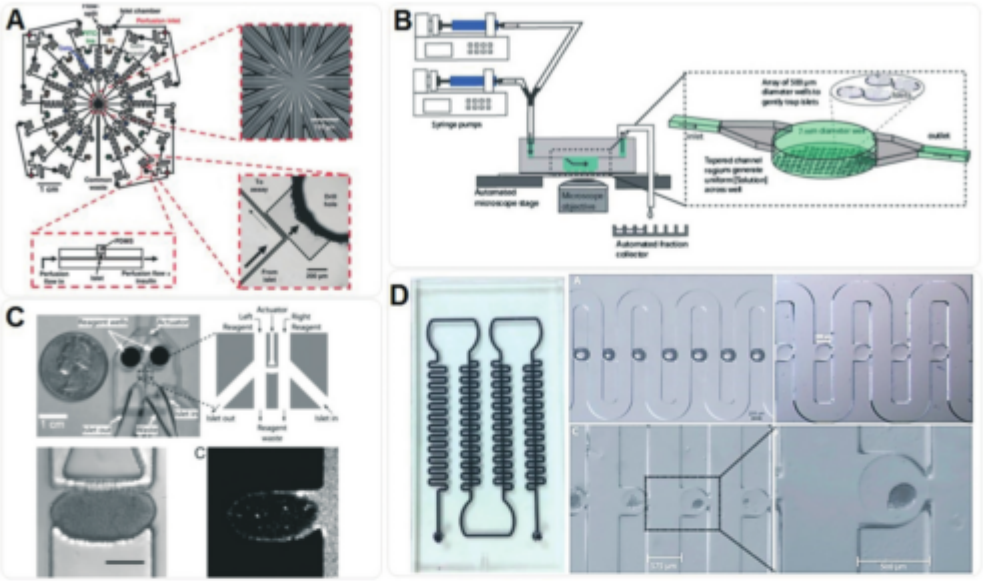

Fig. 5 Examples of various MPS developed for pancreatic islet research. (A) Schematics of a microfluidic chip for monitoring insulin secretion from 15 independent islets (Reproduced from ref. 67 with permission from American Chemical Society Copyright 2009). The device is comprised of a microfluidic channel network, which is indicated by solid black lines. Circles represent the fluidic reservoirs. A side-view representation of an islet perfusion chamber and an on-chip flow-split is also presented. (B) A microfluidic perfusion device for multiparametric islet function assessment through imaging and ELISA (Reproduced from ref. 60 with permission from Springer). (C) A microfluidic device with a single-islet piston-like trap to asses glucose-induced intracellular oscillations of calcium in pancreatic islets (Reproduced from ref. 69 with permission from National Academy of Sciences, U.S.A, Copyright 2004). (D) A microfluidic array for real-time live-cell imaging of microencapsulated pancreatic islets to assess the effect of hypoxia (Reproduced from ref. 59 with permission from American Chemical Society Copyright 2013).

capillary forces and electrokinetic mechanisms inside MPS.[56] Although still in development, in the last decade these features have been successfully introduced to MPS design for applications in islet research (Table 1).

The second major component of islet MPS is an analytical tool or method to monitor glucose-dependent response of the islets. The principal techniques that have been successfully incorporated in MPS up-to-date are capillary electrophoresis immunoassay (CEI) and intracellular Ca^{+2} oscillation monitoring.

CEI provides a technique for the direct detection of secretion from islets with a detection limit of 3 nM for insulin[62] (Fig. 5-A). During experiments, islets are placed in a chamber and effluent is mixed with anti-insulin antibody and fluorescein isothiocyanate labeled insulin (FITC-insulin). Insulin from the islets competes with FITC-insulin for binding sites on the antibody. The mixture is passed into an electrophoresis channel where bound and unbound FITC-insulin is separated. Insulin secretion is then quantified fluorescently through establishing the ratio between bound and free insulin. Similarly, this technique has been applied for detecting glucagon, with a detection limit of 1 nM.[63] Noteworthy, investigating glucagon secretion presents an additional challenge, since α-cells comprise a smaller proportion of the islet than β-cells, resulting in a relatively low amount of glucagon secreted per islet and making it difficult to detect variations in glucagon secretion.[63] This demonstrates that the non-insulin islet hormones, which are secreted in small quantities, can be detected when combining analytical tools with the fluid handling capabilities of microfluidics.

Although many microfluidic devices have employed CEI to perform high-throughput immunoassays on-chip,[64,65] their design was not well-suited for continuous monitoring of living cells.[66] This was mostly because the reported methods required off-line preparation of samples which are not amenable for repetitive sampling and continuous reactions.[66] In this regard, the Kennedy group pioneered the development of a microfluidic CEI to monitor online the fast kinetics of hormone secretion from a single islet with high temporal resolution.[62,66,67] One of the advantages of CEI is that it can be fully integrated on-chip. This technique has proven to be fast and accurate and has been able to detect secretion changes within a few seconds.[62] Recently, the use of this technique has been extended to monitor insulin and islet amyloid polypeptide (IAPP) secretion profiles simultaneously.[68]

Table 1 Summary of selected microfluidic perfusion systems publication used in pancreatic islet research

Detection method	# islets	Specie	Type of trap	Aspect study	Year	Ref.
Capillary electrophoresis immunoassay	1	Mouse	Dam wall-like	Insulin secretion	2003	62
Intracellular calcium oscillation	1	Mouse	Movable wall	Coordination of Ca^{2+} oscillation in islets	2004	69[a]
Capillary electrophoresis immunoassay	1	Mouse	Dam wall-like	Insulin secretion	2005	57
Intracellular calcium oscillation	1	Mouse	Dam wall-like	Role of gap junction on regulating insulin secretion	2006	75
Capillary electrophoresis immunoassay	4	Mouse	Dam wall-like	Continues monitor of insulin secretion on-chip	2007	66
Fluorescence, competitive immunoassay and MALDI-MS	1	Mouse	Hand trapping with micromanipulator	Insulin secretion of a single islet	2008	76
Fluorescence imaging	1	Mouse	Dam wall-like	Effects of glucose gradients on insulin secretion	2009	72
Capillary electrophoresis immunoassay in parallel	15	Mouse	Dam wall-like	Secretion patterns of insulin and free fatty acid lipotoxicity	2009	67[a]
Intracellular calcium oscillation and ELISA	25/100	Mouse/human	Chamber with wells	Islet functionality (mitochondrial potential, insulin secretion)	2009	61
Fluorescent (zinc trapped on droplets)	1	Mouse	Dam wall-like	Insulin secretion	2009	16
Intracellular calcium oscillation	1–15	Mouse	Dam wall-like	Variation of insulin secretion from different mice "islet imprinting"	2009	77
Capillary electrophoresis immunoassay in parallel	1	Mouse	Dam wall-like	Long term operation and performance of electrophoresis device	2009	78
Intracellular calcium oscillation and ELISA	25–30	Mouse	Chamber with wells	Islet functionality under glucose gradients	2010	60[a]
Intracellular calcium oscillation	1	Mouse	Dam wall-like	Insulin secretion cause by different glucose waveforms	2010	79
Intracellular calcium oscillation	100–200	Mouse	Different size of dam wall-like	Separation of islet by size and viability after separation	2010	80
Intracellular calcium oscillation and ELISA	8	Mouse	Dam wall-like	Single islet insulin secretion with passively operated device	2011	81
Mass spectrometry and ELISA	24	Mouse	Polycarbonate or nylon membranes	Collection and concentration of islet secretion	2011	82
Intracellular calcium oscillation/two-photon excitation	4–6	Mouse	Dam wall-like	Effect of microfluidic culture on islet associated endothelial cells	2011	83
Intracellular calcium oscillation and ELISA	10–20	Mouse	Chamber with wells	Effect of hypoxia on insulin secretion	2012	84
Intracellular calcium oscillation and ELISA	4–55	Mouse	Chamber with wells	Insulin secretion kinetics on islet population and mitochondrial potential	2012	85
Intracellular calcium oscillation/two-photon excitation	1	Mouse	Dam wall-like	Dynamics of lipid partitioning in living pancreatic islets	2012	86
Capillary electrophoresis immunoassay	10	Mouse	Dam wall-like	Glucagon secretion	2012	63
Intracellular calcium oscillation	100	Mouse	Chamber with wells	Long term bubble prevention on pancreatic islet culture	2012	87
Fluorescent competitive immunoassay	1	Mouse	Nozzle-like	Secretory dynamics of insulin and IAPP	2013	68
Intracellular calcium oscillation	100	Rat/human	Nozzle-like (encapsulate islets)	Effect of hypoxic conditions on islet viability	2013	59[a]
Intracellular calcium oscillation	5–10	Mouse	Nozzle-like/dam wall-like	Insulin secretion related to epithelial cell lost and effect of shear stress on islets	2013	58
Intracellular calcium oscillation	5–10	Mouse	Dam wall-chamber	Coordination of insulin secretion	2014	73
Intracellular calcium oscillation	16[b]	Single β cell	Micro-orifice driven by pressure	The effect of glucose biases on the spatial distribution of insulin granules	2014	74
Capillary electrophoresis immunoassay	1–10	Mouse	Dam wall-like	Oscillation patterns of Insulin secretion	2014	70

[a] Device shown in Fig. 5. [b] Estimated from images.

However, the setup can be complex since it involves integrating precise external pumps for fluid flow control, power supplies and electrodes for electro-osmotic flow control. Moreover, since most of the secretion products from islets have similar molecular weights, multiplexing using this technique presents a great challenge. Channel clogging, precise temperature control, and requirement of lasers with different wavelengths remain the main issues of working with such a

set-up.[68] Nevertheless, this technique has been useful for long term monitoring of insulin secretion,[57,62] and for understanding heterogeneity in insulin secretion.[66,67,70]

Calcium sensitive dyes[71] (*e.g.* Fluo-3, Indo 1, Quin 2, Calcium Green, Fura Red, *etc.*) have been used to visualize the calcium oscillations that precede insulin exocytosis and thereby to study secretion mechanisms and to indirectly measure islet secretion. Observing these oscillations is often challenging on many of the macro systems commonly employed in biological studies, because of the difficulty in differentiating physiological events that trigger Ca^{+2} oscillation. In contrast, imaging with microfluidic devices can allow exclusive observation of the Ca^{+2} oscillations associated with exocytosis.

Despite the advantages of this method, it presents some limitations regarding quantification and selectivity. For instance, calcium oscillations from different types of cells in the islet may be difficult to distinguish. Moreover, quantification of secretion products is required off-chip using traditional immunoassays such as ELISA.

Nevertheless, this technique has furthered our knowledge regarding important aspects of islet secretion such as the limited coordination of Ca^{+2} oscillations in islets when stimulated with glucose[69] (Fig. 5-C). The mentioned study found that β-cells are electrically coupled through gap junctions, being able to synchronize calcium oscillations but only within glucose-stimulated regions.[69] In addition, this technique has shed light on the cellular dynamics of islets when stimulated with different glucose wave forms, analogous the glucose variations that occur *in vivo*.[72] For instance, Dhumpa, *et al.*[73] developed a MPS to test the hypothesis that negative feedback from the liver synchronizes islet secretion by controlling the blood glucose level. To introduce negative feedback to the on-chip islets, the glucose stimulation level was updated based on the insulin secretion by employing a model. In response to negative feedback, synchronized secretion was observed within groups of islets using calcium imaging and insulin ELISA.

The Ca^{+2} oscillation technique have also been applied to a microfluidic device able to trap single cells, spatially deliver analytes of interest and assess their effects with subcellular resolution.[74] The device employed pancreatic islet β-cells (MIN6) transfected to express insulin-GFP. The cell response evoked by different analytes was visualized using optical microscopy to monitor Ca^{+2} oscillations and insulin-GFP secretion. In particular, the group found that sub-cellular exposure of glucose induced a modification in the spatial distribution of insulin granules (cell polarity) within the β-cell toward the site where glucose was delivered. This tool can help to increase the understanding the dynamics of insulin granules exocytosis due to its precise control of the surrounding chemical environment; however it was only demonstrated with single β-cells.

There are examples of microfluidic platforms specifically designed for pre-assessment of islets destined for transplantation to treat type I diabetes. For instance, Mohammed *et al.*[61] developed a microfluidic islet perfusion device for the assessment of dynamic insulin secretion of multiple pancreatic islets with simultaneous fluorescence imaging of Ca^{2+} oscillations and mitochondrial potential changes. This device was further optimized in order to achieve efficient mixing and uniform distribution of solutions in the perfusion chamber[60] (Fig. 5-B). In another example, Silva, *et al.*[58] developed a microfluidic device that traps islets in cup shaped nozzles, which are connected by channels to allow fluid to bypass the islets. This reduces shear stress on the islet, as demonstrated by healthy islet Ca^{2+} signaling. In addition, the nozzle stimulated intracellular flow through the islets, enhancing β-cell and endothelial cell preservation. This helps address the issue of endothelial cell necrosis in isolated islets, with the goal of stimulating re-vascularisation of islets when transplanted.

Another microfluidic device, developed by Nourmohammadzadeh, *et al.*[59] (Fig. 5-D), determines the effects of hypoxia on alginate encapsulated islets for transplantation. The device simultaneously assesses islet functionality and viability by imaging mitochondrial membrane potential, NADPH and intracellular calcium oscillations. They demonstrated that islet functionality decreases with the increasing hypoxic conditions.

Although some of the aforementioned MPS devices can perform multi-parametric characterization of islets,[60,68] most of them monitor a single parameter to study islet hormone secretion and functionality. Many focus solely on a single islet hormone, mainly insulin or glucagon, which may provide an incomplete profile of islet physiological functionality. Hence many research opportunities exist to expand the amount of hormones detected to measure a larger SF. Here is where one of the major challenges for future islet MPS reside. Additionally, the majority of the MPS have used mouse islets as a proof of concept. Consequently, findings on these devices may require translation to human islets. Table 1 summarizes some of the MPS devices for islets developed to date.

3. Potential analytical tools for islet secretory fingerprint analysis

The analytical techniques mentioned in the previous section prove to be sufficient to follow the fast kinetics of insulin secretion. However, in order to monitor a wide islet SF, integration of novel multiplexed detection tools into MPS is required. The major considerations for detecting secretion from islets are: 1) the temporal resolution of the sensor to assure capturing the fast kinetics of islet hormonal secretion, 2) the dimensions of the sensors to spatially locate islet secretions, 3) the stability of the sensor to allow continuous operation and real time secretion monitoring, and 4) the selectivity of the sensor for a single secreted biomolecule, such as insulin, and not co-secreted products such as amylin and C-peptide. Therefore, the sensing tools must be fast, specific and possess high *spatio-temporal* resolution in order to simultaneously detect changes in the secretion patterns of the different cells composing the islets. In addition, these tools need to be adapted for easy integration with MPS, since the

reduced volume of MPS can concentrate analytes allowing easier detection, particularly for hormones secreted in small quantities (*e.g.* glucagon, PP and somatostatin). Furthermore, since the islet hormones are usually measured in a carrier solution, calibrating the sensor to the respective pH, salts and other molecules is a prerequisite.

The main reported techniques that could provide multiplexed detection of islet secretion kinetics include electrochemical techniques, patch clamp techniques, field effect transistors (FET) and surface plasmon resonance (SPR).[88] The following sections will cover the potential of aforementioned technologies to conceive LOC devices for assessing a pancreatic islet SF.

3.1. Patch clamp

The patch clamp technique is a tool to study the electrophysiological properties of cells by bringing a pipette containing an electrode in contact with the cell membrane. Suction is applied to the pipette to create an ultrahigh resistance seal with the cell membrane. Rupturing the membrane provides electrical contact between the cell interior and the electrode. This setup enables measurement of whole cell currents and cell membrane capacitance, both of which are correlated with exocytosis of cell secretion products.[89]

Patch clamp has been used to study secretion from human β-cells[22,90–92] and α-cells.[25,93,94] During capacitance measurements, exocytosis in β-cells can be invoked using induced voltage clamp depolarisations and secretagogues.[89] This technique can provide quantitative information regarding exocytosis, for example through correlating the rate of capacitance change with the quantity of granules released at a given time.[95]

Since the pipette allows infusion (or dialyzing) of substances into the intracellular environment, observations can be made of the effects of substances on hormone secretion (*i.e.* cyclic AMP, calcium chelators, GTP analogues and sulfonylureas). Likewise, stimulants can be added in the extracellular bathing solution. Furthermore, fluorescent probes can be injected into the cell cytoplasm through the patch pipette. Therefore, a wealth of data can be obtained by simultaneous membrane capacitance and whole cell current measurements obtained using the patch pipette while combining fluorescence imaging.

However, some disadvantages of the patch clamp technique are that it is very low throughput, it provides an indirect measurement of secretion, it can be interfered by endocytic processes, it lacks specificity for individual secretion products and it is invasive. Additionally, this technique requires highly skilled operators in order to trap and manipulate cells.

With the current microfabrication technologies microfluidic platforms with small apertures can be fabricated, which act as the pipette tip. These apertures allow automated trapping lateral to[96] or on the bottom of microfluidic channels.[97–99] For instance, Lau *et al.*[96] developed a PDMS microfluidic patch clamp array that incorporates on chip lateral cell trapping sites and an open access chamber at the top for easy media changes (Fig. 6-i). A challenge associated with using this technique for on-chip applications is the choice of fabrication materials, since fabrication methods can be expensive and complicated. Additionally, the use of substrates with poor dielectric properties can produce low seal resistance, hence decreasing the signal-to-noise ratio. To overcome this problem, Bruhn *et al.*[97] developed a glass pore chip by taking advantage of the high dielectric properties of glass. The device was able to obtain a similar seal resistance as the conventional micropipettes, to automatically trap cells at the bottom and to perform single membrane channel recording (Fig. 6-ii). Currently, some automated patch-clamp systems with multiplexed recording electronics and microfluidics layers, that enable high-throughput measurements, are commercially available.[100,101]

Patch clamp investigations of pancreatic islets have focused primarily on β-cells. But to understand the secretion mechanism of islets as a whole, the technique needs to be extended to other islet cells (δ, ε, *etc.*). However, the lack of reliable methods to identify islet cells adds an extra challenge for patch clamp measurements of intact islets.[25] One proposed solution is to produce genetically modified mice that express fluorescent proteins in α- and β-cells to distinguish them *in situ*.[25] Still, doing this for the various cell types in the islet is time consuming and expensive, and novel identification methods may be required. Nevertheless, studies exist for attaching the patch pipette to single cells within intact islets.[102–104]

The patch clamp technique possesses the required temporal resolution (milliseconds) to monitor secretion kinetics and has sufficient sensitivity to detect single vesicle fusion. After proper identification of individual islet cells, microfluidic devices containing multiple patch clamps can measure secretion kinetics simultaneously. To complement patch clamp measurements, electrochemical sensors can be added on-chip to obtain selective quantification of secretion products as has been previously demonstrated in non-LOC setups.[21,105] Thus, this would provide a high-throughput tool to analyse a single islet SF.

3.2. Amperometry/voltammetry

Amperometric/voltammetric (A/V) techniques provide a method to detect and quantify cell secretions through electrochemical reactions. In amperometry, a potential is applied while the resulting current from oxidized or reduced species is recorded. Conversely, voltammetry measures current as a function of applied potential.

Insulin is an electroactive molecule and hence it can be detected with unmodified electrodes. This has made insulin the prime focus of islet secretion research by means of A/V sensing. However, electrochemical sensing of insulin with unmodified electrodes has been shown to be characterized by fouling, slow kinetics and low sensitivity.[106] To overcome

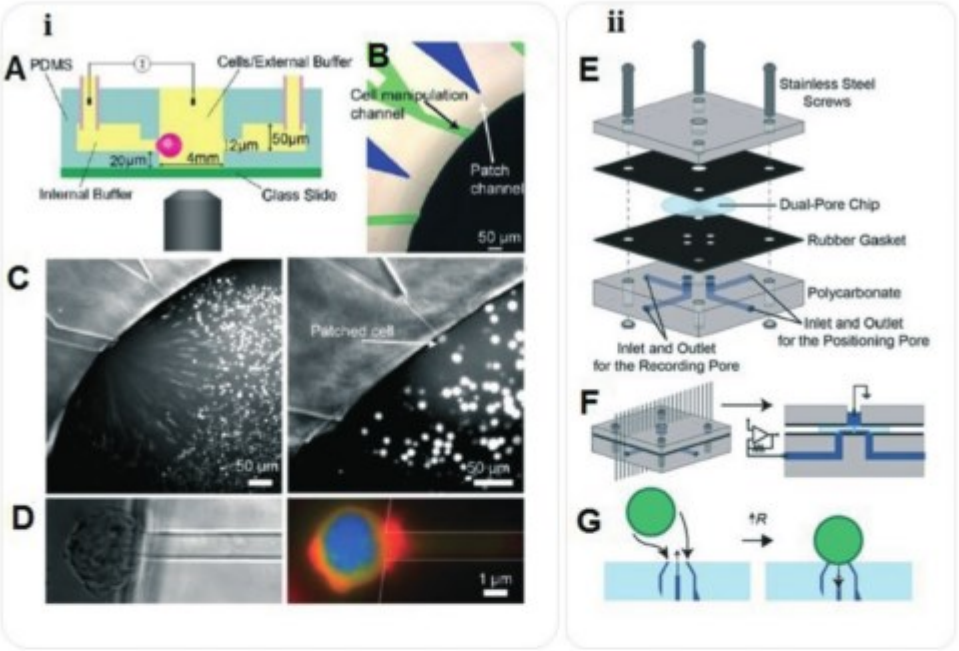

Fig. 6 (i) A microfluidic patch clamp array chip with lateral cell trapping sites. (A) Cross sectional representation showing a cell being trapped in a microfluidic device. (B) Close-up of the device where a channel for patch trapping and cell manipulation can be observed. (C) Optical microscope image of cells being manipulated in order to bring them close to the patch channel. (D) Image showing a cell being trapped and patched on the small channel (Reproduced from ref. 96 with permission from the Royal Society of Chemistry). (ii) Dual pore glass chip. (E) Schematic representation of the assembly of the dual-pore glass chip for cell-attached single-channel patch clamp recording. (F) Cross sectional view of an assembled chip. (G) Representation of a cell trapping mechanism used to establish a high-resistance seal with a cell (Reproduced from ref. 97 with permission from the Royal Society of Chemistry).

these limitations coating catalysts have been developed for the electrodes. Several of these catalysts include those containing ruthenium, iridium oxide, metallodendrimers, and carbon nanotubes. The sensing performance of some of these catalysts have been previously summarized by Rafiee *et al.*[107] and Amini *et al.*[108] Additionally, insulin-specific recognition elements can be added to the electrodes. For instance, insulin aptamers[109] and electrodes modified with molecular imprinted polymers[110] have shown promise for sensing insulin with high specificity. An additional advantage of using aptamers and molecular imprinted polymers as recognition elements is that binding is highly reversible so it is possible to regenerate the sensors with great efficiency.[111] These kinds of selective recognition elements can be developed for other islet hormones which can be advantageous for multiplexed detection.

The majority of A/V sensors have been designed for detecting insulin in blood samples, hence some modification will be required for monitoring insulin secretion from single islets. In addition, some electrodes used a flow injection analysis setup,[107,108] in which the electrode is situated in a constant flow environment. This setup is analogous to the environment in MPS, demonstrating the potential adaptability of these sensors for MPS.

A few A/V sensors have been developed for direct detection of secretions from islets and dispersed β-cells. When monitoring β-cell secretion, alternatives to electrochemically detecting insulin may be preferred to avoid electrode modification steps. For instance, other factors co-secreted with insulin can be readily detected electrochemically. These factors include the electro-active amine, 5-hydroxytryptamine (5HT)[112] and zinc.[113] Zinc is complexed with insulin inside β-cell vesicles and during secretion, the complex dissociates into insulin and free zinc ions. The insulin concentration can be indirectly determined *via* A/V detection of zinc.[114] Conversely, 5HT needs to be incubated with islets prior to experiments, such that the 5HT becomes localized in insulin vesicles, and is subsequently co-secreted with insulin. In this manner, A/V sensing of 5HT has been used to measure secretion from mouse β-cells[115–118] and mouse islets.[119,120]

There are limited reports where A/V sensors have been integrated in MPS systems for monitoring islet secretion. An

example is a microphysiometer chamber containing islets under perfusion, which was coupled with an amperometric insulin sensor composed of a multiwall carbon nanotube film electrode.[121] This platform serves as a proof of concept for LOC devices, which can take advantage of microfabrication and electrode printing technologies to elaborate probes with high *spatio-temporal* resolution. Additionally, nanomaterial modified electrodes with sufficient limit of detection (nM) for single cell analysis are becoming robust and have made inroads into the microfluidic domain, presenting opportunities to apply these sensors to islet research. However, research needs to be expanded into multiplexed A/V detection of islet secretion products to allow screening of an islet SF.

3.3. Impedance spectroscopy

Impedance spectroscopy (IS) (also called electrochemical impedance spectroscopy) is a technique that measures changes in the electrical impedance of a sample over a range of applied electrical frequencies. IS biosensing is based on spectrum changes that take place in response to binding events and reactions associated with analytes of interest. This technique is subdivided into Faradic IS and non-Faradic IS depending on whether a redox reaction is present or not. Faradic IS involves an electrochemical reaction as a sensing step. This reaction can come either from an external chemical compound (redox probe) added to the system or from the sample itself. In contrast, the redox probe is absent in non-Faradaic IS. As a label free technique, IS eliminates costly and cumbersome sample preparation steps.[46] However, as mentioned in the previous section, the electrochemical detection of biological molecules can be non-specific, requiring surface modifications with biomolecules (antibodies, affirmers, aptamers, *etc.*). Additionally, direct detection of analytes can have insufficient sensitivity, requiring catalytic modification of the sensing interface.

Non-Faradic IS has many advantages over Faradaic IS. Firstly, the absence of a redox probe in non-Faradic IS makes the experimental setup simpler and eliminates the need for catalytic modification of the sensing interface. Secondly, the redox probe employed in Faradic IS can be highly toxic for cells. Moreover, depletion of the redox probe can occur, so Faradic IS platforms need to be designed to avoid this issue. Hence, non-Faradic IS is considered more appropriate for integration with LOC devices,[122] especially for investigation of complex biological systems such as human pancreatic islets.

Faradaic IS has been used to detect insulin using immobilized antibodies[123] or silica nanoparticles/nafion.[124] These technologies can be adapted to detect insulin from islet samples. A shared drawback of most electrochemical biosensors is the non-specific interactions that are usually present in complex samples such as blood serum or cell secretions. However, a recent report detected insulin with a non-Faradaic impedance biosensor using a chemically adsorbed zwittorionic polymer (polymer with net charge of zero, but with negative and positive charges within its structure) with attached monoclonal insulin antibodies.[125] Noteworthy, this functionalization confers high specificity to the mentioned sensor, enabling it to detect insulin in the femto-molar concentration in undiluted blood serum. In a similar fashion, the same group developed a non-Faradic IS detection array for protein marker detection.[126] Thermally cross-linked poly(ethylene glycol) on the chip surface provided a simple and robust interface with high antifouling properties. Here, insulin and C-reactive peptide were simultaneously measured in human serum with little cross reactivity despite similarities between the two peptides. The limit of detection was as low as 171 fM and 10 pM respectively.

However, despite the remarkable limit of the detection and antifouling properties of the aforementioned biosensors, as with most biosensors, regeneration of the sensing surface for continuous monitoring of secretion products still remains an issue. A recent review by Goode *et al.*[127] summarizes possible strategies to achieve successful biosensor regeneration. Nevertheless interesting research opportunities exist to extrapolate this technique for multiplexed measurement of islet secretion products. In addition, thin film electrodes modified with robust polymer interfaces can be easily integrated on microfluidic devices with islet perfusion chambers.

3.4. Field effect transistors

A field effect transistor (FET) biosensor is built by modifying the gate surface of a transistor with recognition elements capable of binding an analyte, such as antibodies, antibody fragments, aptamers or DNA (Fig. 7-i). When binding events occur, the electric field is modified, resulting in a detectable change in the transistor conductance.

The concept of FET biosensors has been developed for more than two decades, but only recently has the interest in them increased due to the development of novel nanomaterials. When FETs are coupled with highly conductive nanomaterials, such as nanowires (*e.g.* metal oxide, silicon and carbon based nanowires) and graphene, a very sensitive tool (pg mL^{-1}) for the detection of biomolecules can be fabricated.[128–130]

However, all FET biosensors operate on the principal that the electric field seen by the current carrying element is sensitive to target binding. When immersed in an electrolyte, this requires that binding occur within the order of the Debye length. Beyond this distance the electric field seen by the surface becomes independent of solution composition and binding events.[122] The Debye length is typically restricted to a few nanometers under physiological ionic strength conditions and becomes smaller as the ionic strength increases.[131] Thus, any recognition element must be anchored within this distance, which presents a problem with large macromolecules, such as antibodies (~10 nm). However, it has been demonstrated that recognition elements such as DNA and aptamer (1–2 nm) can efficiently work with FETs.[131] Alternatively, dilution of analytical samples to low ionic strength prior to analysis can be performed.

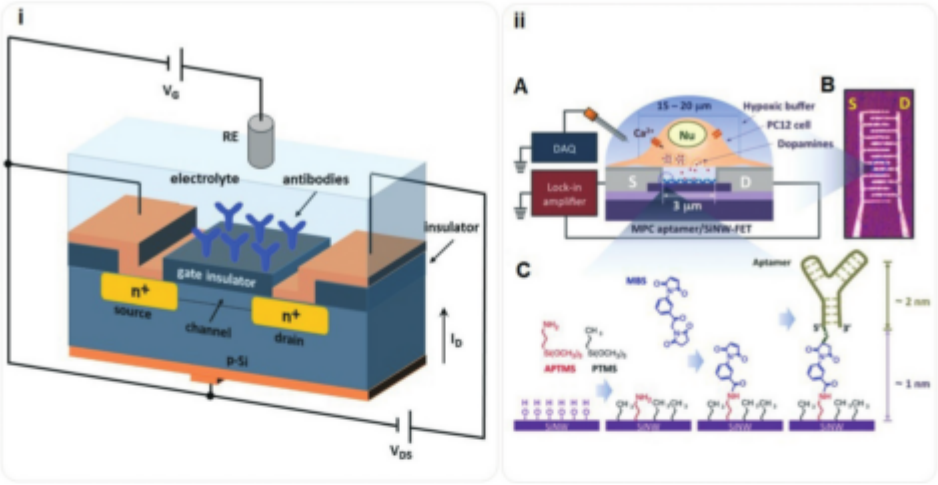

Fig. 7 (i) A typical structure of a FET sensing device functionalized with antibodies. RE stands for reference electrode, VG for gate voltage, VDS for drain–source voltage and ID for drain current. (ii) Multi parallel connected (MPC) silicon nanowire FET. (A) Schematic representation of a DNA-aptamer modified MPC SiNW-FET device for detecting dopamine from stimulated PC12 cells. (B) Microscope image of a SiNW-FET device where "S" stands for source, and "D" for drain. (C) Schematic representation of the DNA-aptamer immobilization procedure on a SiNWFET. APTMS stands for (3-aminopropyl)trimethoxysilane, PTMS for propyltrimethoxysilane and MBS for 3-maleimidobenzoic acid *N*-hydroxysuccinimide ester (Reproduced from ref. 130 with permission from American Chemical Society, Copyright 2013).

The aforementioned limitations have not discouraged the application of this highly sensitive type of biosensor to study cell physiology, especially by coupling them with microfluidics. For instance, Li *et al.*[130] developed a highly specific nanowire FET biosensor embedded in a PDMS microfluidic channel (Fig. 7-ii) to detect dopamine secretion from living chromaffin cells (PC12 cell). The biosensor specificity was achieved using DNA-aptamers, which distinguishes dopamine from other analogues such as catechol, phenethylamine, tyrosine, among others. Although this device does not measure proteins, it is a proof of concept that real-time and label free quantification of secretion products can be achieved with sufficient sensitivity ($<10^{-11}$ M) and selectivity to perform single cell analysis with this technology.

Investigation into the use of FETs to monitor islet secretion products has been limited. Sakata *et al.*[132] developed a FET sensor to monitor the electrical activity of rat pancreatic β-cells by culturing these cells on the FET gate surface. This FET sensor monitored insulin secretion indirectly by measuring pH changes once the β-cells are stimulated with glucose. Sakata identified a correlation between H^+ ion accumulation and insulin secretion through the activation of β-cell respiration activity.

The major advantage of FETs compare to other type of biosensors is that they can be easily multiplexed, miniaturized and manufactured on a large scale, which makes them a good candidate for mass production. Additionally, their small size enables detection of a large islet SF and potentially allow on-chip screening of several secretagogues. As the FET field continues to evolve with improvements in FET microfabrication and nanomaterials development that increase their sensing capabilities, their potential role in secretome research will undoubtedly expand.

3.5. Surface plasmon resonance

By allowing fast detection of binding interactions due to changes in the surface plasmon of a thin gold film, surface plasmon resonance (SPR) sensing has become the gold standard to study biomolecular interactions, particularly affinity based interactions such as DNA–RNA hybridization or antigen–antibody.

The advantage of this technique is its intrinsic dynamic, label free and real-time analysis capabilities. Additionally high-throughput and multiplexed analysis are possible by making arrays of different molecules on the sensing surface.[133]

However, the sensitivity of this technique is insufficient to detect highly diluted analytes or small molecular weight biomolecules such as cancer biomarkers, hormones and antibiotics. To overcome this challenge, sensitivity-enhancing methods have been proposed such as integration of nanostructures, either as amplification tags or as enhancing substrates.[134] As a result, this technique has been able to reach limits of detection of picomolar and attomolar order,[134] opening the possibility to detect protein secretion from single

cells. In addition, the single cell, high-throughput and multiplexed capabilities of this technique can be greatly enhanced by its coupling with microfluidic devices.

There are few reports that attempt to detect cell secretion by the direct application of SPR biosensors.[135–138] Oh *et al.*[137] developed a nanoplasmonic device to study cytokine secretion from immune cells directly derived from human blood (Fig. 8-i). In order to separate the immune cells from the blood, antibody functionalized microbeads targeting specific cell surface biomarkers were employed. Later, these cell/bead conjugates were loaded into the device where they were trapped around a micro-pillar array. The cells were then stimulated and the cytokine secretion was detected on the SPR surface. Another example is a SPR microfluidic device to monitor the dynamic secretion from human monocytic leukemia cells developed by Wu *et al.*[138] The SPR chip was composed of gold nano-slits with immobilized antibodies on a polycarbonate film (Fig. 8-ii). The nano-slit array was integrated with a cell-trapping microfluidic device, to allow for examination of cell secretion dynamics. The cell-trapping system was designed to allow a micrometer separation of target cells from the sensing surface to minimize non-specific signals from cell bodies. An interesting characteristic of this device is the small number of cells required to detect secretion (<10).

Of all analytical techniques mentioned, SPR has been used to detect the widest variety of islet secretion products. SPR biosensors have been used to investigate binding interactions of major secreted islet hormones, namely insulin,[139–141] somatostatin,[142] pancreatic polypeptide[143,144] and ghrelin.[145] Thus, the simultaneous detection of several islet-secreted products in a single device is feasible. However, as with most label free biosensors, specificity can be a challenge, particularly for applications that involve measurements in a complex matrix such as a cell secretome. Thus, novel anti-fouling strategies are a central part of ongoing research in the field. For instance, Frasconi *et al.*[146] were able to detect insulin in human serum using SPR sensing with a surface modified with polymeric dendrimers encapsulated gold nanoparticles. This surface preparation reduced non-specific interaction

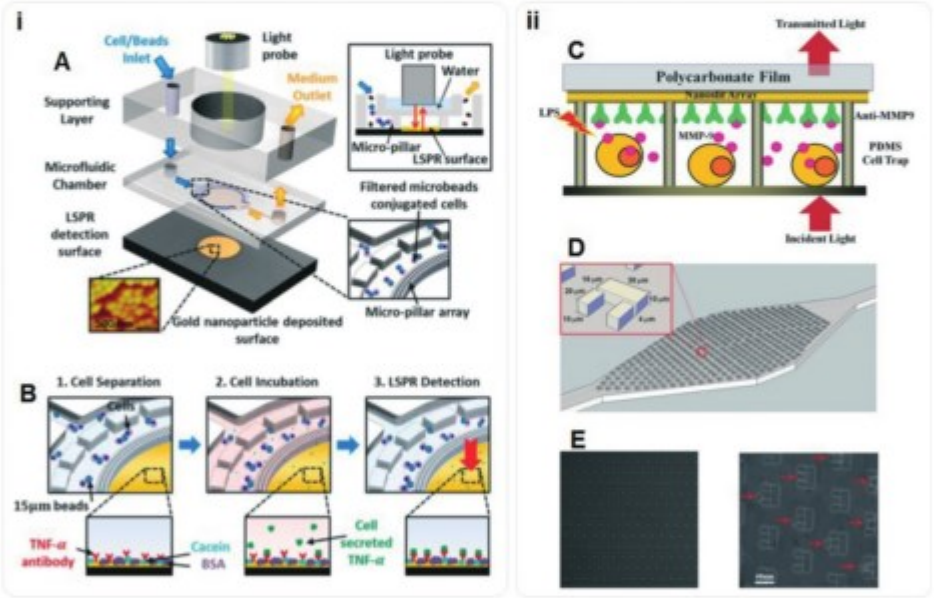

Fig. 8 (i) A microfluidic device with integrated nanoplasmonic sensing for cellular functional immune analysis of human blood. (A) Schematic representation of an integrated localized surface plasmon resonance (LSPR) optofluidic device. The bottom layer is composed of deposited gold nanoparticles. The magnified image at the bottom left is an AFM image of the gold nanostructured surface. The middle layer is composed of a microfluidic chamber and channels. The chamber was integrated with micro pillar arrays, as shown in the middle right schematic, to trap target cells. The cross-sectional view of the device is shown at the upper right corner. (B) The middle layer is composed of a microfluidic chamber and channels. (Reproduced from ref. 137 with permission from American Chemical Society, ACS AuthorChoice 2014). (ii) An optofluidic platform for real-time monitoring of live cell secretion. (C) Schematic representation of the experimental setup to measure cell secretion. The target cells are immobilized in cell traps incorporated in a microfluidic channel. After stimulation, cell secretions bind to antibodies immobilized on a gold nanoslit SPR sensor located above the cells. (D) Schematic representation of the entire microfluidic chamber containing an array of cell traps. The dimensions of the cell traps are shown in the inset on the top left corner. (E) Optical microscope images of the cell trap array showing cells captured in the traps. Each red arrow points to one cell (Reproduced from ref. 138 with permission from John Wiley and Sons).

and provided a limit of the detection in the order of pM in complex biological media. Additionally, a less than 5% loss in performance was observed over 40 regeneration cycles. However, the complex competitive immunoassay scheme, requiring several minutes to perform, reduced its real-time capabilities. Nevertheless, this report presented a strategy to reduce non-specific interaction in SPR sensing when measuring small peptides.

Commercial SPRs are generally based on the traditional prism-coupled SPR configuration. The approach is simple and robust, but not amenable to miniaturization and integration.[147] However, SPR technologies have taken advantage of new advances such as optical fibers and waveguide nanostructures for miniaturization, which have opened new avenues for easy fabrication of SPR LOC devices.[148] With the latter setups, islets can potentially be immobilized in proper microenvironments for secretion detection, similar to devices developed for other cell types (see Fig. 8).

4. Applications of on-chip monitoring of relevant islet secretory fingerprints

4.1. Quality assessment of islet preparations for transplantation

A promising therapeutic avenue for T1D is pancreatic islet transplantation.[149–151] This therapy has provided proof of concept that normoglycemia can be restored in patients with T1D by isolating islets from a cadaveric donor's pancreas and infusing them into the patient's hepatic portal vein (Fig. 9). One of the main limitations of this therapy is the need for more than one donor for each recipient, due to islet apoptosis following isolation.[152] It was estimated that over 50% of the transplanted islets are lost within hours post infusion.[153–157]

This has stimulated interdisciplinary research to increase the long-term survival and functionality of grafted islets.[153,158] LOC technology offers a tremendous opportunity to assess islet quality for transplantation and islet functionality, all of which are part of emerging fields of research. These opportunities can be further increased by analysing the islet secretome and by defining an islet secretory fingerprint that encompass biomarkers that rapidly measures its quality. For the interested reader, other aspects and challenges involved in islet transplantation are thoroughly reviewed elsewhere.[158–160]

Although there are current regulations from the U.S. Food and Drug Administration (FDA) that state the minimum required characteristics for islet preparations, such as safety, identity, purity, viability and potency;[161] it is currently accepted that these specifications provide reasonable estimates of safety, identity, and purity, but do not deliver meaningful measures of viability or potency of the preparation.[163–166]

The current gold standard testing for islet potency is the nude mice bioassay. This bioassay is based on diabetes reversal after islets engraftment under the mouse's kidney capsule.[167–170] Due to the nature of this assay (immune inhibited mice), it is compatible with human islets. This gives the assay a great advantage when predicting the outcome of human engraftments. However, the nude mice bioassay involves a complex surgical procedure, and only works in a retrospective manner, where results are interpretable and accurate only after diabetes reversal has occurred.[168] Despite the drawbacks, whenever a new potency or viability

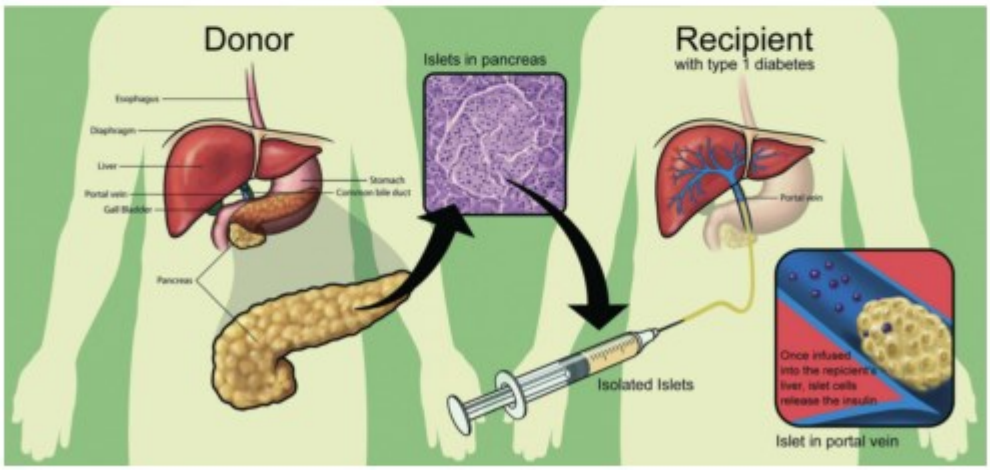

Fig. 9 Islet transplantation through the Edmonton protocol. First, islets are isolated from a donor by collagenase digestion and then they are assessed for identity and quality. Finally the islets are introduced into the hepatic portal veins of the recipient where they are trapped and are able to respond to glucose concentration changes by secreting insulin and glucagon (Reproduced from ref. 162 under the terms of the Creative Commons Public Domain Declaration).

assay is proposed, the predictability of the method should be tested with the nude mice bioassay.

Some promising islet potency and viability assays developed in the last decade include cell membrane integrity tests, cell death, mitochondrial health assays and oxygen consumption rate.[163] Tests that assess mitochondrial function, particularly those measuring oxygen consumption rates of islets, seem to be the most promising and correlate best with transplantation outcomes in the nude mice bioassay. Nevertheless, pancreatic islets are complex micro-organs, and a multiparametric approach can be more accurate than individual assays.

There are few examples of multiparametric tools for assessing islet quality, and the majority of them are based on MPS.[59–61,84] For instance, the Eddington and Oberholzer group developed a microfluidic device where islets are trapped in a well array at the bottom of a micro-chamber. There, mitochondrial membrane potential and Ca^{+2} oscillations were simultaneously measured.[60,61] This device was improved by adding dynamic oxygen control during glucose stimulation.[84] Later, the group developed a microfluidic islet array with hydrodynamic trapping for islet immobilization and an improved oxygen control in order to assess the response of microencapsulated islets to hypoxic conditions.[59] With this configuration, simultaneous analysis of Ca^{+2} oscillations, mitochondrial potential and NAD(P)H of human pancreatic islets was achieved. The advantages of such multiparametric MPS for islet quality assessment and functionality are numerous. It enables precise control over the islet microenvironment, it has high *spatio-temporal* resolution, and it avoids damaging the islets during measurements.

Similar multiparametric MPS could potentially become a new gold standard for islet quality assessment. However, in order to fully establish a new standard, it is still necessary to corroborate the device outcome of islet quality assessment with the nude mice bioassay. Furthermore, these kinds of MPS still rely on elaborate imaging techniques that require trained personnel, complicating their use as point-of-care devices and compromising their commercialisation potential. The development of fully automated LOC devices with integrated sensors that reduce the human factor from the measurements is needed to allow surgeons to immediately assess islet quality prior to transplantation.

By defining a SF for viable and functional islets, it should be possible to develop novel LOC devices to assess in real-time a complex SF of islets in an automated manner. This SF can be comprised of different protein biomarkers for cell death (apoptosis, anoikis, *etc.*), mitochondrial health and secreted hormones. Moreover, assessment of other criteria suggested by the FDA, such as safety and purity, may be also integrated and performed on such LOC devices.

4.2. Islet regeneration

Regeneration of functional pancreatic endocrine tissue in the form of islets, β-cells or other hormone secreting cells, is a potential method to address the issue of donor islet shortages for treating T1D.[171,172] In addition, understanding regeneration pathways could unlock *in vivo* mechanisms for replenishment of pancreatic endocrine tissue.

The activation of transcription factors during fetal pancreatic development has generated interest in their potential applications in β cell regeneration.[173–177] Through better understanding of these transcription factors, new strategies to generate islet tissue from existing β-cells or from pancreatic duct and acinar tissue can be developed.[177] Another strategy is trans-differentiation of cells within islets, for example from α to β-cells.[176] Some members of the Reg family have been shown to affect β cell regeneration and/or neogenesis.[172,178] Another family of proteins, namely the incretins, have also been shown to have implications in regeneration of pancreatic endocrine tissue.[176,179–181] Many of these factors have shown regenerative potential both *in vivo* and *in vitro*.

MPS can enable screening of a large number of transcription factors involved in islet differentiation and thereby improve existing islet regeneration strategies and uncover new regeneration pathways and agents. Such devices would allow the control of the physical and biochemical environment needed to induce differentiation, support long term culture of islets and their differentiation processes (which last several days), and enable the evaluation of the initial state and result of islet differentiation. The microfluidic devices can also serve as a pre-screening tool for regenerating agents, before testing novel strategies *in vivo*.

In addition, the on-chip microenvironment can be tailored to mimic *in vivo* conditions. For instance, incorporation of 3D extracellular matrices that maintain islet–matrix interaction would provide a more optimum environment for islet regeneration. An example of such a platform is reported by Wan *et al.*, where embryoid bodies were differentiated on-chip during long term cultures in 3D collagen matrices.[182] Immunofluorence staining was then utilized to assess the differentiation of embryoid bodies within 3D extracellular matrix cultures.[182] These types of platforms have been recently upgraded by adding microfluidic well arrays to capture embryoids, exposing them to stimulation gradients and allowing easier imaging and more reproducible results.[183] Such platforms can be easily translated for islet studies where immobilization, stimulation and imaging of islets can be performed.

Since islets have been shown to be harmed by shear stress in microfluidic environments,[83] MPS devices can be designed to reduce fluid-induced shear stress on cells. For instance, such devices have been developed to facilitate cell differentiation in sheltered regions away from main flow channels.[183,184] In addition, the perfusion environment can be tailored to control media delivery across cells. Fung *et al.*[185] showed that by exposing both halves of a single embryoid body to different flows, expression of differentiation markers varied across the embryoid body. Such a setup would be very useful to examine the long term effects of stimulation gradients across different regions of the islet. Some microfluidic devices have been developed for delivery of stimulation

gradients to islets[69] and β-cells.[74] These can be adapted to observe the effect of gradients on islet regeneration.

Evaluating the expression and secretion of islet proteins enables tracking of the differentiation process and determination of the regenerated tissue functionality. For instance, when Hui *et al.*[180] induced pancreatic ductal cells to differentiate into insulin secreting cells using an incretin, these cells were tested for insulin gene expression, intracellular insulin content and insulin secretion. Zhou *et al.*[186] differentiated a pancreatic duct cell line into endocrine cells, and used staining for insulin, glucagon and pancreatic polypeptide to evaluate this transformation. Another study demonstrated that islets could be differentiated towards highly proliferative duct-like structures, and then back into islet-like structures, through the action of a Reg family protein.[172] Here, immunodetection of insulin, glucagon, somatostatin and pancreatic polypeptide on different days allowed the differentiation process to be tracked. In addition, immunostaining these hormones within the islet-like structures established their islet-like phenotype. Furthermore the functionality of the islet like structures was demonstrated based on their comparable glucose stimulated insulin release to freshly isolated islets. These studies provide proof of concept for using the SF to monitor and assess islet regeneration. Multiplexed detection of key islet proteins comprising a relevenat SF can provide a more comprehensive evaluation of the islet regeneration process.

Integrated on-chip biosensing tools for an islet SF, as covered in previous sections, can provide tools to assess the success of an islet regeneration strategy. An established SF for freshly isolated islets can be used as a baseline for assessing the functionality of regenerated pancreatic endocrine tissue. The real time capability of cell secretion biosensors can provide continuous assessment of the multiple phases of regeneration processes. In addition to SF biosensing, multiple cell parameters can be measured using other techniques, for example by coupling with fluorescence imaging for differentiation markers. Hence, MPS coupled with real time monitoring of a relevant SF have the potential to provide powerful tools to enhance understanding and control over islet regeneration strategies and furthermore provide quality assessment of regenerated endocrine tissue.

4.3. Drug development and screening for diabetes

Type II diabetes (T2D) is usually characterized by insulin resistance in adipose tissue, skeletal muscles and liver tissue, and by a reduction in insulin production by the pancreas. In order to treat this disease, different therapeutic agents are used to stimulate insulin production (*e.g.* sulfonylureas and meglitinides), or to reduce insulin resistance in target tissues (*e.g.* thiazolidinediones and metformins).

The process for developing new anti-diabetic drugs usually starts with *in vivo* and *in vitro* models. These models are used to assess the absorption, distribution, metabolism, excretion and toxicity (ADMET) of the novel therapeutics. Current models for diabetes drug discovery and research include: chemically induced *in vivo* models (streptozotocin and alloxan) and genetic models of diabetes such as the fa/fa rat, Goto-Kakizaki rats, the db/db mouse, and the ob/ob mouse. The advantages and disadvantages of these models have been extensively reviewed elsewhere.[187,188] Additionally, *in vitro* models include: islet preparations from humans and other species along with insulin-secreting cell lines (RIN, HIT, β-TC, MIN6 and INS-1 cells), to assess compounds that enhance insulin secretion; hepatocytes, muscle cells (L6 and C2C12) and adipocytes (3T3-L1 cells) for compounds that reduce insulin resistance. The interested reader is redirected to relevant reviews of these *in vitro* models.[187,189,190]

Despite the demonstrated value of these *in vivo* and *in vitro* models to better understand diabetes, as in islet transplantation, there is a lack of predictability when results are extrapolated to humans. This predictability challenge may have its origin in vital anatomical and physiological differences that are rarely taken into account.[18] Evidence of these differences can be found in a recent work where re-aggregated human pancreatic islets were assessed and compared to native human islets and rat islets for secondary drug screening.[191] The response of the different islets were significantly different when tested against a variety of compounds such as the calcium channel agonist Bay K 8644, glibenclamide, tolbutamide, caffeine, carbachol, glucagon-like peptide-1, among others. As the authors pointed out, islet re-aggregates may represent a more homogenous model for drug screening since native islets present size and compositional heterogeneity. As a result, they can improve assay repeatability and quality and due to their enhanced response to therapeutics and secretagogues, islet re-aggregates may also provide an important alternative source for transplantation. However, caution may be needed when studying ADMET in clinical trials, since ultimately islet re-aggregates will not reflect the response of native islets due to possible alterations of important cell–cell contacts (juxtacrine signaling) or paracrine effects.[25,192] This may have important consequences for the outcome of human trials.

In a distorted metabolic disease such as T2D, glucose homeostasis is achieved through systemic signaling between different cells and tissues. Thus, an *in vitro* metabolic network comprising human primary cells represents a more accurate model of T2D pathophysiology. However, long term culture is a key consideration when designing such network platforms for drug screening (ADMET), particularly for toxicity studies where 28–90 days culture is usually required.[193] Moreover, interconnected cell networks bring additional challenges because contamination or death of one cell line within the network will compromise the entire network. Despite the challenges, these networks have promise to replace animal models and to provide a more reliable clinical model for drug screening, as shown by the emerging concept of body-on-a-chip.[194]

To date, there is no report of a pancreas-on-chip and there are few reports of metabolic networks aiming to assess the

pathophysiology of T2D and the effect of therapeutics. One of such reports is a setup that incorporates a 3D culture of pancreatic islets and adipocytes derived from Sprague-Dawley rats.[195] A perfusion system was used to stimulate glucose dependent insulin secretion from the islets within a 3D scaffold seeded with adipocytes. After long term exposure to high glucose, the adipocytes started behaving like obese adipocytes secreting more leptin and resistin. This in time decreased and delayed the insulin secretion from the islets.

Another report shows a 3D tissue *in vitro* model where hepatocytes, adipocytes and endothelial cells were cultured in modular bioreactors with a common medium flowing between them[196] (Fig. 10). The goal of this work was to probe crosstalk between tissues and determine how each tissue contributes to the entire body metabolic profile. In this system, inflammatory markers (IL-6, TNL-α, and E-selectin) and metabolites (glucose, FFA, triacylglycerides, alanine, lactate, glycerol, and albumin) were monitored over time in response to energetic substrate imbalances such as glucose excess or reduced insulin within the system. Noteworthy, the system was developed using human cells exclusively. It also demonstrated how an imbalance of energetic substrates changes the overall equilibrium of the model system, just as it occurs in a complex *in vivo* model. If islets are incorporated in such a system, it could provide a useful model for islet response in a metabolic network.

By defining a meaningful SF of healthy pancreatic islets and monitoring it in real-time for ADMET, it may be possible to monitor a future *in vitro* pancreas model that replaces the equivalent animal model. Likewise, the concepts of a secretome signature and a SF can be extended to other cells in a metabolic network such as the aforementioned. Thus, different subpopulations of cells with the potential to become the target of novel T2D therapeutic agents might be identified. Additionally, a platform with real-time capabilities will be able to simultaneously monitor many aspects of ADMET within these networks, comprising a high-throughput screening system. These platforms should minimize resource consumption and increase the correlation between clinical trials and *in vitro* models, hence reducing costs from drug discovery to commercialization.

Thus, different subpopulations of cells with the potential to become the target of novel T2D therapeutic agents might be identified. Additionally, a platform with real-time capabilities will be able to simultaneously monitor many aspects of ADMET within these networks, comprising a high-throughput screening system. These platforms should minimize resource consumption and increase the correlation between clinical

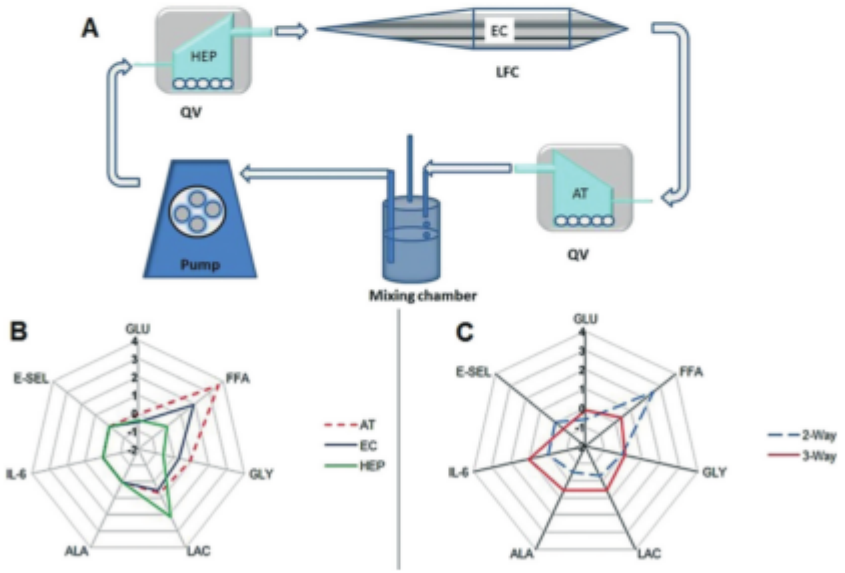

Fig. 10 (A) Schematic representation of a 3D tissue network (ref. 196). In the quasi-vivo (QV) chambers, hepatocytes (HEP) and adipocytes (AT) are cultured in a low shear laminar flow regimen. In the laminar flow chamber (LFC), endothelial cells (EC) are cultured under a high shear laminar flow regimen. (B) Fractional variation in metabolite concentrations for 1-way dynamic cultures of AT, EC and HEP. (C) Fractional variation in metabolite concentrations for a 2-way (AT+EC) cell culture network and 3-way (AT+EC+HEP) cell culture network. GLU (glucose), GLY (glycerol), LAC (lactate), ALA (L-alanine), E-SEL (E-selectin). (Reproduced from ref. 196 under the terms of the Creative Commons Public Domain Declaration).

trials and *in vitro* models, hence reducing costs from drug discovery to commercialization.

5. Conclusion and future perspective

In this review, we have provided a general overview of the secretome and the potential determination of it for pancreatic islets. We presented the state of the art of analytical tools and microfluidic platforms for monitoring a relevant islet SF. We have also proposed that defining a particular SF for healthy islets, diseased islets and viable islets can be used as a baseline to dynamically monitor islet functionality and viability. Thus, SF monitoring has applications in islet quality assessment before transplantation, islet regeneration studies and drug screening. In the case of transplantation, monitoring a SF can provide an assessment of islet viability and potency from both human and alternative sources. For islet regeneration, the SF can be used to assess the quality and functionality of pancreatic endocrine tissue after testing the outcome of a regeneration strategy. LOC platforms can provide tools to more easily screen a wide variety of biochemical environments and reagents as candidates for improved regeneration strategies in a repeatable manner. For drug screening, SF monitoring can be integrated with a pancreas organ-on-chip device to assess ADMET. Moreover, by extending this concept to a cell network, it will be possible to model a complex metabolic disease such as T2D, where novel mechanisms for therapeutics based on the cross talk within the cell network can be discovered. This in time may replace the expensive use of animal models and increase the correlation between *in vitro* models and human trials. Noteworthy, due to the challenges and complexity of maintaining islets in long term culture, to date there is no reports of a pancreas-on-chip for drug screening. In addition to these applications, novel physiological aspects of human pancreatic islets, such as islet paracrine and autocrine effects in native and re-aggregated islets can be studied. This may lead to the discovery of novel therapeutic agents able to regulate these effects.

Biomedical problems often require creative multidisciplinary approaches, especially in the case of pancreatic islets. Interest in secretomics has increased in recent years, because it has the potential to provide new libraries of diagnostic biomarkers and to identify novel therapeutic targets. Increasing collaboration between different fields such as engineering, biology, medicine and analytical chemistry may contribute in developing functional technologies to investigate the secretome of a wide variety of cells and to define and dynamically monitor relevant SFs.

Available platforms for single islet analysis and drug screening do not yet offer multiplexed techniques and are burdened by highly complex operation. The ability to easily monitor several functional parameters from a single human islet would offer a significant technical advantage over current techniques.

MPS are well-established tools and their technology continues to evolve. Once more advanced micro- and nano-analytical technologies are incorporated into MPS, entire metabolic networks or a body-on-chip can be achieved. Furthermore, these platforms can combine SF monitoring techniques with traditional techniques employed in the "-omic" fields such as mass spectrometry or RNA sequencing to comprise a robust tool for systems biology. The potential of these platforms is enormous, but many challenges still remain to be addressed. Herein lays considerable opportunities for interdisciplinary research teams, particularly in secretion biosensing and in coupling and automatizing "-omics" tool with MPS. This in time may provide relevant applications in systemic or metabolic diseases such as diabetes, lowering the economic burden on health systems and increasing the quality of life of diabetic patients.

Acknowledgements

The authors acknowledge the financial support from the Natural Science and Engineering Research Council of Canada (NSERC), the Fonds de recherche nature et technologies-Team Grant, the NSERC-CREATE in ISS, and FRC scholarship from Consejo Nacional de Ciencia y Teconologia de México (CONACyT) and Secretaria de Educaión Pública de México (SEP). The authors are also thankful to T. Johns, M. Mekhail, for their insightful comments and editing of this manuscript.

Notes and references

1 G. K. Agrawal, N. S. Jwa, M. H. Lebrun, D. Job and R. Rakwal, *Proteomics*, 2010, **10**, 799–827.
2 P. Mukherjee and S. Mani, *Biochim. Biophys. Acta, Proteins Proteomics*, 1834, **2013**, 2226–2232.
3 Y. Hathout, *Expert Rev. Proteomics*, 2007, **4**, 239–248.
4 M. Niepel, S. L. Spencer and P. K. Sorger, *Curr. Opin. Chem. Biol.*, 2009, **13**, 556–561.
5 A. A. Cohen, N. Geva-Zatorsky, E. Eden, M. Frenkel-Morgenstern, I. Issaeva, A. Sigal, R. Milo, C. Cohen-Saidon, Y. Liron and Z. Kam, *Science*, 2008, **322**, 1511–1516.
6 K. E. Gascoigne and S. S. Taylor, *Cancer Cell*, 2008, **14**, 111–122.
7 J. G. Yovos, *Diabetes Res. Clin. Pract.*, 2011, **93**, S25–S26.
8 T. Otonkoski, M. Banerjee, O. Korsgren, L. E. Thornell and I. Virtanen, *Diabetes, Obes. Metab.*, 2008, **10**, 119–127.
9 P. Rorsman and M. Braun, *Annu. Rev. Physiol.*, 2013, **75**, 155–179.
10 K. Polonsky, B. Given and E. Van Cauter, *J. Clin. Invest.*, 1988, **81**, 442.
11 P. Lefebvre, G. Paolisso, A. Scheen and J. Henquin, *Diabetologia*, 1987, **30**, 443–452.
12 P. Gilon, R. M. Shepherd and J.-C. Henquin, *J. Biol. Chem.*, 1993, **268**, 22265–22268.
13 A. G. Jones and A. T. Hattersley, *Diabetic Med.*, 2013, **30**, 803–817.
14 P. Westermark, A. Andersson and G. T. Westermark, *Physiol. Rev.*, 2011, **91**, 795–826.
15 D. Brandenburg, *Exp. Diabetes Res.*, 2008, **2008**, 576862.

16 C. J. Easley, J. V. Rocheleau, W. S. Head and D. W. Piston, *Anal. Chem.*, 2009, **81**, 9086–9095.
17 O. Cabrera, D. M. Berman, N. S. Kenyon, C. Ricordi, P. O. Berggrern and A. Caicedo, *Proc. Natl. Acad. Sci. U. S. A.*, 2006, **103**, 2334–2339.
18 A. Caicedo, *Semin. Cell Dev. Biol.*, 2013, **24**, 11–21.
19 D. Bosco, M. Armanet, P. Morel, N. Niclauss, A. Sgroi, Y. D. Muller, L. Giovannoni, G. Parnaud and T. Berney, *Diabetes*, 2010, **59**, 1202–1210.
20 S. T. Hanna, G. M. Pigeau, J. Galvanovskis, A. Clark, P. Rorsman and P. E. MacDonald, *Pfluegers Arch.*, 2009, **457**, 1343–1350.
21 M. Braun, R. Ramracheya, S. Amisten, M. Bengtsson, Y. Moritoh, Q. Zhang, P. R. Johnson and P. Rorsman, *Diabetologia*, 2009, **52**, 1566–1578.
22 M. Braun, R. Ramracheya, M. Bengtsson, Q. Zhang, J. Karanauskaite, C. Partridge, P. R. Johnson and P. Rorsman, *Diabetes*, 2008, **57**, 1618–1628.
23 M. Braun, in *Pancreatic Beta Cell*, ed. G. Litwack, Elsevier Academic Press Inc, San Diego, 2014, vol. 95, pp. 165–193.
24 N. Wierup, F. Sundler and R. S. Heller, *J. Mol. Endocrinol.*, 2014, **52**, R35–R49.
25 S. J. Le Marchand and D. W. Piston, *J. Biol. Chem.*, 2010, **285**, 14389–14398.
26 X. Wang, L. Yi, C. Guillo and M. G. Roper, *Electrophoresis*, 2015, **36**, 1172–1178.
27 E. Gylfe and A. Tengholm, *Diabetes, Obes. Metab.*, 2014, **16**, 102–110.
28 K. Dezaki, B. Damdindorj, H. Sone, O. Dyachok, A. Tengholm, E. Gylfe, T. Kurashina, M. Yoshida, M. Kakei and T. Yada, *Diabetes*, 2011, **60**, 2315–2324.
29 T. Aizawa, T. Kaneko, K. Yamauchi, H. Yajima, T. Nishizawa, T. Yada, H. Matsukawa, M. Nagai, S. Yamada and Y. Sato, *Life Sci.*, 2001, **69**, 2627–2639.
30 B. Farhat, A. Almelkar, K. Ramachandran, S. J. Williams, H. H. Huang, D. Zamierowksi, L. Novikova and L. Stehno-Bittel, *Islets*, 2013, **5**, 87–94.
31 H. H. Huang, L. Novikova, S. J. Williams, I. V. Smirnova and L. Stehno-Bittel, *Islets*, 2011, **3**, 6–13.
32 M. Ahmed, J. Forsberg and P. Bergsten, *J. Proteome Res.*, 2005, **4**, 931–940.
33 P. Bergsten, *Diabetes, Obes. Metab.*, 2009, **11**, 97–117.
34 M. Ahmed, in *The Islets of Langerhans*, Springer, 2010, pp. 363–390.
35 Z. Yousefi, J. Sarvari, K. Nakamura, Y. Kuramitsu, A. Ghaderi and Z. Mojtahedi, *Folia Histochem. Cytobiol.*, 2012, **50**, 368–374.
36 E. Imperlini, I. Colavita, M. Caterino, P. Mirabelli, D. Pagnozzi, L. Del Vecchio, R. Di Noto, M. Ruoppolo and S. Orru, *J. Cell. Biochem.*, 2013, **114**, 2577–2587.
37 C. A. Formolo, R. Williams, H. Gordish-Dressman, T. J. MacDonald, N. H. Lee and Y. Hathout, *J. Proteome Res.*, 2011, **10**, 3149–3159.
38 M. K. Jha, M. Seo, J.-H. Kim, B.-G. Kim, J.-Y. Cho and K. Suk, *Biochim. Biophys. Acta, Proteins Proteomics*, 1834, **2013**, 2418–2428.
39 J. H. Yoon, J. Kim, P. Song, T. G. Lee, P.-G. Suh and S. H. Ryu, *Adv. Biol. Regul.*, 2012, **52**, 340–350.
40 J. Zhong, S. A. Krawczyk, R. Chaerkady, H. L. Huang, R. Goel, J. S. Bader, G. W. Wong, B. E. Corkey and A. Pandey, *J. Proteome Res.*, 2010, **9**, 5228–5238.
41 M. Chevallet, H. Diemer, A. Van Dorssealer, C. Villiers and T. Rabilloud, *Proteomics*, 2007, **7**, 1757–1770.
42 G. Kulkarni and C. McCulloch, *J. Cell Sci.*, 1994, **107**, 1169–1179.
43 I. Charles, A. Khalyfa, D. M. Kumar, R. R. Krishnamoorthy, R. S. Roque, N. Cooper and N. Agarwal, *Invest. Ophthalmol. Visual Sci.*, 2005, **46**, 1330–1338.
44 S. Pirkmajer and A. V. Chibalin, *Am. J. Physiol.*, 2011, **301**, C272–C279.
45 A. Gallotta, E. Orzes and G. Fassina, *Clin. Lab. Med.*, 2012, **32**, 33–45.
46 J. S. Daniels and N. Pourmand, *Electroanalysis*, 2007, **19**, 1239–1257.
47 C.-H. Liu and S.-M. Hwang, *Cytokine+*, 2005, **32**, 270–279.
48 W. A. LaFramboise, D. Scalise, P. Stoodley, S. Graner, R. D. Guthrie, J. Magovern and M. Becich, *Am. J. Physiol.*, 2007, **292**, C1799–C1808.
49 Y. Lu, J. J. Chen, L. Y. Mu, Q. Xue, Y. Wu, P. H. Wu, J. Li, A. O. Vortmeyer, K. Miller-Jensen, D. Wirtz and R. Fan, *Anal. Chem.*, 2013, **85**, 2548–2556.
50 E. K. Sackmann, A. L. Fulton and D. J. Beebe, *Nature*, 2014, **507**, 181–189.
51 R. Fan, O. Vermesh, A. Srivastava, B. K. Yen, L. Qin, H. Ahmad, G. A. Kwong, C.-C. Liu, J. Gould and L. Hood, *Nat. Biotechnol.*, 2008, **26**, 1373–1378.
52 Q. Chen, J. Wu, Y. Zhang and J.-M. Lin, *Anal. Chem.*, 2012, **84**, 1695–1701.
53 C. Ma, R. Fan, H. Ahmad, Q. Shi, B. Comin-Anduix, T. Chodon, R. C. Koya, C.-C. Liu, G. A. Kwong and C. G. Radu, *Nat. Med.*, 2011, **17**, 738–743.
54 K. Galler, K. Brautigam, C. Grosse, J. Popp and U. Neugebauer, *Analyst*, 2014, **139**, 1237–1273.
55 Y. Liu and A. K. Singh, *JALA*, 2013, **18**, 446–454.
56 Y. Wang, J. F. Lo, J. E. Mendoza-Elias, A. F. Adewola, T. A. Harvat, K. P. Kinzer, D. Lee, M. Qi, D. T. Eddington and J. Oberholzer, *Bioanalysis*, 2010, **2**, 1729–1744.
57 J. G. Shackman, G. M. Dahlgren, J. L. Peters and R. T. Kennedy, *Lab Chip*, 2005, **5**, 56–63.
58 P. N. Silva, B. J. Green, S. M. Altamentova and J. V. Rocheleau, *Lab Chip*, 2013, **13**, 4374–4384.
59 M. Nourmohammadzadeh, J. F. Lo, M. Bochenek, J. E. Mendoza-Elias, Q. Wang, Z. Li, L. Y. Zeng, M. G. Qi, D. T. Eddington, J. Oberholzer and Y. Wang, *Anal. Chem.*, 2013, **85**, 11240–11249.
60 A. F. Adewola, D. Lee, T. Harvat, J. Mohammed, D. T. Eddington, J. Oberholzer and Y. Wang, *Biomed. Microdevices*, 2010, **12**, 409–417.
61 J. S. Mohammed, Y. Wang, T. A. Harvat, J. Oberholzer and D. T. Eddington, *Lab Chip*, 2009, **9**, 97–106.
62 M. G. Roper, J. G. Shackman, G. M. Dahlgren and R. T. Kennedy, *Anal. Chem.*, 2003, **75**, 4711–4717.

63 J. G. Shackman, K. R. Reid, C. E. Dugan and R. T. Kennedy, *Anal. Bioanal. Chem.*, 2012, **402**, 2797–2803.
64 S. B. Cheng, C. D. Skinner, J. Taylor, S. Attiya, W. E. Lee, G. Picelli and D. J. Harrison, *Anal. Chem.*, 2001, **73**, 1472–1479.
65 A. Bromberg and R. A. Mathies, *Electrophoresis*, 2004, **25**, 1895–1900.
66 J. F. Dishinger and R. T. Kennedy, *Anal. Chem.*, 2007, **79**, 947–954.
67 J. F. Dishinger, K. R. Reid and R. T. Kennedy, *Anal. Chem.*, 2009, **81**, 3119–3127.
68 A. R. Lomasney, L. Yi and M. G. Roper, *Anal. Chem.*, 2013, **85**, 7919–7925.
69 J. V. Rocheleau, G. M. Walker, W. S. Head, O. P. McGuinness and D. W. Piston, *Proc. Natl. Acad. Sci. U. S. A.*, 2004, **101**, 12899–12903.
70 L. Yi, X. Wang, R. Dhumpa, A. M. Schrell, N. Mukhitov and M. G. Roper, *Lab Chip*, 2014, 823–832.
71 A. Takahashi, P. Camacho, J. D. Lechleiter and B. Herman, *Physiol. Rev.*, 1999, **79**, 1089–1125.
72 X. Zhang and M. G. Roper, *Anal. Chem.*, 2009, **81**, 1162–1168.
73 R. Dhumpa, T. M. Truong, X. Wang, R. Bertram and M. G. Ropert, *Biophys. J.*, 2014, **106**, 2275–2282.
74 K. Terao, M. Gel, A. Okonogi, A. Fuke, T. Okitsu, T. Tada, T. Suzuki, S. Nagamatsu, M. Washizu and H. Kotera, *Sci. Rep.*, 2014, **4**, 6.
75 J. V. Rocheleau, M. S. Remedi, B. Granada, W. S. Head, J. C. Koster, C. G. Nichols and D. W. Piston, *PLoS Biol.*, 2006, **4**, e26.
76 D. Chen, W. Du, Y. Liu, W. Liu, A. Kuznetsov, F. E. Mendez, L. H. Philipson and R. F. Ismagilov, *Proc. Natl. Acad. Sci. U. S. A.*, 2008, **105**, 16843–16848.
77 C. S. Nunemaker, J. F. Dishinger, S. B. Dula, R. Wu, M. J. Merrins, K. R. Reid, A. Sherman, R. T. Kennedy and L. S. Satin, *PLoS One*, 2009, **4**, e8428.
78 K. R. Reid and R. T. Kennedy, *Anal. Chem.*, 2009, **81**, 6837–6842.
79 X. Zhang, A. Grimley, R. Bertram and M. G. Roper, *Anal. Chem.*, 2010, **82**, 6704–6711.
80 K. H. Nam, W. Yong, T. Harvat, A. Adewola, S. Wang, J. Oberholzer and D. T. Eddington, *Biomed. Microdevices*, 2010, **12**, 865–874.
81 L. A. Godwin, M. E. Pilkerton, K. S. Deal, D. Wanders, R. L. Judd and C. J. Easley, *Anal. Chem.*, 2011, **83**, 7166–7172.
82 C. Morris, D. J. Banks, L. Gaweda, S. Scott, X. X. Zhu, M. Panico, P. Georgiou and C. Toumazou, *Conference proceedings : ... Annual International Conference of the IEEE Engineering in Medicine and Biology Society. IEEE Engineering in Medicine and Biology Society. Annual Conference*, 2011, vol. 2011, pp. 8412–8415.
83 K. S. Sankar, B. J. Green, A. R. Crocker, J. E. Verity, S. M. Altamentova and J. V. Rocheleau, *PLoS One*, 2011, **6**, e24904.
84 J. F. Lo, Y. Wang, A. Blake, G. N. Yu, T. A. Harvat, H. Jeon, J. Oberholzer and D. T. Eddington, *Anal. Chem.*, 2012, **84**, 1987–1993.
85 D. Lee, Y. Wang, J. E. Mendoza-Elias, A. F. Adewola, T. A. Harvat, K. Kinzer, D. Gutierrez, M. Qi, D. T. Eddington and J. Oberholzer, *Biomed. Microdevices*, 2012, **14**, 7–16.
86 A. K. Lam, P. N. Silva, S. M. Altamentova and J. V. Rocheleau, *Integr. Biol.*, 2012, **4**, 838–846.
87 Y. Wang, D. Lee, L. Zhang, H. Jeon, J. E. Mendoza-Elias, T. A. Harvat, S. Z. Hassan, A. Zhou, D. T. Eddington and J. Oberholzer, *Biomed. Microdevices*, 2012, **14**, 419–426.
88 Y. X. Huang, D. Cai and P. Chen, *Anal. Chem.*, 2011, **83**, 4393–4406.
89 S. Misler, D. W. Barnett, K. D. Gillis and D. M. Pressel, *Diabetes*, 1992, **41**, 1221–1228.
90 M. Braun, R. Ramracheya, P. R. Johnson and P. Rorsman, *Ann. N. Y. Acad. Sci.*, 2009, **1152**, 187–193.
91 S. Hanna, G. Pigeau, J. Galvanovskis, A. Clark, P. Rorsman and P. MacDonald, *Pfluegers Arch.*, 2009, **457**, 1343–1350.
92 D. S. Luciani and J. D. Johnson, *Mol. Cell. Endocrinol.*, 2005, **241**, 88–98.
93 M. Braun, R. Ramracheya, M. Bengtsson, A. Clark, J. N. Walker, P. R. Johnson and P. Rorsman, *Diabetes*, 2010, **59**, 1694–1701.
94 R. Ramracheya, C. Ward, M. Shigeto, J. N. Walker, S. Amisten, Q. Zhang, P. R. Johnson, P. Rorsman and M. Braun, *Diabetes*, 2010, **59**, 2198–2208.
95 P. Proks, L. Eliasson, C. Ammälä, P. Rorsman and F. M. Ashcroft, *J. Eng. Phys.*, 1996, **496**, 255–264.
96 A. Y. Lau, P. J. Hung, A. R. Wu and L. P. Lee, *Lab Chip*, 2006, **6**, 1510–1515.
97 B. R. Bruhn, H. Y. Liu, S. Schuhladen, A. J. Hunt, A. Mordovanakis and M. Mayer, *Lab Chip*, 2014, **14**, 2410–2417.
98 R. Pantoja, J. M. Nagarah, D. M. Starace, N. A. Melosh, R. Blunck, F. Bezanilla and J. R. Heath, *Biosens. Bioelectron.*, 2004, **20**, 509–517.
99 X. Li, K. G. Klemic, M. A. Reed and F. J. Sigworth, *Nano Lett.*, 2006, **6**, 815–819.
100 J. Dunlop, M. Bowlby, R. Peri, D. Vasilyev and R. Arias, *Nat. Rev. Drug Discovery*, 2008, **7**, 358–368.
101 C. Farre, M. George, A. Brüggemann and N. Fertig, *Drug Discovery Today: Technol.*, 2008, **5**, e23–e28.
102 S. Göpel, T. Kanno, S. Barg and P. Rorsman, *J. Eng. Phys.*, 2000, **528**, 497–507.
103 S. Göpel, T. Kanno, S. Barg, X. G. Weng, J. Gromada and P. Rorsman, *J. Eng. Phys.*, 2000, **528**, 509–520.
104 S. Göpel, T. Kanno, S. Barg, J. Galvanovskis and P. Rorsman, *J. Physiol.*, 1999, **521**, 717–728.
105 C. D. Paras, W. Qian, J. R. Lakey, W. Tan and R. T. Kennedy, *Cell Biochem. Biophys.*, 2000, **33**, 227–240.
106 A. Salimi, M. Roushani, S. Soltanian and R. Hallaj, *Anal. Chem.*, 2007, **79**, 7431–7438.
107 B. Rafiee and A. R. Fakhari, *Biosens. Bioelectron.*, 2013, **46**, 130–135.
108 N. Amini, M. B. Gholivand and M. Shamsipur, *J. Electroanal. Chem.*, 2014, **714–715**, 70–75.
109 J. Y. Gerasimov, C. S. Schaefer, W. Yang, R. L. Grout and R. Y. Lai, *Biosens. Bioelectron.*, 2013, **42**, 62–68.

162 M. A. Naftanel and D. M. Harlan, *PLoS Med.*, 2004, **1**, e58.
163 K. K. Papas, T. M. Suszynski and C. K. Colton, *Curr. Opin. Organ Transplant.*, 2009, **14**, 674–682.
164 T. Yamamoto, A. Horiguchi, M. Ito, H. Nagata, H. Ichii, C. Ricordi and S. Miyakawa, *J Hepatobiliary Pancreat. Surg.*, 2009, **16**, 131–136.
165 C. K. Colton, K. K. Papas, A. Pisania, M. J. Rappel, D. E. Powers, J. J. O'Neil, A. Omer, G. Weir, S. Bonner-Weir and C. Halberstadt, *Characterization of islet preparations*, Elsevier, Amsterdam, 2007.
166 G. Loganathan, M. L. Graham, D. M. Radosevich, S. M. Soltani, M. Tiwari, T. Anazawa, K. K. Papas, D. E. R. Sutherland, B. J. Hering and A. N. Balamurugan, *Transplantation*, 2013, **95**, 1439–1447.
167 C. Ricordi, J. Lakey and B. Hering, *Transplant. Proc.*, 2001, **33**, 1709.
168 F. Bertuzzi and C. Ricordi, *Diabetes Care*, 2007, **30**, 410–417.
169 N. London, S. Thirdborough, S. Swift, P. Bell and R. James, *Transplant. Proc.*, 1991, **23**, 749.
170 C. Ricordi, D. W. Scharp and P. E. LACY, *Transplantation*, 1988, **45**, 994–996.
171 F. W. Pagliuca, J. R. Millman, M. Gürtler, M. Segel, A. Van Dervort, J. H. Ryu, Q. P. Peterson, D. Greiner and D. A. Melton, *Cell*, 2014, **159**, 428–439.
172 A. Jamal, M. Lipsett, R. Sladek, S. Laganiere, S. Hanley and L. Rosenberg, *Cell Death Differ.*, 2005, **12**, 702–712.
173 N. Ben-Othman, M. Courtney, A. Vieira, A. Pfeifer, N. Druelle, E. Gjernes, B. Faurite, F. Avolio and P. Collombat, *Diabetes Res. Clin. Pract.*, 2013, **101**, 1–9.
174 S. Puri and M. Hebrok, *Dev. Cell*, 2010, **18**, 342–356.
175 H. Kaneto, T. Miyatsuka, Y. Fujitani, H. Noguchi, K.-H. Song, K.-H. Yoon and T.-A. Matsuoka, *Diabetes Res. Clin. Pract.*, 2007, **77**, S127–S137.
176 J. M. Mellado-Gil, N. Cobo-Vuilleumier and B. R. Gauthier, *J. Transplant.*, 2012, **2012**, 9.
177 L. C. Murtaugh, *Development*, 2007, **134**, 427–438.
178 J.-L. Liu, W. Cui, B. Li and Y. Lu, *Endocr., Metab. Immune Disord.: Drug Targets*, 2008, **8**, 1–10.
179 A. Migliorini, E. Bader and H. Lickert, *Mol. Metab.*, 2014, **3**, 268–274.
180 H. Hui, C. Wright and R. Perfetti, *Diabetes*, 2001, **50**, 785–796.
181 J. Zhou, M. A. Pineyro, X. Wang, M. E. Doyle and J. M. Egan, *J. Cell. Physiol.*, 2002, **192**, 304–314.
182 C. R. Wan, S. Chung and R. D. Kamm, *Ann. Biomed. Eng.*, 2011, **39**, 1840–1847.
183 E. Cimetta and G. Vunjak-Novakovic, *Exp. Biol. Med.*, 2014, **239**, 1255–1263.
184 T. Cambier, T. Honegger, V. Vanneaux, J. Berthier, D. Peyrade, L. Blanchoin, J. Larghero and M. Thery, *Lab Chip*, 2015, **15**, 77–85.
185 W. T. Fung, A. Beyzavi, P. Abgrall, N. T. Nguyen and H. Y. Li, *Lab Chip*, 2009, **9**, 2591–2595.
186 J. Zhou, M. A. Pineyro, X. Wang, M. E. Doyle and J. M. Egan, *J. Cell. Physiol.*, 2002, **192**, 304–314.
187 M. J. Reed and K. A. Scribner, *Diabetes, Obes. Metab.*, 1999, **1**, 75–86.
188 N. Sakata, G. Yoshimatsu, H. Tsuchiya, S. Egawa and M. Unno, *Exp. Diabetes Res.*, 2012, **2012**, 256707.
189 V. Dave, R. Sharma, S. Sharma, P. Jain and S. Yadav, *Int. J. Adv. Pharm. Sci.*, 2013, **4**, 1–8.
190 V. Poitout, L. K. Olson and R. P. Robertson, *Diabetes Metab.*, 1996, **22**, 7–14.
191 K. Ramachandran, X. Peng, K. Bokvist and L. Stehno-Bittel, *Br. J. Pharmacol.*, 2014, **171**, 3010–3022.
192 A. Chowdhury, O. Dyachok, A. Tengholm, S. Sandler and P. Bergsten, *Diabetologia*, 2013, **56**, 1557–1568.
193 Oecd, *OECD Guidelines for the Testing of Chemicals, Organization for Economic*, 1994.
194 S. N. Bhatia and D. E. Ingber, *Nat. Biotechnol.*, 2014, 760–772.
195 M. G. Xu, Y. N. Yan, X. H. Wang and Ieee, *Modeling insulin secretion dysfunction in a three-dimensional culture system by cell-assembly technique*, Ieee, New York, 2009.
196 E. Iori, B. Vinci, E. Murphy, M. C. Marescotti, A. Avogaro and A. Ahluwalia, *PLoS One*, 2012, **7**, e34704.

RightsLink®

Home | Account Info | Help

Title: Multiplex Surface Plasmon Resonance Imaging-Based Biosensor for Human Pancreatic Islets Hormones Quantification

Author: F. Rafael Castiello, Maryam Tabrizian

Publication: Analytical Chemistry

Publisher: American Chemical Society

Date: Mar 1, 2018

Logged in as:
Francisco Castiello Flores
McGill University
Account #:
3000911160

LOGOUT

PERMISSION/LICENSE IS GRANTED FOR YOUR ORDER AT NO CHARGE

This type of permission/license, instead of the standard Terms & Conditions, is sent to you because no fee is being charged for your order. Please note the following:

- Permission is granted for your request in both print and electronic formats, and translations.
- If figures and/or tables were requested, they may be adapted or used in part.
- Please print this page for your records and send a copy of it to your publisher/graduate school.
- Appropriate credit for the requested material should be given as follows: "Reprinted (adapted) with permission from (COMPLETE REFERENCE CITATION). Copyright (YEAR) American Chemical Society." Insert appropriate information in place of the capitalized words.
- One-time permission is granted only for the use specified in your request. No additional uses are granted (such as derivative works or other editions). For any other uses, please submit a new request.

BACK | CLOSE WINDOW

analytical chemistry

Article

Cite This: Anal. Chem. 2018, 90, 3132−3139

pubs.acs.org/ac

Multiplex Surface Plasmon Resonance Imaging-Based Biosensor for Human Pancreatic Islets Hormones Quantification

F. Rafael Castiello[†] and Maryam Tabrizian[*,†,‡]

[†]Biomedical Engineering Department and [‡]Faculty of Dentistry, McGill University, Montreal, Quebec H3A 2B4, Canada

Supporting Information

ABSTRACT: Diabetes arises from secretory defects in vascularized micro-organs known as the islets of Langerhans. Recent studies indicated that furthering our understanding of the paracrine effect of somatostatin on glucose-induced insulin secretion could represent a novel therapeutic avenue for diabetes. While many research groups are interested in insulin and glucagon secretion, few are particularly focused on studying the paracrine interaction in islets' cells, and none on monitoring a secretory fingerprint that contemplates more than two hormones. Surface plasmon resonance imaging can achieve high-throughput and multiplexed biomolecule quantification, making it an ideal candidate for detection of multiple islet's secretion products if arrays of hormones can be properly implemented on the sensing surface. In this study, we introduced a multiplex surface plasmon resonance imaging-based biosensor for simultaneous quantification of insulin, glucagon, and somatostatin. Performing this multiplex biosensing of hormones was mainly the result of the design of an antifouling sensing surface comprised by a mixed self-assembly monolayer of CH_3O-PEG-SH and 16-mercaptohexadecanoic acid, which allowed it to operate in a complex matrix such as an islet secretome. The limit of detection in multiplex mode was 1 nM for insulin, 4 nM for glucagon, and 246 nM for somatostatin with a total analysis time of 21 min per point, making our approach the first reporting a label-free and multiplex measurement of such a combination of human hormones. This biosensor holds the promise of providing us with a mean for the further understanding of the paracrine effect of somatostatin on glucose-induced insulin secretion and consequently help develop novel therapeutic agents for diabetes.

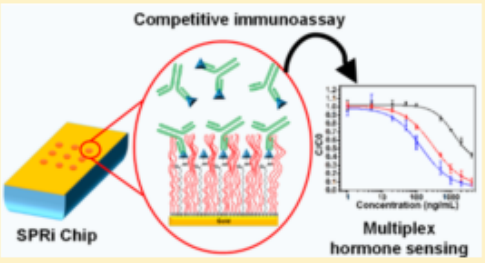

Diabetes mellitus affects 12.9% of the adult population in North America and the Caribbean region, from which type 2 diabetes (T2D) accounts for 90−95% of the cases.[1] Diabetes arises from secretory defects in the pancreatic islets of Langerhans, which are endocrine clusters of cells with an average diameter of 150 μm.[2] The islets are vascularized micro-organs with five different types of cells (α, β, δ, PP, and ε) that cooperate for hormone secretion in response to metabolic changes.[2,3]

Recent studies indicate that the pancreatic islet's anatomy and physiology are species-dependent and that the unique cytoarchitecture of human islets has significant consequences for cell-to-cell communication within the islets.[4] For instance, secreted hormones from the different islets' cells may exert paracrine interaction on their neighbor cells,[3,5,6] particularly somatostatin whose inhibition has been shown to increase glucose-induced insulin secretion.[7] Further understanding of these paracrine effects may represent a therapeutic avenue for T2D.[5,6]

Up until now, most of the pancreatic islet research depends on traditional bioassays for hormone quantification such as patch clamp,[8−12] capillary electrophoresis immunoassays (CEI),[13−16] and ELISA.[16−18] Patch clamp has been used to study the secretion from individual islet β-cells[8−10] and α-cells.[11,12] This technique provides quantitative information regarding exocytosis, by correlating the rate of capacitance change with the number of granules released at a given time.[19] However, the patch clamp technique requires highly skilled operators to trap and manipulate individual cells, is low throughput, it only provides an indirect measurement of secretion, and it lacks specificity for individual secretion products. On the other hand, CEI has been used for direct detection of insulin[14] and glucagon[15] from pancreatic islets. During CEI experiments, islets are placed in a chamber and the effluent is mixed with the targeted hormone antibodies and fluorescent-labeled hormones. The secreted hormones from the islets then compete with fluorescent-labeled hormones for binding sites on the antibody. This mixture is then passed into an electrophoresis channel where bound and unbound fluorescent hormones are separated. Hormone secretion is then quantified fluorescently by establishing the ratio between bound and free hormone. As with patch clamp, CEI requires skilled operators to work effectively, precise temperature control, overcoming channel clogging, and the integration of lasers with different wavelengths.[15] Finally, although operation-

Received: October 17, 2017
Accepted: January 29, 2018
Published: January 29, 2018

DOI: 10.1021/acs.analchem.7b04288
Anal. Chem. 2018, 90, 3132−3139

ally simpler, ELISA is difficult to use for simultaneous quantification, is time-consuming, and is expensive. Moreover, all the mentioned techniques face many challenges when trying to expand them for simultaneous analysis of multiple targets.

While many research groups are interested in insulin and glucagon secretion,[20−23] few are particularly focused on studying the paracrine interaction in islets' cells,[5] and none on monitoring a secretory fingerprint (SF) for more than two hormones. Hence, to monitor an islets' SF, implementation of multiplexed analytical tools is required.

In this context, surface plasmon resonance imaging (SPRi) could be a useful tool to measure a pancreatic islet's SF. SPRi is now established as the gold standard to study biomolecular interactions such as antigen−antibody.[24] In addition to label-free and real-time analysis, SPRi can achieve high-throughput and multiplexed measurements through arrays of different molecules on the sensing surface.[24] In the past decade, SPR biosensors have mostly been used to investigate fundamental physiological aspects of the major secreted islet hormones, namely, insulin,[25−27] somatostatin,[28] pancreatic polypeptide,[29,30] and ghrelin.[31] However, there are no reports of a SPRi multiplex biosensor aiming to dynamically quantify more than two of the major secreted hormones. SPRi biosensors present an additional advantage for this particular application that involves measurements in a complex matrix such as the islet secretome. This advantage is provided by designing antifouling surfaces using self-assembled monolayers (SAM) that reduce interferences caused by nonspecific adsorption of molecules on the sensor surface.[32]

Here in, we introduce an SPRi-based biosensor for multiplexed detection of insulin, glucagon, and somatostatin. First, we studied the effect of composition on the antifouling properties of a mixed SAM of a thiolated polyethylene glycol (CH_3O-PEG-SH) and 16-mercaptohexadecanoic acid (MHDA). The antifouling properties of the biosensor were investigated by injecting two proteins: bovine serum albumin (BSA) and lysozyme (LYZ). Next, a competitive immunoassay protocol for insulin, glucagon, and somatostatin was implemented, and the biosensor performance for individual hormones was determined. Finally, the biosensor performance was tested in multiplex mode performing simultaneous competitive immunoassays for the three hormones, and the limit of detection (LOD) and dynamic range were determined for each hormone in the mixture.

EXPERIMENTAL SECTION

Materials and Apparatus. Absolute ethanol was purchased from Fisher Scientific (Fair Lawn, NJ), and phosphate-buffered saline (PBS) tablets, Tween 20, and glycine were purchased from BioShop Canada Inc. (Burlington, Ontario, Canada). Ethanolamine hydrochloride, *N*-(3-(dimethylamino)-propyl)-*N*′-ethylcarbodiimide hydrochloride (EDC), *N*-hydroxysuccinimide (NHS), bovine serum albumin (BSA), hydrochloric acid (HCl), human glucagon, human somatostatin, and lysozyme (LYZ) were purchased from Sigma-Aldrich (St. Louis, MO). Tris-buffered saline (TBS) with 1% casein was purchased from BIO-RAD. Anti-insulin antibody (6.2 mg/mL) and human insulin were purchased from PROSPECT (Ness, Ziona, Israel). Anti-glucagon and anti-somatostatin antibodies (200 μg/mL each) were purchased from Santa Cruz Biotechnologies, Inc. (Mississauga, ON, Canada). CH_3O-PEG-SH (MW 1200 Da) was purchased from Rapp Polymere GmbH (Tübingen, Germany). 16-Mercaptohexadecanoic acid (MHDA) was purchased from ProChimia Surfaces Sp. (Zacisze, Sopot, Poland).

SPRi detection was performed using a scanning-angle SPRi instrument (model SPRi-Lab+, Horiba, France). The SPRi apparatus, equipped with an 800 nm LED source, a CCD camera, and a microfluidic flow cell, was placed in an incubator at 25 °C (Memmert Peltier, Rose Scientific, Canada).

SPRi Measurements. For all experiments, the slope of the plasmon curves was automatically computed by the instrument's software to facilitate the selection of the working angle for kinetic analysis. This slope corresponds to the point of the plasmon curve at which the slope was maximum. Reflectivity shift (ΔR (%)) for all experiments was acquired upon stabilization of the baseline. Measured values were the average of at least three spots for each sample including controls, and each experiment was repeated at least three times. At each step, the substrate was washed with the running buffer PBS-T (PBS with 0.002% Tween 20), and the difference in the reflected intensity was measured by taking into account the difference between the initial and final buffer signal. An injection loop with a fixed volume of 200 μL was used during the experiments. A flow rate of 20 μL/min was used for all experiments, with the exception of functionalization steps where the flow rate was adjusted depending on the required contact time.

Substrate Preparation. For single hormone-sensing, cleaned microscope glass slides (12 mm × 25 mm × 1 mm, n = 1.518) substrates were coated with 2 nm Cr as an adhesion layer, followed by the deposition of a thin Au layer of 48 nm using electron-beam physical vapor deposition under high vacuum. Microscope glass slides were then coupled to an SF11 equilateral triangular prism ($n_{SF\text{-}11}$ = 1.765) using a refractive index matching liquid. For multiplex sensing, similar gold-coated prisms (n = 1.765) purchased from Horiba Scientific-GenOptics, France, were used as received.

Surface Functionalization. Substrates were cleaned by subsequent immersion in absolute ethanol and deionized (DI) water and dried with a stream of nitrogen. Ethanolic solutions of 0.5 mM CH_3O-PEG-SH and 0.5 mM MHDA were prepared and mixed at different molar ratios from 100% MHDA to 90% CH_3O-PEG-SH−10% MHDA. Substrates were immersed in the above-mentioned ethanolic solutions overnight to allow the self-assembly monolayer (SAM) formation. Finally, the substrates were thoroughly rinsed with absolute ethanol and DI water and dried under a stream of nitrogen.

Microscope slides with freshly prepared SAMs were immediately placed on the SPRi system for subsequent functionalization. First, conditioning was performed by 4 serial injections (contact time of 2 min each) of a regeneration solution containing 1 M glycine pH 2.5 (1M-Gly). Then, the surface was rinsed with PBS-T until the baseline was stable. Next, NHS/EDC chemistry was used to covalently bind insulin, glucagon, or somatostatin as reported by Gobi et al.[33] Briefly, 200 μL of an aqueous solution containing 2 mg/mL NHS, 2 mg/mL EDC, and 50 μg/mL of the desired hormone were flowed over the sensor with a contact time of 1 h. Next, an injection of 200 μL (contact time 10 min) of 1 M ethanolamine hydrochloride pH 8.5 was performed to inactivate unfunctionalized −COOH groups on the sensor surface. Then, two serial injections of regeneration solution (contact time 1 min each) were performed to remove weakly bound hormones. Finally, a blocking solution containing 1% casein and 5% BSA in TBS buffer was injected with a contact time of 30 min, and subsequently, at least 3 injections of the regeneration solution

DOI: 10.1021/acs.analchem.7b04288
Anal. Chem. 2018, 90, 3132−3139

were made to remove weakly bound proteins. Figure 1 shows a graphical representation of a typical sensor functionalization.

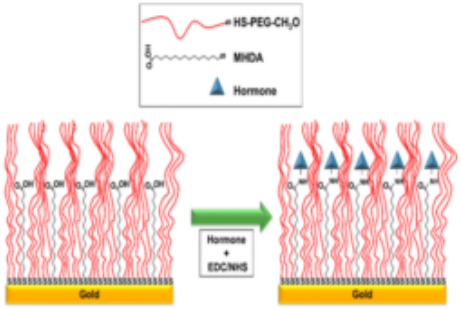

Figure 1. Schematic representation of the surface functionalization of thin Au films used in this study. The surface is composed of a mix SAM of 16-mercaptohexadecanoic (MHDA) as a linker and a thiolated PEG (CH_3O-PEG-SH) as a spacer and antifouling agent incubated overnight. Targeted hormones are covalently immobilized to the surface using EDC/NHS chemistry in an aqueous solution.

For the functionalization of gold-coated prisms in multiplex measurement mode, the procedure described for microscope slides was followed with some minor changes. After conditioning, 4 individual solutions containing NHS/EDC (2 mg/mL each) and 50 μg/mL of insulin, glucagon, somatostatin, or BSA were spotted (150 nL) in triplicate on the surface of the prism and incubated in a humidity chamber for 1 h. Immediately after, the prism was rinsed with a copious amount of DI water and subsequently immersed in 1 M ethanolamine hydrochloride pH 8.5 for 10 min. Next, the prism was immersed in the blocking solution for 30 min, subsequently rinse with DI water and placed in the SPR flow chamber. Then, the regeneration solution was injected at least three times to obtain a stable baseline before beginning with the competitive immunoassays.

Competitive Immunoassay. For multiplex assays, standard solutions containing insulin, glucagon, and somatostatin were prepared in PBS-T buffer at a concentration range of 1−4000 ng/mL and mixed with a cocktail of antibodies containing anti-insulin (1 μg/mL), anti-glucagon (2 μg/mL), and anti-somatostatin (2 μg/mL). These mixtures were incubated for 2 min under gently mixing and serially injected over the spotted sensor chip from highest to lowest hormone concentration (contact time of 10 min) starting with a blank solution containing only the antibody cocktail. Each sensing cycle comprised: sample injection 10 min, 5 min buffer washing, and 2 injections of regeneration solution (1M-Gly) with a contact time of 25 s with 3 min washing with buffer in-between. For individual immunoassays, the same conditions were used, with the exception of somatostatin, for which the assay concentration ranged from 50 to 8000 ng/mL. For all competitive immunoassays, the optimal antibody concentration was defined as the concentration that could generate a small but detectable SPR signal of $\Delta R \approx 1$, which has been previously reported as a reliable ΔR for this type of assays.[34]

Statistics. For all competitive immunoassays, relative binding (C/C_0) was calculated by dividing the response of the standard solutions containing hormones (C) by the response of the blank solution containing only a fixed concentration of antibodies (C_0). To generate calibration curves C/C_0 was plotted against hormone concentration. The calibration curves were fitted using a nonlinear 4 parameter logistic (4PL) model. The lower limit of detection (LOD) for all immunoassays was calculated from the calibration curves as the blank signal (C_0) minus 3 times the standard deviation. The dynamic range for the competitive immunoassay was established between $0.2C/C_0$ and $0.8C/C_0$. All data is expressed as the average of at least 3 independent experiments ± standard deviation (SD).

RESULTS AND DISCUSSION

Effect of SAM Composition on the Sensor Response. SAMs are typically used as a linker layer for immobilization of biological components at the transducer surface of biosensors.[32] A necessary procedure when developing a competitive immunoassay is limiting the amount of competing antigen and antibody in order to maximize the assay's sensitivity. Typically, commercial SPR chips achieve this by fixing the SAM composition and controlling the surface density of the analyte, either by changing the contact time or the concentration of the analyte during functionalization.[35] However, in a mass-sensitive technique such as SPR, the detection of small molecules (such as the target peptides in this study) is challenging, requiring careful design of the surface chemistry to ensure optimal sensitivity.[36] Thus, the linker to spacer ratios must be studied in detail on a case basis.

In this work, a mixed SAM comprised of a linear thiol with a carboxyl end group (MHDA) was used for hormone immobilization, along with a low molecular weight thiolated PEG (CH_3O-PEG-SH) that acts as a spacer and as an antifouling agent.[37] These compounds are used on a regular basis for biosensor development; however, this work presents the first report using them in combination. Additionally, contrary to the majority of the reports in the literature,[32] our study presents a long chain compound as a spacer and a short chain as an anchor. Thus, the results obtained could be counterintuitive when compared to previous reports. In addition, SAM composition plays an important role on the final surface density of immobilized biomolecules; thus, a preliminary study was performed to evaluate its effect on the sensor's response. Since somatostatin was the smallest of the targeted hormones, it was used as the "reference" hormone for this study.

Figure 2 shows the change in reflectivity for a fixed amount of antisomatostatin antibodies (1 μg/mL) over different SAM compositions. With 100% and 50% MHDA, a large signal can be observed. Interestingly a change occurred after 50% PEG molar fraction, the signal abruptly diminished and it was barely present for the 70% and 90% PEG molar fractions. This could be explained by the fact that mixtures of *n*-alkanethiols of different chain lengths tend to form SAMs with a composition enriched with the longer alkanethiol.[32] Thus, a very little amount of linker is left on the surface to covalently bind somatostatin.

For 70% and 90% PEG molar fractions, it was necessary to increase 20−30 times the antisomatostatin antibody concentration to obtain a measurable SPR signal. This presents some disadvantages for the sensor operation for the following reasons: (1) for a competitive immunoassay, a large amount of antibodies will be poorly inhibited by a small amount of analytes.[38] (2) Each data point in this type of assay requires the

DOI: 10.1021/acs.analchem.7b04288
Anal. Chem. 2018, 90, 3132−3139

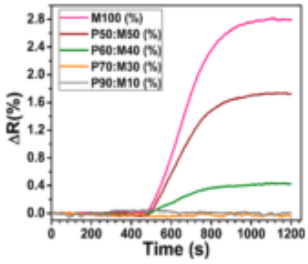

Figure 2. SPR reflectivity change response of 1 μg/mL of antisomatostatin antibody for different SAM compositions. P and M stand for CH_3O-PEG-SH and MHDA, respectively.

injection of a fresh antibody solution; hence, a high amount of antibodies will increase reagent consumption and operational costs.

On the other hand, 100% and 50% MHDA surface regeneration proved to be challenging when compared to 40% MHDA (Figure S1). Thus, we set the final composition of SAM as 60% PEG−40% MHDA to incorporate the maximum amount of PEG and still get a detectable signal, even with a relative low antibody concentration.

Single-Step Hormone Immobilization. The hormones used in this work are small peptides possessing an N-terminal group which could be used for immobilization on the sensor surface, through an amide bond formation with the carboxyl group on the MHDA. The surface functionalization was performed in a single step as reported by Gobi et al.[33] Compared to typical two-step NHS/EDC processes where buffer solutions with a variety of pH are required,[39,40] the single step functionalization offers the advantage of reducing the functionalization time and pH adjustments for all hormones since the reaction is performed in aqueous solution. This is particularly advantageous when preparing SPR surfaces using several hormones solutions.

After chip conditioning, individual hormones and the immobilization reagent (a mixture of NHS/EDC) were injected over the sensor chip. Once the solution reached the surface, the SPR angle decreased slightly followed by a steady angle increase to nearly reach a plateau representing surface saturation. At the end of the injection, the surface was washed with running buffer until a stable baseline was obtained. Finally, in order to make the sensor surface homogeneous, a blocking agent containing 5% BSA and 1% casein (w/w) in TBS buffer was injected with a total contact time of 30 min. At the end of the injection, running buffer was allowed to wash the surface until stabilization of the SPR signal occurred. After this point, at least 2 injections of regeneration solution were used to remove any weakly adsorbed BSA and casein. Once the baseline was stabilized, the difference in SPR angle before and after the blocking step was measured.

Table 1 shows the corresponding mean reflectivity change observed after the individual hormone functionalization and its corresponding blocking step (n = 3). Interestingly, since the available functionalization sites are fixed, the reflectivity change values for each hormone functionalization proved to be proportional to their differences in molecular weight (MW insulin > glucagon > somatostatin).

Biosensor Performance for Individual Immunoassays. Direct immunoassays of small molecules by SPR can be challenging since the SPR signal is directly related to the change in mass at the sensor surface. Consequently, the immunoassays in the present work were performed in a competitive manner where inhibition of antibody binding is due to binding occurring with hormones in solution. Thus, the higher the concentration of hormones in solution, the smaller the SPR signal and vice versa (Figure 3).

Table 1. SPR Mean Reflectivity Change after Individual Hormone Functionalization and Their Corresponding Blocking Step

hormone	ΔR (%) functionalization	ΔR (%) blocking
insulin	8.26 ± 0.57	0.3 ± 0.07
glucagon	4.57 ± 0.32	0.26 ± 0.06
somatostatin	3.36 ± 0.66	0.89 ± 0.17

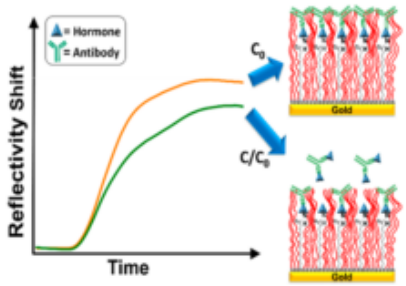

Figure 3. Graphical representation of a competitive immunoassay over the sensor surface. After formation of a mixed SAM and functionalization with the targeted hormone covalently linked to the SAM, inhibition of the blank solution with optimal antibody concentration (C_0) follows due to binding occurring with hormones in solution (C/C_0). Thus, the higher the concentration of hormones in solution, the smaller the SPR signal and vice versa.

In general, competitive immunoassays require the use of a small antibody concentration so that slight amounts of the analyte can inhibit antibody binding to the surface.[38] For this reason, the optimal antibody concentration for each hormone was defined as the concentration of the antibody that could generate a small but detectable SPR signal of $\Delta R \approx 1$.[34] This corresponded to an antibody concentration of 1, 2, and 2 μg/mL for anti-insulin, anti-glucagon, and anti-somatostatin, respectively.

To study the sensor performance, standard solutions containing either insulin, glucagon, or somatostatin were prepared in PBS-T. Then, the optimal amount of antibody was added to the standard solution and gently mixed for a predefined period of time before injecting into the SPR system. Somatostatin was particularly sensitive to incubation conditions during this step. After testing different times and mixing conditions, it was found that 2 min incubation under gently manual agitation provided optimal conditions for sensing (data not shown).

Figure 4 shows the sensor calibration curves for insulin (Figure 4A), glucagon (Figure 4B), and somatostatin (Figure 4C). For each hormone, mean relative binding values (C/C_0) were plotted as a function of hormone concentration (ng/mL). For each experiment, the entire sensor surface was functionalized, and the mean SPR shift was measured on at least 10

DOI: 10.1021/acs.analchem.7b04288
Anal. Chem. 2018, 90, 3132−3139

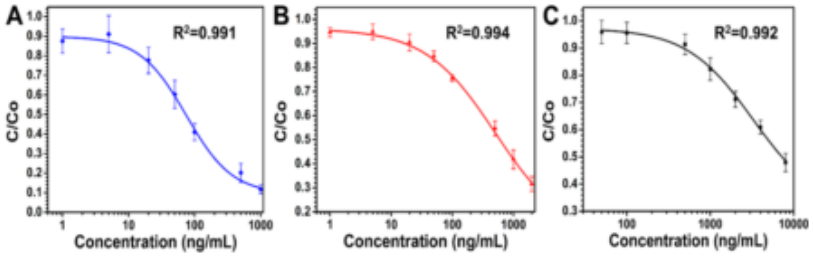

Figure 4. Individual hormone calibration curves in PBS-T for (A) insulin, (B) glucagon, and (C) somatostatin. For each hormone, mean relative binding values (C/C_0) were plotted as a function of hormone concentration (ng/mL). Relative binding was calculated by dividing the response for each concentration (C) by the response from a solution containing only the optimal concentration of individual antibodies (C_0). Solid lines correspond to the fitting of a nonlinear 4PL model. Error bars represent the standard deviation from 3 independent experiments (n = 3).

spots from different regions of the chip. Then, an average of these SPR shifts from three independent sensors was calculated and the bars in Figure 4 represent the corresponding SD. The LOD and dynamic range for individual immunoassays are shown in Table 2.

Table 2. SPR Sensing Performance for Single Hormones[a]

hormone	ΔR (%) (C_0)	LOD (ng/mL)	LOD (nM)	dynamic range (ng/mL)
insulin	1.47 ± 0.06	12	2	15−338
glucagon	1.25 ± 0.02	4	1	72−2000[b]
somatostatin	1.11 ± 0.03	409	250	1237−8000[b]

[a]All values were calculated from the nonlinear 4PL fit equation derived from individual calibration curves. The reported LOD was calculated as the response of the blank (C_0) minus 3 times the standard deviation. [b]Highest concentration tested.

Additionally, we tested different sensor regeneration solutions including 10−50 mM NaOH, 10 mM NaOH 1−20% (v/v)−acetonitrile, 0.1−1 M glycine (pH 2−3), 0.1−1 M glycine−1% (v/v) DMSO, and 2 M $MgCl_2$, 0.1−1 M glycine−1% (v/v) DMSO, and 2 M $MgCl_2$(data not shown). From these solutions, 1 M glycine with a pH = 2.5 provided the more efficient conditions for surface regeneration.

Finally, the sensor's resistance to nonspecific absorption of proteins was determined by separately injecting BSA and LYZ with a final concentration of 1 mg/mL. The injection of these solutions was performed at the end of each calibration curve experiment under the same experimental conditions as the standard solutions used during hormone sensing. The shift in reflectivity was measured after 10 min of contact time and 5 min PBS-T wash. For all cases, during BSA injection the SPR angle increased abruptly and later returned to a slightly smaller baseline value, likely due to the high bulk refractive index change during the injection. This can be interpreted as a

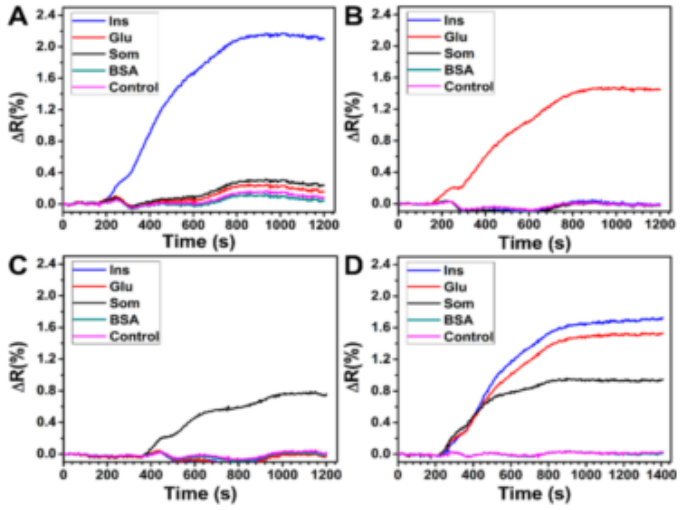

Figure 5. Spot specificity on a multiplex sensing surface for (A) anti-insulin, (B) anti-glucagon, and (C) anti-somatostatin. (D) Typical blank solution response (C_0) for multiplex immunoassays. Immobilized BSA (green line) and the bare SAM surface, identified in the graphs as "Control" (pink line), were used as negative controls.

DOI: 10.1021/acs.analchem.7b04288
Anal. Chem. 2018, 90, 3132−3139

negligible accumulation of BSA on the sensor surface. In the case of LYZ injection, the sensor registered a positive increase in the baseline value immediately after the buffer washing step. The adsorbed amount of LYZ was less than 100 pg/mm^2 for all hormone-functionalized surfaces. This value is consistent with the definition of an antifouling surface.[37] Moreover, a single injection of regeneration solution for 25 s returned the baseline to its original value, indicating a weak interaction of LYZ on the sensor's surface. Table S1 in the Supporting Information shows the mean (n = 3) SPR response to BSA and LYZ immediately after buffer washing

Biosensor Performance for Multiplex Immunoassays. Multiplex hormone detection was achieved by simultaneously performing three immunoassays. Once the different hormones were immobilized on the surface and the chip blocked, the spot cross-reactivity was investigated. Figure 5 shows the sensor response to individual injection of the optimal antibody concentration of anti-insulin (Figure 5A), anti-glucagon (Figure 5B), and anti-somatostatin (Figure 5C). The typical sensor response to a blank solution (mix of all antibodies) is shown in Figure 5D. Each injection caused an increase in SPR signal on the relevant spot, indicating specific binding and low cross-contamination between the spots. A certain level signal variation was observed between individual injections of antibodies (Figure 5A–C) and the injection of the antibody mix (Figure 5D). This signal variability may arise due to subsequent injection and regeneration of the sensor's surface since the multiplex sensor presented a similar performance to that of the individual sensors, as shown later in this section. This did not represent a major drawback during the sensor operation, as we recorded consistent and reproducible measurement during all of our experiments.

For this experiment, two negative controls were used: the bare SAM surface and spots functionalized with BSA, as identified by "Control" (pink color) and BSA (green color) in Figure 5. As it can be seen in Figure 5D, there was a negligible response on the BSA and "Control" spots when exposed to the blank solution, indicating the high antifouling properties of the sensor.

To further determine the antifouling properties of the sensor in multiplex mode, separate injections of BSA and LYZ with a final concentration of 1 mg/mL were performed. As with individual sensing experiments, BSA injection resulted in a small decrease of the baseline while LYZ lead to a slight increase in the baseline value measured after buffer washing. Similarly to individual assays, the adsorbed amount of LYZ was well within the definition of an antifouling surface[37] (less than 100 pg/mm^2). The mean SPR response of the multiplex sensor for BSA and LYZ immediately after buffer washing is reported in the Supporting Information (Table S2).

For the multiplex assays, freshly prepared standard solutions (PBS-T) containing a mixture of insulin, glucagon, and somatostatin were prepared. The optimal amount of antibodies was then added and gently mixed for 2 min before injecting into the SPR system. Figure 6 shows the calibration curves for multiplex sensing of insulin (blue), glucagon (red), and somatostatin (black). For each hormone, mean relative binding values (C/C_0) were plotted as a function of hormone concentration (ng/mL). During experiments, the mean SPR shift was measured in at least 3 spots for each hormone and the controls. Then, an average of these SPR shifts from 3 independent sensors was calculated, and the bars in Figure 6 represent the corresponding SD. The LOD and dynamic range

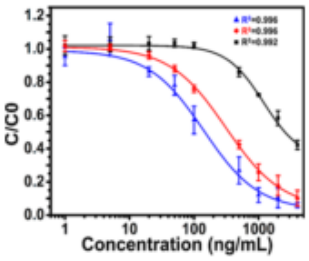

Figure 6. Multiplex hormone calibration curves in PBS-T for insulin (blue), glucagon (red), and somatostatin (black). For each hormone, mean relative binding values (C/C_0) were plotted as a function of hormone concentration (ng/mL). Relative binding was calculated by dividing the response of a range of standard solutions containing a mix hormones (C) by the response of the blank solution containing only a fixed concentration of antibodies (C_0). Solid lines correspond to the fitting of a nonlinear 4PL model. Error bars represent the standard deviation from 3 independent experiments (n = 3).

for multiplex immunoassays are shown in Table 3. Typical SPR curves for the multiplex detection mode can be found in the Supporting Information (Figures S3–S6).

Table 3. SPR Sensing Performance for Multiplexed Immunoassays[a]

hormone	max ΔR (%) (C_0)	LOD (ng/mL)	LOD (nM)	dynamic range (ng/mL)
insulin	1.69 ± 0.02	8	1	34–633
glucagon	1.52 ± 0.01	14	4	85–1592
somatostatin	0.93 ± 0.03	403	246	719–4000[b]

[a]All values were calculated from the nonlinear 4PL fit equation derived from individual calibration curves. The reported LOD was calculated as the response of the blank (C_0) minus 3 times the standard deviation. [b]Highest concentration tested.

The LOD of the sensor in multiplex mode was very similar to that of individual sensors. However, it can be noticed that the dynamic range for each hormone is different from each other. This could be as a result of variations in the hormones' surface density caused by the surface functionalization of the gold-coated prism outside of the SPR system.

Interestingly, the LOD of the SPR immunoassays in the multiplex mode were 1 order of magnitude higher than their corresponding ELISA assays (pg/mL). However, the high sensitivity of the ELISA method is not necessarily required for the detection of hormones directly secreted by a population of islets. For instance, previous reports demonstrated the individual detection of insulin[13] and glucagon[14] secreted (LOD) from 10 islets was 10 and 5 nM, respectively, at 15 mM glucose.

Since the number of somatostatin secreting cells within the islets is usually smaller than that of insulin or glucagon secreting cells,[4] further protocol optimization could be required. Nevertheless, if the future detection of islet secretion products requires signal amplification, this could be readily addressed using gold nanoparticles, either within the sensing surface itself or as signal enhancing agent to increase the LOD of the present SPR immunoassays.[41]

DOI: 10.1021/acs.analchem.7b04288
Anal. Chem. 2018, 90, 3132–3139

CONCLUSIONS

In this work, we introduced a strategy for label-free and multiplex detection of pancreatic islet hormones with a LOD of 1 nM for insulin, 4 nM for glucagon, and 246 nM for somatostatin with a total analysis time per point of 21 min using a SPRi-based biosensor. The sensor showed comparable performance to previous reports where direct secretion of insulin and glucagon from a population of islets have been studied. The sensor exhibited excellent antifouling properties and specificity due to the design of a mixed SAM of a thiolated polyethylene glycol and 16-mercaptohexadecanoic acid showing a negligible response to a concentration of 1 mg/mL of BSA and a very little response to LYZ. This show promise for the future operation of the sensor in a complex matrix such as a pancreatic islet secretome. The present SPRi-based biosensor could be easily integrated with previously developed microfluidic perfusion devices, which trap and reproduce the natural *in vivo* conditions of the islets, allowing real-time secretion analysis of pancreatic islet secretion. Such biosensing platform holds the potential to monitor a small islet's secretory fingerprint, allowing further understanding of the paracrine effect of somatostatin on glucose inducing insulin secretion as well as comprising a drug screening platform for the discovery of novel therapeutic agents for the treatment of diabetes

ASSOCIATED CONTENT

Supporting Information

The Supporting Information is available free of charge on the ACS Publications website at DOI: 10.1021/acs.analchem.7b04288.

Quantitative data of nonspecific adsorption of BSA and LYZ on individual and multiplex mode and typical SPR curves for multiplex mode sensing (PDF)

AUTHOR INFORMATION

Corresponding Author

*E-mail: maryam.tabrizian@mcgill.ca.

ORCID

Maryam Tabrizian: 0000-0002-5050-4480

Notes

The authors declare no competing financial interest.

ACKNOWLEDGMENTS

The authors acknowledge the financial support from the Natural Science and Engineering Research Council of Canada (NSERC), the Fonds de Recherche Nature et Technologies-Team Grant, the NSERC-CREATE in ISS, and FRC scholarship from Consejo Nacional de Ciencia y Teconología de México (CONACyT) and Secretaría de Educación Pública de México (SEP). The authors are also thankful to F. Melaine for her insightful discussions during the development of this work.

REFERENCES

(1) International Diabetes Federation. OpenURL, 2015.
(2) Hall, J. E.; Guyton, A. C. *Guyton and Hall Textbook of Medical Physiology*, 12th ed.; Saunders Elsevier: Philadelphia, PA, 2011.
(3) Yovos, J. G. *Diabetes Res. Clin. Pract.* **2011**, *93*, S25−S26.
(4) Cabrera, O.; Berman, D. M.; Kenyon, N. S.; Ricordi, C.; Berggrern, P. O.; Caicedo, A. *Proc. Natl. Acad. Sci. U. S. A.* **2006**, *103* (7), 2334−2339.
(5) Caicedo, A. *Semin. Cell Dev. Biol.* **2013**, *24* (1), 11−21.
(6) Wierup, N.; Sundler, F.; Heller, R. S. *J. Mol. Endocrinol.* **2014**, *52* (1), R35−R49.
(7) Braun, M. In *Pancreatic Beta Cell*; Litwack, G., Ed.; Elsevier Academic Press Inc: San Diego, CA, 2014; Vol. *95*, pp 165−193.
(8) Braun, M.; Ramracheya, R.; Johnson, P. R.; Rorsman, P. *Ann. N. Y. Acad. Sci.* **2009**, *1152* (1), 187−193.
(9) Hanna, S. T.; Pigeau, G. M.; Galvanovskis, J.; Clark, A.; Rorsman, P.; MacDonald, P. E. *Pfluegers Arch.* **2009**, *457* (6), 1343−1350.
(10) Luciani, D. S.; Johnson, J. D. *Mol. Cell. Endocrinol.* **2005**, *241* (1), 88−98.
(11) Braun, M.; Ramracheya, R.; Bengtsson, M.; Clark, A.; Walker, J. N.; Johnson, P. R.; Rorsman, P. *Diabetes* **2010**, *59* (7), 1694−1701.
(12) Ramracheya, R.; Ward, C.; Shigeto, M.; Walker, J. N.; Amisten, S.; Zhang, Q.; Johnson, P. R.; Rorsman, P.; Braun, M. *Diabetes* **2010**, *59* (9), 2198−2208.
(13) Roper, M. G.; Shackman, J. G.; Dahlgren, G. M.; Kennedy, R. T. *Anal. Chem.* **2003**, *75* (18), 4711−4717.
(14) Shackman, J. G.; Reid, K. R.; Dugan, C. E.; Kennedy, R. T. *Anal. Bioanal. Chem.* **2012**, *402* (9), 2797−2803.
(15) Lomasney, A. R.; Yi, L.; Roper, M. G. *Anal. Chem.* **2013**, *85* (16), 7919−7925.
(16) Castiello, F. R.; Heileman, K.; Tabrizian, M. *Lab Chip* **2016**, *16* (3), 409−431.
(17) Xing, Y.; Nourmohammadzadeh, M.; Elias, J. E. M.; Chan, M. W.; Chen, Z. Q.; McGarrigle, J. J.; Oberholzer, J.; Wang, Y. *Biomed. Microdevices* **2016**, *18* (5), 9.
(18) Lee, D.; Wang, Y.; Mendoza-Elias, J. E.; Adewola, A. F.; Harvat, T. A.; Kinzer, K.; Gutierrez, D.; Qi, M.; Eddington, D. T.; Oberholzer, J. *Biomed. Microdevices* **2012**, *14* (1), 7−16.
(19) Proks, P.; Eliasson, L.; Ammälä, C.; Rorsman, P.; Ashcroft, F. M. *J. Physiol.* **1996**, *496* (1), 255−264.
(20) Yang, L.; Ji, W.; Xue, Y.; Chen, L. *J. Mol. Med.* **2013**, *91* (8), 929−938.
(21) Süss, C.; Solimena, M. *Exp. Clin. Endocrinol. Diabetes* **2008**, *116* (S 01), S13−S20.
(22) Li, Y. V. *Endocrine* **2014**, *45* (2), 178−189.
(23) Rorsman, P.; Braun, M. *Annu. Rev. Physiol.* **2013**, *75*, 155−179.
(24) Singh, P. *Sens. Actuators, B* **2016**, *229*, 110−130.
(25) Nault, L.; Guo, P.; Jain, B.; Brechet, Y.; Bruckert, F.; Weidenhaupt, M. *Acta Biomater.* **2013**, *9* (2), 5070−5079.
(26) Hiep, H. M.; Nakayama, T.; Saito, M.; Yamamura, S.; Takamura, Y.; Tamiya, E. *Jpn. J. Appl. Phys.* **2008**, *47* (2), 1337−1341.
(27) Grasso, G.; Bush, A. I.; D'Agata, R.; Rizzarelli, E.; Spoto, G. *Eur. Biophys. J.* **2009**, *38* (4), 407−414.
(28) Gao, J.; Tong, H.; Huang, Z.; Liu, R.; Li, X.; Qjang, O.; Tang, C. *Anal. Methods* **2013**, *5* (13), 3201−3206.
(29) Lerch, M.; Kamimori, H.; Folkers, G.; Aguilar, M. I.; Beck-Sickinger, A. G.; Zerbe, O. *Biochemistry* **2005**, *44* (25), 9255−9264.
(30) Zou, C.; Kumaran, S.; Markovic, S.; Walser, R.; Zerbe, O. *ChemBioChem* **2008**, *9* (14), 2276−2284.
(31) Takagi, K.; Legrand, R.; Asakawa, A.; Amitani, H.; François, M.; Tennoune, N.; Coëffier, M.; Claeyssens, S.; Do Rego, J. C.; Déchelotte, P.; Inui, A.; Fetissov, S. O. *Nat. Commun.* **2013**, *4*, 2685.
(32) Love, J. C.; Estroff, L. A.; Kriebel, J. K.; Nuzzo, R. G.; Whitesides, G. M. *Chem. Rev.* **2005**, *105* (4), 1103−1169.
(33) Gobi, K. V.; Iwasaka, H.; Miura, N. *Biosens. Bioelectron.* **2007**, *22* (7), 1382−1389.
(34) Estevez, M. C.; Belenguer, J.; Gomez-Montes, S.; Miralles, J.; Escuela, A. M.; Montoya, A.; Lechuga, L. M. *Analyst* **2012**, *137* (23), 5659−5665.
(35) Biacore Life Sciences, GE Healthcare, Uppsala, Sweden, 2003.
(36) Mitchell, J. *Sensors* **2010**, *10* (8), 7323−7346.
(37) Vaisocherova, H.; Brynda, E.; Homola, J. *Anal. Bioanal. Chem.* **2015**, *407* (14), 3927−3953.
(38) Mitchell, J. S.; Wu, Y.; Cook, C. J.; Main, L. *Steroids* **2006**, *71* (7), 618−631.
(39) Cui, X.; Yang, F.; Sha, Y.; Yang, X. *Talanta* **2003**, *60* (1), 53−61.
(40) Haasnoot, W.; Gerçek, H.; Cazemier, G.; Nielen, M. W. F. *Anal. Chim. Acta* **2007**, *586* (1), 312−318.

DOI: 10.1021/acs.analchem.7b04288
Anal. Chem. 2018, 90, 3132−3139

(41) Bedford, E. E.; Spadavecchia, J.; Pradier, C. M.; Gu, F. X. *Macromol. Biosci.* **2012**, *12* (6), 724−739.

DOI: 10.1021/acs.analchem.7b04288
Anal. Chem. 2018, 90, 3132−3139

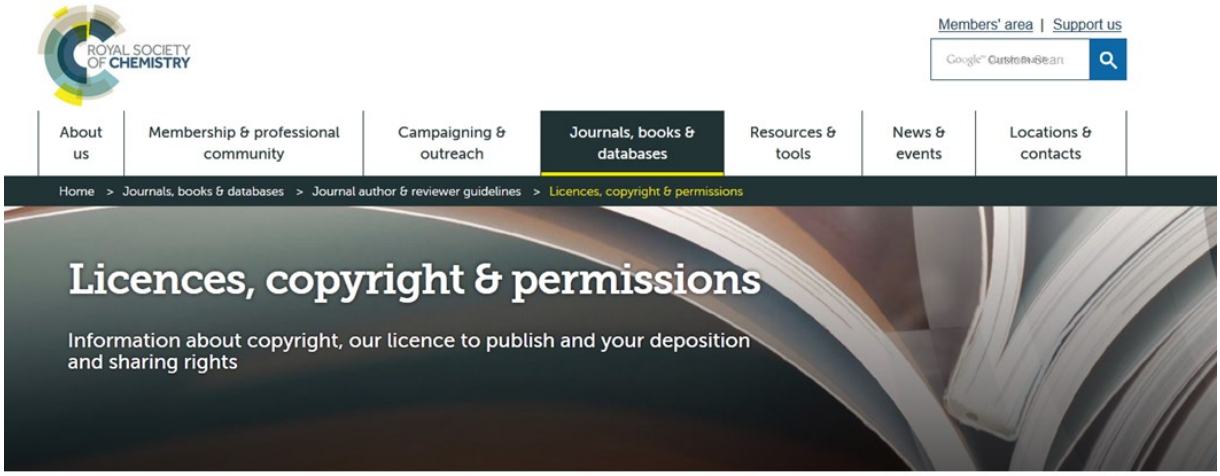

Deposition and sharing rights

The following details apply only to authors accepting the standard licence to publish. Authors who have accepted one of the open access licences to publish, or are thinking of doing so, should refer to the details for open access deposition rights.

When the author accepts the licence to publish for a journal article, he/she retains certain rights concerning the deposition of the whole article. This table summarises how you may distribute the accepted manuscript and version of record of your article.

Sharing rights	Accepted manuscript	Version of record
Share with individuals on request, for personal use	✓	✓
Use for teaching or training materials	✓	✓
Use in submissions of grant applications, or academic requirements such as theses or dissertations	✓	✓
Share with a closed group of research collaborators, for example via an intranet or privately via a scholarly communication network	✓	✓
Share publicly via a scholarly communication network that has signed up to STM sharing principles	⧗	×
Share publicly via a personal website, institutional repository or other not-for-profit repository	⧗	×
Share publicly via a scholarly communication network that has not signed up to STM sharing principles	×	×

⧗ Accepted manuscripts may be distributed via repositories after an embargo period of 12 months

Analyst

PAPER

View Article Online
View Journal

Cite this: DOI: 10.1039/c9an00140a

Gold nanoparticle amplification strategies for multiplex SPRi-based immunosensing of human pancreatic islet hormones†

F. Rafael Castiello[a] and Maryam Tabrizian *[a,b]

In this work, we demonstrate the potential use of SPRi for secretion-monitoring of pancreatic islets, small micro-organs that regulate glucose homeostasis in the body. In the islets, somatostatin works as a paracrine inhibitor of insulin and glucagon secretion. However, this inhibitory effect is lost in diabetic individuals and little is known about its contribution to the pathology of diabetes. Thus, the simultaneous detection of insulin, glucagon and somatostatin could help understand such communications. Previously, the authors introduced an SPRi biosensor to simultaneously monitor insulin, glucagon and somatostatin using an indirect competitive immunoassay. However, our sensor achieved a relatively high LOD for somatostatin detection (246 nM), the smallest of the three hormones. For this reason, the present work aimed to improve the performance of our SPRi biosensor using gold nanoparticles (GNPs) as a means of ensuring somatostatin detection from a small group of islets. Although GNP amplification is frequently reported in the literature for individual detection of analytes using SPR, studies regarding the optimal strategy in a multiplexed SPR setup are missing. Therefore, with the aim of finding the optimal GNP amplification strategies for multiplex sensing we compared three architectures: (1) GNPs immobilized on the sensor surface, (2) GNPs conjugated with primary antibodies (GNP-Ab_1) and (3) GNPs conjugated with a secondary antibody (GNP-Ab_2). Among these strategies an immunoassay using GNP-Ab_2 conjugates was able to achieve multiplex detection of the three hormones without cross-reactivity and with 9-fold LOD improvement for insulin, 10-fold for glucagon and 200-fold for somatostatin when compared to the SPRi biosensor without GNPs. The present work denotes the first report of the simultaneous detection of such hormones with a sensitivity level comparable to ELISA assays, particularly for somatostatin.

Received 21st January 2019,
Accepted 27th February 2019
DOI: 10.1039/c9an00140a
rsc.li/analyst

Introduction

Pancreatic islets are small micro-organs that regulate glucose homeostasis in the body.[1] Deficiencies in the islet's secretory pathways give rise to diabetes mellitus. However, little is understood about the paracrine communications occurring during glucose regulation.[1] For instance, it has been shown that somatostatin, secreted by the third most abundant cell type in the islets, is a potent paracrine inhibitor of the secretion of both insulin and glucagon.[2,3] In a healthy adult, somatostatin secretion is normally stimulated by glucose; however, this triggering effect is lost in type 1 and type 2 diabetes. This has been proposed to contribute to the impaired regulation of glucagon secretion in diabetes.[4,5] Thus, monitoring a secretory fingerprint (SF) of pancreatic islets including the three most abundant secreting cells in the islets could help to better understand such paracrine communications.

Pancreatic islet research to date has involved mostly the use of traditional bioassays for hormone quantification such as ELISA,[6–8] patch clamp,[9–14] and capillary electrophoresis (CE).[15–17] However, these techniques have a low throughput, are time-consuming, are labor intensive and can detect only one hormone at a time. Moreover, they face several challenges when attempting their implementation for multiplex analysis.

Most of these shortcomings could be addressed using optical, electrical, mechanical or magnetic biosensors.[18] Among these biosensing technologies, sensors based on the optical excitation of surface plasmons have increased in popularity in the last decade due to their simple, easy to use, non-invasive and label-free nature.[19] Surface plasmon resonance (SPR) biosensors present an additional advantage for the multiplex screening of biomolecular interactions when combined with imaging capabilities (SPRi).[20] For instance, H. J. Lee *et al.*[21] demonstrated the simultaneous detection of 3 low molecular weight protein biomarkers using SPRi, by creating a

[a]Biomedical and Biological Engineering Department, McGill University, Montreal, QC, Canada. E-mail: maryam.tabrizian@mcgill.ca
[b]Faculty of Dentistry, McGill University, Montreal, QC, Canada

†Electronic supplementary information (ESI) available: Gold nanoparticle functionalization characterization: including surfaces and GNP-Ab conjugates. See DOI: 10.1039/c9an00140a

high-density antibody microarray achieving multiplex detection of the three protein markers down to 1 nM concentrations. This makes SPRi a very desirable technique for secretion-monitoring of pancreatic islets.

In a recent work reported by the authors, a multiplex SPRi-based biosensor was introduced as a viable tool for simultaneous quantification of insulin, glucagon, and somatostatin by performing three simultaneous competitive assays with monoclonal antibodies.[22] In this work an innovative surface chemistry was introduced and optimized for the detection of the three targeted peptides in a competitive immunoassay format with high antifouling properties, obtaining limits of detection (LODs) of 1 nM for insulin, 4 nM for glucagon, and 246 nM for somatostatin in multiplexed mode with a total analysis time of 21 min per point. These LODs are satisfactory for the detection of insulin and glucagon as demonstrated by previous reports where these hormones were detected individually from secretions of a small group of islets within a microfluidic device.[15,16] However, there are no available reports regarding the required LOD for somatostatin within a similar islet population. Moreover, it is known that the number of somatostatin secreting cells within pancreatic islets is usually lower than that of insulin or glucagon secreting cells.[23]

Considering the important role of somatostatin in regulating insulin and glucagon secretion,[2,3] and before moving to precious and scarce human islet studies, the aim of the present work was to improve the performance of the previously developed SPRi biosensor to ensure that somatostatin secreted from a small group of islets can effectively, accurately and simultaneously be detected with other towed hormones.

Since their introduction by L. Lyon *et al.*,[24] gold nanoparticles (GNPs) have been the most commonly used method for improving the performance of SPR immunosensors. Two configurations are typically considered for the use of GNPs in SPR signal amplification: (1) the sensor surface modification with GNPs and (2) the labeling of a recognition element with GNPs. These strategies rely either on the coupling of the local plasmon resonance of the GNP with the surface plasmon resonance of the system or on the increased mass attached to the recognition element for signal enhancement.[25,26] Both GNP amplification strategies have been frequently reported in the literature for individual detection of hormones such as insulin,[27] progesterone,[28] and testosterone[29] and other small analytes;[26,30,31] however, studies regarding the application of these strategies for multiplex hormone detection are scarce. Moreover, few reports exist regarding the use of GNP amplification in a multiplex setting and they focus on the detection of DNA sequences[32] or cancer biomarkers by means of localized SPR using microscopy.[33] Although these reports demonstrated the detection of target analytes in femtomolar levels in multiplexed mode, there is a lack of formal studies regarding the optimal GNP amplification strategy for SPRi systems.

Thus, to establish the optimal signal amplification configuration for the multiplexed sensing of a SF of pancreatic islets with SPRi, three GNP amplification strategies were investigated including (1) GNPs immobilized on the sensor surface, (2) GNPs conjugated with primary antibodies (GNP-Ab_1) and (3) GNPs conjugated with a secondary antibody (GNP-Ab_2). For this study, somatostatin was used as the 'reference' hormone, as it is the smallest among the three SFs of pancreatic islets, to first test the performance of the aforementioned SPR signal amplification strategies in an indirect competitive assay. Then, the biosensor performance was assessed in multiplexed mode to determine the LOD and dynamic range for the three targeted hormones simultaneously.

Experimental section

Materials and methods

20 nm gold nanoparticles (GNPs) in citrate buffer, ethanolamine hydrochloride, *N*-hydroxysuccinimide (NHS), *N*-(3-dimethylaminopropyl)-*N*′-ethylcarbodiimide hydrochloride (EDC), hexa(ethylene glycol) dithiol (HEGD), bovine serum albumin (BSA), hydrochloric acid (HCl), glycerol, sodium hydroxide (NaOH), human glucagon and human somatostatin were purchased from Sigma-Aldrich (St Louis, MO, USA). Absolute ethanol was purchased from Fisher Scientific (Fair Lawn, NJ, USA), and phosphate-buffered saline (PBS) tablets, Tween 20 and glycine were purchased from BioShop Canada Inc. (Burlington, Ontario, Canada). 3,3′-Dithiobis(sulfosuccinimidyl propionate) (DTSSP) was purchased from ThermoFisher Scientific. Tris-buffered saline (TBS) with 1% casein and goat anti-mouse IgG1 and goat anti-rat IgG2a secondary polyclonal antibodies were purchased from Bio-Rad. The anti-insulin antibody (6.2 mg mL^{-1}) and human insulin were purchased from PROSPECT (Ness, Ziona, Israel). Anti-somatostatin monoclonal antibodies (200 μg mL^{-1} each) were purchased from Santa Cruz Biotechnology, Inc. (Mississauga, ON, Canada). Anti-glucagon monoclonal antibodies were purchased from Abcam (Cambridge, MA, USA). CH_3O-PEG-SH (MW 1200 Da) was purchased from Rapp Polymers GmbH (Tübingen, Germany). 16-Mercaptohexadecanoic acid (MHDA) was purchased from ProChimia Surfaces Sp. (Zacisze, Sopot, Poland). Borate buffer (0.5 M, pH 8.5) was purchased from Alfa-Aesar (USA).

Substrate preparation

Cleaned microscope glass slide (12 mm × 25 mm × 1 mm, n = 1.518) substrates were coated with 2 nm Cr as an adhesion layer, followed by the deposition of a thin Au layer of 48 nm using E-beam vapor deposition under high vacuum. The slides were then coupled to an SF11 equilateral triangular prism (nSF-11 = 1.765) using a refractive index matching liquid. Gold-coated prisms (n = 1.765) were purchased from Horiba Scientific, France, and used as received.

SPRi measurements

SPRi detection was performed using a scanning-angle SPRi instrument (model SPRi Lab+, Horiba, France). The SPRi apparatus is equipped with an 800 nm LED source, a CCD camera, and a microfluidic flow cell. All experiments were per-

formed at 25 °C by keeping the instrument inside an incubator (Memmert Peltier, Rose Scientific, Canada).

To select the working angle for kinetic analysis, the slope of the plasmon curves was computed automatically using the instrument's software. The selected angle corresponds to the point of the plasmon curve at which the slope was maximum. Reflectivity shift (ΔR (%)) was measured upon stabilization of the baseline. After each analyte injection, the substrate was rinsed with running buffer PBS-T (PBS with 0.002% Tween 20), and ΔR was calculated by the difference between the buffer signals before and after the analyte injection. The signal was recorded at least on three spots for each analyte and controls to determine the average ΔR values. All experiments were performed using an injection loop with a fixed volume of 200 μL and a constant flow rate of 20 μL min^{-1}, with the exception of functionalization steps where the flow rate was adjusted depending on the required contact time.

All SPR plots are presented as a function of reflectivity shift (ΔR (%)) *vs.* time. A Savitzky–Golay smoothing polynomial function of second order was applied to all plots using OriginLab 2018 (b.9.5.5.409).

Surface immobilization of hormones

Following a protocol previously developed by the authors,[22] an ethanolic solution of 0.5 mM CH_3O-PEG-SH and 0.5 mM MHDA was prepared and mixed at a molar ratio of 40% MHDA and 60% PEG (60-PEG/40-MHDA). Gold-coated prisms and slides were immersed in the ethanolic solution overnight to allow self-assembled monolayer (SAM) formation. Finally, they were thoroughly rinsed with absolute ethanol, DI water and dried under a stream of N_2.

For individual somatostatin sensing experiments, SAM-functionalized slides were placed on the SPRi system for subsequent functionalization. An initial conditioning step was performed by four serial injections of a 1 M glycine (pH 2.5) (1 M-Gly) solution (contact time of 2 min each). Then, PBS-T was allowed to run until a stable baseline was obtained. Next, covalent immobilization of insulin, glucagon or somatostatin *via* NHS/EDC chemistry was performed following the protocol reported by Gobi *et al.*.[34] Briefly, an aqueous solution containing 2 mg mL^{-1} NHS, 2 mg mL^{-1} EDC and 50 μg mL^{-1} of the desired hormone was injected into the system with a contact time of 1 h. Next, an injection of 1 M ethanolamine hydrochloride (pH 8.5) (contact time of 10 min) was performed to inactivate any unfunctionalized –COOH groups. Then, two serial injections of 1 M-Gly solution (contact time of 1 min each) were performed to remove weakly bound hormones. Finally, a blocking solution containing 5% BSA and 1% casein in TBS buffer was injected (contact time of 30 min) and subsequently, at least 3 injections of the 1 M-Gly solution were made to remove weakly bound proteins. Fig. 1A shows a schematic representation of a typical surface hormone functionalization.

For multiplex measurements, gold-coated prisms were functionalized using the procedure described for glass slides

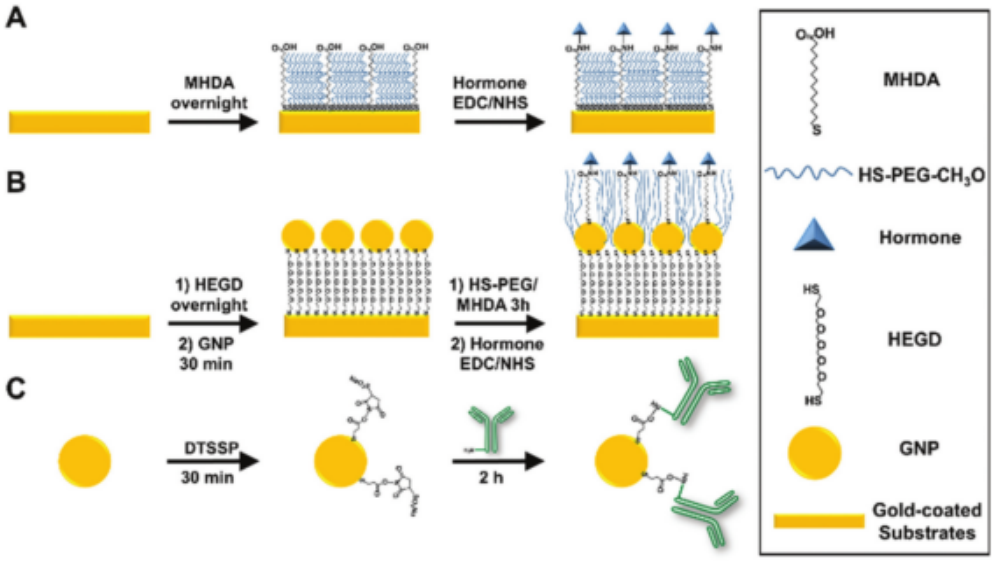

Fig. 1 Schematic representation of the typical surface functionalization of (A) gold-coated substrates functionalized with a self-assembled monolayer (SAM) of 16-mercaptohexadecanoic acid (MHDA)/CH_3O-PEG-SH (PEG) and subsequently with the targeted hormone, (B) gold-coated substrate surface functionalized with a SAM of hexa(ethylene glycol) dithiol (HEGD), GNPs and subsequently with the targeted hormone and (C) covalent antibody functionalization for the formation of GNP-conjugates using (3,3'-dithiobis(sulfosuccinimidyl propionate)) (DTSSP).

outside of the SPR system. After conditioning, four individual solutions containing NHS/EDC and each targeted hormone (insulin, glucagon, and somatostatin) or a control (BSA) were spotted (150 nL) in triplicate on the prisms and incubated in a humidity chamber for 1 h. After incubation, the prisms were rinsed with DI water and exposed to 1 M ethanolamine hydrochloride (pH 8.5) for 10 min. Next, the prisms were exposed to the blocking solution for 30 min and subsequently rinsed with PBS-T. Finally, the prisms were placed in the SPR system and a 1 M-Gly solution was injected at least three times to obtain a stable baseline before starting the experiments.

Immobilization of GNPs on the gold-coated sensor's surface

In this work, commercial 20 nm GNPs were selected since it has been reported in the literature as an optimal size for SPR amplification either when immobilized in the sensor's surface or for antibody modified GNP immunoassays of small molecules.[28,35,36]

The immobilization of commercial 20 nm GNPs on the gold-coated sensor's surface was achieved according to a protocol developed by Taufik *et al.*[37] with minor modifications. After cleaning, gold-coated slides were immersed in an ethanolic solution of 2 mM HEGD overnight to allow SAM formation. After rinsing with ethanol and DI water, the slides were exposed to an aqueous solution containing 20 nm GNPs (OD_{520} = 1.0) and incubated for one hour. Next, the slides were rinsed with DI water and placed in a 60-PEG/40-MHDA ethanolic solution for 3 hours. Finally, hormone functionalization was performed according to the procedure described in the previous section. Fig. 1B shows a schematic representation of the surface functionalization with GNPs and hormones.

Antibody–GNP functionalization

The functionalization protocol for commercial 20 nm GNPs (OD_{520} = 1) with primary and secondary antibodies was adapted from a previous report by J. D. Driskell *et al.*[38] using DTSSP as a bifunctional crosslinker. Briefly, 134 μL of 50 mM borate buffer (pH 8.5) was added to a 1 mL suspension of 20 nm GNPs to adjust the pH. Next, 26 μL of 20 μM DTSSP was added to the GNPs and incubated for 30 min to form a thiolate monolayer through cleavage of the DTSSP disulfide bond. The suspension was then centrifuged at 17 500*g* for 30 min. Then, the supernatant containing excess DTSSP was removed and the GNPs were resuspended in 1 mL of 2 mM borate buffer. Immediately afterward, 20 μg of the desired antibody was added to the DTSSP-GNP suspension and incubated for 1.5 hours. The suspension was then centrifuged at 17 500*g* for 30 min, the supernatant was removed, and the GNPs were resuspended in 1 mL of 2 mM borate buffer containing 1% (m/v) BSA and incubated for 30 min to allow the BSA to block any unreacted DTSSP and nonspecific binding sites. The centrifugation/resuspension cycle was repeated two additional times using 2 mM borate buffer for resuspension to remove excess antibody and BSA. The final volume of the solution after the centrifugation/resuspension cycles was fixed to approximately 200 μL ($OD_{525} \approx 4$) and the solution was stored at 4 °C. The functionalized GNPs were diluted to the desired concentration in PBS-T prior to use in immunoassays. Fig. 1C shows a schematic representation of antibody–GNP functionalization. Successful GNP functionalization for all antibodies was confirmed by the shift in the absorbance maxima of the GNPs from 520 to 525 nm (Fig. S2 provided in the ESI†).

Competitive immunoassays

The four configurations used for indirect competitive immunoassays consisted of a surface with (Fig. 2A) and without GNPs (Fig. 2B), primary antibody–GNP (GNP-Ab_1) conjugates (Fig. 2C) and secondary antibody–GNP (GNP-Ab_2) conjugates (Fig. 2D). Since somatostatin was the smallest of the targeted hormones, it was used as the "reference" hormone in all individual hormone assays. The optimal primary anti-somatostatin antibody, GNP-Ab_1 and GNP-Ab_2 concentrations were defined as the concentration that could generate a small but detectable SPR signal of $\Delta R \approx 1$, previously reported as a reliable ΔR for this type of assay.[39]

Standard somatostatin solutions were prepared by serial dilution in PBS-T buffer with concentrations ranging between 0.01 and 4000 ng mL^{-1}. These solutions were then mixed with 2 μg mL^{-1} of anti-somatostatin antibody for assays involving only primary antibodies, 0.6 μg mL^{-1} of antibody for the assay with GNP-Ab_2 conjugates or a 1 : 50 dilution (from $OD_{525} \approx 4$) of GNP-Ab_1 conjugates. All mixtures were incubated for 2 min with gentle mixing by inverting upside down and then injected into the system from the highest to the lowest hormone concentration (contact time of 10 min) starting with a blank solu-

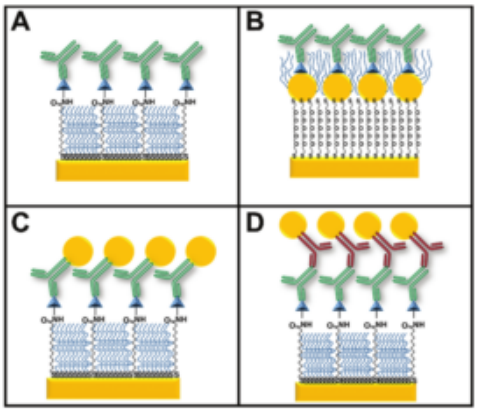

Fig. 2 Schematic representation of the four configurations of competitive immunoassays used for this work: (A) an assay involving only primary antibodies and the hormone immobilized on a gold surface used as the control, (B) an assay where GNPs are present on the surface and the hormone is immobilized on top of the GNPs, (C) an assay where GNPs are conjugated with monoclonal primary antibodies (GNP-Ab_1) and (D) an assay involving amplification using GNPs conjugated with a polyclonal secondary antibody (GNP-Ab_2) after a primary competitive assay.

tion containing only anti-somatostatin antibodies or GNP-Ab_1 conjugates. For secondary antibody conjugate assays, immediately after anti-somatostatin antibody injection, GNP-Ab_2 conjugates were injected (1 : 50 dilution from $OD_{525} \approx 4$). The optimal primary anti-somatostatin antibody, GNP-Ab_1 and GNP-Ab_2 concentrations were defined as the concentration that could generate a small but detectable SPR signal of $\Delta R \approx 1$, previously reported as a reliable ΔR for this type of assay.[39]

During calibration curve experiments, different sensor regeneration solutions were tested including 10–50 mM NaOH, 50 mM NaOH with 5–50% (v/v) glycerol, 0.1–1 M glycine (pH 1.5), 0.1–1 M glycine (pH 1.5) with 1% (v/v) DMSO, and 2 M $MgCl_2$. From these solutions, 50 mM NaOH with 25% glycerol provided the most efficient conditions for regeneration and it was used throughout all the experiments.

For multiplex assays, standard solutions having a mixture of insulin, glucagon, and somatostatin were prepared in PBS-T buffer in a concentration range of 0.01–4000 ng mL^{-1} and mixed with a cocktail of primary antibodies containing anti-insulin (0.2 μg mL^{-1}), anti-glucagon (0.05 μg mL^{-1}) and anti-somatostatin (0.6 μg mL^{-1}). Similar to individual somatostatin assays, the mixtures were incubated for 2 min with gentle mixing and serially injected over the spotted sensor chip from the highest to the lowest hormone concentration (contact time of 10 min) starting with a blank solution containing only the antibody cocktail. Subsequently, a GNP-Ab_2 mixture containing GNPs conjugated to anti-mouse IgG1 (1 : 100 dilution from $OD_{525} \approx 4$) and anti-rat Ig2a (1 : 50 dilution from $OD_{525} \approx 4$) was injected into the system. Each sensing cycle comprised: hormone primary antibody mixing and incubation for 2 min, cocktail injection for 10 min, 3 min buffer washing, 10 min injection of a GNP-Ab_2 mixture and 2 injections of a regeneration solution with a contact time of 30 s with 3 min washing with buffer in between.

Statistics

Relative binding (C/C_0) was calculated for all competitive immunoassays, by dividing the response of the standard solutions containing hormones (C) by the response of the blank solution containing only a fixed concentration of antibodies (C_0). To generate calibration curves C/C_0 was plotted against the hormone concentration. The calibration curves were fitted using a nonlinear 4 parameter logistic (4PL) model using OriginLab 2018 (b.9.5.5.409). The LOD for all immunoassays was calculated from the calibration curves as the blank signal (C_0) minus three times its standard deviation. The dynamic range for the competitive immunoassay was established between $0.2C/C_0$ and $0.8C/C_0$. All data are expressed as the average of at least 3 independent experiments ± standard deviation (SD).

Results and discussion

GNP amplification strategy comparison for competitive immunoassays

First, the formation of a chemically linked layer of GNPs was performed using a SAM of a dithiol alkane (HEGD). HEGD allowed anchoring of the GNPs to the gold-coated sensor's surface through the thiol group at each end of the molecule.[37] AFM analysis indicated the successful immobilization of the GNPs by a significant change in surface morphology from a clean gold surface to a GNP-modified surface as clearly observed in Fig. S1 provided in the ESI.† This was further confirmed by a change in surface RMS roughness from 0.68 nm to 2.41 nm and later to 5.36 nm from a clean surface to a SAM-functionalized surface and to a GNP-functionalized surface. The signal amplification rationale here is that the activation of the GNP localized SPR due to the proximity of the immobilized GNPs to the sensor's surface can lead to different resonance properties of the overall SPR system with additional resonance shifts, resulting in an enhanced sensitivity of the biosensor.[25]

For all GNP–antibody conjugates, functionalization was confirmed by a shift observed in the maximum absorption peak from 520 to 525 nm (Fig. S2 in the ESI†). In the case of GNP-Ab_1 conjugates, the rationale behind this strategy is that the increased mass of the antibody due to the linked GNPs will result in a higher refractive index change on the SPR surface, thereby producing a larger SPR shift.[26] Additionally, due to the close proximity of the GNPs to the SPR surface (<15 nm) signal enhancement is also linked to electromagnetic field coupling between surface SPR and the GNP localized SPR.[26] Regarding the use of GNP-Ab_2 conjugates, the signal amplification is only expected from the increased mass of the antibody due to the linked GNPs, as the GNPs are quite far from the surface.[26]

Fig. 3 shows the sensor calibration curves for somatostatin detection where the mean relative binding values (C/C_0) are plotted as a function of hormone concentration for all sensing strategies. For these experiments, detection without GNPs was used as a control assay (Fig. 3A). Additionally, the entire

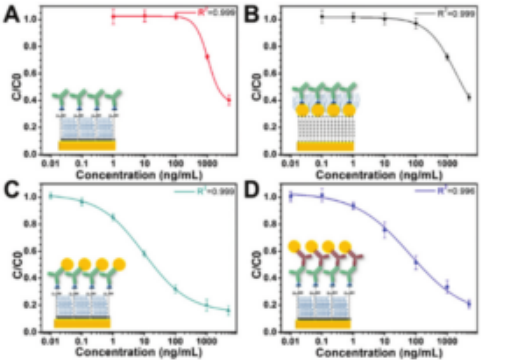

Fig. 3 Somatostatin sensing calibration curves in PBS-T for competitive immunoassays involving (A) only primary antibodies, (B) GNPs on the sensor's surface, (C) GNPs conjugated with monoclonal primary antibodies (GNP-Ab_1) and (D) an assay with GNPs conjugated with a polyclonal secondary antibody (GNP-Ab_2). Solid lines correspond to the fitting of a nonlinear 4PL model. Error bars represent the standard deviation from 3 independent experiments (n = 3).

Table 1 SPR sensing performance for somatostatin using different immunosensing strategies

Strategy	ΔR (%) (C_0)	LOD [ng mL^{-1}]	LOD [nM]	Dynamic range [ng mL^{-1}]
Primary antibodies	1.10 ± 0.03	450	275	754–4000[a]
GNPs on surface	1.72 ± 0.05	404	247	626–4000[a]
GNP-Ab$_1$	1.26 ± 0.02	0.24	0.15	1.54–780
GNP-Ab$_2$	0.93 ± 0.04	1.75	1.07	7.5–4000[a]

[a] Highest concentration tested.

sensor surface was functionalized with somatostatin, and the SPR shift for all sensing events was obtained as the mean of at least 10 spots from different regions of the chip. Then, an average of ΔR of three independently prepared chips was calculated representing their corresponding standard deviation (SD). The LOD and dynamic range for each sensing strategy are shown in Table 1.

It is noteworthy that the concentration of the control assay (Fig. 3A) and the strategy using a GNP-modified surface (Fig. 3B) was set to 2 μg mL^{-1} to facilitate comparison and to easily observe SPR signal enhancement. Interestingly, these two sensing strategies presented similar LODs. However, the GNP-modified surface showed a higher SPR signal (Fig. S3 in the ESI†) compared to the signal obtained for the surface without GNPs as clearly observable in the ΔR (%) (C_0) values in Table 1. Indeed, this seems consistent with recent reports where the LOD of the calibration curve of an indirect competitive immunoassay using GNP-modified sensors did not change even when the SPR signal was enhanced.[31,40] A possible explanation is that the performance of an indirect competitive immunoassay highly depends on the affinity constant of the immunoreaction.[31] Therefore, only strategies affecting the affinity of the antigen–antibody system such as the GNP-Ab conjugation could improve the LOD of the SPR sensor.[31]

Finally, from all immunosensing strategies, the competitive immunoassay using GNP-Ab$_1$ conjugates presented the best performance decreasing the LOD by three orders of magnitude compared to the control assay from 450 ng mL^{-1} to 240 pg mL^{-1}. Hence, this immunoassay amplification strategy was selected for further development of the multiplex hormone-sensing assay.

GNP-amplified multiplex hormone sensing

Fig. 4A–C show the assessment of cross-reactivity for primary antibodies. Individual injection of each antibody caused an increase in the SPR signal only on its relevant spot, demonstrating specificity and low cross-contamination between spots. Moreover, there was a negligible response on the control spots, indicating good antifouling properties.

However, when a similar experiment was performed using GNP-Ab$_1$ conjugates (Fig. 4D–G), high cross-reactivity was observed. This effect was particularly large for GNP-anti-insulin conjugates which generated a non-specific signal increase in all the functionalized spots including the two negative controls (Fig. 4D). When GNP-anti-glucagon conjugates were injected,

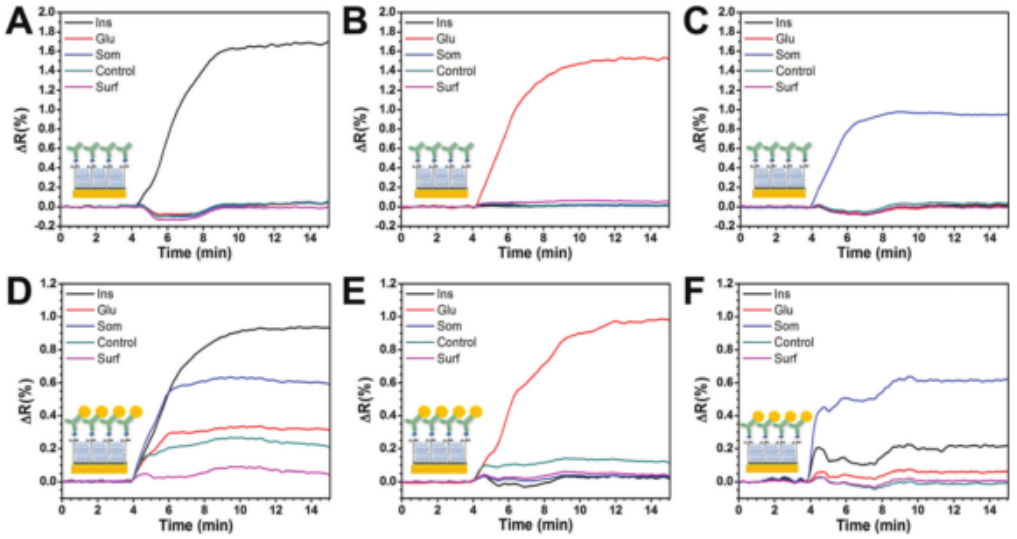

Fig. 4 Comparison of the sensor specificity in multiplexed mode. The first row shows the specificity of the sensor without signal amplification for (A) anti-insulin, (B) anti-glucagon, and (C) anti-somatostatin. The second row shows the specificity of the sensor on the same surface with signal amplification for (D) GNP–anti-insulin, (E) GNP–anti-glucagon and (F) GNP–anti-somatostatin. Immobilized BSA ("Control") and the bare SAM surface ("Surf") were used as negative controls.

cross-reactivity with insulin and somatostatin spots was not observed; however some degree of non-specific interactions was detected for the negative control spots (Fig. 4F). For GNP-anti-somatostatin conjugates, cross-reactivity was also observed mostly with insulin spots (Fig. 4G). Additional antibodies from different species and companies were used for GNP-Ab_1 conjugates for anti-insulin and anti-somatostatin. However cross-reactivity was always present (data not shown). This has been reported in the literature as a recurring problem for multiplex immunoassays[41,42] particularly for GNP conjugates since it has been shown that such conjugations can modify the activity of the antibodies. In theory, a combination of GNP-Ab_1 conjugates with little or null cross-reactivity for our system could be achieved; however testing a library of antibodies would be time consuming and cost-ineffective. Due to this dilemma, the second-best amplification strategy (GNP-Ab_2) was selected for further development of our multiplex immunosensor. For this strategy, some degree of cross-reactivity could occur since the secondary antibodies are similarly conjugated to GNPs. In general, antibody conjugation is known to affect the antibody's affinity;[31] however this did not seem to hinder the possibility for multiplex sensing as later demonstrated in this section.

The nonspecific binding effect of the GNP-Ab_2 conjugates on the analyte spots was determined prior to the multiplex assay through the injection of a mixture of GNP-goat anti-mouse IgG1 and GNP-goat anti-rat IgG2a over the sensor surface. As seen in Fig. 5A, a minimum SPR angle shift was detected during the injection with the signal returning to similar baseline levels after a few minutes of PBS-T washing, indicating a negligible nonspecific binding effect of the GNP-Ab_2 conjugates to the different surface spots.

Fig. 5B shows a typical sensor response to a blank solution (mixture of all antibodies) and the subsequent amplification effect of the GNP-Ab_2 conjugates. First, the injection caused a small increase in the SPR signal on the relevant hormone spots while an almost no response for the control spots, indicating specific binding. For these experiments, the initial concentration of primary antibodies (C_0) was fixed to 0.2 μg mL^{-1} for anti-insulin, 0.05 μg mL^{-1} for anti-glucagon and 0.6 μg mL^{-1} for anti-somatostatin. This Ab_1 concentration produced a small signal of ≈0.15ΔR for all hormone spots. The subsequent injection of GNP-Ab_2 conjugates generated an SPR signal enhancement of ≈10 times, which was consistent with previous literature reports where 20 nm GNP-Ab_2 conjugates have been used for signal amplification.[28,43]

It is noteworthy that the C_0 signal obtained for somatostatin during individual GNP-Ab_2 was smaller (ΔR = 0.93, Table 1) compared to that obtained during the multiplex assay (ΔR = 1.51, Table 2). This difference is likely due to some cross-reactivity between the different species of secondary antibodies in GNP-Ab_2. However, due to the absence of non-specific interactions with the hormone spots and the controls, it was possible to use these conjugates for multiplex detection since the sensor response (ΔR) was always consistent and reproducible for all targeted hormones.

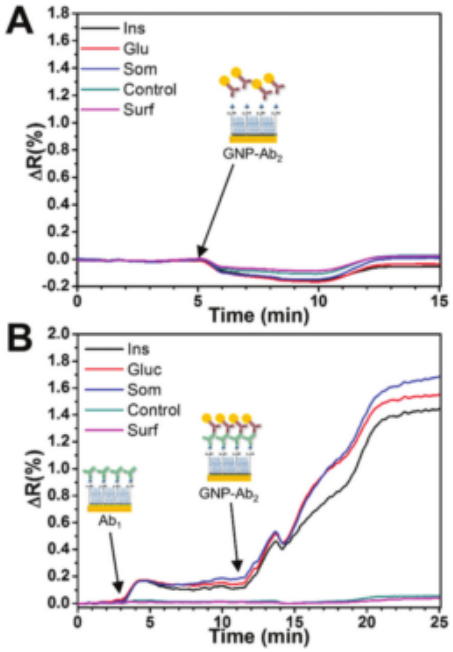

Fig. 5 Real-time SPR angle shift sensorgrams of (A) the nonspecific binding effect of GNP-Ab_2 conjugates and (B) the specific binding effect of GNP-Ab_2 conjugates after primary antibody injection (blank injection C_0). Immobilized BSA and the bare SAM surface identified as "Control" and "Surf" were used as negative controls.

Table 2 SPR sensing performance for a GNP-Ab_2 multiplex immune assay for insulin, glucagon and somatostatin. The presented ΔR (%) (C_0) is the sensor's response to the GNP-Ab_2 conjugates

Hormone	ΔR (%) (C_0)	LOD [ng mL^{-1}]	LOD [nM]	Dynamic range [ng mL^{-1}]
Insulin	1.32 ± 0.03	0.90	0.15	3.9–270
Glucagon	1.40 ± 0.03	1.35	0.39	5.0–1977
Somatostatin	1.51 ± 0.04	2.00	1.22	6.6–4000[a]

[a] Highest concentration tested.

To further assess the sensor's resistance to non-specific adsorption of proteins, at the end of each calibration curve, two solutions containing either BSA or LYZ, both with a final concentration of 1 mg mL^{-1}, were injected to the system following the same protocol as that for the hormone immunoassay. After an abrupt increase in the SPR signal during the injections due to the high bulk refractive index of the solution, the shift in reflectivity was measured after 10 minutes of contact time and 5 minutes of PBS-T wash. Since LYZ presented the largest ΔR among the two tested proteins, it was used as a reference to quantitatively evaluate the antifouling properties of the sensor. The mean (n = 3) ΔR response to BSA

and LYZ from the hormone-functionalized spots and controls is shown in Table S1 in the ESI.† It was found that the adsorbed amount of LYZ was ≈100 pg mm^{-2} for all spots assuming that 1 RU = 1 μRIU = 1 pg mm^{-2} of surface mass shift for a fixed wavelength of 800 nm.[44] This was very consistent with the definition of an antifouling surface.[45] Moreover, a short (30 s) injection of a regeneration solution returned the baseline to its original value, indicating a weak interaction of LYZ and BSA on the sensor's surface.

Fig. 6 shows the average calibration curves for the multiplex sensing of serially diluted mixtures of insulin, glucagon, and somatostatin in PBS-T obtained from three independent sensor chips. The calculated LOD and dynamic range obtained (Table 2) for the three hormones in multiplexed mode were somehow comparable to those of ELISA kits (0.001–40 ng mL^{-1} depending on the hormone targeted) assessing individual hormone quantification. However, our sensing approach has the advantage of multiplexing, a larger working range and a relatively low analysis time of 32 min per point. Moreover, each multiplex SPRi immunosensing surface showed good stability on which over 21 binding/regeneration cycles were performed.

The use of GNPs for SPR signal amplification led to a remarkable LOD improvement for all tested hormones. An increase of 9-fold for insulin, 10-fold for glucagon and 200-fold for somatostatin detection was obtained as compared to the multiplex sensing approach without using GNP conjugate amplification.[22] Noteworthy is the fact that somatostatin showed a dramatic improvement in the LOD. This could be explained by the fact that somatostatin is the smallest of the targeted hormones in this study (MW = 1637.88 Da). Thus, under the same immobilization conditions, the maximum amount of immobilization is expected to be lower than that of the higher MW hormones.[46] This could lead to less steric hindrance for binding of the large GNP-Ab$_2$ conjugates. This is corroborated by the fact that despite showing a similar response for primary antibody injection, somatostatin produced a slightly larger SPR shift for GNP-Ab$_2$ conjugates (Fig. 5).

The LOD achieved in this study is in accordance with previous studies where detection of insulin[15] and glucagon[16] secreted from 10 islets was achieved at 15 mM glucose. Therefore, the somatostatin secreted from this small population of islets could be effectively and accurately detected by our proposed approach, opening the possibility of gaining better understanding of its paracrine communications associated with abnormal islets' function in diabetes.

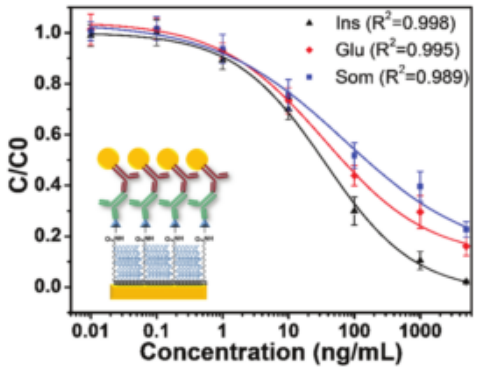

Fig. 6 Calibration curves for a multiplex immunoassay using GNP-Ab$_2$ conjugates as the amplification strategy in PBS-T. Solid lines correspond to the fitting of a nonlinear 4PL model for different concentrations of insulin (blue), glucagon (red), and somatostatin (black). For each hormone, mean relative binding values (C/C_0) were plotted as a function of hormone concentration (ng mL^{-1}). The mean SPR shift was measured in sets of triplicate spots for each hormone and the controls. Then, the average SPR shift was calculated using 3 independent multiplex sensors (n = 3) corresponding to the reported SD.

Conclusions

To address the challenges in the detection of low molecular weight hormones secreted in very low concentrations by human islets such as somatostatin, we investigated three GNP amplification strategies using an SPRi-based biosensing approach. Although the amplification method involving the conjugation of primary antibodies with GNPs showed the best performance for sensing of individual hormones, it presented large cross-reactivity during multiplex experiments. This cross-reactivity was successfully circumvented using an immunoassay with secondary antibodies conjugated to GNPs as amplification. We successfully achieved multiplex detection of three pancreatic islet related hormones with LODs of 0.15 nM, 0.39 nM and 1.22 nM for insulin, glucagon and somatostatin, respectively, with a total analysis time of 32 min per point. This performance is comparable with the previously reported detection sensitivity of insulin and glucagon secreted from 10 islets as well with the individual hormone sensing using conventional ELISA kits.

The possibility of working with a small pancreatic islet population combined with the advantage of multiplexing, a wide working concentration window and a low analysis time makes our sensor very suitable for its future application in secretion-monitoring of pancreatic islets, particularly for understanding the paracrine effect of somatostatin on glucose-induced insulin and glucagon secretion. Furthermore, integrating a microfluidic perfusion platform with the proposed sensing approach could allow one to perform multiparametric analysis of a SF of pancreatic islets in the context of discovery of novel drugs for diabetes treatment.

Conflicts of interest

There are no conflicts to declare.

Acknowledgements

The authors acknowledge the financial support from the Natural Science and Engineering Research Council of Canada

(NSERC) and the NSERC-CREATE in ISS grants and the FRC scholarship from Consejo Nacional de Ciencia y Teconología de México (CONACyT) and Secretaría de Educación Pública de México (SEP). The authors are also thankful to Dr. F Melaine for her help during the initial exploration of GNPs as the amplification strategy.

References

1 F. R. Castiello, K. Heileman and M. Tabrizian, *Lab Chip*, 2016, **16**, 409–431.
2 M. Braun, R. Ramracheya, S. Amisten, M. Bengtsson, Y. Moritoh, Q. Zhang, P. R. Johnson and P. Rorsman, *Diabetologia*, 2009, **52**, 1566–1578.
3 S. J. Le Marchand and D. W. Piston, *J. Biol. Chem.*, 2010, **285**, 14389–14398.
4 V. Grill, M. Gutniak, A. Roovete and S. EfendiĆ, *J. Clin. Endocrinol. Metab.*, 1984, **59**, 293–297.
5 O. Segers, M. Vroede, Y. Michotte and G. Somers, *Diabetic Med.*, 1989, **6**, 232–238.
6 K. Ramachandran, X. Peng, K. Bokvist and L. Stehno-Bittel, *Br. J. Pharmacol.*, 2014, **171**, 3010–3022.
7 D. T. Nguyen, D. van Noort, I. K. Jeong and S. Park, *Biofabrication*, 2017, **9**, 015021.
8 Y. Xing, M. Nourmohammadzadeh, J. E. M. Elias, M. W. Chan, Z. Q. Chen, J. J. McGarrigle, J. Oberholzer and Y. Wang, *Biomed. Microdevices*, 2016, **18**, 9.
9 M. Braun, R. Ramracheya, P. R. Johnson and P. Rorsman, *Ann. N. Y. Acad. Sci.*, 2009, **1152**, 187–193.
10 S. T. Hanna, G. M. Pigeau, J. Galvanovskis, A. Clark, P. Rorsman and P. E. MacDonald, *Pflug. Arch. Eur. J. Physiol.*, 2009, **457**, 1343–1350.
11 D. S. Luciani and J. D. Johnson, *Mol. Cell. Endocrinol.*, 2005, **241**, 88–98.
12 M. Braun, R. Ramracheya, M. Bengtsson, A. Clark, J. N. Walker, P. R. Johnson and P. Rorsman, *Diabetes*, 2010, **59**, 1694–1701.
13 R. Ramracheya, C. Ward, M. Shigeto, J. N. Walker, S. Amisten, Q. Zhang, P. R. Johnson, P. Rorsman and M. Braun, *Diabetes*, 2010, **59**, 2198–2208.
14 K. Terao, M. Gel, A. Okonogi, A. Fuke, T. Okitsu, T. Tada, T. Suzuki, S. Nagamatsu, M. Washizu and H. Kotera, *Sci. Rep.*, 2014, **4**, 6.
15 M. G. Roper, J. G. Shackman, G. M. Dahlgren and R. T. Kennedy, *Anal. Chem.*, 2003, **75**, 4711–4717.
16 J. G. Shackman, K. R. Reid, C. E. Dugan and R. T. Kennedy, *Anal. Bioanal. Chem.*, 2012, **402**, 2797–2803.
17 A. R. Lomasney, L. Yi and M. G. Roper, *Anal. Chem.*, 2013, **85**, 7919–7925.
18 J. P. Lafleur, A. Jonsson, S. Senkbeil and J. P. Kutter, *Biosens. Bioelectron.*, 2016, **76**, 213–233.
19 S. S. Hinman, K. S. McKeating and Q. Cheng, *Anal. Chem.*, 2018, **90**, 19–39.
20 G. Spoto and M. Minunni, *J. Phys. Chem. Lett.*, 2012, **3**, 2682–2691.
21 H. J. Lee, D. Nedelkov and R. M. Corn, *Anal. Chem.*, 2006, **78**, 6504–6510.
22 F. R. Castiello and M. Tabrizian, *Anal. Chem.*, 2018, **90**, 3132–3139.
23 O. Cabrera, D. M. Berman, N. S. Kenyon, C. Ricordi, P. O. Berggrern and A. Caicedo, *Proc. Natl. Acad. Sci. U. S. A.*, 2006, **103**, 2334–2339.
24 L. A. Lyon, M. D. Musick and M. J. Natan, *Anal. Chem.*, 1998, **70**, 5177–5183.
25 J. Jung, K. Na, J. Lee, K. W. Kim and J. Hyun, *Anal. Chim. Acta*, 2009, **651**, 91–97.
26 S. Szunerits, J. Spadavecchia and R. Boukherroub, *Rev. Anal. Chem.*, 2014, **33**, 153–164.
27 M. Frasconi, C. Tortolini, F. Botre and F. Mazzei, *Anal. Chem.*, 2010, **82**, 7335–7342.
28 J. S. Mitchell, Y. Wu, C. J. Cook and L. Main, *Anal. Biochem.*, 2005, **343**, 125–135.
29 J. S. Mitchell and T. E. Lowe, *Biosens. Bioelectron.*, 2009, **24**, 2177–2183.
30 S. W. Zeng, D. Baillargeat, H. P. Ho and K. T. Yong, *Chem. Soc. Rev.*, 2014, **43**, 3426–3452.
31 D. C. Kabiraz, K. Morita, K. Sakamoto and T. Kawaguchi, *Talanta*, 2017, **172**, 1–7.
32 I. E. Sendroiu, L. K. Gifford, A. Lupták and R. M. Corn, *J. Am. Chem. Soc.*, 2011, **133**, 4271–4273.
33 J. U. Lee, A. H. Nguyen and S. J. Sim, *Biosens. Bioelectron.*, 2015, **74**, 341–346.
34 K. V. Gobi, H. Iwasaka and N. Miura, *Biosens. Bioelectron.*, 2007, **22**, 1382–1389.
35 S. Takae, Y. Akiyama, Y. Yamasaki, Y. Nagasaki and K. Kataoka, *Bioconjugate Chem.*, 2007, **18**, 1241–1245.
36 L. Huang, G. Reekmans, D. Saerens, J.-M. Friedt, F. Frederix, L. Francis, S. Muyldermans, A. Campitelli and C. V. Hoof, *Biosens. Bioelectron.*, 2005, **21**, 483–490.
37 S. Taufik, A. Barfidokht, M. T. Alam, C. Jiang, S. G. Parker and J. J. Gooding, *J. Electroanal. Chem.*, 2016, **779**, 229–235.
38 J. D. Driskell, C. A. Jones, S. M. Tompkins and R. A. Tripp, *Analyst*, 2011, **136**, 3083–3090.
39 M. C. Estevez, J. Belenguer, S. Gomez-Montes, J. Miralles, A. M. Escuela, A. Montoya and L. M. Lechuga, *Analyst*, 2012, **137**, 5659–5665.
40 T. Kawaguchi, D. R. Shankaran, S. J. Kim, K. Matsumoto, K. Toko and N. Miura, *Sens. Actuators, B*, 2008, **133**, 467–472.
41 D. Juncker, S. Bergeron, V. Laforte and H. Li, *Curr. Opin. Chem. Biol.*, 2014, **18**, 29–37.
42 J. T. Dias, L. Lama, J. Gantelius and H. Andersson-Svahn, *Nanoscale*, 2016, **8**, 8195–8201.
43 J. Martinez-Perdiguero, A. Retolaza, L. Bujanda and S. Merino, *Talanta*, 2014, **119**, 492–497.
44 R. B. Schasfoort, *Handbook of surface plasmon resonance*, Royal Society of Chemistry, United Kingdom, 2nd edn, 2017.
45 H. Vaisocherova, E. Brynda and J. Homola, *Anal. Bioanal. Chem.*, 2015, **407**, 3927–3953.
46 J. Lahiri, L. Isaacs, J. Tien and G. M. Whitesides, *Anal. Chem.*, 1999, **71**, 777–790.

Appendix B: Curriculum Vitae

F. Rafael Castiello

EDUCATION

M. Sc. in Material Science and Engineering
2013
National Autonomous University of Mexico (UNAM), Mexico
- Graduation with honors

B. Sc. in Chemical Engineering
2009
Guadalajara University, Guadalajara, Mexico
- Minors in food chemistry and environmental engineering
- Exchange Program, IMC University of Applied Sciences Krems, Austria

RESEARCH EXPERIENCE

Master research **2011 – 2013**
Department of Nanostructures, National Autonomous University of Mexico, Ensenada, Mexico
- Synthesis and characterization of multiwall carbon nanotubes and gold nanoparticles
- Functionalization of carbon nanotubes with cyclodextrin and gold nanoparticles as potential biosensors
- Test of nanomaterials as potential biosensors using Locally Enhanced Raman Spectroscopy

Research Assistant **2008 – 2009**
Department of Food Technology at Center for Technological Assistance and Design from Jalisco State (CIATEJ), Mexico
- Development of thermo-resistant biopolymeric systems for bakeable jams
- Study of rheological/thermal properties of developed jams and tests on finished products

Research Assistant **2006**
Department of Synthesis and Characterization of polymeric materials**,** Guadalajara University, Mexico
- Mechanical properties of polymeric materials
- Synthesis kinetics of polymeric hydrogels

ACADEMIC EXPERIENCE

Teaching Assistant, Bioperformance and Biomaterials course
2017
McGill University, Montreal, QC
- Taught, graded and assisted student with final project

Lecturer of Nano-biomaterials course **2013**
Autonomous University of Baja California, Mexico
- Syllabus elaboration
- Design of laboratory practices and evaluation exams

OTHER EXPERIENCE

Project Engineer **2009 – 2010**

Promotora la Loma S.A. de C.V., Guadalajara, México

- Design of a novel process to transform residual material to a high value product
- The project included a viability study and the experimental design

TRAININGS

Leadership Workshop Series **2017**
McGill University, Montreal, QC

NSERC-CREATE Training Program in Integrated Sensor Systems (ISS)
2014 – 2016
McGill University, Montreal, QC

- **Hands-on workshops:** Surface and materials characterization, Surface chemistry, Micro and Nano bioengineering, Silicon microfabrication
- **Professional skills short courses:** Basic Business Skills, Learn to Teach Day, Academic Integrity, Commercialization of Biomedical Research, Intellectual Property, Process Control and Project Management
- **Chair of the Graduate Student Program Committee** for the organization of a winter networking event

SKILLS

Laboratory techniques: UV-Vis Spectroscopy, Infrared Spectroscopy (FT-IR), Quartz Crystal Microbalance (QCMD), Impedance Spectroscopy, Raman Spectroscopy, Surface Plasmon resonance imaging (SPRi), Atomic force microscopy (AFM), Fluorescence Microscopy, Thermogravimetric analysis (TGA), Differential Scanning Calorimetry (DSC) and Microfabrication
Field expertise: Pancreatic islets (Diabetes), Biosensors, Microfluidics, Surface characterization and Nanomaterials
Software: Word, Excel, PowerPoint, MS Project, COMSOL, Origin Lab, ChemDraw, AutoCAD, MATLAB
Languages: Spanish, English (Fluent), French (intermediate), German (Basic)

AWARDS

NSERC-CREATE Integrated Sensor Systems (ISS) Fellowship Award **2014 – 2016**
Fellowship for academic excellence (valued at 12,800 CAD/annually)
National Council of Science and Technology of Mexico International PhD Fellowship **2013 – 2017**
Fellowship for academic excellence (valued at 28,000 USD/annually)
National Council of Science and Technology of Mexico National M.Sc. Fellowship **2011 – 2013**
Fellowship for academic excellence (valued at 7,000 USD/annually)
Ernst Mach Grant **2008**
Academic Cooperation and Mobility Office of Austria (ÖAD/ACM) (valued at 6,400 EUR)

ACTIVITIES & INTERESTS

Private Tutor: mathematics, chemistry and physics (high school level) **2005 – 2009**
Sports: Gym and swimming
Music: Enthusiastic classic piano and guitar player
Interest: Reading (Science fiction, science, and self-development), learning through short courses

PUBLICATION & PRESENTATIONS

Articles:

- **Castiello, F.R** and Tabrizian M. *Multiplex SPRi-based immunoassay using gold nanoparticle amplification strategies for quantification of human pancreatic islet hormones*. Submitted to the journal ACS Sensors on December 12, 2018.

- **Castiello, F.R,** Porter J., Modarres P. and Tabrizian M. *Interfacial capacitance immunosensing using interdigitated electrodes: effect of the insulation/immobilization chemistry. Submitted to the journal ACS OMEGA on November 28, 2018.*
- **Castiello, F.R** and Tabrizian M. *Multiplex Surface Plasmon Resonance Imaging-Based Biosensor for Human Pancreatic Islets Hormones Quantification.* Anal. Chem. 2018, 90, 3132-3139.
- Nayef, L.; **Castiello, R**.; Tabrizian, M., *Washless Method Enables Multilayer Coating of an Aggregation-Prone Nanoparticulate Drug Delivery System with Enhanced Yields*, Colloidal Stability, and Scalability. Macromolecular Bioscience 2017.
- **F. Rafael Castiello**, Khalil Heileman, Maryam Tabrizian, *Microfluidic perfusion systems for secretion fingerprint analysis of pancreatic islets: applications, challenges and opportunities*, Lab Chip, 2016, 16, 409-431.
- J. M. Romo-Herrera, A. L. González, L. Guerrini, **F. R. Castiello**, G. Alonso-Nuñez, O. E. Contreras and R. A. Alvarez-Puebla, *A study of the depth and size of concave cube Au nanoparticles as highly sensitive SERS probes,* Nanoscale, 2016, 8, 7326-7333.
- **Castiello, F.R**.; Romo-Herrera, J.; Farías, M.; Guerra, E.; Contreras, O.; Berhault, G.; Kochkar, H.; Fuentes, S.; Alonso-Nuñez, G., "Green" seed-mediated synthesis and morphology of Au nanoparticles using β-cyclodextrin. Gold Bulletin 2016, 49 (1-2), 45-51.

International conferences:

- **Castiello, F. R**.; Tabrizian, M. *Impedance Biosensors as a Tool for Dynamic Monitoring of Cell Secretion, 32nd International Symposium on Microscale Separations and Bioanalysis*. Niagara on the lake, Canada, April 3-7, 2016. (Oral presentation)
- **Castiello, F. R**., Heileman, K., and Tabrizian, M. Dielectric/Impedance spectroscopy as a tool to analyze pancreatic islet secretion and functionality on-chip. Poster presented at Lab-on-a-chip Microfluidics & Microarrays World Congress, San Diego, California, USA. September 28-30, 2015. (Poster presentation)